



Endothelial Cross-Talks in the Aging Heart

Dissertation

zur Erlangung des Doktorgrades der
Naturwissenschaften

vorgelegt beim Fachbereich 15 (Biowissenschaften)

der Johann-Wolfgang-Goethe-Universität

in Frankfurt am Main

von

Julian Uwe Gabriel Wagner

aus Limburg an der Lahn

Frankfurt 2019

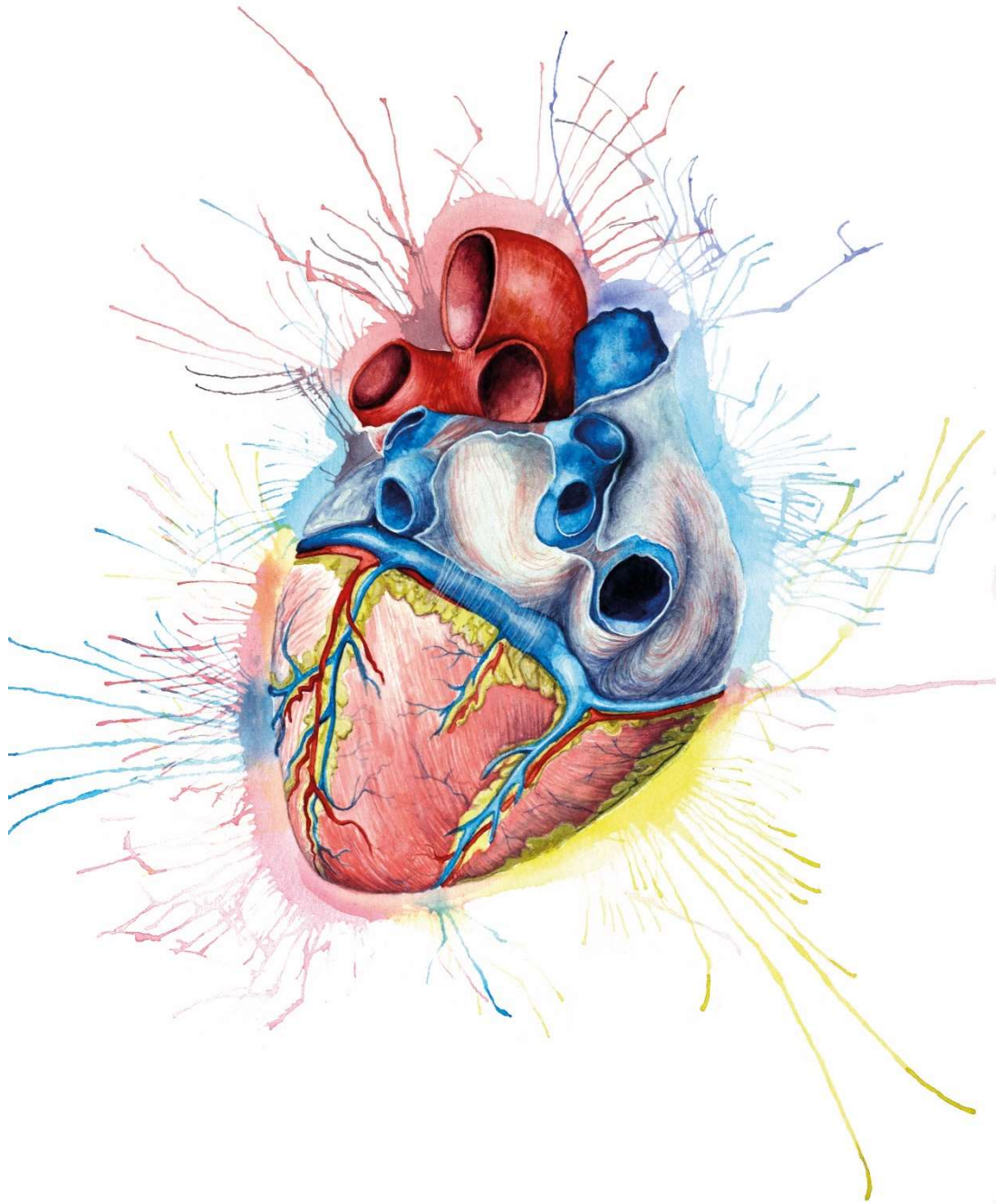
(D 30)

vom Fachbereich 15 (Biowissenschaften) der
Johann-Wolfgang-Goethe-Universität als Dissertation angenommen.

Dekan: Prof. Dr. Sven Klimpel

Gutachter: Prof. Dr. Stefanie Dimmeler
Prof. Dr. Amparo Acker-Palmer

Datum der Disputation: 20.08.2020



*So eine Arbeit wird eigentlich nie fertig, man muss sie für fertig erklären,
wenn man nach der Zeit und den Umständen das Möglichste getan hat.*

-Johann Wolfgang von Goethe

Abbreviations

3D	three-dimensional
A	adenine
ACh	acetylcholine
Adgrl3	adhesion G protein-coupled receptor L3
AGE	advanced glycation end-products
AMI	acute myocardial infarction
AMPK	5'-AMP-activated protein kinase
ANG2	angiopoietin-2
Ang-II	angiotensin II
ANOVA	analysis of variance
AU	absorption unit
BBE	bovine brain extract
BCECF, AM	2',7'-bis-(2-carboxyethyl)-5-(and-6)-carboxyfluorescein, acetoxymethyl ester
BDM	2,3-Butanedione monoxime
BM	basement membrane
BMP4	bone morphogenic factor 4
BSA	bovine serum albumin
C	cytosine
°C	degree Celsius
Ca	calcium
CD	cluster of differentiation
Cdh5/CDH5	cadherin 5
cDNA	complementary DNA
cFB(s)	cardiac fibroblast(s)
CM(s)	cardiomyocyte(s)
CST	Cell Signaling Technologies
Ctrl.	control
CV	cardiovascular
CVD(s)	cardiovascular disease(s)
CO ₂	carbon dioxide
Co	control
Col	collagen
Cx	connexin
d	days
DAMPs	danger-associated molecular patterns
DAPI	4',6-Diamidin-2-phenylindol
DDR2	Discoidin Domain Receptor Tyrosine Kinase 2
DEG(s)	differentially expressed gene(s)
Dll4	delta-like 4
DMEM	Dulbecco's modified eagle's medium

DMSO	dimethylsulfoxid
DNA	deoxyribonucleic acid
DPBS	Dulbecco's phosphate buffered saline
E	embryonic day
EBM	endothelial basal medium
EC(s)	endothelial cells
ECAR	extracellular acidification rate
ECM	extracellular matrix protein
EDTA	ethylene diaminetetraacetic acid
EdU	5-ethynyl-2'-desoxyuridin
Efemp1	EGF-containing fibulin-like extracellular matrix protein 1
EGF	endothelial growth factor
EHS	Engelbrecht Holm-Swarm
EM	electron microscopy
EMT	epithelial-to-mesenchymal transition
EndMT/EndoMT	endothelial-to-mesenchymal transition
eNOS	endothelial nitric oxide synthase
ET-1	endothelin-1
et al.	et alii; lat. for "and others"
FB(s)	fibroblast(s)
FCS/FBS	fetal calve serum / fetal bovine serum
FGF2	fibroblast growth factor 2
Fig.	figure
FMT	fibroblast-to-myofibroblast transition
FN	fibronectin
FSP1	fibroblast specific protein 1
g	gravity constant or gram
G	guanine
GDF-11	growth differentiation factor 11
GFP	green fluorescence protein
GFR	growth factor reduced
GO	gene ontology
h	hour
HBSS	Hank's balanced salt solution
HCAEC	human coronary artery endothelial cells
HEK	human embryo kidney
HF	heart failure
HFpEF	heart failure with preserved ejection fraction
HFrEF	heart failure with reduced ejection fraction
HIF 1 α	hypoxia induced factor 1 α
hr	human recombinant
HRP	horseradish peroxidase
HS	horse serum
HUVEC	human umbilical vein endothelial cells

Hz	Hertz
IL	interleukin
iNOS	inducible NOS
IRAK-3	IL-1 receptor-associated kinase
ITGB1	Integrin β 1
JAG1	JAGGED-1
KLF2	Krüppel-like factor 2
KO	knockout
L	liter
LA	left atrium
Lama/LAMA	laminin alpha chain
Lamb/LAMB	laminin beta chain
Lamc/LAMC	laminin gamma chain
LM	laminin
LV	left ventricle
m	meter
M	Molar
MendoT	mesenchymal-to-endothelial transition
Mg	magnesium
MI	myocardial infarction
min.	minutes
mL	milliliter
MMP	matrix metalloprotease
mRNA	messenger RNA
MuIV	murine leukemia virus
n	nano or sample number
n.s.	not significant
N-cadherin	neural cadherin
NF1	neurofibromatosis type-1
NO	nitric oxide
NOS	nitric oxide synthase 3
NOX	NADPH oxidase
Npas4l	helix–loop–helix-Per–ARNT–Sim (bHLH-PAS) protein neuronal PAS domain-containing protein 4-like protein
NRP1	neuropilin-1
OCN	osteocalcin
PDGFR α	platelet-derived growth factor receptor α
PE	phenylephrine
PBS	phosphate buffered saline
PCR	polymerase chain reaction
Pecam 1	platelet endothelial cell adhesion molecule 1
qPCR	quantitative PCR
Rgs6	Regulator of G-protein signaling 6
RNA	ribonucleic acid

rpm	rounds per minute
RT	reverse transcription
RT	room temperature
s	seconds
scRNA seq	single-cell RNA sequencing
SD	standard deviation
SEM	standard error of the mean
SHG	second harmonics generation
siRNA	small interfering RNA
SM22 α	Transgelin
SMC(s)	smooth muscle cell(s)
snRNA seq	single-nucleus RNA sequencing
stauro	staurosporine
T	thymine
TGF β	transforming growth factor β
TLR	toll-like receptor
TNF α	tumor necrosis factor α
Tris	tris(hydroxymethyl)-aminomethan
TRP	transient receptor potential
t-SNE	t-distributed stochastic neighbor embedding
T β RI	TGF β receptor I
VE-cadherin	vascular endothelial cadherin
VEGF	vascular endothelial growth factor
VEGFR	VEGF receptor
Vim	Vimentin
VSMCs	vascular smooth muscle cells
vWF	von-Willebrandt-factor
WHO	World Health Organization
α -SMA	α -smooth muscle actin
μ	micro

Table of Content

Zusammenfassung	1
Summary	7
1 Introduction	12
1.1 General Introduction	12
1.2 The Heart	12
1.2.1 Anatomical Structure of the Heart	12
1.2.2 The Wall of the Heart	13
1.3 The Vascular System	14
1.3.1 Vessel Structure	14
1.3.2 Development of the Vasculature: Vasculogenesis and Angiogenesis	16
1.3.3 The Basement Membrane	20
1.4 Cardiovascular Diseases	23
1.4.1 Atherosclerosis	24
1.4.2 Myocardial Infarction	24
1.4.3 Heart Failure	25
1.5 Cellular Cross-Talk and Heterogeneity in the Heart	26
1.5.1 Cellular Heterogeneity and Cellular Cross-Talk in the Healthy Heart	26
1.5.2 Cellular Processes and Cross-Talk during post-MI Cardiac Remodeling	31
1.6 Aging	34
1.6.1 Cardiovascular Aging	34
1.6.2 Changes in Cellular Mechanisms in the Aging Heart	36
1.7 Cellular Plasticity in the Adult Heart	40
1.8 The Vascular Niche Function	42
1.9 The Use of single-cell RNA Sequencing to Study Cardiac Cellular Heterogeneity ..	44
2 Objectives	47
3 Results and Discussion	48
3.1. Role of Laminin β 1 and Laminin β 2 in the Endothelial Niche of the Aging Heart	48
3.2. Transcriptional Heterogeneity of Fibroblasts as a hallmark of Cardiac Aging	52
3.3. Generation of a Cardiac Tissue Mimetic to dissect Cellular Cross-Talk of the Heart ..	57
3.4. Conclusions and Future Perspectives	63
4 References	65
5 Permissions to Reprint	83
6 Author Contribution	84
6.1 Author contribution for Appendix 1	84

6.2 Author contribution for Appendix 2.....	84
6.3 Author contribution for Appendix 3.....	85
6.4 Author contribution for Appendix 4.....	86
7 Schriftliche Erklärung	87
8 Acknowledgments.....	88
9 Appendix	90
9.2 Appendix 1	90
9.3 Appendix 2.....	117
9.4 Appendix 3.....	131
9.5 Appendix 4.....	172
10 Curriculum Vitae	208

Zusammenfassung

Erkrankungen des Herz-Kreislauf-Systems gelten nach wie vor als Haupttodesursache in den modernen Industrienationen. Der Überbegriff „Herz-Kreislauf-Erkrankungen“ ist jedoch nicht einheitlich definiert. Er beschreibt im Wesentlichen Erkrankungen des Herzens und der Blutgefäße und umfasst Krankheiten wie zum Beispiel Bluthochdruck, Arteriosklerose, Herzinfarkt, Herzinsuffizienz, koronare Herzkrankheiten, rheumatische Herzkrankheiten und Herzklappenfehler. Neben den wohlbekanntesten Risikofaktoren, wie Übergewicht, Rauchen, Hypercholesterinämie und mangelnde Bewegungen, ist das Alter ein Hauptrisikofaktor, der maßgeblich an der Ausbildung von Herz-Kreislauf-Erkrankungen beteiligt ist. Dies ist insbesondere in einer älter werdenden Gesellschaft ein größer werdendes Problem.

Doch wie kommt es dazu, dass die Prävalenz für Herz-Kreislauf-Erkrankungen im Alter steigt? Im Allgemeinen geht man von altersabhängigen Veränderungen auf zellulärer Ebene aus, die die krankhaften Gewebsveränderungen im Herzen und den Gefäßen bedingen. Wichtige Mechanismen wie Autophagie, oxidativer Stress, mitochondrielle Dysfunktionen, genomische Instabilität, zelluläre Seneszenz und Störungen in der Signaltransduktion von Wachstumsfaktoren spielen dabei eine entscheidende Rolle. So kommt es im Alter zur Hypertrophierung von Herzmuskelzellen, die sich in einer Herzwandverdickung, sowie einer veränderten Herzkammergeometrie äußert. Chronische Endzündungsreaktionen, parakrine sowie altersabhängige Zell-intrinsische Faktoren führen zudem zu einer Aktivierung kardialer Fibroblasten mit erhöhter Zellproliferation, Kollagen-Sekretion und Matrix-Quervernetzung. Die Folgen sind interstitieller und paravaskulärer Fibrosen, die das Herz und die Blutgefäße versteifen lassen. Oxidativer Stress und Endzündungen greifen zusätzlich die Blutgefäße an und beeinträchtigen die Endothelfunktion, die durch etwaige Vorerkrankungen wie *Diabetes mellitus* und Bluthochdruck zusätzlich verschlechtert wird.

In den vergangenen Jahrzehnten lag das Hauptaugenmerk daher auf der Erforschung dieser altersabhängigen Veränderungen, in der Hoffnung die kardiovaskuläre Alterung besser zu verstehen und mögliche regenerative Interventionen zu entwickeln. Durch die Erforschung der Reparaturmechanismen anderer Organe wie den Lungen und dem Knochenmark, zeigte besonders das Endothel eine hohe regenerative Kapazität, die die Proliferation und Zellfunktion der umliegenden Zellen beeinflusst.

Lange war die allgemeine Meinung, dass das Endothel lediglich die innere Auskleidung der Blut- und Lymphgefäße, sowie der Herzkammern sei, das als einschichtige Barriere die Integrität der Blutgefäße garantiert und damit im ständigen Kontakt mit dem Blut und mit den darin enthaltenden Bestandteilen steht. Die Endothelzellen, die diese Barriere bilden sind jedoch –abhängig von der Art des Blutgefäßes und dem Gewebe, das sie versorgen– sehr heterogen und übernehmen dabei zentrale Aufgaben. Neben der Barrierefunktion regulieren Endothelzellen zusätzlich den Stoffaustausch zwischen Blut und Gewebe, stimulieren die Bildung neuer Blutgefäße und remodellieren bereits bestehende Gefäßnetze. Sie sind weiterhin in der Lage die extrazelluläre Matrix, die sie umgibt umzustrukturieren. Dabei entlassen sie nicht nur Matrixproteine, sondern auch Zytokine und Wachstumsfaktoren in den Extrazellularraum, die dort gespeichert werden. Diese Faktoren werden dann bei Bedarf freigesetzt und stimulieren beispielsweise Angiogenese oder Zellproliferation. Die Sezernierung verschiedener Matrixproteine stabilisiert nicht nur die zelluläre Nachbarschaft, sondern reguliert zudem diverse Zellfunktionen.

Durch die Modellierung des endothelialen Milieus – der sogenannten vaskulären Nische – sind Endothelzellen also in der Lage mit den umliegenden Zellen zu kommunizieren. Infolge dessen wurde sogar ein regenerativer Effekt der vaskulären Nische bereits in diversen Organen beschrieben. In der Leber etwa wurde gezeigt, dass erhöhte Konzentrationen an endotheliale Ang2 und verringertem endotheliale Aktivin A nach partieller Hepatektomie die Proliferation von Hepatozyten und somit die Leberregeneration anregen. Im Knochenmark mobilisieren Endothelzellen Stammzellen via Stickstoffmonoxid und in den Lungen setzt endotheliale MMP14 Wachstumsfaktoren aus der extrazellulären Matrix frei, die die Epithelzellproliferation nach partieller Pneumektomie stimulieren. Ob ein solcher regenerativer Effekt der vaskulären Nische auch im Herzen eine Rolle spielt ist allerdings weitgehend unbekannt.

Da sich sowohl die regenerative Kapazität des Herzens als auch die endotheliale Funktion im Alter abnehmen, war das Ziel der vorliegenden Dissertation die Rolle der vaskulären Nische bzw. der endothelialen Zellkommunikation im gealterten Herzen zu untersuchen. Im Zuge dessen wurde auf humane Zelllinien, sowie Maus- und artifizielle Rattenmodelle zurückgegriffen. Da sich es bei dieser Arbeit um eine kumulative Dissertation mit teilweise publizierten Originalarbeiten handelt, teilt sich die Arbeit in drei Teile auf.

Im ersten Teil dieser Arbeit wurden im Speziellen die Transkriptomsignatur sekretorischer Gene im Endothel von alten Herzen studiert. Dazu wurden perfundierte Endothelzellen aus Herzen von jungen (12 Wochen alte Tiere) und alten Mäusen (20 Monate alte Tiere) isoliert und für *bulk RNA sequencing* verwendet. Unter den top-regulierten Genen befanden sich die beiden Matrixproteine Laminin $\beta 1$ und $\beta 2$. Während Laminin $\beta 2$ besonders im jungen kardialen Endothel exprimiert war, war Laminin $\beta 1$ vorwiegend im alten Endothel zu finden. Dieser Wechsel in der Lamininexpression wurde histologisch auf Proteinebene bestätigt und dessen autokrine Funktion *in vitro* untersucht. Um die *in vivo*-Situation *in vitro* nachzuahmen, wurden Zellkulturschalen mit humanen rekombinanten Laminin 421 bzw. Laminin 411 beschichtet und mit humanen Endothelzellen aus der Nabelvene (HUVEC) besät. Diverse funktionelle Untersuchungen zeigten, dass Endothelzellen in der Gegenwart von Laminin 411 schlechter migrieren und adhären, während in Matrigel-Assays beobachtet werden konnte, dass HUVEC in der Gegenwart von LM 411 vermindert endotheliale Netzwerke ausbildeten.

Unser *bulk RNA sequencing* Datensatz zeigte zudem neben dem Wechsel in der Lamininexpression auch Hinweise für Endothel-zu-Mesenchym Transition im gealterten kardialen Endothel. *In vitro* Experimente ergaben, dass Endothelzellen sowohl basal als auch durch die Stimulation mit TGF $\beta 2$ vermehrt mesenchymale Gene exprimieren, wenn sie auf LM411 kultiviert werden.

Auf mechanistischer Ebene wurden diverse Faktoren gefunden, die die beschriebenen Ergebnisse bedingen können. So wurde herausgefunden, dass HUVEC in der LM411-Kultur weniger FGF2 –ein bekannter Inhibitor für Endothel-Mesenchym Transition– und Thrombospondin 2 –ein wichtiger Regulator im kardiovaskulären System– sezernieren. Weiterhin war -verglichen zu LM421- durch die Kultivierung auf LM411 vor allem die aktive Konformation des Matrixproteinrezeptors Integrin $\beta 1$ weniger detektierbar, die für die verringerte Adhäsion und Migration verantwortlich gemacht werden konnte.

Im zweiten Teil dieser Doktorarbeit, wurde eine globale Transkriptomanalyse des gesamten jungen und alten Mäuseherzen durchgeführt. Durch den Einsatz von *single-nucleus RNA sequencing* war es möglich das Transkriptom auf Einzelkernebene zu untersuchen und Veränderungen nicht nur im Endothel, sondern im gesamten Herzen zu studieren, wodurch putative interzelluläre Interaktionen mit Endothelzellen untersucht werden konnten.

Insgesamt wurden 14.827 Zellkerne von drei jungen (12 Wochen alte) und 12.981 Zellkerne von drei alten (18 Monate alte) Mäusen isoliert und für die Transkriptomanalysen verwendet. Unter Verwendung eines bioinformatischen *t-distributed stochastic neighbor embedding* plots konnten die Einzelkerndaten in einer zweidimensionalen Darstellung zusammengefasst und 15 spezifische Zellpopulationen bestimmt werden. Besonders kardiale Fibroblasten zeigten unter allen kardialen Zellen die stärkste Veränderung in der Genregulation im Alter und wurden daher gesondert analysiert. Eine *Pseudotime Analyse* ordnete die gesamte Fibroblastenpopulation in eine lineare Darstellung an und gruppierte die Fibroblasten in 11 Untergruppen, die entweder von jungen oder alten Zellen prädominiert wurden. Signalweganalysen ergaben, dass besonders die vorwiegend „alten“ Fibroblastengruppen überwiegend Gene exprimieren, die in inflammatorischen, angiogenen und osteogenen Signalwegen wiederzufinden sind.

Zunächst haben wir uns mit der Regulation der Angiogenese-assoziierten Gene in Fibroblasten befasst. Da besonders sekretorische angiogene Gene in alten Fibroblasten reguliert waren, wurde eine bioinformatische Liganden-Rezeptor-Analyse durchgeführt, um etwaige zelluläre Interaktionen vorherzusagen. Die Analyse ergab, dass während der Alterung besonders Fibroblasten mit Endothelzellen interagieren könnten, wobei Fibroblasten maßgeblich parakrine Faktoren und Endothelzellen die dazugehörigen Rezeptoren exprimieren würden. Diese Hypothese wurde mit einem HUVEC Matrigel-Assay untersucht, bei dem HUVEC für 24 Stunden mit konditionierten Fibroblastenkulturüberständen stimuliert wurden, die zuvor von isolierten Fibroblasten aus jungen und alten Mäuseherzen generiert wurden. Interessanterweise zeigten HUVEC, die mit „alten“ Fibroblastenmedium behandelt wurden eine verschlechterte Netzwerkbildung als HUVEC, die mit „jungen“ Fibroblastenmedium kultiviert wurden. Mitglieder der Serpin-Familie wurden als Hauptverursacher dieses Effekts bestimmt, die vermehrt auf RNA- und Protein-Ebene in „alten“ Fibroblasten gefunden wurden. Durch den Einsatz von neutralisierenden Serpin-Antikörpern war es schließlich möglich den antiangiogenen Effekt des „alten“ Fibroblastenmediums zu stoppen. Im weiteren Verlauf lag der Fokus auf der Regulation der Osteogenese-assoziierten Gene in Fibroblasten. Die Einzelkerndaten zeigten zu Beginn, dass in „alten“ Fibroblasten die Faktoren *Runx2* und *Cepbp*, beides wichtige Regulatoren der Osteoblastendifferenzierung, exprimiert waren. Während RT-qPCR und *bulk RNA sequencing* Daten die Expression von *Runx2* in isolierten Mausfibroblasten validierten, zeigten his-

tologische Färbungen im alten Mäuseherz PDGR α -positive Zellen, die Osteokalzin exprimieren. Diese „osteogenen Fibroblasten“ waren fast ausschließlich im Epikard alter Herzen zu finden. Das Epikard junger Herzen war nahezu frei von solchen Zellen. Darüber hinaus wurden durch von-Kossa-Färbungen, neben den Herzklappen, einzelne Kalzifizierungen ausschließ im Epikard alter Herzen gefunden. Das junge Herz zeigte keinerlei Kalkablagerungen im Epikard.

Zusammenfassend konnte gezeigt werden, dass sich besonders Fibroblasten im gealterten Herzen verändern. Während sie über Serpinexpression die Angiogenese hemmen, nehmen sie im Epikard einen osteogenen Phänotypen an. Ob jedoch diese osteogenen Zellen tatsächlich von Fibroblasten oder epikardiale Zellen abstammen, muss in *linage-tracer* Versuchen validiert werden.

Im dritten und letzten Teil dieser Dissertation wurde eine neuartige dreidimensionale sphäroidale Zellkultur (*Cardiac Tissue Mimetic*; CTM) entwickelt, um die interzellulären Kommunikationswege zwischen Endothelzellen, Herzmuskelzellen und kardialen Fibroblasten in einer möglichst physiologischen Umgebung zu untersuchen. Zur CTM-Generierung wurden in einem ersten Schritt Herzmuskelzellen und Fibroblasten aus neonatalen Rattenherzen isoliert und in einem Verhältnis von 5:1 in hängenden Tropfen kultiviert. Nach vier Tagen ballten sich die Zellen zu Sphäroiden zusammen, die in einem zweiten Schritt zunächst mit Matrigel und dann mit grün-fluoreszierenden HUVEC überzogen wurden. Der Einsatz grün-fluoreszierender HUVEC ermöglichte dabei die Beobachtung von Gefäßbildungen *in situ*. Zehn Tage lang wurden die CTMs in Kultur gehalten und die Gefäßausbildung unter diversen Stimuli studiert. Zunächst wurden CTMs mit dem Sympathomimetikum Phenylephrin (PE) behandelt. Die Stimulation mit PE förderte die CTM-Hypertrophierung, -Reifung und -Schlagfrequenz, verglichen mit CTMs ohne Stimulation. Zudem konnte die Bildung eines ausgeprägten Endothelnetzes beobachtet werden. Während PE keinen direkten Effekt auf Endothelzellen zu haben schien, konnte bewiesen werden, dass PE die Sekretion von VEGF in Herzmuskelzellen erhöhte, das parakrin die Endothelsprossung induzierte. Das Sekretom von Fibroblasten zeigte unter PE jedoch keine pro-angiogenen Veränderungen. Da PE nicht nur das Sekretom veränderte, sondern auch die CTM-Kontraktion beeinflusste, wurde angenommen, dass PE zusätzlich über eine mechanische Aktivierung die Endothelsprossung induziert. Um die Kontraktion aus dem Zellkultursystem zu entkoppeln, wurden CTMs mit einer Kombination aus PE und jeweils den β -Blockern Metoprolol und Propranolol stimuliert. Alle genannten β -Blocker waren in der Lage die

CTM-Kontraktion zu senken. Zudem war die Endothelsprossung nahezu gänzlich unterdrückt. Dass die verwendeten β -Blocker einen direkten Effekt auf Endothelzellen oder einen direkten Effekt auf die VEGF-Expression in Herzmuskelzellen haben, konnte durch diverse funktionelle Experimente widerlegt werden und implizierte, dass die mechanische Aktivierung von Endothelzellen durch Herzmuskelzellen die Gefäßbildung im kardialen Milieu induziert.

Im weiteren Verlauf wurde das CTM-Modell verwendet, um pathophysiologische Zustände, wie sie bei Ischämien und bei Remoderierungsprozessen nach einem Herzinfarkt auftreten, zu untersuchen. Die Behandlung der CTMs mit dem pro-fibrotischen Wachstumsfaktor TGF β 2 zeigte zwar nur eine marginal erhöhte Endothelzellensprossung im Vergleich zu Kontroll-CTMs, allerdings war besonders die Kollagenablagerung in TGF β 2-stimulierten CTMs erhöht, was mit einer verstärkten Fibrose gleichzusetzen ist. Außerdem exprimierten vereinzelnde Endothelzellen mesenchymale Marker, die besonders bei der Endothel-Mesenchym-Transition eine Rolle spielen. Die Kultivierung von CTMs unter starker Hypoxie induzierte ebenfalls Kollagenablagerungen, verminderte aber die Endothelsprossung.

Zusammenfassend konnte eine neuartige Zellkultur generiert werden, die der Untersuchung von Endothelzellen in einer kardialen Umgebung dient. Neben der direkten Beobachtung des Gefäßwachstums, kann dieses Modell auch zur Untersuchung diverser Therapeutika in Hinblick auf Nebenwirkungen genutzt werden.

Summary

Cardiovascular diseases are still regarded as the main cause of death in the modern world. However, the generic term "cardiovascular diseases" is not uniformly defined. It essentially describes diseases of the cardiovascular system and includes diseases such as hypertension, arteriosclerosis, myocardial infarctions, heart failure, coronary heart diseases, rheumatic heart diseases and heart valve defects. In addition to the well-known risk factors such as obesity, smoking, hypercholesterolemia and lack of exercise, age is a further risk factor that plays an important role in the development of cardiovascular diseases. As the modern societies age; this becomes an increasing problem.

But why does the prevalence of cardiovascular diseases increase with age? In general, age-dependent changes at the cellular level are assumed to be responsible for the pathological changes in the cardiac and vascular tissues. Important mechanisms such as autophagy, oxidative stress, mitochondrial dysfunctions, genomic instability, cellular senescence and disturbances in signaling pathways of growth factors play a decisive role. In old age, myocardial hypertrophy occurs, which results in cardiac wall thickening and an altered geometry of the ventricle. Chronic inflammations, paracrine and age-dependent cell-intrinsic factors further lead to activation of cardiac fibroblasts with increase cell proliferation, collagen secretion and matrix cross-linking. The consequences are interstitial and perivascular fibrosis, which stiffen the heart and blood vessels. Oxidative stress and inflammations additionally attack the blood vessels and impair endothelial function, which is further aggravated by possible pre-existing conditions such as diabetes mellitus and hypertension.

In the past decades, the main focus has therefore been on researching these age-dependent changes in the hope of better understanding cardiovascular ageing and developing possible regenerative interventions. By studying the repair mechanisms of other organs such as the lungs and the bone marrow, the endothelium in particular showed a high regenerative capacity, which influences the proliferation and cell function of the surrounding cells.

For a long time, the general opinion was that the endothelium is only the internal lining of blood and lymphatic vessels, as well as the heart chambers, which as a single-layer barrier guarantees the integrity of the blood vessels. However, endothelial cells are very heterogeneous, depending on the type of blood vessel and the type of tissue they

serve. In addition to their barrier function, endothelial cells also regulate the exchange of substances between blood and tissue, stimulate the formation of new blood vessels and re-model existing vascular networks. They are also able to restructure the extracellular matrix that surrounds them. They release not only matrix proteins, but also cytokines and growth factors into the extracellular space. On demand, these factors are then released and stimulate angiogenesis or cell proliferation. In addition, the secretion of various matrix proteins not only stabilizes the cellular neighborhood, but also regulates various cell functions.

By modelling the endothelial environment - the so-called vascular niche - endothelial cells are able to communicate with the surrounding cells. As a result, a regenerative effect of the vascular niche has already been described in various organs. In the liver, for example, it has been shown that increased concentrations of endothelial Ang2 and decreased endothelial activin A after partial hepatectomy stimulate the proliferation of hepatocytes and thus liver regeneration. In the bone marrow, endothelial cells mobilize stem cells via nitric oxide and in the lungs, endothelial MMP14 releases growth factors from the extracellular matrix, which stimulate epithelial cell proliferation after partial pneumectomy. Whether such a regenerative effect of the vascular niche also plays a role in the heart is largely unknown.

Since both the regenerative capacity of the heart and endothelial function decrease with age, the aim of this dissertation was to investigate the role of the vascular niche and endothelial cell communication in the aged heart. Human cell lines as well as mouse and artificial rat models were used for these investigations. Since this thesis is a cumulative dissertation with partially published papers, it is divided into three parts.

In the first part of this thesis, the transcriptional signature of secretory genes in the aged cardiac endothelium was studied. Perfused endothelial cells from hearts of young (12-week-old animals) and old mice (20-month-old animals) were isolated and used for bulk RNA sequencing. The two matrix proteins laminin β 1 and β 2 were among the top-regulated genes. While laminin β 2 was particularly expressed in the young cardiac endothelium, laminin β 1 was predominantly found in the old endothelium. This change in laminin expression was confirmed histologically at protein level and its autocrine function was investigated *in vitro*. To mimic the *in vivo* situation *in vitro*, cell culture dishes were coated with human recombinant laminin 421 or laminin 411 and sutured with human endothelial cells from the umbilical vein (HUVEC). Diverse functional investigations showed that endothelial cells migrated and adhered poorly in the presence

of laminin 411, while in Matrigel tube formation assays HUVEC formed reduced endothelial networks when cultured on LM 411.

In addition to the change in laminin expression, our bulk RNA sequencing data set showed indications for endothelial-to-mesenchymal transition in the aged cardiac endothelium. *In vitro* experiments have shown that endothelial cells express more mesenchymal marker genes both basally and by stimulation with TGF β 2 when cultured on LM411.

At mechanistic level, various factors have been found that may influence the described results. It was found that HUVEC cultured on LM411 secrete less FGF2 -a well-known inhibitor of endothelial mesenchymal transition- and thrombospondin 2 -an important regulator in the cardiovascular system. Furthermore, LM411 reduces the activity of the matrix protein receptor integrin β 1, which was found to be responsible for the reduced adhesion and migration.

In the second part of this thesis, a global transcriptome analysis of the entire young and old mouse heart was performed. The use of single-nucleus RNA sequencing made it possible to study the transcriptome at the single nucleus level and to study changes not only in the endothelium but in the entire heart, thus revealing putative intercellular interactions with endothelial cells.

A total of 14,827 nuclei from three young (12 weeks old) and 12,981 nuclei from three old (18 months old) mouse hearts were isolated and used for transcriptome analysis. Using bioinformatic t-distributed stochastic neighbor embedding plots, the single nucleus data could be summarized in a two-dimensional representation showing 15 specific cell populations. Among all cardiac cells, fibroblasts in particular showed the strongest gene regulation in aged hearts and were therefore analyzed separately. A pseudotime analysis arranged the entire fibroblast population into a linear representation and grouped the fibroblasts into 11 subgroups, which were either predominated by young or old cells. Signaling pathway analyses further showed that especially the "old" fibroblast groups predominantly express genes found in inflammatory, angiogenic as well as osteogenic signaling pathways.

Initially, we focused on the regulation of angiogenesis-associated genes in fibroblasts. Since particularly secretory angiogenic genes were regulated in old fibroblasts, a bioinformational ligand-receptor analysis was used to predict possible cellular interactions. The analysis predicted that in particular fibroblasts could increasingly interact with endothelial cells during aging, with fibroblasts expressing paracrine factors and

endothelial cells expressing the corresponding receptors. This hypothesis was confirmed with a HUVEC Matrigel assay in which HUVEC were stimulated for 24 hours with conditioned fibroblast culture supernatants, generated from isolated fibroblasts from young and old mouse hearts. Interestingly, HUVEC treated with "old" fibroblast medium showed a worsened network formation than HUVEC cultured with "young" fibroblast medium. Members of the serpin family were identified as the main causative agents of this effect, which were increasingly found at both the RNA and protein levels in "old" fibroblasts. By using neutralizing serpin antibodies, it was possible to completely rescue the anti-angiogenic effect of the "old" fibroblast medium.

In the further course the focus was on the regulation of the osteogenesis-associated genes in fibroblasts. First, the single-nucleus data showed that the factors Runx2 and Cepbp, both important regulators in osteoblast differentiation, were expressed in "old" fibroblasts. While RT-qPCR and bulk RNA sequencing data validated the expression of Runx2 in isolated mouse fibroblasts, histological staining in old mouse hearts showed PDGFR α -positive cells expressing osteocalcin (an osteoblast marker gene). These "osteogenic fibroblasts" were found almost exclusively in the epicardium of old hearts. The epicardium of young hearts was almost completely free of such cells. In addition, von-Kossa stainings found (except for calcified cardiac valves) individual calcifications exclusively in the epicardium of old hearts. The young heart did not show any calcium deposits in the epicardium at all.

In summary, it could be shown that in particular cardiac fibroblasts are affected by aging. While they inhibit angiogenesis through serpin expression, they might require an osteogenic phenotype in the epicardium. However, whether these osteogenic cells originate from fibroblasts or epicardial cells has to be further validated in lineage-tracer experiments.

In the third part of this dissertation, a novel three-dimensional spheroidal cell culture model (Cardiac Tissue Mimetic; CTM) was developed to investigate the intercellular communication pathways between endothelial cells, cardiomyocytes and cardiac fibroblasts in a physiological environment. In a first step, cardiomyocytes and fibroblasts were isolated from neonatal rat hearts and cultured in a ratio of 5:1 in hanging droplets. After four days, the cells clumped together and formed spheroids, which in a second step were first coated with matrix and then with GFP-positive HUVEC. The use of GFP-positive HUVEC made it possible to observe the vessel formation *in situ*. The CTMs

were kept in culture for ten days and vessel formation was studied under various stimuli. CTMs were first treated with the sympathomimetic phenylephrine (PE). Stimulation with PE promoted CTM hypertrophy, maturation and contraction frequency compared to CTMs without stimulation. Using the GFP-positive HUVEC, pronounced endothelial sprouting and vessel formation were observed in PE stimulated CTMs. While PE did not appear to have a direct effect on endothelial cells, it was shown that PE increased VEGF secretion in cardiomyocytes and hence induced endothelial sprouting in a paracrine manner. By contrast, the secretome of fibroblasts showed no pro-angiogenic changes upon PE stimulation. Since PE not only altered the secretome but also influenced CTM contraction, it was assumed that PE also induced endothelial progression via mechanical activation. In order to uncouple mechanical activation, CTMs were stimulated with a combination of PE and the β blockers metoprolol and propranolol. All of the aforementioned β blockers were able to reduce CTM contraction. In addition, endothelial sprouting was almost completely suppressed.

We were further able to exclude that the used β blockers have a direct effect on endothelial cells and a direct effect on VEGF expression in cardiomyocytes by using various functional experiments and implied that the mechanical activation of endothelial cells by cardiomyocytes is sufficient to induce endothelial sprouting.

Finally, the CTM model was used to investigate pathophysiological conditions such as those occurring in ischemia and remodeling processes upon myocardial infarctions. In line with known remodeling processes, the treatment of CTMs with the pro-fibrotic growth factor TGF β 2 showed pronounced collagen deposition but only marginally increased vessel formation compared to control CTMs. In addition, single endothelial cells expressed mesenchymal markers indicating occurrence of endothelial-mesenchymal transition. The cultivation of CTMs under severe hypoxia also induced collagen deposition, but diminished vessel formation.

In summary, a novel three-dimensional cell culture system was generated that can be used for investigating endothelial cells in a cardiac environment in terms of intercellular cross-talk.

1 Introduction

1.1 General Introduction

The heart is a central unit in the human body. As a muscular organ, it pumps blood through the blood vessels of the circulatory system and forms together with the blood vessel system the cardiovascular (CV) system. By being a systemically distributed organ, the CV system spans almost all tissues in humans and provides the cells with oxygen, nutrients and metabolites.

Disorders or diseases of this central system are summarized in the umbrella term cardiovascular diseases (CVDs) and include pathophysiological states like -among others- atherosclerosis, heart failure, hypertension and coronary heart disease. Although modern medical care has tremendously enhanced in the past decades, CVDs are still the primary cause of death globally and represents more than 30% of all deaths. The World Health Organization (WHO) illustrates this fact by stating that in 2016 more than 17.9 million people died from CVDs worldwide¹. This state is expected to worsen as the Western societies age, whereas especially the elderly is prone to CVDs. Interestingly, both the incidence and prevalence of CVDs keenly increase in men at about age 45 and at about age 55 in women. At about age 70 the risk is even worse^{2,3}.

Although the CV system has been studied for centuries, aged-dependent alterations in cell communication within the heart, within the vascular system and between heart and vasculature still need to be elucidated. By deciphering the impact of aging, novel strategies might be developed lowering CVD mortality.

1.2 The Heart

1.2.1 Anatomical Structure of the Heart

By pumping blood through the entire body, the heart supplies nearly each tissue with oxygen, nutrients and metabolites but also clears the organs from wastes. In humans, mammals and birds, the heart is divided into four chambers: the right and left atrium as well as the right and left ventricle^{4,5}. Functionally and structurally the heart can be further divided into the right heart (right atrium and right ventricle) and the left heart (left atrium and left ventricle) that are separated from each other by the atrioventricular septum (Figure 1)⁴. Whereas the right heart conducts deoxygenated blood through the

lungs, the left heart pumps the oxygenated blood through the body. Under physiological conditions, the superior and inferior vena cava collect deoxygenated blood from the body in the right atrium. An underpressure in the right ventricle pulls the blood through the tricuspid valve into the right ventricle that pumps blood through the pulmonary valve into the lungs. In the lungs, blood is oxygenated, passes the pulmonary veins and is collected in the left atrium of the heart. From there on, the blood is pulled through the mitral valve into the left ventricle that pumps blood through the aortic valve into the circulatory system of the body. Since the left ventricle has to supply the whole body and the right ventricle only the lungs, the myocardium of the left ventricle is thicker compared to the myocardium of the right ventricle⁴.

1.2.2 The Wall of the Heart

The wall of the heart is formed by three layers; the inner endocardium, the middle myocardium and the outer epicardium. The endocardium consists of a continuous mono-layer of endothelial cells (ECs) that line all cardiac chambers, the cardiac valves and the entire vascular system. Whereas the myocardium is formed by a specific type of striated myocytes, the so-called cardiomyocytes (CMs) that are embedded in a collagen matrix, the epicardium mostly contains fibroblasts. A fourth layer, the pericardium, is covering the whole heart like an elastic sack. It protects the heart from infections and keeps the heart position stable within the chest⁴.

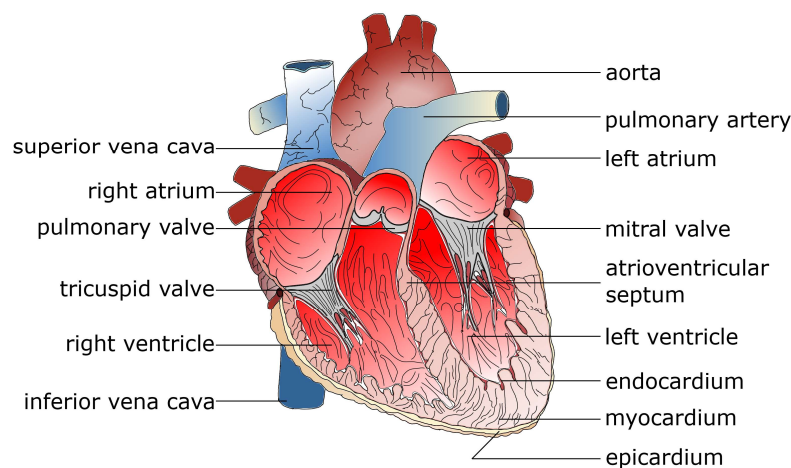


Figure 1: Anatomical structure of the human heart. Shown is a schematic cross section of the human heart. The figure is adapted from the review article in *Appendix 1*.

1.3 The Vascular System

The vascular network of humans and other vertebrates can be classified into two major vessel types: blood vessels and lymphatic vessels. Whereas blood vessels supply tissues and cells with nutrients, metabolites and oxygen but also remove waste products, lymphatic vessels filter excess interstitial fluids and serve as transport system for immune cells^{6,7}. Although the blood vessel and the lymphatic vessel system serve different functions, both are lined by a specific type of epithelium, the endothelium. This specialized cell layer consists of ECs that forms a mono-layer that serves as a systemically distributed organ spanning almost all expanses of the vertebrate body^{8,9}.

Blood and lymphatic vessels are hierarchically organized. In the blood vessel system large arteries conduct blood away from the heart, bifurcate into smaller arterioles and further into a distinct capillary network. Small venules drain capillaries and merge into larger veins that transport blood back to the heart. In the lymphatic system, blind-ended lymphatic capillaries, pre-collecting and collecting lymphatic vessels drain excess interstitial fluids from the tissues and conduct these to the venous system (Figure 2). Besides draining and transporting excessive fluids (called lymph), lymphatic capillaries provide an entry site for tissue-resident immune cells into the lymphatic and thereby later into the venous system⁹.

1.3.1 Vessel Structure

Vessel morphology differs among blood and lymphatic vessels. Both arteries and veins consist of three distinct layers: Tunica intima, tunica media and tunica adventitia (Figure 2). The tunica intima is the innermost layer of the vessel wall and is formed by a continuous mono-layer of ECs that are attached to extracellular matrix proteins: the basement membrane (BM). Tunica media is the middle layer and contains mostly elastic fibers as well as smooth muscle cells (SMCs) that grant -especially in arteries- the ability of vessel constriction or dilation. This layer is overemphasized in arteries but reduced in veins. The outermost layer of blood vessels is formed by the tunica adventitia containing predominantly elastic fibers which is more pronounced in veins to compensate the reduced tunica media and to grant vessel stability. Capillaries and small lymphatic vessels consist of a tunica intima only. These vessels are exclusively formed by ECs coated by a BM layer. Additional SMCs and pericytes might cover these vessels to stabilize vessel structure.

Furthermore, vessels can differ not only morphologically within a vascular network but also among different vascular beds. As described above, tunica media and adventitia vary between arteries and veins in their sizes. In respect to tunica intima, veins and lymphatic vessels additionally contain luminal valves that helps pumping and prevents backflow of blood or lymph⁹. Whereas arteries and veins are lined by a continuous EC layer, the endothelium of capillaries can be continuous, discontinuous or fenestrated depending on its vascular bed. Fenestrated ECs are characteristic for tissues that are involved in filtration, such as the kidney glomeruli and discontinuous ECs are typical for sinusoidal vascular beds that are found in the bone marrow or liver⁹. The capillary network of the heart consists of an continuous endothelium.

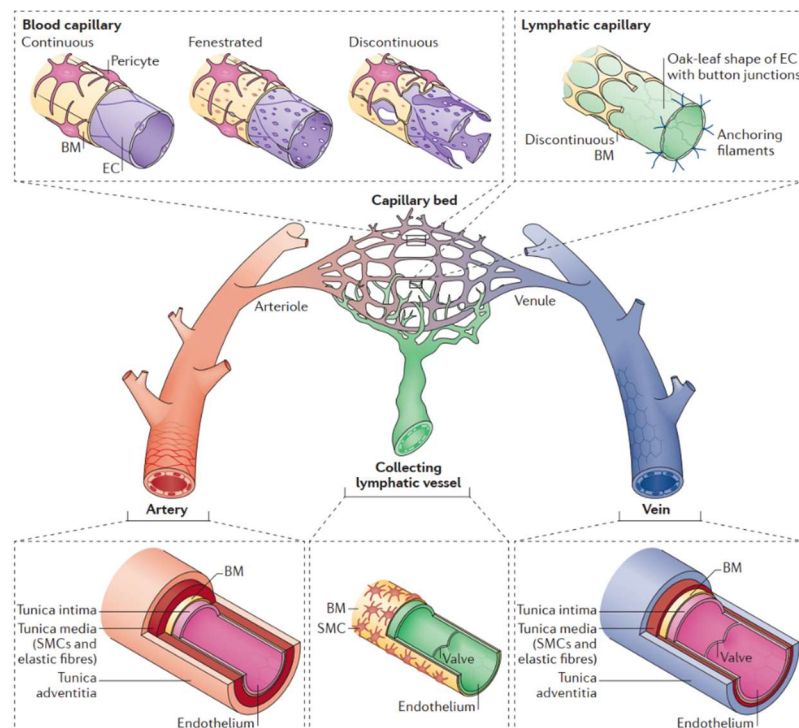


Figure 2: Organization of the vessel system. The vascular system is hierarchical structured. Arteries (red) leave the heart and branch into smaller arterioles and further into a defined capillary network. Small venules drain the capillaries and merge into large veins (blue) that conduct blood back to the heart. Excess interstitial fluid is drained by small blind-ended further by larger collecting lymphatic vessels (green), that transport the lymph into the venous system. The vessel wall of arteries and veins is formed by three layers: the inner tunica intima that is formed by the endothelium and its basement membrane (BM), the middle tunica media, consisting of smooth muscle cells (SMCs) and the outer tunica adventitia containing elastic fibers. Capillaries and lymphatic vessels contain only an endothelial layer that is covered by its BM and partially distributed SMCs or pericytes. Depending on the vascular bed, the endothelium of capillaries can be continuous, fenestrated or discontinuous, whereas the endothelium of lymphatic vessels contains oak-leaf shaped ECs but a discontinuous BM. The figure is adapted from Potente and Mäkinen, 2017⁹.

1.3.2 Development of the Vasculature: Vasculogenesis and Angiogenesis

The development of vasculature is directly connected to the demands of the organ that it serves. Whereas a shortage of nutrients or oxygen leads to blood vessel formation, excessive interstitial fluid pressure stimulates lymphatic vessel development¹⁰. The vasculature can develop through diverse molecular mechanisms and cellular origins that -depending on the developmental or pathophysiological state- rely on two distinct key processes: vasculogenesis and angiogenesis.

1.3.2.1 Vessel Development through Vasculogenesis

In prenatal development, the vasculature is formed through vasculogenesis, a process that has been excessively studied in zebrafish and mouse embryo studies^{11–18}. In zebrafish embryos, the transcription factor Npas4l (helix–loop–helix–Per–ARNT–Sim (bHLH-PAS) protein neuronal PAS domain-containing protein 4-like protein) has turned out to be a key coordinator of this process. Npas4l mobilizes multipotent mesodermal cells and drive their differentiation towards angioblasts¹¹. Angioblasts are endothelial precursor cells that originate from the lateral plate mesoderm. They merge into the large axial and cranial vessels, as well as the pharyngeal arch artery which later assemble the dorsal aorta and the cardinal vein^{12,13,18}. Further studies report that angioblasts form common progenitor tubes and subsequently differentiate within the tube into arterial or venous ECs^{14,15}. However, Kohli and coworkers have shown an alternative model of vessel formation in 2013. According to them, arterial and venous ECs might arise from distinct angioblast pools stemming from different locations¹⁶. This hypothesis is supported by Npas4l-loss-of-function studies which had been performed by Didier Stainier's laboratory from the Max-Planck Institute in Bad Nauheim. Stainier and his colleagues were able to report that zebrafish embryos being deficient for Npas4l indeed lacked most but not all ECs¹². Comparable to zebrafish, also the vascular network of mouse embryos develops from mesodermal cells that form early angioblasts and a primitive vessel plexus. NPAS4, the mammalian homologue to Npas4l, has also been found being expressed in mouse mesodermal cells that orchestrates as transcription factor the endothelial lineage¹¹. Independent of cellular origins, vessel formation can also be induced by various growth factors. In this regard, the vascular en-

dothelial growth factor (VEGF), fibroblast growth factor 2 (FGF2) or the bone morphogenic factor 4 (BMP4) were found to drive EC differentiation from mesodermal stem cells^{9,17}.

1.3.2.2 Vessel Development through Angiogenesis

While the *de novo* formation of primordial ECs or vessels is referred to as vasculogenesis, angiogenesis is defined as the remodeling of a vascular network by sprouting from pre-existing blood vessels¹⁷. This process is responsible for further vessel formations in both embryonal and adult vasculature and occurs in physiological, as well as pathophysiological states by which ECs sprout from existing vessels, branch, migrate and form mature vessels¹⁹ (Figure 3). Tissue-derived growth factors, like VEGF attract ECs in a chemotactic manner by stimulating them to become motile, invasive and to form filopodia²⁰. ECs sense VEGF via VEGF receptor 2 and 3 (VEGFR2 and 3) and the VEGF co-receptor neuropilin-1 (NRP1). Whereas these receptors stimulate sprouting, VEGFR1 inhibits sprouting. Since ECs and mural cells share a common BM that enwraps the endothelial tubule like a sleeve, ECs first need to breakdown the BM to liberate themselves (Figure 3A). By secreting matrix metalloproteases (MMPs), such as MMP1, ECs degrade the BM²¹. This process often liberates further angiogenic growth factors that were bound in the extracellular matrix protein (ECM) network²². These factors can be pro- or anti-angiogenic and fine-tune the angiogenic process by stimulating or preventing branching²³. Due to ECM degradation, mural cells detach from the vessel which stimulates ECs to secrete further pro-angiogenic factors, such as Angiopoietin-2 (Ang2). The liberated ECs or so-called “tip cells” invade the surrounding tissue and use their filopodia to follow the growth factor gradient chemotactically. Proliferative ECs, so-called stalk cells, follow the tip cell and elongate the nascent sprout by cell proliferation and migration. They also establish the vessel lumen, secrete BM proteins and recruit mural cells to stabilize the newly formed endothelial tubule. To prevent an excessive sprout formation, tip cells are selected by lateral inhibition, a process that is controlled by the Notch signaling pathway²⁴. Notch is a receptor protein that suppresses tip cell behavior and is more active in stalk cells²⁵. Conversely, tip cells were shown to express low levels of Notch but high levels of the Notch ligand Delta-like protein 4 (Dll4) that inhibits filopodia formation and tip cell transition in stalk cells²⁶. In contrast to Dll4, the Notch ligand JAGGED-1 (JAG1) is primarily expressed by stalk

cells. JAG1 antagonizes Dll4 in stalk cells and hence prevents Dll4 back signaling to tip cells²⁴ (Figure 3B). Unlike tip cells, stalk cells are equipped with a high proliferative capacity. They elongate the sprout by proliferation and stabilize it by expressing high levels of the adherence junction protein VE-cadherin (vascular endothelial cadherin or cadherin 5; Cdh5) (Figure 3C). The deposition of ECM proteins to form a new BM, as well as the recruitment of mural cells (pericytes or SMCs) further strengthen the newly formed branch. By anastomosing with neighboring sprouts, tip cells finally form a vessel loop and create a new blood vessel^{7,24,27}. Finally, the onset of blood flow into the lumen shapes the newly formed vessel and activates the shear-stress-responsive transcription factor Krüppel-like factor-2 (KLF2). KLF2 upregulates the endothelial nitric oxide synthase (eNOS) that keeps vessel lumen dilated and downregulates VEGFR2 to prevent further tip-cell formation. Together with oxygen and nutrient supply, KLF2 shifts the ECs to a quiescence state and end the angiogenic process²⁰.

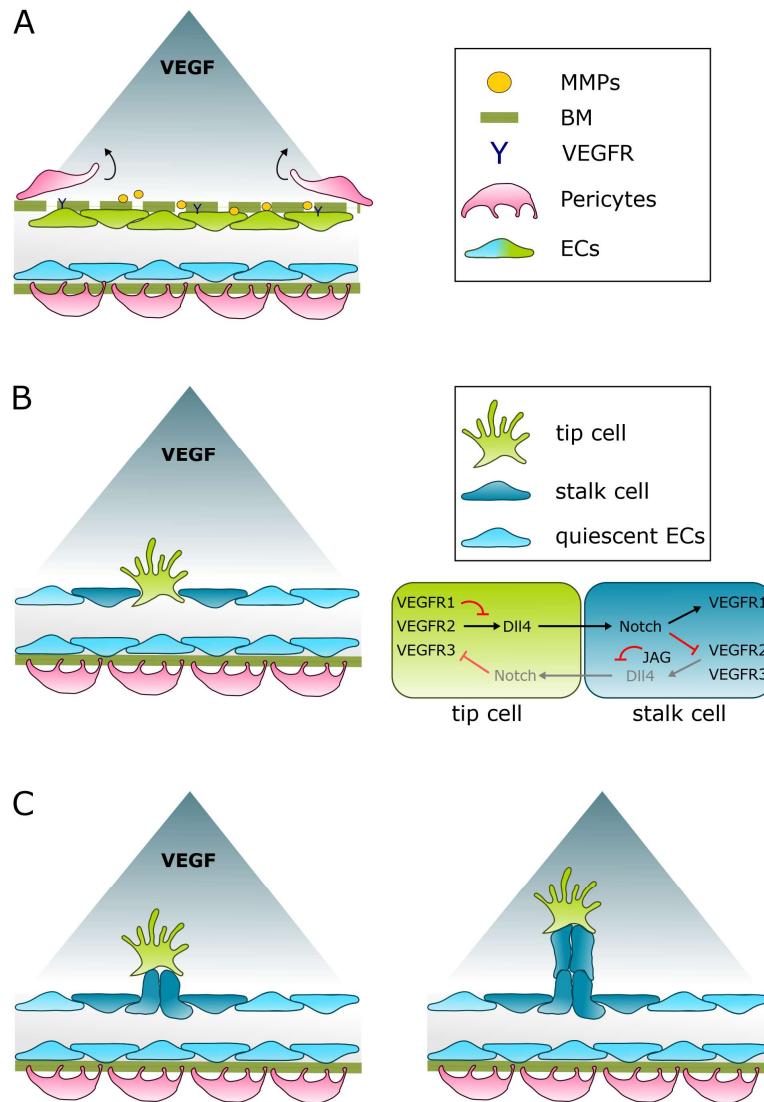


Figure 3: Vessel development through angiogenesis. (A) During angiogenesis, endothelial cells (ECs) respond to tissue-derived VEGF. These leads to the expression and release of matrix metalloproteases (MMPs) that degrade the basement membrane (BM) that liberates the ECs and cause pericyte detachment. (B) The liberated EC undergo filopodia formation to probe the environment to follow the VEGF gradient. Lateral inhibition prevents hypersprouting, by which delta-like 4 (DII4) is highly expressed by tip cells. DII4 stimulates Notch receptors of the neighboring ECs and stimulate them to become stalk cells. Conversely to DII4, JAGGED (JAG) antagonizes DII4 in stalk cells to prevent DII4 back signaling to the tip cells. (C) While tip cells are less proliferative and follow the VEGF gradient, stalk cells elongate the new branch by cell proliferation and form the lumen. The figure is adapted and modified from Potente, Gerhardt and Carmeliet, 2011²⁰.

1.3.3 The Basement Membrane

The basement membrane or basal membrane (BM) is an important structural element of cellular monolayers, that grant stability and structural integrity. Some smaller capillaries and angiogenic sprouts are only stabilized by a single BM layer. It composes of a variety of ECM proteins and can be found in electron-microscopic images as a 50-100 nm thick and electron-dense layer, separating endothelial, as well as epithelial cells from the underlying connective tissue (Figure 4A). Similar to blood vessels, also the BM can be very heterogeneous depending on the tissue where it is formed²⁸. Besides being a structural element, the BM can also modulate cellular behaviors by sequestering growth factors and cytokines, by regulating its temporal and spatial distribution and by forming concentration gradients²⁹.

1.3.3.1 Composition and Function of the Basement Membrane

The BM is a very complex structure and its composition differs among different tissues, developmental stages or pathophysiological states. In the past, the BM was extensively studied, especially in the mouse Engelbrecht Holm-Swarm (EHS) sarcoma model, using Matrigel^{28,30}. Matrigel is a complex BM-like composite derived from EHS tumor cells and is commonly used in *in vitro* models to mimic the BM for ECs. However, tumor cells and their BM differ from physiological cells with their BM in many aspects, which makes the use of Matrigel in many *in vitro* assays debatable³¹⁻³⁴. Although the BM primarily anchors endothelial cells to the underlying connective tissue, it can also influence cell adhesion, migration, differentiation, function and survival (Figure 4), which is controlled by the complex composition of ECM proteins within the BM²⁸.

The main components of the BM are the extracellular proteins laminin, type IV collagen, nidogen/entactin and perlecan²⁸. Laminin and type IV collagen are crucial for BM stability and maintain its integrity. These large molecules are expressed in distinct subunits that self-assemble into supramolecular structures³⁵⁻³⁷. The BM stability is further increased by perlecan and nidogen/entactins that interconnect laminins and collagens. Together with other ECM components, such as agrin, fibulin, fibronectin, SPARC, osteonectin and BM90, the complexity and heterogeneity of the BM is further increased²⁸.

1.3.3.2 Laminin

Besides collagen, laminin is the predominant BM component in blood vessels. It is expressed throughout all BMs and its composition changes depending on the developmental stage, age and tissue. Laminins are T- or cross-shaped heterotrimeric glycoproteins consisting of one α -, one β - and one γ -chain³⁵ (Figure 4). To date, five distinct α -, four β - and three γ -chains are known³⁵ that have been identified to form 16 laminin combinations. Four further combinations have been proposed relying on both *in vivo* and *in vitro* studies^{35,38}. By the growing number of isoforms, two laminin nomenclatures have evolved in the past decades. The first or “the old” system uses Arabic numerals to describe laminin isoforms and bases on the order of laminin discovery. In this context, laminins are referred to as laminin-1, laminin-2, laminin-3, etc³⁹. However, this system failed to describe the composition of the polypeptide chains that are present in the respective laminin isoform. By contrast, the alternative or “new” system indicates each laminin polypeptide as a number. For example, the laminin isoform 421 (LM421) consists of the laminin α 4-, β 1- and γ 1-chain. A full list of all known laminins is shown in the following table (Table. 1).

Table 1: Nomenclature of laminins. The table was adapted from Yao, 2017³⁸.

Old Nomenclature	New Nomenclature
Laminin-1	Laminin-111
Laminin-2	Laminin-211
Laminin-3	Laminin-121
Laminin-4	Laminin-221
Laminin-5	Laminin-3(A)32
Laminin-5B	Laminin-3B32
Laminin-6	Laminin-311
Laminin-7	Laminin-321
Laminin-8	Laminin-411
Laminin-9	Laminin-421
Laminin-10	Laminin-511
Laminin-11	Laminin-521
Laminin-12	Laminin-213
Laminin-13	Laminin-323
Laminin-14	Laminin-423
Laminin-15	Laminin-523
-	Laminin-212
-	Laminin-222
-	Laminin-333
-	Laminin-522

As a major BM protein, laminin not solely interconnects with other ECM components. Accumulating studies in the past have shown that laminins play multiple crucial roles in the embryonal development and even most laminin knockout models were reported to be embryonically lethal^{36,40,41}. This can be explained by the fact that laminins bind to and subsequently activate cell-surface receptors, such as the heterodimeric integrin and thereby modulate cell functions. These activities can be mapped to globular domains that are present within each laminin chain^{27,35}. The laminin polypeptide chains are composed of multiple globular domains (LG), coiled-coil domains, rod-like structures or repeats of epidermal growth factor-Like (LE) domains. Especially the globular domains can be further subdivided into the laminin N-terminal globular domain (LN), laminin four (LF) domain and L4 domains (Figure 4B)^{35,38,42}. Multiple laminin receptors bind to these structures. These receptors can be divided into integrins and non-integrins. It is known that at least eight integrin receptors ($\alpha1\beta1$, $\alpha2\beta2$, $\alpha3\beta1$, $\alpha6\beta1$, $\alpha1\beta4$, $\alpha7\beta1$, $\alpha9\beta1$ and $\alpha v\beta3$) bind to laminin, whereas most of them bind preferentially to the laminin α -chain's LN and LG domains^{43,44}.

Integrins represents the main class of laminin receptors. Their stimulation activates multiple signaling proteins, such as Src, FAK, Rho or PI3K and their long-term activation controls cell proliferation, survival and differentiation (Figure 4C)⁴⁵. Non-integrin laminin receptors are represented by dystroglycans, syndecans, Lutheran blood group glycoproteins and the soluble 67 LR^{35,46}. Their affinity to laminins is rather weak compared to integrins and they play a minor role in laminin signaling.

Activation of laminin receptors is not only modulated by matrix composition and growth factors that are sequestered in the BM but also by tissue and BM stiffness. Recent studies have shown that matrix stiffness controls not only focal adhesion formation but also neural stem cell differentiation^{47,48}. However, the molecular mechanism behind the concept of matrix stiffness is still not fully understood yet.

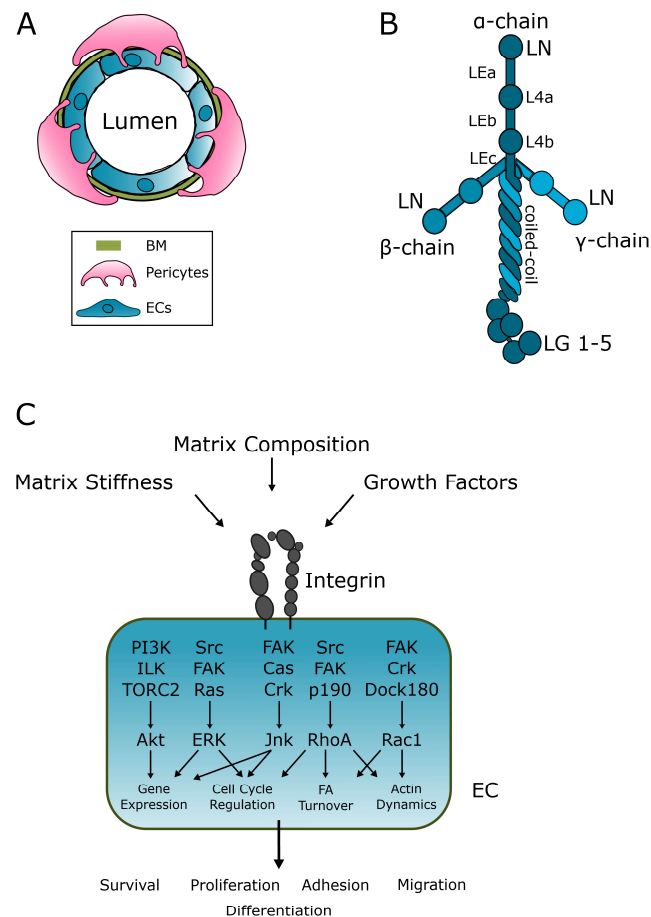


Figure 4: The basement membrane. (A) The basement membrane (BM) is a layer of ECM proteins that separates endothelial cells (EC) from underlying cells or tissues. (B) Among others, laminins are the major BM component. Laminin-111 is shown in this figure consisting of the α 1-, β 1- and γ 1-chain. Each chain contains further structures that are referred to as LN, LE or LG domains and a coiled-coil structure. BM components, growth factors or the BM stiffness can modulate ECM receptor (integrin) activation and activate pathways including PI3K, Src and FAK, resulting in survival, proliferation, adhesion, migration or differentiation. The figure is modified from ^{35,38,45}.

1.4 Cardiovascular Diseases

The umbrella term cardiovascular disease (CVD) describes a class of diseases that involves the heart and the entire blood vessel system. CVDs include diseases such as myocardial infarction, coronary heart disease, atherosclerosis, heart failure, cardiomyopathy, as well as hypertensive diseases. However, their underlying mechanisms can be very diverse. According to the WHO, CVDs are still the primary cause of death globally¹. Since the Western societies age and since elderly are more prone to CVDs, the situation is expected to become worse². In this aspect, it is of major interest to shed light on the cellular and molecular changes during disease and aging to establish novel therapeutic strategies.

1.4.1 Atherosclerosis

Atherosclerosis (Greek; *athera*: artery and *sklerosis*: hardening) is a chronic inflammation of arteries that is characterized by the accumulation of lipids and fibrous structures in the vessel wall leading to artery narrowing and finally artery occlusion⁴⁹. The underlying causes are very complex and include endothelial lesions, as well as high levels of cholesterol-rich lipoproteins⁴⁹. Hypertension or alterations in blood flow dynamics cause lesions of the endothelium with EC detachments which shifts the endothelium to a pro-inflammatory phenotyp^{49–51}. Specific sites of arteries, such as bifurcations are more prone to hemodynamic turbulences than others and thereby more vulnerable to endothelial lesions. The activation of the endothelium increases its permeability to low-density lipoproteins (LDL) that results in a further activation of ECs. Monocytes and other leucocytes are recruited by pro-inflammatory ECs and absorb the infiltrated LDL resulting in sub-endothelial accumulation of cholesterol-engorged macrophages, the so-called foam cells⁴⁹. Although these fatty lesions are not of clinical significance, they serve as precursors of larger lesions where lipid-rich necrotic debris and SMCs aggregate⁵⁰. This fibrous lesion forms an atherosclerotic plaque that typically contains a fibrotic cap containing ECM proteins like fibronectin, as well as a necrotic core, containing cellular debris and leukocytes. Especially leukocytes from the necrotic core were shown to secrete multiple interferons and MMPs that degrade the fibrotic cap. In progressing clinical manifestation, the degradation of the cap structure leads to plaque instability and ultimately to plaque rupture⁴⁹. A ruptured plaque may float within the blood flow as emboli causing ischemic events, such as myocardial infarction^{49,50}.

1.4.2 Myocardial Infarction

The myocardial infarction (MI) is a very acute form of CVDs and contributes significantly to CVD mortality⁵². MI is mainly caused by occlusions of a coronary artery followed by a prevented oxygen and nutrient supply of the underlying cardiac tissue. As a consequence, underlying ECs, FBs and CMs die from necrosis and apoptosis. Following MI, the heart and especially the left ventricle (LV) undergo structural and cellular changes that are referred to as pathophysiological cardiac remodeling⁵³. To compensate the loss of CMs and to prevent ventricular wall rupture, resident cardiac FBs become active and form first a preliminary fibrin clot and later a mature collagen

scar^{54,55}. The scar formation and the loss of CMs reduce LV function and cause LV dilation, as well as an altered chamber geometry (Figure 5)⁵⁶. As a matter of compensation, the remaining CMs undergo cardiac hypertrophy during the cardiac remodeling process⁵⁷. The molecular and cellular changes during cardiac remodeling are described in detail below.

In basic and medical research, mouse models are often used to mimic MI and to study cardiac remodeling. During a mouse surgery, a permanent ligation of the left anterior descending (LAD) artery is induced. The LAD artery belongs to the coronary artery system and usually supplies about 50% of the LV myocardium. The occlusion of this artery prevents blood supply of the underlying LV tissue and causes an acute myocardial infarction (AMI) (Figure 5).

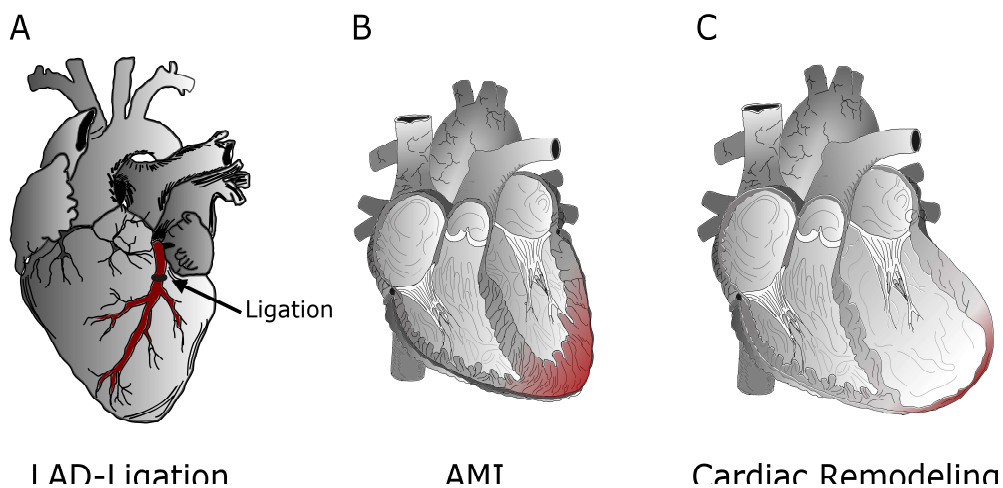


Figure 5: The LAD-ligation model. (A) In mouse models, an acute myocardial infarction is induced by a permanent ligation of the left anterior descending artery (LAD). (B) The LAD-ligation results in an acute myocardial infarction (AMI). (C) Following AMI, necrotic cardiomyocytes are replaced by a collagen-based scar and heart undergoes hypertrophy and left ventricle dilation (cardiac remodeling). Panel B and C were adopted and modified from the review article in *Appendix 1*.

1.4.3 Heart Failure

Heart failure (HF) is a chronic CVD that is characterized by a reduced cardiac function where the heart is not able to conduct blood sufficiently through the circulatory system of the body or the lung. As a consequence, the body is no longer supplied with blood sufficiently during physical exercises or at rest. Common symptoms are a shortness of breath, tiredness, as well as leg edema and the symptoms become worse when doing physical exercises⁵⁸. Causes of HF are other underlying CVDs such as coronary artery and heart diseases, cardiomyopathy, atherosclerosis, hypertension, atrial fibrillation or

a previous MI that are followed by severe cardiac remodeling processes⁵⁹. The clinical manifestation further worsens through multiple compensating neurohumoral changes, such as an activation of the sympathetic system⁶⁰.

In general, the left part of the heart, the right part of the heart or both sides can suffer from HF. A left heart HF can be further classified into a HF with preserved ejection fraction (HFpEF) or HF with reduced ejection fraction (HFrEF), depending on the ability of the LV to contract or relax, as well as the ability to eject the LV blood volume sufficiently^{58,61}.

1.5 Cellular Cross-Talk and Heterogeneity in the Heart^a

1.5.1 Cellular Heterogeneity and Cellular Cross-Talk in the Healthy Heart

Cellular specification and cross-talk are essential for an organ to function and fulfill specific tasks. Multicellularity and intercellular interactions, as well as cellular signaling determine cardiac development and cardiac homeostasis in the adulthood. In the following, the main three cell populations in the heart, as well as the cardiac ECM as an important modulatory system will be described in respect to their intercellular cross-talk (Figure 6).

Cardiac endothelial cell: Cardiac endothelial cells (cECs) form the inner lining of the heart chambers and the entire macro- and microvasculature that supplies the myocardium with blood. By doing so, an enormous number of cECs is required and hence it is not surprising that cECs outnumber CMs by an estimated ratio of 3:1^{62,63}. By making up to about 60% of the non-myocyte population, cECs were shown to be the most important non-myocyte population within the heart⁶². They strongly interact with CMs, especially during cardiac development by expressing neuregulin, neurofibromatosis type-1 (NF1) and platelet-derived growth factor β (PDGF β)⁶⁴. The auto- and paracrine signaling of CMs and cECs is pivotal to maintain cardiac function. Both CMs and ECs are able to release nitric oxide (NO) by expressing three NO synthases: iNOS (inducible NOS), eNOS and NOS, whereas the endothelial eNOS is four-times more active than the CM-derived iNOS⁶⁵. On the one hand, NO acts on the blood vessels' tunica

^a Parts of section 1.5 "Cellular Cross-Talk and Heterogeneity in the Heart" and section 1.6 "Aging" were re-written and used for the submitted review article that can be found in *Appendix 1*.

media and results in vasodilation by relaxing vascular SMCs. On the other hand, NO can also signal in CMs and attenuate CM contraction leading to a reduced heart beating rate^{65,66}. Another cEC-derived factor is endothelin-1 (ET-1). ET-1 can act as paracrine factor on CMs via the ET_A receptor and as autocrine factor via the endothelial ET_B receptor⁶³. In CMs, ET-1 was found to induce hypertrophy and seems to be involved in cardiac remodeling in the diseased heart⁶⁴. In ECs, ET-1 was reported to mediate EC survival via FOXO¹⁶⁷ but also to potentiate TGFβ-mediated endothelial-to-mesenchymal transition in CVDs and hence promote fibrosis⁶⁸. A more cardiac protective role can be annotated to the EC-derived neuregulin that was shown to reduce apoptosis in CMs⁶⁹. The importance of EC-CM cross-talk was further elucidated by Narmoneva et al. in 2004. By using a EC-CM co-culture system, the group showed that ECs promote CM survival by reduced apoptosis and necrosis, as well as spatial remodeling and synchronized contraction in CMs that can also be of interest during cardiac regeneration⁷⁰ (Figure 6A).

Cardiac fibroblast: Cardiac FBs (cFBs) are small elongated spindle-shaped cells with a strong secretory phenotype. They display a granular cytosol containing a pronounced rough endoplasmic reticulum. Unlike CMs, that are organized in a defined structure within the heart, cFBs are roughly distributed throughout the entire myocardium and are located in the interstitial space between CMs⁷¹. By today, there is no unique or specific cFB marker gene available. However, the expression of multiple markers, such as Vimentin, platelet-derived growth factor receptor α (PDGFRα), fibroblast-specific protein 1 (FSP1) or DDR2 can be used to define cFBs or FB-like cells histologically. Taken this in consideration, cFBs seem to be a mixture of multiple FB-subtypes, that arise from multiple origins. Whereas cFBs can arise from the epicardium or the atrio-ventricular septum, it is estimated that about 20% of all cFBs have an endothelial origin, through a process that is referred to as endothelial-to-mesenchymal transition (EndoMT; see section “*Cellular Plasticity in the Adult Heart*”)^{71,72}. To date, mostly bulk experiments have been used to characterize the FB composition of the heart. Hence single-cell RNA sequencing (scRNA Seq) will be a powerful tool to shed light on the origin and heterogeneity of cFBs in the near future.

Usually cFBs interact with other cells by ECM protein deposition (Figure 6B). They release -among others- collagens, laminins and other glycoproteins that contain growth factor-like domains which stimulate cellular growth or angiogenesis⁷³. Integrins are heterodimeric ECM receptors that are directly connected to the cytoskeleton. They are

expressed throughout CMs, cFBs and also ECs and form a physical connection between ECM and cytoskeleton⁷⁴. By remodeling the ECM, cFBs directly influence cell signaling via kinase signaling cascades and allow mechanical interactions with other cell types, especially with CMs^{75,76}. Nevertheless, the ECM primarily forms a scaffold that stabilizes CM position and keeps the myocardium in shape.

However, cFBs are not solely providers for ECM proteins. Surprisingly, Camelliti and coworkers demonstrated in 2004 that sheep cFB do express three gap junction connexins Cx40, Cx43 and Cx45⁷⁷. A more recent study from the group of Peter Kohl even documented connexin-based electric coupling of FB-like cells with CMs using optogenetics⁷⁸. But still, the exact role of cFBs in electric coupling and whether cFBs are involved in electric signal conduction is not well characterized and needs to be further elucidated.

Apart from ECM deposition and electric coupling, cFBs also release auto- and paracrine factors, including IL6, transforming growth factor β (TGF β), endothelin-1 (ET1) and other cytokines that significantly impact CMs⁷⁹. Since most of these pathways occur during pathologies, the auto- and paracrine signaling of cFBs will be specifically described below.

Cardiomyocytes: CMs are the contractile element of the myocardium. Their synchronized contraction maintains a proper cardiac movement that is needed to pump blood through the circulatory system. To maintain cardiac contraction throughout a whole lifespan, CMs are equipped with a very large cytoplasm that is crammed with sarcomeres, the contractile unit of myocytes and mitochondria to meet their high energy demand⁶⁴. However, although the heart's volume consists mostly of CMs⁶⁴, they only account for up to 35% of the entire cardiac cellular composition^{72,80,81}.

The main interaction partners of CMs are neighboring CMs (Figure 6C). The connection is established by specific gap junctions, so-called intercalated disks that are usually formed by connexins⁶⁴. These junction proteins allow the direct exchange of ions, small molecules as well as small peptides between CMs and also electrically couple the entire myocardium⁶⁴. The 3D structure as well as tissue integrity is maintained by gap junctions that stabilize the relative position of CMs to each other⁷⁶. Disorganizations or disorders of cardiac gap junctions can cause severe disfunctions and often occur during CVDs. In this regard, Michael Gollob and his coworkers from the University of Ottawa reported that patients suffering from a mutation in connexin 40 (Cx40)

GJA5 develop idiopathic atrial fibrillation that was predisposed by impaired gap junction assembly or insufficient electric coupling⁷⁵. Furthermore, loss of neural cadherin (N-cadherin), an further adherens junction protein, had been shown to lead to a dilated cardiomyopathy and sudden death in a loss-of-function mouse model⁸².

Admittedly, CMs are not only able to interact via junction proteins. Auto- and paracrine factors like acetylcholine (ACh), interleukin 6 (IL6) or tumor necrosis factor α (TNF α) can also be secreted by CMs to communicate with other cells. ACh is a well-known neurotransmitter of the parasympathetic nervous system. Interestingly, Roy et al. demonstrated in 2013 that CMs can be a non-neural source of ACh which can counterbalance the sympathetic influence in the heart⁸³ (Figure 6D). Pro-inflammatory cytokines such as IL6⁸⁴ or TNF α ⁸⁵ are secreted by CMs during ischemic events. Clinical studies reported IL6 to be detrimental to the heart and being a prognostic predictor for chronic heart failure^{86,87}. Furthermore, CMs also secrete pro-angiogenic factors, such as VEGF-A and angiopoietin-1, to activate ECs and stimulate vessel growth^{64,88}. CM-derived VEGF-A plays a crucial role not only during ischemic events, but also during cardiac development. In this regard, CM-specific VEGF-A knockout (KO) mice suffered from defective angiogenesis with a degenerated vascular system, but also suffered from ventricular wall thinning⁸⁹.

Extracellular Matrix: The myocardial extracellular matrix (ECM) is a very complex structure that includes several hundred different glycoproteins, such as collagen, laminin, fibronectin, proteoglycans and MMPs⁵³. Whereas most of these components serve structural tasks, some of them rather play regulatory roles and influence cellular behavior^{90–92}. In principle, the cardiac ECM can be divided into the interstitial ECM that accommodates proteins such as collagen and fibronectin and the BM that mostly contains laminins and collagens⁹³. The BM can be mainly found as a thin layer on the surface of ECs, where it stabilizes the microvasculature, as well as the endocardium and modulates cell functions.

In the past, the cardiac ECM was reported to contain mostly fibrillar collagens, where type I collagen makes up to about 85% of the entire collagen content and type III collagen only 11% of the total collagen content⁵³. Fibrillar collagen primarily serves as a scaffold in the heart that stabilizes CMs within the myocardium. In addition to type I and III collagen, collagen type XIII was found in intercalated discs between CMs to maintain CM-CM connections⁹⁴. Collagens are expressed as polypeptide chains that

assemble to large supramolecular structures in the extracellular space and are protected from degradation via cross-linking of collagen-subunits which is facilitated by the lysyl oxidase⁹⁵.

Fibronectin is a glycoprotein and a further main component of the cardiac ECM. It serves important functions during cardiac development, where it is mostly expressed by cFBs and cECs but plays a rather minor role in the healthy heart⁹⁶. In the adult heart, fibronectin serves as scaffold for FBs and infiltrating immune cells and is mostly involved in inflammatory events. Especially the splice variant fibronectin extra domain A (EDA) was shown to be a pro-inflammatory factor after MI and maintain cardiac remodeling⁹⁷.

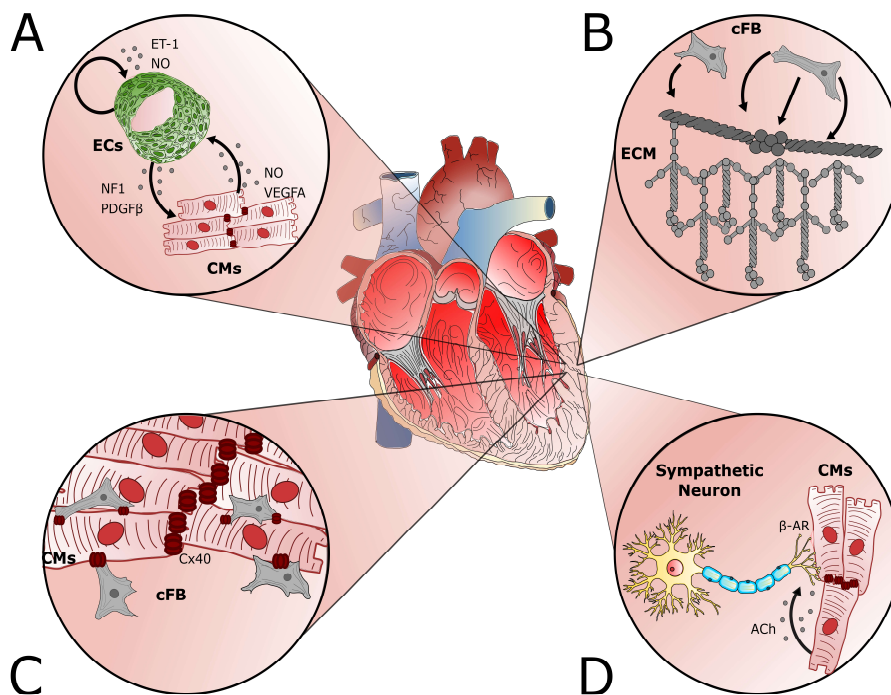


Figure 6: Cellular cross-talk in the healthy heart. (A) CMs and endothelial cells (ECs) interact via nitric oxide (NO) secretion that serves as vessel protective substance and VEGFA that induces angiogenesis. Whereas EC-derived NF1 and PDGF β plays an important role during cardiac development, ET-1 maintains EC-survival. (B) Cardiac FBs are small amorph cells that reside in the intercellular space between CMs within the myocardium. They mostly secrete extracellular matrix (ECM) proteins, such as laminin and collagen, that stabilize the myocardium but also modulate cellular behavior. (C) The myocardium is formed mostly by cardiomyocytes (CMs) that are electrically coupled via the gap junction protein connexin 40 (Cx40). Cardiac fibroblasts (cFBs) support electric signal conduction by forming Cx40 junctions between cFBs and CMs. (D) CMs are also able to secrete auto- and paracrine substances. They can be a source of non-neuronal acetyl choline (ACh) that counterbalances activations of the β -adrenergic receptor (β -AR) by sympathetic neurons. The figure is modified from the review article in *Appendix 1*.

1.5.2 Cellular Processes and Cross-Talk during post-MI Cardiac Remodeling

Since the adult heart and especially the CMs within the myocardium have only limited regenerative capacities, MI triggers transient inflammatory processes to initiate cardiac repair. Despite its regenerative effect, the post-infarct inflammatory response is implicated with severe pathological remodeling processes, such as fibrosis and altered chamber geometry.

MIs are typically caused by occlusions of the coronary arteries. This results in missing blood and nutrient supply in the underlying tissue, followed by necrosis of ECs, FBs and CMs^{54,98,99}. This loss of cells can be counterbalanced in the neonatal mouse heart that is able to regenerate the myocardium within the first week after birth⁵⁴. By contrast, the adult heart has lost its ability to regenerate after injury and replaces necrotic CMs with ECM components. The acute sudden-death of CMs causes the secretion of pro-inflammatory chemokines and cytokines. In this regard, necrotic CMs tend to express TNF α , IL-1 β and members of the IL-6 family to recruit leukocytes¹⁰⁰. Dying CMs and damaged ECM both further releases danger-associated molecular patterns (DAMPs) that trigger additional inflammatory reactions via toll-like receptor (TLR) signaling. Reactive oxygen species (ROS) that additionally triggers the immune response, are increasingly formed and released by CMs due to the hypoxic conditions¹⁰⁰ (Figure 7A). Upon these inflammatory signals, cFBs from the border zone are activated and start to secrete MMPs to degrade the ECM^{101,102}. ECM degradation allows immune cells (macrophages and dendritic cells) to infiltrate the infarcted zone and clear it from cellular debris and degraded ECM components^{103,104} (Figure 7B). Subsequently, activated FBs migrate into the infarct zone and rebuild the ECM scaffold¹⁰⁵. By secreting collagen type I and type III, FBs form a scar tissue that stabilizes the infarcted area and prevents ventricular wall rupture^{99,106,107}. The deposition of fibronectin and its splice variant EDA further restores the ECM scaffold that can be used by further activated FBs to migrate towards the infarcted zone, but also modulates the post-infarct inflammation⁵⁴.

In advanced post-infarct cardiac remodeling, some activated FBs differentiate to myofibroblasts⁵⁴. Myofibroblasts are key players in cardiac repair and scar formation (Figure 7C). They are able to contract due to their high content of contractile proteins (α -smooth muscle actin: α -SMA) and contribute significantly to matrix protein secretion that forms the collagen-scar¹⁰⁰. The process of fibroblast-to-myofibroblast transition is mediated by an increased ECM stiffness, that activates mechanosensitive receptors,

such as integrins. Integrins are ECM receptors that are directly linked to proteins of the cytoskeleton, such as actinin and vinculin. Their activation stimulates the GTP-binding protein RhoA that regulates the formation of stress fibers containing the contractile components α -SMA and F-actin^{54,108,109}. An alternative pathway is induced by transient receptor potential (TRP) channels, like TRPV4 and TRPC6 that are both activated by TGF β . Additionally, ECM rigidity also activates TRP channels via β 1-integrin signaling. The activation of TRP channels in FBs leads to a Ca²⁺ influx and myofibroblasts differentiation^{46,54,110}.

The laboratory of Jeffrey Molkentin further elucidated FB heterogeneity in post-MI hearts. He and his co-worker postulate that some myofibroblasts in the scar acquire a rather quiescent state and turn into Acta2-positive matrifibrocytes. These cells are less proliferative compared to myofibroblasts but maintain the scar tissue integrity by secreting ECM components¹⁰⁵.

To restore tissue homeostasis and induce reparative processes after the post-infarct remodeling, pro-inflammatory signals need to be inhibited. IL1 receptor-associated kinase 3 (IRAK-3) was found to be an endogenous inflammation inhibitor¹¹¹. It functions as a repressor for macrophage-driven inflammation and FB-dependent ECM breakdown¹⁰⁰. IRAK-3 was reported to be expressed by distinct macrophage populations and FBs to inhibit pro-inflammatory cytokines¹¹². In addition to endogenous signals, soluble anti-inflammatory factors are also secreted. Among them, IL10 and members of the TGF β family were found to repress post-infarct inflammations. In particular, the source of TGF β is quite diverse. It can be secreted by several immune cells but can also be stored in the ECM and is liberated by matrix breakdown¹⁰⁰. TGF β mediates cellular differentiations processes, such as fibroblast-to-myofibroblast transition and endothelial-to-mesenchymal transition^{54,113}. Both pathways increase the pool of active mesenchymal cells that play important roles in scar formation and detrimental cardiac remodeling⁵⁴. Both transition processes will be discussed in detail below.

The elevated level of TGF β in the post-MI heart stimulates ECs especially in the mitral valve leaflets to undergo endothelial-to-mesenchymal transition (EndoMT). As a consequence, EndoMT leads to an increased mesenchymal cell formation and excessive collagen secretion that results in valvular stiffness and subsequently in mitral stenosis¹¹³.

As part of the post-MI remodeling, the cardiac ECM also undergoes structural changes. Following the acute inflammatory phase, collagen deposition still remains increased

over ECM degradation in the LV. Advanced glycation end-products (AGE) and lysyl oxidase are both elevated in the post-MI heart. They cross-link collagen chains causing collagen accumulation and interstitial fibrosis as well as LV stiffness⁵³.

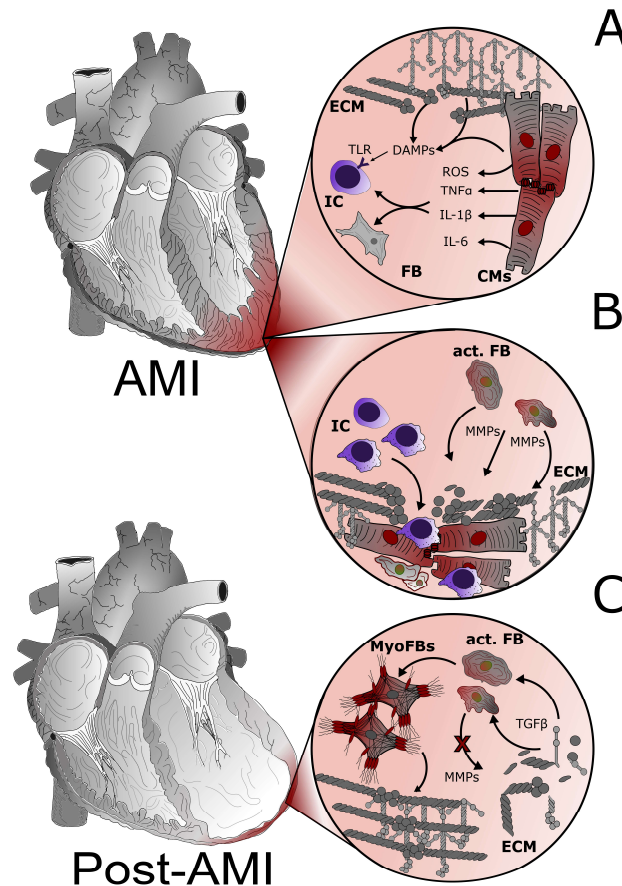


Figure 7: Cellular cross-talk in the AMI heart. (A) Acute myocardial infarction (AMI) and thereby lack of oxygen stimulates cardiomyocytes (CMs) to release pro-inflammatory cytokines, such as TNF α , IL-6, IL-1 β and danger-associated molecular patterns (DAMPs). In addition, degraded ECM proteins release further DAMPs that trigger additional inflammatory reactions via toll-like receptor (TLR) signaling on immune cells (IC). Reactive oxygen species (ROS) are increasingly induced due to the lack of oxygen and modulate inflammatory events, as well. (B) Upon release of pro-inflammatory cytokines, fibroblasts (FB) become active (act. FB) and start to degrade the extra cellular matrix (ECM) by secreting matrix-metalloproteases (MMPs). ICs are able to invade the infarcted area and clear the tissue from ECM debris and necrotic cells. (C) ECM degradation liberates anti-inflammatory growth factors, such as transforming growth factor β (TGF β) that stimulates –among others- fibroblast-to-myofibroblast transition. In this process, FBs shift from a degrading to an ECM secreting phenotype. Myofibroblasts (MyoFBs) forms a collagen-scar that prevents ventricular rupture and replaces CMs. The figure was modified from the review article in *Appendix 1*.

1.6 Aging

To understand and decipher the molecular and cellular changes during cardiac aging, one has to answer the question: What is aging? This is a very tough question, that many researchers in this field keep on asking. Carlos Lopez-Otin and his coworkers define aging as a consequence of accumulated loss of physiological integrity and functions leading to increased vulnerability to death¹¹⁴. In their review article they define the nine cellular “hallmarks of aging” and state that aging is accompanied by stem cell exhaustion, altered intercellular communication, genome instability, telomere shortening, epigenetic changes, the loss of proteostasis, deregulated nutrient sensing, mitochondrial dysfunction and cellular senescence¹¹⁴. Barbosa et al. even extended this number of hallmarks by taking deregulated autophagy and oxidative stress into account, too¹¹⁵. Also, further researchers describe aging as a manifestation of time-dependent molecular and cellular failures leading to chronic inflammations, altered cell communication and finally the loss of organ functions. In this context, aging can be seen as a time-dependent disease rather than a physiological condition¹¹⁶.

However, other theories suggest that aging is a result of the limited number of divisions somatic cells can undergo (“Hayflick limit”) or a result of random accumulations of damages (“Stochastic Theory”)^{115,117,118}.

In the following sections, the variety of cardiovascular aging will be discussed in detail.

1.6.1 Cardiovascular Aging

As the modern medical care and life conditions have tremendously improved in the past century, life-expectancy has –especially in industrialized countries- remarkably increased. Whereas the life expectancy was around 50 years in the 1900s, the life expectancy has increased to over 80 years at the present time¹¹⁶. However, aging is described as the major risk factor for severe diseases, such as CVDs and is therefore increasing in prevalence in the elderly. As CVDs are the primary cause of death globally¹, it is of major interest to understand how aging increases the risk for CVDs.

In the aging heart, many changes of the intra- and extracellular signaling are known that lead to severe age-dependent cardiac remodeling¹¹⁹. The underlying cellular changes causing cardiac remodeling will be discussed in detail in section “*Changes in Cellular Mechanisms in the Aging Heart*”, whereas the structural cardiac remodeling will be described below.

The aging heart. With advanced age, characteristic cardiac remodeling processes can be observed. Most of them affect alterations of the cardiac chamber geometry such as increased diameter of the left atrium (LA)¹¹⁹. A correlation of LA dilation with other risk factors for CVDs, such as hypertension and increased body mass index, was shown by a 16-year follow-up Framingham study¹²⁰. In addition, participants in the Multi-Ethnic Study of Atherosclerosis cohort with age-related LA dilation displayed higher degrees of myocardial fibrosis and other disorders¹²¹.

Further age-related structural changes can be found in the LV. During aging, the LV undergoes hypertrophic changes, such as increased wall thickness, altered chamber geometry and chamber dilation, as well as interstitial fibrosis^{119,122}. These alterations base on several molecular and cellular changes, like age-related oxidative stress, impaired calcium regulation and increased CM-loss¹²³. Especially the loss of CMs stimulate the remaining CM population to undergo hypertrophy that causes wall thickening and the increased degree of interstitial fibrosis conditions ventricular stiffness¹¹⁹. As a consequence, patients tend to develop pathophysiologic conditions like HFpEF.

Besides cardiac chamber abnormalities, age-dependent valvular alterations may also occur. Among of them, the aortic valve stenosis is the most prevalent valvular disorder in the aging heart¹²⁴. Interestingly, the valvular remodeling share many common risk factors with atherosclerosis, such as hypertension, smoking, age, high LDL level and gender¹¹⁹. Like atherosclerosis, aortic stenosis is attributed to chronic inflammations as well as tissue calcifications leading to increased tissue stiffness and narrowing^{124,125}.

A further valvular disease is mitral stenosis, that contributes to a significant portion of cases in industrialized countries¹²⁶. Mitral stenosis (MS) is caused by valvular calcification and inflammation and its prevalence was shown to increase with advanced age. MS is characterized by severe ECM stiffness and hardening, as well as an increased valvular mass. ECs that line the mitral valve were shown to transit to mesenchymal cells that further contributes to ECM protein production as well as stiffness and cellular mass¹²⁶.

Age-dependent changes can also be found in the pericardium. Increased interstitial fibrosis, as well as increased deposition of adipose tissue are the main age-related changes in this compartment^{119,127}. Fei et al reported in 2010, that especially the pericardial adipose tissue secretes pro-inflammatory cytokines, so-called adipokines, that

tempt to further increase interstitial fibrosis and impair the cardiac electric conductivity system^{127,128}.

The aging vasculature. In vascular aging, changes can be observed in large arteries as well as in the microvasculature. Large arteries display an age-related increase in wall thickening, especially in the intima. This is due to a reduced proliferative capacity of ECs with aging resulting in a loss of endothelial integrity. As a consequence, vascular SMCs invade the intimal layer leading to an increase in wall thickness up to 3-fold¹²⁹. Rigidity of vasculature is further promoted by calcification which is partially driven by the loss of calcification inhibitors, like (among others) osteopontin and pyrophosphate¹¹⁹.

Similar to larger vessels, vessels of the aging microcirculatory system display also an outward hypertrophic remodeling including enlarged lumen diameter and increased wall thickness¹³⁰.

Age-related changes of the ECM can be observed in both the macro- and microvasculature. Excessive production of fibrotic ECM components (elastin, collagen and fibronectin) and cross-linkers increase ECM rigidity and thereby promote vascular stiffness^{119,130}.

Especially upon ischemic injury, aging can be associated with reduced angiogenesis, accompanied by impaired EC function and reduced VEGF expression¹³¹.

1.6.2 Changes in Cellular Mechanisms in the Aging Heart

In general, it is thought that the increased vulnerability to CVDs in the elderly is based on age-dependent cellular changes. As indicated in the previous section “*Cardiovascular Aging*”, multiple cellular mechanisms are altered or impaired upon age¹¹⁴ (Figure 8). Among of them, autophagy, mitochondrial oxidative stress, telomere shortening, insulin-like/insulin growth factor 1 (IGF1) pathways, growth differentiation factor 11 (GDF11) and 5'-AMP-activated protein kinase (AMPK) pathways seem to be the most affected mechanisms¹¹⁹. In the following, each mechanism will be pointed out to describe the cellular processes during age.

Impaired autophagy. Autophagy is a highly conserved biological process by which cells clear their cytosols from cytotoxic proteins and dysfunctional organelles. By form-

ing membranous intracellular vesicles, cellular components (organelles, proteins, pathogens, etc.) are engulfed, delivered to the lysosome, degraded and recycled¹³². Currently, three distinct forms of autophagy have been described: macroautophagy, microautophagy and chaperon-mediated autophagy¹³². Especially, macroautophagy seems to play an important role, since it decreases with cardiac age¹¹⁹. The experimental induction of macroautophagy showed a promotion of longevity, and its “anti-aging” effect is thought to base on the clearance of cytotoxic components and dysfunctional organelles^{114,119,133–135}. Whereas macroautophagy also increases the general “fitness” of cells and was reported to be up-regulated during cardiac ischemia¹¹⁹, a decrease in macroautophagy is associated with multiple CVDs¹³⁶. In this respect, the deletion of the autophagy-related gene *Atg5* caused HFrEF in mice, whereas the induction of autophagy reduces *Ang-II* (angiotensin II)-induced cardiac hypertrophy^{137,138}.

Increase in oxidative stress. Already in the 1950s, Denham Harman postulated the free radical theory of the aging heart by stating that increasing levels of ROS damage macromolecules that accumulate in the heart and gradually lead to organ dysfunction¹³⁹. In the aging and diseased heart, levels of superoxides, the most abundant cardiac ROS, are elevated. Superoxides are generated in the mitochondrial respiratory chain by the NADPH oxidase 1, 2, 4 and 5 (NOX1-5)¹¹⁹. Whereas NOX up-regulation leads to oxidative stress, the antioxidant enzymes superoxide dismutase, catalase and glutathione peroxidase degrade superoxides and reduce excessive ROS production^{119,140}. Interestingly, the antioxidant capacity of myocyte mitochondria is impaired in HF, causing oxidative stress. The increased ROS level affects CMs by altering the intracellular contractility signaling pathway, as well as inducing cell death and thereby impairing ventricular function. In ECs, ROS disrupts the protective effect of NO and causes EC dysfunction and subsequently promote arterial stiffness and finally atherosclerosis (Figure 8A).

Telomere shortening. Telomeres are nucleoprotein caps of chromosomes that shorten with each cell division throughout the lifespan. If a specific telomere length is reached, cell cycle inhibitors are activated resulting in apoptosis or cellular senescence. Whereas telomere attrition plays a minor role in CM aging, it may be involved in EC dysfunction¹¹⁹. Especially the guanine-rich stretches of telomeres are vulnerable

to ROS and shortened telomeres were in particular found in vessels, prone to atherosclerosis. Telomere shortening may furthermore be responsible for the loss of stem and progenitor cells that reduces the regenerative capacity of the aging heart^{119,141,142}.

Alterations in IGF-1 signaling. IGF1 signaling plays a very controversial role in cardiac aging. There are emerging evidences for both protective and detrimentally effects in the aging heart. In vascular SMCs, IGF1 was reported to induce DNA damages, increase ROS production and induce cellular senescence^{143,144}. In contrast, IGF1 deficient mice showed an increased life expectancy and the same association was seen in human^{143–145}. In addition, the blood IGF1 level that peaks in the adolescence, gradually decreases throughout the life¹⁴⁴. Multiple studies even confirm a protective role for IGF1 in the aging CV system by reporting an association of low IGF1 levels with an increased risk for coronary artery diseases, such as atherosclerosis, and HF^{144,146}. On the one hand, Higashi and his coworkers consider IGF1 to be anti-inflammatory and atheroprotective that rather prevents atherosclerosis¹⁴⁷ and also others report that IGF1 overexpression prevent LV dilation and hypertrophy¹⁴³. On the other hand, multiple different IGF1 overexpression studies demonstrate an increased development of HF and cardiac hypertrophy (Figure 8B), as well as an worsen recovery after MI¹⁴³. These examples show that the specific role of IGF1 in the aging heart is not completely understood. In the end it might depend on the cardiac compartment and cell type, whether IGF1 is cardiac protective or detrimental to the heart.

Increased interstitial fibrosis. In the post-MI heart, fibrosis plays an important role in cardiac repair and remodeling. However, this reparative mechanism is detrimental to the aging heart. Cardiac fibrosis (Figure 8C) increases during aging and is associated with cardiac stiffness, as well as LV hypertrophy¹⁴⁸. The factors causing cardiac fibrosis can be diverse, whereas chronic inflammation and age-related elevated collagen deposition were reported to mainly drive interstitial and perivascular fibrosis. In addition, aged cardiac FBs were reported to increase lysyl oxidase and AGE expression that excessively cross-link collagen and promote ventricular stiffness(Figure 8D)⁵⁴. Furthermore, Ang-II promotes FB proliferation, FB activation and collagen deposition leading to cardiac hypertrophy and fibrosis^{119,148,149}. On the other hand, AMPK plays a cardiac protective role in myocardial ischemia, angiogenesis and cardiac injury^{119,143}. It is considered to delay the formation of fibrosis by inhibition of inflammation, inhibition of FB activation and blocking of ECM deposition^{119,150,151}. AMPK additionally inhibits CM size

and hypertrophy¹⁵². However, there are increasing numbers of sources demonstrating that AMPK expression decreases in CMs and myofibroblasts during aging, indicating the lack of AMPK as a cause for cardiac fibrosis^{119,151,153,154}. Similar to AMPK, GDF-11 (a member of the TGF β family) shows a decrease in cardiac aging and its low serum levels are associated with LV stiffness and hypertrophy¹¹⁹. Both the decrease in AMPK and GDF-11 with age favors fibrogenesis.

Fibrotic alterations not only occur during physiological cardiac aging, but also in the healing processes of the aging heart. Previous articles reported about impaired healing processes in the aging heart after MI^{155,156} which is worsen by age-related alterations of ECM deposition and reduced growth factor receptor sensitivity^{156,157}. Although collagen deposition is elevated in the aged heart, mouse studies demonstrated reduced collagen secretion in the scar tissue and an increased serum level of MMPs upon MI in aged mice^{156,157}. The increased MMP level could damage the ECM and results in an insufficient scar formation.

In addition, fibroblast-myofibroblast transition is impaired in the aged heart, probably caused by a diminished response of FBs towards TGF β ¹⁵⁸. The reduced TGF β sensitivity bases on a decrease in TGF β receptor I (T β RI) expression¹⁵⁸ and thereby impairs myofibroblast formation. Fibroblast-myofibroblast transition may also be reduced by a lack of periostin expression. Periostin is a matrix protein that is deposited by FBs and which is reduced in the aging heart¹⁵⁷. It plays a minor structural role but rather modulates cell-matrix adhesion, as well as cell functions. Periostin was shown to activate FBs via α_v -integrin and thereby promote myofibroblast formation by inducing α -SMA expression^{54,159}. Both the age-related decline in periostin, as well as the reduced expression of T β RI impair myofibroblast recruitment and subsequently impair cardiac repair in the aging heart.

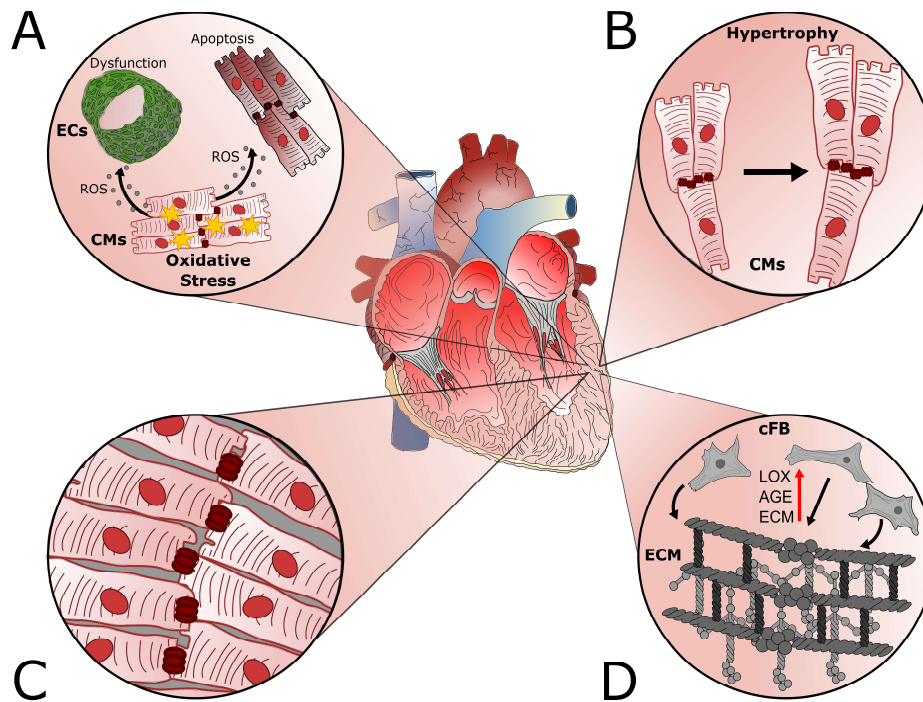


Figure 8: Cellular alterations in the aging heart. (A) Aging is also associated with an increased production of reactive oxygen species (ROS) that leads to endothelial, as well as cardiomyocyte (CM) dysfunction. (B) Multiple signaling pathways and the loss of CMs stimulate the remaining CMs to undergo hypertrophy. (C) During aging, the cardiac chambers undergo severe changes. One of them is the formation of interstitial fibrosis that causes ventricular stiffness. (D) Fibroblasts (FB) display elevated extracellular matrix (ECM) production and additionally an increased expression of lysyl oxidase (LOX) and advanced glycation end-products (AGE) that excessively cross-link collagens and thereby promote ventricular stiffness. The figure was modified from the review article in *Appendix 1*.

1.7 Cellular Plasticity in the Adult Heart

The ability of cells to differentiate is fundamental for cardiac development and repair processes in many CVDs. Two prominent examples of cellular plasticity in the heart are fibroblast-to-myofibroblast transition (FMT) and endothelial-to-mesenchymal transition (EndoMT). Since both mechanisms are of major interest in physiological, as well as pathophysiological cardiac aging, FMT and EndoMT will be further described below.

Fibroblast-to-myofibroblast transition (FMT). FMT is a process that is involved in both physiological and pathophysiological events (Figure 9A). However, its primary role has been described for pathophysiological conditions such as MI (scar formation)⁵⁴ or wound healing¹⁶⁰ and the process typically develops in two phases¹⁶¹. In the initial phase, activated FBs transdifferentiate into an immature myofibroblast form that is referred to as pro-myofibroblast which then matures to a full myofibroblast¹⁶¹. FB-pro-myofibroblast transition is mediated by a variety of stimuli, like mechanical tension

(caused by ECM rigidity or tension within the wound), humoral (cytokines, growth factors, interleukins) and mechanical factors (ECM components). Fibronectin EDA, PGDF and TGF β are among the main drivers of this process that stimulate stress fiber formation and increase FB motility. Pro-myofibroblasts are characterized by expressing β - and γ -actin as stress fiber components and N-cadherin that reduces cell-matrix adhesion and thereby promote motility¹⁶². Upon a prolonged exposure to pro-FMT factors, pro-myofibroblasts starts to form α -SMA containing stress fibers and gradually transit into fully mature myofibroblasts. By expressing OB-cadherin, myofibroblasts possess focal adhesion kinases and increase cell-matrix adhesion¹⁶³. As a consequence, myofibroblasts become less motile and less proliferative but enhance contractility, as well as ECM deposition¹⁶¹.

Endothelial-to-mesenchymal transition (EndoMT). To date, multiple studies showed that ECs are able to undergo a trans-differentiation process, that is known as endothelial-to-mesenchymal transition (EndoMT) (Figure 9B). EndoMT is a biological mechanism that has been identified in the past years by which ECs lose their phenotype and acquire mesenchymal-like features, such as a migratory and contractile phenotype¹⁶⁴. ECs undergoing EndoMT lose endothelial-specific markers like von-Willebrand factor, CD31, VE-cadherin and eNOS but express mesenchymal-specific markers, such as calponin, vimentin, α -SMA, transgelin, fibronectin EDA, collagen type I and III and FSP-1.

EndoMT can be induced by different stimuli. In the diseased heart, mostly inflammatory or fibrotic factors, such as hypoxia or TGF β 2 drive EndoMT. Hypoxia induces EndoMT through hypoxia-induced factor 1 α (HIF1 α) that activates the transcription factor Snail1 and thereby stimulates the expression of mesenchymal genes^{164,165}. TGF β 2 can initiate EndoMT via a canonical and multiple non-canonical pathways¹⁶⁴. The most common form of TGF β -signal transduction is the canonical pathway. In the canonical pathway, TGF β 2 binds to the heterodimeric, transmembrane TGF β -receptor that phosphorylates Smad2 and Smad3^{164,166–168}. Phosphorylated Smad2 and Smad3 form a complex with Smad4 that translocates to the nucleus. The Smad2/3/4 complex binds to Smad-binding elements and activates the expression of mesenchymal genes, as well as the pro-EndoMT factors Snail1 and Snail2 that further promotes EndoMT^{164,168}.

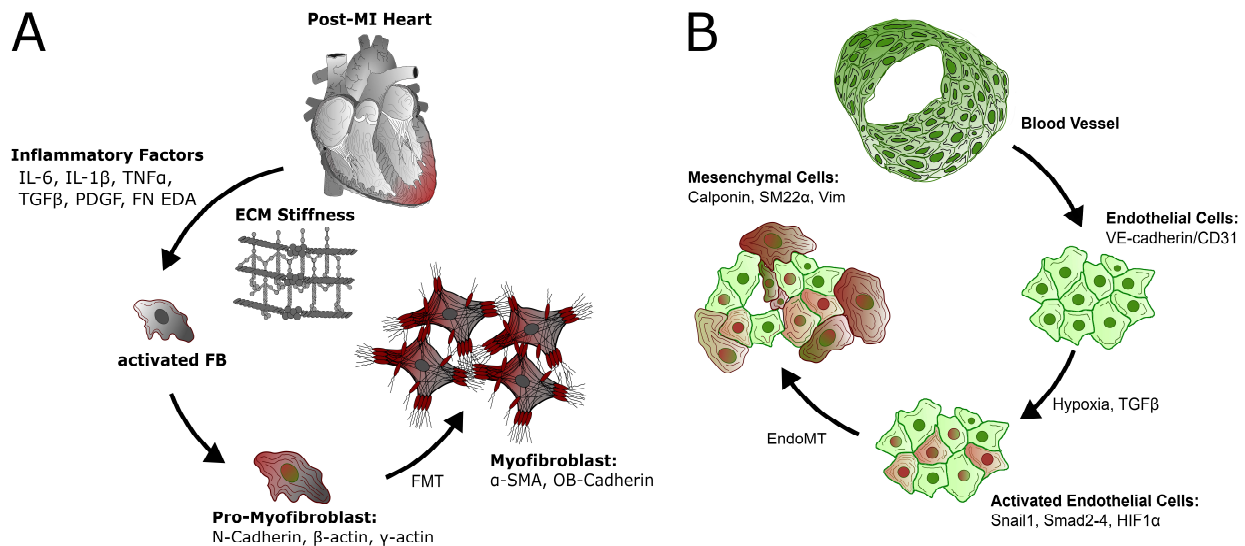


Figure 9: Cellular plasticity – FMT and EndoMT. (A) Fibroblast-to-myofibroblast transition (FMT) typically occurs during diseases. ECM stiffness and pro-inflammatory cytokines stimulates activated fibroblasts (FBs) to transit into pro-myofibroblasts. Upon prolonged pro-inflammatory stimuli, pro-myofibroblasts transit to fully mature myofibroblasts. (B) Endothelial-to-mesenchymal transition (EndoMT) is initiated through -among others- hypoxia and TGF β . Whereas hypoxia activates via HIF1 α , TGF β stimulates phosphorylation of Smad2 and Smad3 that form a complex with Smad4. Both hypoxia and TGF β drive the reduction of endothelial gene expression but stimulates expression of mesenchymal genes. The figure was modified from the review article in *Appendix 1*.

1.8 The Vascular Niche Function

The vascular or endothelial niche can be considered as the microenvironment that is formed by ECs and mural cells of the vessel wall¹⁶⁹. By secretion of matrix proteins or auto-/paracrine factors, the vascular niche is able to modulate the function and behavior of adjacent cells. However, the term vascular niche does not exclude that non-vascular cells such as tissue-resident cells may also influence the vascular microenvironment and thereby modulate cell functions¹⁶⁹. As example for non-vascular modulators, CMs may release VEGF or angiopoietin-1 to activate ECs^{64,88}. CM-derived NO acts on SMCs residing in the tunica media and leads to vasodilation⁶³.

Cellular components of the vascular niche: ECs are the most important cellular component of the vascular niche. They form blood vessels that supply the underlying tissues with oxygen, allow plasma to enter the tissue, as well as secrete BM components to stabilize the vessel and affect auto-/paracrine signaling pathways. Since vessels are initially leaky, ECs need to recruit mural cells that stabilizes the preliminary tube. Mural cells, such as SMCs and pericytes are the second major class of cellular components within the vascular niche¹⁶⁹. They reinforce the vascular tube and secrete

further pro- and anti-angiocrine factors to modulate vessel growth²⁰. However, the vascular niche of capillaries and of the microvasculature is more complex than the vascular niche of larger vessels. Since a proper vessel wall is missing, tissue-specific cells surrounding capillaries have a deep impact on vascular niche modulation¹⁶⁹.

Basement membrane as non-cellular component of the vascular niche: The vascular BM is the major non-cellular component of the vascular niche. It not only grants capillary stability but can also modulate cell behavior as described in the section “1.3.3. *Composition and Function of the Basement Membrane*”. In the past, many groups described that changes in the endothelial BM composition modulate cell function. These changes often occur during diseases or development. In this regard, the laboratory of Lydia M. Sorokin demonstrated that laminin 411 and laminin 511 are involved in T-cell recruitment across the blood-brain barrier (BBB) during encephalomyelitis¹⁷⁰. In addition to this, Wu et al. dissected the laminin subunits and reported that the encephalomyelitis-related expression of laminin $\alpha 5$ is responsible for the impairment of T-cell extravasation¹⁷⁰.

Regenerative capacity of the vascular niche: The vascular niche is not solely a storage for angiogenic factors or responsible for immune cell recruitment. It also shows a high regenerative capacity that drives multiple repair mechanisms. In the past decades, multiple studies demonstrated a regenerative effect of the vascular niche in liver, lungs and the bone marrow^{171–176}. In the bone marrow (Figure 10A), EC-derived NO was shown to be essential for stem and progenitor cell mobilization¹⁷². Additionally, Iktin et al. described a ROS-dependent mobilization of haematopoietic progenitor cells that is driven by ECs¹⁷³. Helmut Augustin’s laboratory elucidated the role of the endothelial niche in liver regeneration (Figure 10B) by demonstrating a partial-hepatectomy-dependent down-regulation of Ang2 in sinusoidal ECs that drives hepatocyte proliferation¹⁷⁵. Furthermore, Manavski et al. reported from EC-derived KLF2 which induces activating A expression and thereby inhibits hepatocyte proliferation after liver regeneration¹⁷⁶. Apart from liver and bone marrow, Shahin Rafii studied the regeneration of pulmonary tissues (Figure 10C). He and his co-workers displayed that upon unilateral pneumonectomy, pulmonary ECs start to secrete MMP14 to liberate cryptic EGF-like domains from the ECM that promote epithelial cell expansion. This in turn, supports alveolarization¹⁷¹. However, whether the vascular niche drives repair mechanisms in the heart remains unknown.

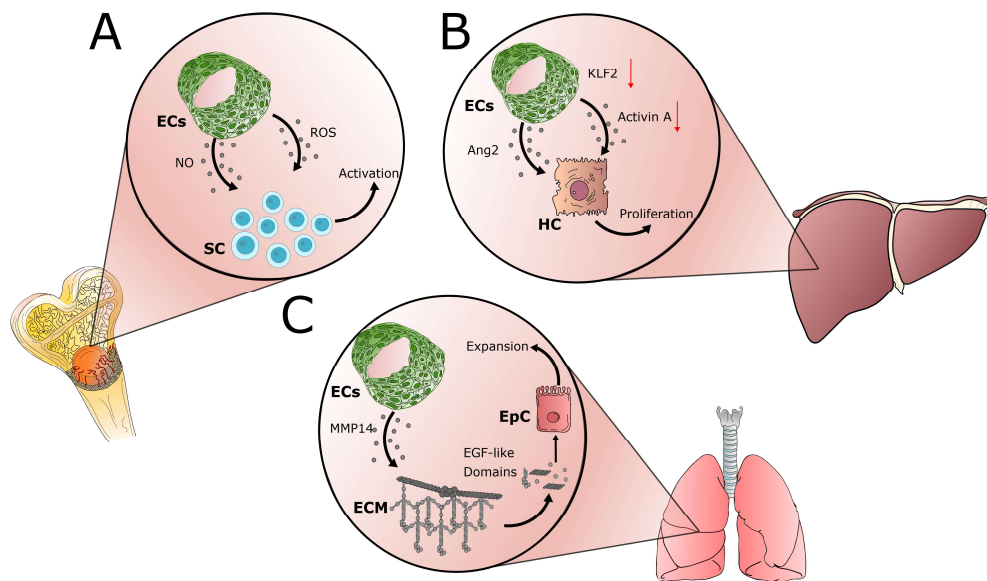


Figure 10: Regenerative capacity of the vascular niche. (A) In the bone marrow, endothelial cells (ECs) can activate stem cells (SC) via NO and ROS production. (B) Upon liver damage, regeneration is driven by the vascular niche through EC-derived Ang2 and reduced KLF2/activin-A that stimulates hepatocyte (HC) proliferation. (C) In the lung, ECs release MMP14 to degrade ECM components. ECM breakdown liberates cryptic EGF-like domains that induce epithelial cell (EpC) expansion.

1.9 The Use of single-cell RNA Sequencing to Study Cardiac Cellular Heterogeneity

The heart is a complex organ, containing a specific heterogeneous composition of myocytes and non-myocytes. This cellular heterogeneity results in a remarkable cellular interaction network that allows the heart to function as an integrate unit. To decipher the cardiac cell composition and cellular interactions, mostly bulk or population experiments have been used in the past. However, these types of experiments dilute out lower cellular signals and fail to provide any information about the origin of specific cellular subpopulations¹⁷⁷.

Recent advances in RNA sequencing enable whole transcriptome analysis on single-cell level that emerge into a new methodology called single-cell RNA sequencing (scRNA seq)^{177,178}. In very recent studies, scRNA seq has successfully been used to study cellular heterogeneity in the healthy and diseased heart^{179–182}. In this respect, the group of Richard Harvey gave a comprehensive analysis of the non-myocyte populations in both healthy and injured mouse hearts. By clustering more than 30,000 single cells, he and his coworkers found more than 30 cell populations including an

previously undescribed cardiac FB lineage, as well as novel myofibroblasts in the post-AMI heart¹⁸⁰. By contrast, the laboratory among Joseph Wu used scRNA seq to shed light on CM heterogeneity to define transcription factors that can be useful for differentiation protocols for human induced pluripotent stem cell-derived CMs¹⁸¹.

Apart from cellular heterogeneity, it is of major interest to understand also the intercellular communication within or between specific cell populations. Richard Harvey and his group provided an elegant way to predict the interactome in a recent study via scRNA seq¹⁸⁰. Using a bioinformational method that was provided by Rmilowski et al. in 2015¹⁸³, he and his group represented a cell-cell communication network by predicting ligand-receptor interactions. They implemented a directed, weighted network by taking four layers of nodes into account that can be describes as follows: The first layer of nodes refers to the cell populations expressing ligands (the source of ligands), whereas the second layer of nodes refers to the ligands that are expressed. The third layer represents the receptor targets of the ligands and the fourth layer refers to the target cell population expressing the receptors. Although, anatomical barriers cannot be modeled in this analysis, potential interactions can be found to race further hypotheses. Such a ligand-receptor analysis has already been used also by Nadia Rosenthal's laboratory in 2017 which was able to predict interconnections of non-myocytes in male versus female mouse hearts¹⁷⁹.

Although scRNA seq is a powerful tool for cardiac research, there are still some limitations that could distort scientific conclusions. One of the most important issues is the separation of cardiac tissue to receive a single-cell suspension. Enzymatic or mechanical tissue dissociation is relatively harsh and often results in the disruption of many cells which could result in the loss of small cellular subpopulations. In addition to this, the transcriptional profile may change upon tissue dissociation due to the loss of the natural cellular environment and by the mechanical force that is needed for tissue dissociation. A further bias can occur during cell sorting. Pipelines of various commercially available platforms, such as the 10X Genomics or Fluidigm C1 systems sort cells of a specific range of size. For instance, large cells, like CMs are often too big to pass the pipelines which makes current scRNA seq platforms unable to reliably display the relative abundance of cardiac cells so that either myocytes or non-myocytes are used for scRNA seq^{177,178}. These limitations can be overcome using a modified form of scRNA seq, called single-nucleus RNA sequencing (snRNA seq). The advantage of snRNA seq is that cardiac tissue being snap-frozen in liquid nitrogen can be used. The nuclei

can be isolated afterwards without changing the transcriptional profile. This procedure enables also long-term tissue storage, outsourcing of nucleus isolation or snRNA seq and prevents transcriptional changes during tissue dissection due to the fact that no intact cells are needed. The use of single nuclei instead of single cells also bypasses the sorting bias that occur during scRNA seq and allows to capture a snap-shot of the entire cellular make-up of the heart. In this respect, Hu et al. has already used this technique in combination with droplet-sequencing to investigate cellular diversity in postnatal hearts and captured both cardiac myocyte and cardiac non-myocytes¹⁸².

2 Objectives

Studying the remarkable intercellular cross-talk in the adult heart is a fundamental challenge in cardiac research. Especially improving the understanding of alterations during aging will be of major interest to develop novel interventions for elderly patients. Therefore, the present dissertation aimed to shed light on the intercellular changes and impairments that appear during cardiac aging, by covering the following objectives:

1. Elucidating the role of endothelial cells in the aging cardiac vascular niche (see published work in *Appendix 2*).
2. Studying the cellular heterogeneity and cross-talk of the aging heart by applying snRNA seq on adult and aged mouse hearts (see accepted work in *Appendix 3*), while the current literature on intercellular communication in regenerating, diseased and aged heart is reviewed in *Appendix 1*.
3. Establishment of a novel cell culture model to study intercellular communication of endothelial cells, fibroblasts and cardiomyocytes in a cardiac environment (see submitted work in *Appendix 4*).

3 Results and Discussion

3.1. Role of Laminin β 1 and Laminin β 2 in the Endothelial Niche of the Aging Heart^b

Endothelial cells are not solely the inner lining of blood vessels that supply all tissues with oxygen and blood. They also maintain vessel integrity by interacting with surrounding cells and are the main cell type forming the vascular microenvironment, the so-called “endothelial niche”¹⁶⁹. By secreting ECM proteins or releasing auto- and paracrine factors, ECs are able to modulate the endothelial niche and thereby control cell functions such as adhesion and motility especially during angiogenesis¹⁸⁴, but also control tissue homeostasis by sequestering growth factors in their ECM. The function of the vascular niche has been extensively studied in the past decades showing that the endothelial niche additionally maintain tissue regeneration upon injury, particularly in bone marrow, lungs and the liver^{171–176}. Whether the endothelial niche drives repair and regeneration in the heart is unknown.

However, the reparative capacity of the heart decreases with age^{155,156}, associated with a endothelial impairment and dysfunction¹³¹. As a matter of fact, one may argue that an impairment of the endothelial niche and consequently an impaired intercellular communication might be responsible for the increased vulnerability of the aging heart. Hence, we aimed to decipher the role of the endothelial microenvironment underlying EC impairment in the aging heart.

To address our aim, we first isolated perfused ECs from hearts of young (12-15 weeks old) and aged (18 months old) mice followed by total RNA isolation. By using bulk RNA sequencing, we intended to assess age-dependent changes in the endothelium and observed several genes clustered in aged and young mice. To specifically monitor changes in the endothelial niche, we strongly focused on genes that encode for secreted proteins and particularly observed a switch in the expression of laminin β -chain 1 (*Lamb1*) and 2 (*Lamb2*). Whereas *Lamb1* expression was increased, *Lamb2* was decreased with age. However, the expression of laminin α and γ chains remained unchanged. Interestingly, the same switch in laminin β chain expression was observed in mouse hearts upon acute myocardial infarction (AMI). Immunohistological analysis

^b This chapter is a summary of the most important findings from the previously published manuscript¹⁸⁶. The full manuscript can be found in the *Appendix 2*.

confirmed the dysregulation of *Lamb1* in the aging as well as AMI hearts and revealed also changes in the localization of *Lamb1*. In young mouse hearts, *Lamb1* was profoundly localized with the myocardial BM as assessed by laminin $\alpha 2$ immunostainings, whereas in aged mice, *Lamb1* was co-localized with endothelial cells.

The antipodal expression from *Lamb2* to *Lamb1* in the aging endothelium suggested that laminins carrying these two beta chains might have distinct functions on EC. To verify this suggestion, we switched to the human system and mimicked the *in vivo* situation by culturing HUVECs (human umbilical vein endothelial cells) on laminin 421 (LM421) as “young matrix” and laminin 411 (LM411) as “aged matrix”. Both laminin isoforms, LM421 and LM411 carried the major endothelial laminin $\alpha 4$ -chain¹⁸⁵ and the laminin $\gamma 1$ -chain, which was the only γ -chain expressed in young and aged cardiac ECs according to the bulk RNA sequencing data set¹⁸⁶. Only the laminin β -chains differed in both isoforms. HUVECs were cultured on both matrices. After 10 days, a significantly reduced number of HUVECs was observed on the LM411 matrix compared to the LM421 matrix. To determine if this observation is due to alterations in cell proliferation or cell death, we applied HUVEC proliferation and apoptosis microplate assays. Interestingly, neither HUVEC proliferation (as assessed by EdU incorporation) nor apoptosis (by determining caspase 3/7 activity) were altered by the respective matrices. However, we found that cell-matrix adhesion was impaired in the presence of LM411, thus explaining the reduced number of HUVECs in the initial finding. In addition to this, LM411 also reduced the migratory as well as tube formation capacity of HUVECs when compared to the LM421 matrix. Comparable results were found in human coronary artery ECs by assessing migration assays demonstrating that the findings are not unique for HUVECs.

Since replicative aging was shown by *in vitro* assays to induce endothelial-to-mesenchymal transition (EndoMT) in human ECs¹⁸⁷ and since EndoMT marker genes were up-regulated in aged cardiac ECs on RNA level, we questioned whether LM411 and LM421 also affect TGF β 2-induced EndoMT. Indeed, HUVECs cultured on the LM411 matrix showed an increased mRNA expression of the mesenchymal markers SM22 α , calponin and vimentin compared to HUVECs on LM421, in both the presence and absence of TGF β 2. Distinct morphological alterations and SM22 α -induction were further observed in TGF β 2-stimulated HUVECs cultured on LM411. The cells showed a de-

creased VE-cadherin (as EC marker) expression as well as less pronounced VE-cadherin localization, compared to HUVECs cultured on LM421, implicating that LM411 augments EndoMT *in vitro*.

In the aging heart, EndoMT was shown to occur in human atherosclerotic lesions¹⁸⁸, where acute events may be triggered by plaque erosions¹⁸⁹. To determine whether erosion might be affected by the different laminin matrices, we performed a HUVEC detachment assay. In line with the cell-matrix adhesion assay, HUVECs showed significantly increased detachment when cultured on LM411 compared to HUVECs on LM421, suggesting a putative role of laminin β 1 during atherosclerotic plaque erosion.

After having found several cellular functions that were changed in the presence of LM411, the mechanism underlying these alterations needed to be elucidated. Integrins are well known to be the main receptor for laminins regulating cellular functions⁴⁴. Among of the different integrin subtypes, integrin β 1 (ITGB1) is the key unit that is functionally important and expressed in ECs¹⁹⁰. Thereby, we determined the activation of ITGB1 in HUVECs cultured on LM421 and LM411 using a monoclonal antibody that binds to the activated conformation of ITGB1. Interestingly, HUVECs cultured on LM421 showed a significant higher activation of ITGB1 compared to HUVECs on LM411. Moreover, siRNA-mediated silencing of ITGB1 reduced the adhesion of HUVECs to LM421 to the level of control HUVECs on LM411 and completely abolished adhesion towards LM411.

In summary, the data of the first part of this thesis provides insights in the age-dependent dysregulation of the endothelial laminin β -chains (Figure 11). Whereas *Lamb2* is profoundly expressed in ECs of young mouse hearts, aged cardiac ECs switch the expression to *Lamb1*. This *Lamb2/Lamb1* switch was found to regulate multiple cellular functions and EC phenotype. HUVEC adhesion and migration were decreased by LM411, most likely because of a reduction in ITGB1 activation. Interestingly, LM411 stimulates HUVECs to lose their endothelial phenotype and acquire a more mesenchymal-like identity, suggesting that *Lamb1* contributes to the induction of EndoMT in the aging heart. On the one hand, EndoMT was described in multiple studies to contribute to cardiac fibrosis¹⁹¹ and atherosclerosis^{188,192}, two diseases that are prototypical for age-associated diseases. On the other hand, this switch might also be a compensatory mechanism, since a similar *Lamb2/Lamb1* switch was observed in hearts upon AMI and a transient or partial EndoMT may induce angiogenic sprouting¹⁹³. Moreover, ECs are known to drive tissue regeneration in other organs in a paracrine as well

as autocrine manner and thereby balance tissue repair and fibrosis^{171–176}. It can be speculated that an impaired endothelial matrix expression not only affects EC functions but also alters the endothelial paracrine environment and hence contribute to age-associated disorders. Indeed, we observed dysregulations of various growth factors and cytokines measured in supernatants of HUVECs cultured on LM411 versus LM421. In this regard, we found thrombospondin-2 and FGF2 to be less secreted by HUVECs cultured on the LM411 matrix compared to HUVECs on LM421. Whereas thrombospondin-2 is in fact involved in CVDs¹⁹⁴, FGF2 is known to inhibit EndoMT¹⁹⁵. Thus, a reduction of FGF2 release might even promote EndoMT during cardiac aging. To further investigate the role of Lamb1 and Lamb2 in the aging heart *in vivo*, conditional knock-out mice have to be generated. Since Lamb1-knock-out is lethal in mice at E5.5¹⁹⁶ and Lamb2-knock-out is lethal within 3 weeks after birth^{197–199}, conditional knock-out mice would be a better option. In this regard, conditional Lamb2-knock-out animals could be then used to investigate the role of Lamb2 during AMI and EndoMT, when combined with endothelial lineage-tracer lines.

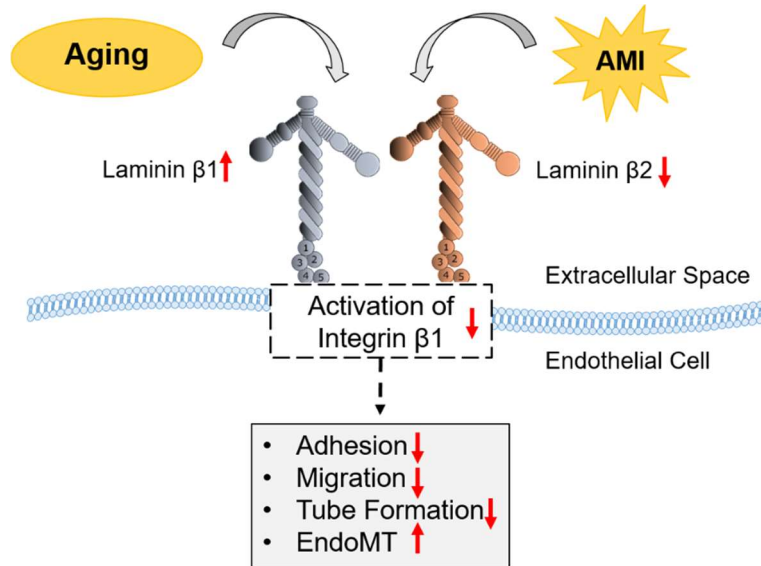


Figure 11: Switch in *Lamb2* to *Lamb1* controls cell functions in cardiac endothelial cells. Upon aging and acute myocardial infarction (AMI) cardiac endothelial cells shift the expression from *Lamb2* to *Lamb1*. This switch decreases the activation of integrin β1, thereby reducing cell-matrix adhesion, migration and tube formation. However, endothelial-to-mesenchymal transition (EndoMT) is elevated. Figure is adapted from the online available graphical abstract of the previously published manuscript¹⁸⁶.

3.2. Transcriptional Heterogeneity of Fibroblasts as a hallmark of Cardiac Aging^c

Aging is described as the major risk factor for cardiovascular diseases (CVDs)¹¹⁹, which represent the main cause of deaths globally¹. Especially cardiac aging gained attention, since the aging heart is associated with severe cardiac remodeling such as increased vascular and ventricular rigidity, perivascular and interstitial fibrosis, LV wall thickening as well as impaired angiogenesis upon hypoxic injuries^{119,200}. Interventions with cardio-protective drugs were shown to decrease the development of CVDs and significantly expand life expectancy²⁰¹. Many of the above mentioned remodeling processes can be linked to maladaptations on cellular levels that are accompanied by impaired intercellular communications and replicative senescence¹¹⁴. By now, among others, fibroblast (FB) activation, disturbed angiogenesis as well as cardiomyocyte (CM) hypertrophy are known to drive cardiac remodeling during age^{119,202}. Additionally, increased numbers of monocyte-derived macrophages and granulocytes were further found in the aging heart²⁰³. To what extent the communication and heterogeneity of cardiac cells are altered and how they control cardiac remodeling during aging is surprisingly little understood.

To shed light on the heterogeneity and intercommunication of cardiac cells in the adult and aged mouse heart, we applied single-nucleus RNA sequencing (snRNA seq) on young (12 weeks) and aged (18 months) mouse hearts. By including 3 mice per group, we received a total number of 14,827 nuclei from young and 12,981 nuclei from aged hearts that were bioinformatically assessed using a t-distributed stochastic neighbor embedding plot (short: t-SNE plot)²⁰⁴. This procedure allowed us to visualize clusters of nuclei that share similar transcriptomic signatures. Unsupervised clustering resulted in a total of 15 distinct nuclei clusters that were annotated to specific cell types using the expression of cell-specific genes and by using already published scRNA / snRNA seq data sets^{179,205}. In this way, we determined 7 major cell types among of which FBs, CMs, ECs, pericytes, immune cells, epicardial cells and adipocytes were present, whereas FBs contained 2 sub-clusters and ECs as well as CMs contained 3 sub-clusters each.

Although cell cycle activity as well as relative nuclei distribution were not significantly altered by aging, 128 uniquely differentially expressed (non-redundant) genes (DEGs)

^c This chapter summarizes the key findings of the recently accepted manuscript shown in the *Appendix 3*.

were identified in young versus aged nuclei. Among of the DEGs, 107 genes were uniquely up- and 21 genes were uniquely down-regulated in aged hearts. Surprisingly, the majority of all DEGs were associated with FBs, suggesting that cardiac aging mainly influences this cell population. Thus, we turned our main attention to cardiac FBs and performed a FB sub-clustering. We ended up with a total of 12 distinct FB sub-clusters, whereas four sub-cluster were mainly populated by young nuclei and six sub-cluster predominantly populated by old nuclei. Each sub-cluster showed distinct gene expression that were used for gene ontology (GO) analysis. Interestingly, sub-clusters from young FB nuclei displayed an enrichment for GO terms associated with cardio-protective pathways (energy generation, regulation of muscle system processes), whereas sub-clusters from old FB nuclei showed GO terms connected to “angiogenesis”, “EC proliferation”, “migration” and “osteoblast differentiation”. Genes connected to inflammatory responses were also enriched in aged FBs which is in line with the current literature showing a pro-inflammatory response of FBs during remodeling and cardiac fibrosis²⁰⁶. In addition, genes that are associated with “epithelial cell proliferation” were also enriched in sub-clusters that were mostly populated by old FB nuclei. We considered this GO term as FB expansion in the aging heart and confirmed our hypothesis by Picrosirius Red stainings showing increased perivascular and interstitial fibrosis in aged compared to young hearts. However, whether certain FBs gain a rather angiogenic and osteogenic phenotype during age, was so far unknown.

To receive more detailed insights into the trajectory of aging FBs, we applied a pseudotemporal analysis of the entire FB population allowing the sorting of all FB nuclei in a linear order. The pseudotemporal representation displayed the dynamics of FBs during aging and revealed 11 specific states. In line with the previous sub-clustering we found states that were predominantly populated by aged nuclei and states that contained mostly young nuclei. Also GO term analysis showed that young nuclei enriched genes that are connected to cardiac and FB functions (e.g. ECM structure organization), while old nuclei enriched genes associated with angiogenesis, osteoblasts, inflammation and cell proliferation. RNA-Velocity analysis further showed higher amounts of pre- or un-spliced mRNA in old nuclei versus young nuclei, indicating a higher transcriptional activity (“RNA verlocity”²⁰⁷) in aged FBs. This was true especially for states that were connected to the GO terms “angiogenesis” and “osteoblast differentiation”.

To address the functional consequences of the observed “angiogenic” FB states, we first focused on the angiogenesis-related genes that were enriched in these states. Interestingly, we observed that some of the genes were connected to ECM and secreted proteins, leading us to the assumption that the paracrine signaling between FBs and ECs might be changed upon cardiac age. Driven by this notion, we applied a weighted ligand-receptor analysis¹⁸³ on the entire snRNA seq data set. The ligand-receptor analysis predicted a potential interaction network, demonstrating that FBs represent the most ligand providing population and ECs express most corresponding receptors in the aging heart. To confirm alterations of the paracrine activity of FBs *in vitro*, we collected conditioned culture media of FBs isolated from young and aged mouse hearts and applied them to HUVEC tube formation assays. Whereas conditioned medium derived from young cardiac FBs improved the angiogenic capacities of HUVECs, aged FB medium reduced HUVEC tube formation, demonstrating an impaired paracrine signaling between FBs and ECs with age. In line with these observations, we found that aged FB nuclei expressed several anti-angiogenic factors such as Efemp1, which is known to reduce angiogenesis in tumors²⁰⁸ and multiple members of the anti-angiogenic serpin family, including serpin E1 and E2²⁰⁹. A mouse proteome profiler array confirmed increased levels of serpin E1 in conditioned medium of aged FBs, while increased levels Efemp1 were validated by RT-qPCR in isolated FBs from young versus aged hearts. By using neutralizing antibodies, we depleted serpins and Efemp1 from the conditioned media of aged FBs and repeated the tube formation assay. Interestingly, neutralization of serpins was sufficient to rescue the anti-angiogenic effect of the aged FB medium completely, whereas depletion of Efemp1 did not alter the aged phenotype. In summary, these data showed that cardiac FBs increase serpin expression upon aging which promotes an anti-angiogenic effect on ECs.

In line with the “hallmarks of aging” described by Lopez-Otin in 2013¹¹⁴, aged FB medium further increased inflammatory gene expression but decreased autophagy in HUVECs as demonstrated by *in vitro* studies. However, replicative senescence as well as mitochondrial dysfunctions could not be observed.

Next, we aimed to assess the meaning of the osteogenic genes, that were enriched in 2 of the aged FB states. Since cardiac FB were shown to acquire osteogenic properties during pathological remodeling upon AMI²¹⁰, it seemed plausible that a comparable transition also occurs in the aging heart. We found in the aged FB states several genes that were associated with osteoblast function and differentiation such as Cebpb, Ddr2

and Runx2 which were further validated by bulk RNA sequencing. Histological analysis of young and aged mouse hearts confirmed that Osteocalcin, a further canonical osteoblast marker²¹⁰, was profoundly expressed by Pdgfra⁺ FBs in aged hearts. However, these specific FB population was -besides in valves- found in the epicardium of aged mouse hearts. In line with this, punctiform calcifications were observed in the aged epicardium, unlike the young epicardium, where no calcification was found.

In summary, the present study comprehensively compared the transcriptional signature of the main cell types of the adult and aged mouse heart on single-nucleus level. In our data set, aging affected mostly FBs that displayed major changes in heterogeneity and gene expression. Especially FB fates were changed, indicating a decreased number of functional FBs and subsequently a decline in cardiac function upon age. Interstitial fibrosis is such an impairment that includes a dysregulation of FBs acquiring an inflammatory phenotype²¹¹. Those findings can be recapped in our pseudotemporal analysis, where certain FB states enriched pro-inflammatory genes and genes that are connected to cell proliferation. In addition, Picrosirius Red stainings confirmed interstitial and perivascular fibrosis in the aging heart.

Due to the ligand-receptor analysis, we gained further insights in the endothelial cross-talk. We predicted that ECs were the most “signal receiving” cells in the aging heart. Functional assays strengthened our hypothesis, demonstrating an age-related impairment of angiogenesis driven by FB-derived serpins signaling (Figure 12). Serpins belongs to the well-known anti-angiogenic protein family²⁰⁹ that are profoundly expressed by senescent cells²¹². They further have a pro-inflammatory effect that may enhance fibrotic activity in aged hearts²¹³ while a serpin depletion might be cardioprotective. A study by Khan et al. indicates that a SERPINE1 null mutation protects from biological aging in humans. By studying 177 subjects of the Berne Amish community including 43 subjects carrying a null SERPINE1 allele, SERPINE1 heterozygosity was associated with lower fasting insulin levels together with lower prevalence for diabetes mellitus and significant longer leukocyte telomeres. Carriers of the null SERPINE1 allele even had a longer life span in the extended Amish kindred²¹⁴. In this regard, FB might be able to remodel the endothelial niche in the aging heart. By expressing serpins, they may control EC functions and trigger inflammations. However, the contribution of further cytokines and matrix proteins cannot be excluded since the *in vivo* conditions are certainly more complex and needs to be further explored.

Moreover, we observed that aged FBs acquire osteogenic properties (Figure 12). Aging is associated with vascular calcification, but an osteogenic transition of FBs was so far only reported in hearts upon AMI²¹⁰. A recent publication demonstrated that aged skin-FBs acquire adipogenic features, indicating that aging has a tissue specific effect on FBs. Indeed, our data implicates that aged cardiac FBs acquire osteogenic properties, especially in the epicardium, but whether this phenotype has a functional impact or contributes to ventricular stiffness or impaired epicardial function needs to be further investigated.

Future studies may continue on this and investigate the role of osteogenic FBs in the aging heart. Osteocalcin- or Runx2-tracer mice can be used to capture a time course giving the age of mice when FBs acquire osteogenic traits. A second possibility could be the characterization of isolated aged cardiac FBs and testing their ability to transit to osteogenic cells as described previously²¹⁰. Since an osteogenic transition of FBs was reported in hearts upon AMI²¹⁰, osteogenic FBs in the aging heart might not be too absurd.

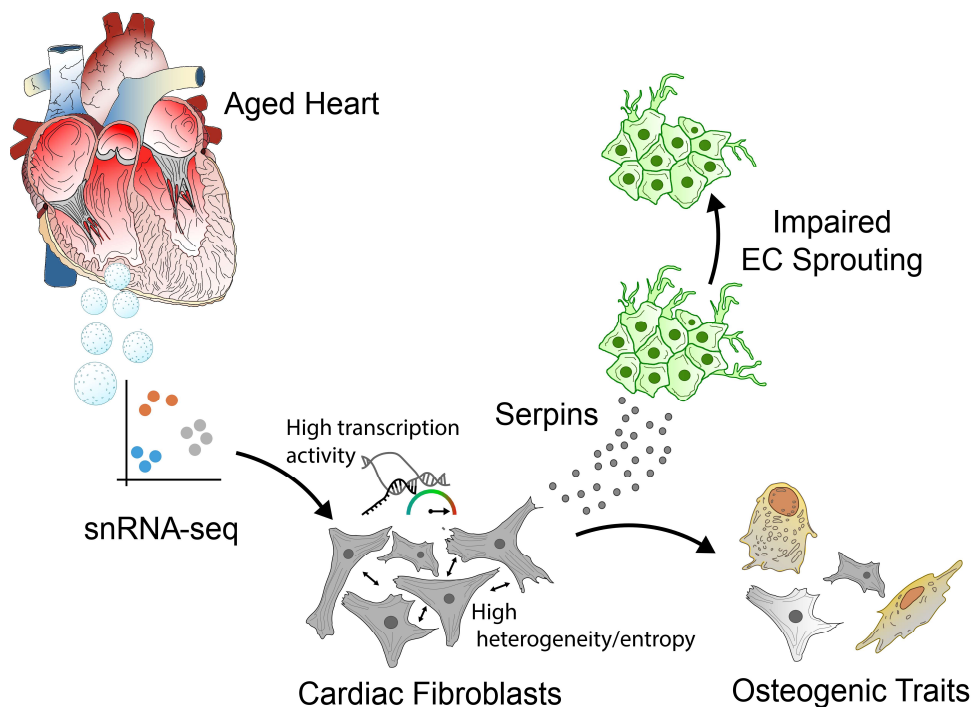


Figure 12: Cardiac fibroblasts control angiogenesis and acquire osteogenic traits upon aging. Single-nucleus RNA sequencing (snRNA seq) of young and aged mouse hearts revealed that cardiac fibroblasts impair endothelial cell (EC) sprouting by expressing serpins and acquire osteogenic properties as seen by expression of Osteocalcin and calcifications, especially in the epicardium. The figure is adopted from the graphical abstract (suppl. figure 11) of the accepted manuscript that can be found in the *Appendix 3*.

3.3. Generation of a Cardiac Tissue Mimetic to dissect Cellular Cross-Talk of the Heart^d

The heart consists of a variety of different cell populations, including CMs, ECs and FBs resulting in a remarkable cellular cross-talk that maintains tissue homeostasis during physiological as well as pathophysiological states and aging^{215,216}. To date, mostly two-dimensional CM cultures were used to study pathophysiology and effects of therapeutics in the cardiac system²¹⁷. Yet, two-dimensional cultures lack CM maturity as well as spatial organization and are hence not able to resemble the *in vivo* situation properly²¹⁸. To overcome this issue, three-dimensional CM monocultures were generated. Although, spatial orientations and CM interactions can be studied, three-dimensional CM monocultures ignore the cross-talk between ECs, FBs and CMs which is characteristic for the native myocardium^{215,216}. In *in vivo* situations, pathologic stimuli were demonstrated to induce angiogenesis and EC growth to meet the oxygen and nutrient demands of the remodeled heart^{219,220}. These EC adaptations were reported to occur in parts via the release of CM-derived pro-angiogenic factors, such as VEGF⁸⁹, angiopoietins^{221,222}, NO²²³ and CM-derived extracellular vesicles²²⁴. However, ECs not solely provide blood and oxygen to the tissues, they were also found to signal back to CM and induce CM growth, protection and fibrosis^{225–227}. The fact that ECs and FBs forms up to 80% of the heart's cell count^{228,229} further underlines the importance of using a multicellular culture system.

So far, multiple groups established different three-dimensional multicellular *in vitro* models to recapitulate the cellular heterogeneity and cross-talk of the heart. In this regard, engineered CM tissues, scaffolds, biodegradable matrices and similar other constructs were generated^{230–232}. Adding primary or iPS-derived ECs lead to rudimentary vascularization^{233–236}. Despite some exceptions^{237–239}, most models fail to display a proper network formation, making these models inadequate to study angiogenesis in a cardiac-like environment²⁴⁰. Therefore, we aimed to establish a three-dimensional spheroid system including CM, FB and EC to study hetero-cellular interactions under physiological and pathophysiological conditions in particular in terms of angiogenesis.

^d This chapter summarizes the key findings from the previously submitted manuscript that can be found in the *Appendix 4*.

To establish a three-dimensional spheroid system, we isolated primary CMs and FBs from neonatal (P1-2) rat ventricles. For each spheroid, we used 62,000 CMs and 6,400 FBs that formed a spheroid in a hanging drop. After 4 days, spheroids were collected, coated with growth factor reduced Matrigel and distributed in a 96-well U-bottom plate. Spheroids were allowed to recover in an incubator and 10,000 HUVECs transduced with a GFP-expressing lentivirus were added per spheroid. The spheroids (referred to as “cardiac tissue mimetics” or CTMs) were then cultured for 10 days in the presence and absence of the hypertrophic α -adrenergic receptor agonist phenylephrine (PE)²⁴¹.

First, we assessed how the CTMs respond to PE. Interestingly, in the presence of PE CTMs displayed hypertrophic growth and maturation as assessed by CM size, adult-type titin expression and sarcomere organization. In line with the known effects of PE treatment²⁴¹, CTMs showed increased contractile amplitude and contraction frequency. We further observed a metabolic switch upon PE-treatment, showed by increased mitochondrial function and increased oxidative metabolism.

Since we wanted to study endothelial cross-talk in terms of angiogenesis, we then turned our focus to vascularization. As reported by previous *in vivo* studies^{242,243}, PE stimulation increased vascular density also in the CTM system as determined by increased sprout length, sprout thickness and number of branch points. Increased filopodia formation indicated further augmented angiogenesis in the presence of PE. To assess whether vascularization was driven by a direct influence of PE on ECs, we used a HUVEC-spheroid based angiogenic sprouting assay, where we stimulated HUVECs with PE, a positive control (VEGF) or no stimulus. Surprisingly, PE did not affect HUVEC sprouting at all, whereas VEGF profoundly induced sprouting, leading us to the assumption, that if PE has no direct effect on ECs, it might stimulate CMs or FBs to release pro-angiogenic factors. Driven by this notion, we generated conditioned media of FB- and CM-monocultures in the presence and absence of PE and used these as adding for HUVEC-spheroid sprouting assays. Indeed, conditioned medium - derived from CMs stimulated with PE – significantly induced HUVEC sprouting, while medium from untreated CMs did not. Conditioned medium from untreated FBs also induced HUVEC sprouting which was not further increased upon PE stimulation. Hence, we hypothesized that PE induces the secretion of pro-angiogenic factors in CMs. Since pro-hypertrophic stimulation of CMs was reported to induce VEGF secretion²⁴³ and since we found increased levels of VEGF in culture media from CMs treated with PE, we determined the contribution of VEGF in our conditioned medium system. By using

neutralizing antibodies, we depleted VEGF from the PE-CM-conditioned medium and repeated the HUVEC-spheroid sprouting assay. Indeed, VEGF-depletion was sufficient to reduce EC sprouting to the level of untreated HUVEC-spheroids. In line with these findings, PE-stimulated CTMs showed a significant reduction in sprouting, when treated with neutralizing antibodies. Together, these data suggest that the three-dimensional CTM platform is able to mimic already published *in vivo* findings showing intercellular communications between CMs and ECs mediated by VEGF²⁴⁴.

Since PE stimulation increased CTM contraction, we additionally questioned whether PE-mediated mechanical force induces EC sprouting in the CTM model. To answer this question, we uncoupled the contribution of contraction on angiogenic sprouting by applying the β -adrenergic receptor antagonists propranolol (β 1/2-specific antagonist) and metoprolol (β 1-specific antagonist)^{245,246} to PE-treated CTMs. First of all, both β -blockers significantly reduced CTM contraction frequency, while propranolol additionally decreased CTM growth. Surprisingly, uncoupling of contraction significantly diminished vascularization compared to CTMs without β -blocker treatment. Because β -adrenergic receptor antagonists were shown to directly affect vascularization^{247,248}, we tested propranolol and metoprolol on HUVEC monocultures using tube formation assays. However, we were not able to see any direct effects of propranolol or metoprolol on HUVECs. To finally exclude that the used β -blockers cause secretomic changes in CMs, we collected conditioned medium from CMs treated with PE, PE in combination with propranolol and PE in combination with metoprolol. The conditioned media were then used on HUVEC-spheroid sprouting assays again. Interestingly, we could not find any effect on HUVEC sprouting, suggesting that PE-induced contractile force likely mediate -in addition to paracrine effects- angiogenesis.

Next, we turned our focus to possible applications and thus tested, whether the CTM platform can be used to study pathological or inflammatory stress. Thus, we cultured mature CTMs (CTMs being already treated with PE for 10 days) for 3 days either in medium containing TGF β 2 (as previously described¹⁸⁶) to induce EndoMT or under hypoxic conditions (0.1 % O₂). Interestingly, TGF β 2 marginally but significantly increased vascularization. However, immunostainings against vimentin suggested increased FB activation in TGF β 2-treated CTMs, accompanied by increased collagen deposition as assessed by second harmonic generation and Picrosirius Red stainings. As TGF β 2 is a well-known driver of EndoMT, we scanned CTM cryo-sections for ECs expressing mesenchymal markers such as vimentin, SM22 α and collagen III. Single

ECs located to both the CTM's surface and center were double-positive for endothelial and mesenchymal markers such as vimentin, demonstrating the occurrence of EndoMT.

In contrast to TGF β 2-treated CTMs, hypoxic CTMs displayed diminished vascularization but also increased collagen deposition.

In summary, we have established a three-dimensional *in vitro* cardiac tissue mimetic (CTM) containing CMs, FBs and ECs which can be used to study intercellular communication between CMs and ECs. The study demonstrated that the treatment with the hypertrophic α -adrenergic receptor agonist phenylephrine promotes CTM vascularization which was mediated at least partially by VEGF (Figure 13). However, depletion of VEGF didn't fully diminish CTM vascularization, suggesting the contribution of further pro-angiogenic cytokines and ECM proteins secreted by CMs or FBs as well as the contribution of mechanical activation by contracting CMs.

Although many other three-dimensional culture systems have been established for drug screenings, only few uses engineered tissues and cultures for mechanistic studies²³⁶. Our study provides a more in-depth analysis of the cardiac microenvironment and intercellular cross-talk especially in terms of CM-EC interaction. In addition to the communication via CM-derived VEGF, we demonstrated that mechanical activation may contribute to cardiac vascularization. The use of β -adrenergic receptor antagonists diminished CTM contraction and thereby CTM vascularization. We excluded direct effects of the used β -blockers on ECs and demonstrated that conditioned media of CMs treated with β -blockers did not affect angiogenesis, suggesting a potential direct influence of mechanical activation on EC sprouting. However, the influence of further angiogenic factors such as matrix proteins cannot be excluded in our experimental set-up.

Finally, we assessed whether our model can be used to study pathophysiological conditions (Figure 13). By addition of the pro-fibrotic cytokine TGF β 2, CTMs displayed augmented vascularization and increased collagen deposition. Additionally, we found EndoMT occurring within the CTMs suggesting that the CTM platform may be used to study EndoMT in a more cardiac relevant environment. The combination of TGF β 2 with further inflammatory cytokines (such as IL-1 β) might be an option to mimic chronic inflammation in cardiac remodeling. By contrast, severe hypoxic conditions fully diminished CTM vascularization but augmented collagen deposition.

In addition, we established a robust three-dimensional cardiac tissue mimetic that can be used for drug screenings going beyond targeting CM intrinsic functions only. The system may allow to study putative therapeutic benefits or side effects and to investigate intercellular communication under physiological and pathophysiological conditions. In following studies, CTMs may also be adjusted to mimic an aged phenotype. They might bridge the gap between two-dimensional *in vitro* cultures and *in vivo* models. By using CMs and FBs from aged mouse or rat hearts, CTMs may be a useful tool to study intercellular cross-talk during aging. In spite of this, the effect of various matrix proteins could be tested. During CTM formation, CM-FB spheroids are coated with Matrigel. One might use other ECM components such as fibronectin, collagen or laminins to study the impact of ECM components on CTM function and vascularization. However, the extensive culturing duration might be too long to observe any effects, taking the quick ECM turn-over into considerations.

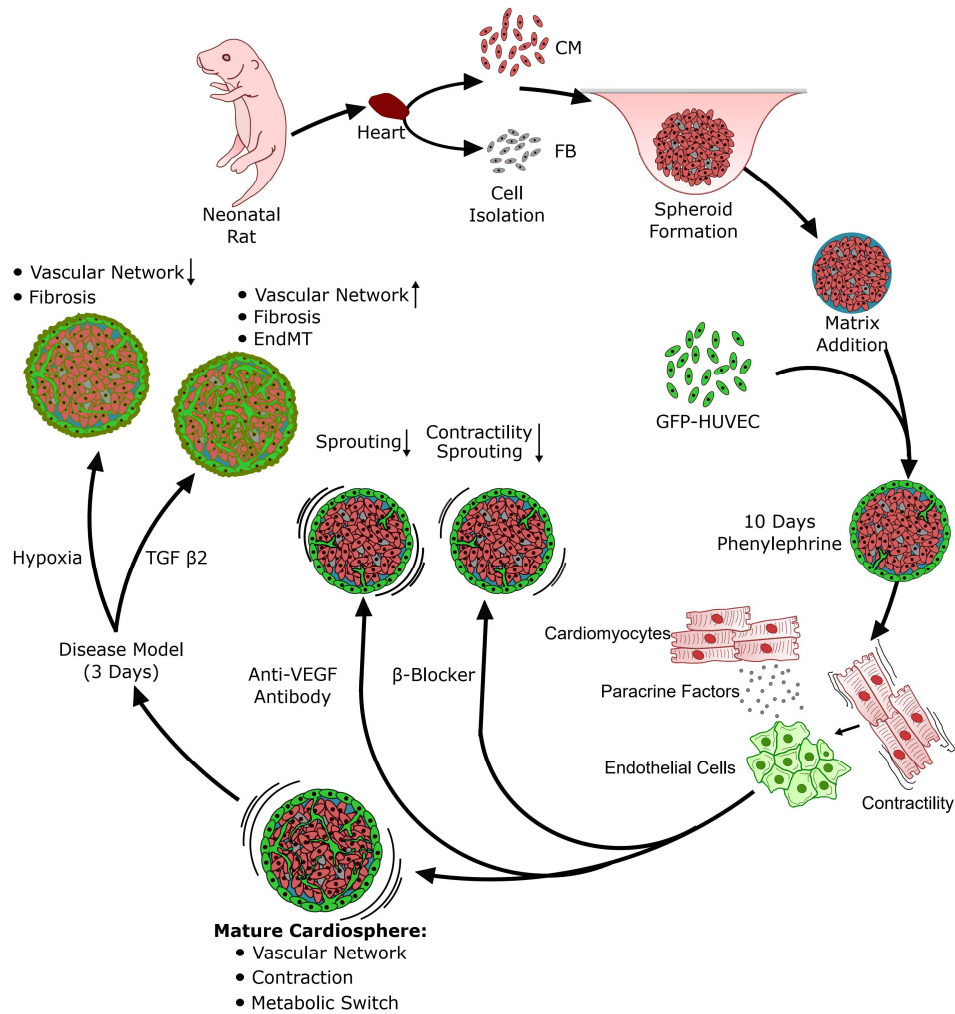


Figure 13: Generation of a cardiac tissue mimetic to study intercellular cross-talk. To study intercellular cross-talks in the heart during physiological and pathophysiological conditions, cardiomyocytes (CM) and fibroblasts (FB) were isolated from neonatal rat and allowed to form spheroids in hanging drops. Spheroids were harvested, coated with growth factor reduced Matrigel and coated with GFP-transduced HUVEC. By culture the cardiac tissue mimetics (CTM = spheroids + HUVECs) for 10 days under phenylephrine, it was found that CM-derived factors as well as CM contraction increased vascularization which was impaired by VEGF depletion and the use of β -blockers. Stress conditions were resembled by treating mature CTMs with TGF β 2 or hypoxia (0.1% O₂). Whereas TGF β 2 induced vascularization, collagen deposition and EndoMT, hypoxia diminished vascularization but induced fibrosis. Figure is adapted adopted from figure 4H of the submitted manuscript in *Appendix 4*.

3.4. Conclusions and Future Perspectives

The data of the present dissertation provide novel insights in the endothelial cross-talk in the aging heart on both autocrine and paracrine level (Figure 14).

By using bulk RNA seq of ECs derived from young and aged mouse hearts, we identified an autocrine interaction of cardiac ECs upon aging. We documented a dysregulation of the endothelial matrix proteins Lamb1 and Lamb2, showing that the endothelial-derived Lamb1 reduces EC migration, matrix adhesion but contribute to the induction of EndoMT. A novel paracrine cross-talk was discovered between FBs and ECs, by using snRNA seq, in which aged cardiac FBs may reduce endothelial sprouting via serpin signaling. Finally, the use of our novel cardiac tissue mimetic model revealed that upon PE stimulation CMs induce endothelial sprouting via VEGF expression and putatively through mechanical activation via contraction. However, we cannot exclude that CMs express further factors such as matrix proteins which modulate angiogenesis, as well.

Of note, these results reveal certain limitations, since most of the data were raised by *in vitro* studies. Animal models need to be utilized to validate their *in vivo* significance. In this regard, conditional endothelial *Lamb2* or *Lamb1* knockout mice may be a helpful tool to study the impact of laminin in the diseased and aging heart. Likewise, the relevance of serpins in the aging heart might be targeted by *Serpine1*-deficient mice. Given the fact that we found a putative FB-EC paracrine interaction by conditioned media studies *in vitro* does not necessarily mean that this cross-talk spatially happen in the heart. Hence, an aging mouse study with *Serpine* knockout mice may shed light on this interesting point. However, since the generation of transgenic mice, breeding, crossing (also with lineage tracer lines) and aging would take years, both the *Lamb* and *Serpine* knockout studies are beyond the scope of the present dissertation. To bridge the gap between *in vitro* and *in vivo*, the cardiac tissue mimetic model may be used where the FB-CM spheroids might be covered with laminin 421 or 411 before HUVEC addition or *Serpine*-deficient FBs might be used for spheroid formation.

Nevertheless, the results of this thesis provide interesting and novel insights into the cellular interaction within the aging heart. Particularly, the first “atlas” of the aging heart is a rich data source, that provides putative targets for further studies and therapeutic interventions.

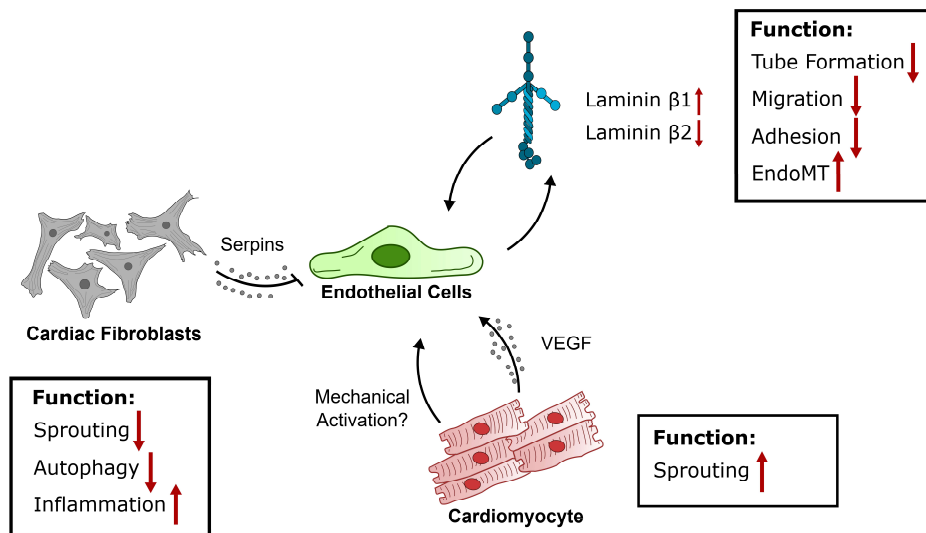


Figure 14: Graphical summary of the present dissertation. Age-dependent changes of endothelial cells can be found on both autocrine and paracrine level. On the one hand, aging shifts the expression of laminin $\beta 2$ to laminin $\beta 1$ in cardiac endothelial cells and thereby controls endothelial functions (tube formation, migration, adhesion and EndoMT) on autocrine level. On the other hand, aging also affects fibroblasts that control angiogenesis, endothelial autophagy and inflammation via the release of serpins and hence control endothelial function on a paracrine level. Paracrine changes can be further studied using artificial cardiac tissue mimetics. By using this platform, it was found, that cardiomyocytes promote endothelial sprouting upon phenylephrine stimulation, by releasing VEGF and putatively by mechanical activation via cardiomyocyte contraction. Parts of this figure were taken from the manuscripts in the *Appendix 1, 3 and 4*.

4 References

1. WHO Report on Cardiovascular diseases (CVDs). (2017).
2. Lakatta, E. G. Journal of Molecular and Cellular Cardiology So ! What ' s aging ? Is cardiovascular aging a disease ? *J. Mol. Cell. Cardiol.* **83**, 1–13 (2015).
3. Lakatta, E. G. & Levy, D. Arterial and cardiac aging: major shareholders in cardiovascular disease enterprises: Part I: aging arteries: a 'set up' for vascular disease. *Circulation* **107**, 139–146 (2003).
4. Schünke, M., Schulte, E. & Schumacher, U. *PROMETHEUS Innere Organe*. (Thieme, 2018).
5. Müller, W. A., Frings, S. & Möhrlen, F. Tier- und Humanphysiologie: Eine Einführung. *Springer Spektrum* **6**, 1–919 (2019).
6. Tammela, T. & Alitalo, K. Lymphangiogenesis : Molecular Mechanisms and Future Promise. *Cell* **140**, 460–476 (2010).
7. Carmeliet, P. & Jain, R. K. Molecular mechanisms and clinical applications of angiogenesis. *Nature* **473**, 298–307 (2011).
8. Aird, W. C. Endothelium and haemostasis. *Hamostaseologie* **35**, 11–16 (2015).
9. Potente, M. & Mäkinen, T. Vascular heterogeneity and specialization in development and disease. *Nat. Publ. Gr.* **18**, 477–494 (2017).
10. Planas-paz, L., Strilic, B. & Breier, G. Mechanoinduction of lymph vessel expansion. *EMBO J.* **31**, 788–804 (2012).
11. Reischauer, S. *et al.* Cloche is a bHLH-PAS transcription factor that drives haemato-vascular specification. *Nat. Publ. Gr.* **535**, 294–298 (2016).
12. Paffett-lugassy, N. *et al.* Heart field origin of great vessel precursors relies on nkx2.5-mediated vasculogenesis. *Nat. Cell Biol.* **15**, 1362–1369 (2014).
13. Proulx, K., Lu, A. & Sumanas, S. Cranial vasculature in zebra fi sh forms by angioblast cluster-derived angiogenesis. *Dev. Biol.* **348**, 34–46 (2010).
14. Herbert, S. P. *et al.* Arterial / Venous Segregation by Selective Cell Sprouting : An Alternative Mode of Blood Vessel Formation. *Science (80-)*. **326**, 294–298 (2010).
15. Lindskog, H. *et al.* Molecular identification of venous progenitors in the dorsal aorta reveals an aortic origin for the cardinal vein in mammals. *Development* **141**, 1120–1128 (2014).

16. Kohli, V., Schumacher, J., Desai, S., Rehn, K. & Sumanas, S. Arterial and Venous Progenitors of the Major Axial Vessels Originate at Distinct Locations. *Dev. Cell* **25**, 196–206 (2014).
17. Marcelo, K., Goldie, L. & Hirschi, K. Regulation of Endothelial Cell Differentiation and Specification. *Circ. Res.* **112**, 1272–1287 (2013).
18. Siekmann, A. F., Standley, C., Fogarty, K. E., Wolfe, S. A. & Lawson, N. D. Chemokine signaling guides regional patterning of the first embryonic artery. *Genes Dev.* **23**, 2272–2277 (2009).
19. Pavel, M. & Rubinsztein, D. C. Mammalian autophagy and the plasma membrane. *FEBS J.* **284**, 672–679 (2017).
20. Potente, M., Gerhardt, H. & Carmeliet, P. Basic and therapeutic aspects of angiogenesis. *Cell* **146**, 873–887 (2011).
21. Blasi, F. & Carmeliet, P. uPAR: a versatile signalling orchestrator. *Nat. Rev.* **3**, 932–943 (2002).
22. Arroyo, A. G. & Iruela-arispe, M. L. Extracellular matrix , inflammation , and the angiogenic response. *Eur. Soc. Cardiol.* **1**, 226–235 (2010).
23. Nyberg, P., Xie, L. & Kalluri, R. Endogenous Inhibitors of Angiogenesis. *Am. Assoc. Cancer Res.* **65**, 3967–3980 (2005).
24. Eilken, H. M. & Adams, R. H. Dynamics of endothelial cell behavior in sprouting angiogenesis. *Curr. Opin. Cell Biol.* **22**, 617–625 (2010).
25. Huang, H., Bhat, A., Woodnutt, G. & Lappe, R. Targeting the ANGPT – Tie2 pathway in malignancy. *Nat. Publ. Gr.* **10**, 575–585 (2010).
26. Thurston, G., Noguera-troise, I. & Yancopoulos, G. D. less tumour growth. *Nat. Rev. Cancer* **7**, 327–331 (2007).
27. Phng, L. & Gerhardt, H. Angiogenesis : A Team Effort Coordinated by Notch. *Dev. Cell* **16**, 196–208 (2009).
28. LeBleu, V. S., Macdonald, B. & Kalluri, R. Structure and function of basement membranes. *Exp. Biol. Med. (Maywood).* **232**, 1121–1129 (2007).
29. Yue, B. Biology of the Extracellular Matrix : An Overview. *J Glaucoma* **23**, 20–23 (2014).
30. Wisdom, B. J. J., Gunwar, S., Hudson, M. D., Noelken, M. E. & Hudson, B. G. Type IV collagen of Engelbreth-Holm-Swarm tumor matrix: identification of constituent chains. *Connect. Tissue Res.* **27**, 225–234 (1992).

31. Lei, H., Kalluri, R., Furth, E. E., Baker, A. H. & Strauss, J. F. 3rd. Rat amnion type IV collagen composition and metabolism: implications for membrane breakdown. *Biol. Reprod.* **60**, 176–182 (1999).
32. Kalluri, R., Hudson, B. G. & Neilson, E. G. Isoform switching of type IV collagen is developmentally arrested in X-linked Alport syndrome leading to increased susceptibility of renal basement membranes to endoproteolysis. Find the latest version : *J. Clin. Invest.* **99**, 2470–2478 (1997).
33. Kahsai, T. Z. *et al.* Seminiferous Tubule Basement Membrane. *J. Biol. Chem.* **272**, 17023–17032 (1997).
34. Gunwar, S. *et al.* Glomerular Basement Membrane. *J. Biol. Chem.* **273**, 8767–8775 (1998).
35. Durbeej, M. Laminins. *Cell Tissue Res.* **339**, 259–268 (2010).
36. Miner, J. H., Li, C., Mudd, J. L., Go, G. & Sutherland, A. E. Compositional and structural requirements for laminin and basement membranes during mouse embryo implantation and gastrulation. *Development* **131**, 2247–2256 (2004).
37. Poschl, E. *et al.* Collagen IV is essential for basement membrane stability but dispensable for initiation of its assembly during early development. *Development* **131**, 1619–1628 (2004).
38. Yao, Y. Laminin: loss-of-function studies. *Cell. Mol. Life Sci.* **74**, 1095–1115 (2017).
39. Burgeson, R. E. *et al.* A New Nomenclature for the Laminins. *Matrix Biol.* **14**, 9–11 (1994).
40. Scheele, S. *et al.* Laminin α 1 globular domains 4–5 induce fetal development but are not vital for embryonic basement membrane assembly. *PNAS* **102**, 1–5 (2005).
41. Edwards, M. M. *et al.* Mutations in Lama1 Disrupt Retinal Vascular Development and Inner Limiting Membrane Formation. *JBC* **285**, 7697–7711 (2010).
42. Aumailley, M. The laminin family. *Cell Adhes. Migr.* **7**, 48–55 (2013).
43. Suzuki, N., Yokoyama, F., Nomizu, M., Suzuki, N. & Yokoyama, F. Functional Sites in the Laminin Alpha Chains Functional Sites in the Laminin Alpha Chains. *Connect. Tissue Res.* **8207**, (2009).
44. Nishiuchi, R. *et al.* Ligand-binding specificities of laminin-binding integrins: A comprehensive survey of laminin–integrin interactions using recombinant α 3h1, α 6h1, α 7h1 and α 6h4 integrins. *Matrix Biol.* **25**, 189–197 (2006).

45. Legate, K. R., Wickström, S. A. & Fässler, R. Genetic and cell biological analysis of integrin outside-in signaling. *Genes Dev.* **23**, 397–418 (2009).
46. Davis, J., Burr, A. R., Davis, G. F., Birnbaumer, L. & Molkenin, J. D. A TRPC6-dependent pathway for myofibroblast transdifferentiation and wound healing in vivo. *Dev. Cell* **23**, 705–715 (2012).
47. Zhu, Y. *et al.* Matrix stiffness modulates the differentiation of neural crest stem cells in vivo. *J. Cell. Physiol.* **234**, 7569–7578 (2019).
48. Hassanisaber, H. *et al.* The effect of substrate bulk stiffness on focal and fibrillar adhesion formation in human abdominal aortic endothelial cells. *Mater. Sci. Eng. C. Mater. Biol. Appl.* **98**, 572–583 (2019).
49. Lusis, A. J. Atherosclerosis. *Nature* **407**, 233–241 (2000).
50. Tabas, I., García-cardena, G. & Owens, G. K. Recent insights into the cellular biology of atherosclerosis. *JCB* **209**, 13–22 (2015).
51. Gimbrone, M. A., Topper, J. N., Nagel, T., Anderson, K. R. & Garcia-cardena, G. Endothelial Dysfunction, Hemodynamic Forces, and Atherogenesis. *Ann NY Acad Sci.* **902**, 230–239 (2000).
52. Mozaffarian, D. *et al.* Heart Disease and Stroke Statistics-2016 Update: A Report From the American Heart Association. *Circulation* **133**, e38–360 (2016).
53. Nielsen, S. H. *et al.* Understanding cardiac extracellular matrix remodeling to develop biomarkers of myocardial infarction outcomes. *Matrix Biol.* **75–76**, 43–57 (2019).
54. Trial, J. & Cieslik, K. A. Extracellular Matrix in Cardiovascular Pathophysiology Changes in cardiac resident fibroblast physiology and phenotype in aging. *J Physiol Hear.* **315**, H754–H755 (2018).
55. Ertl, G. & Frantz, S. Healing after myocardial infarction. *Cardiovasc. Res.* **66**, 22–32 (2005).
56. Benjamin, E. J. *et al.* Heart Disease and Stroke Statistics-2017 Update: A Report From the American Heart Association. *Circulation* **135**, e146–e603 (2017).
57. Nickel, A. & Lo, J. Myocardial energetics in heart failure. *Basic Res Cardiol* **108**, 358 (2013).
58. *Chronic Heart Failure: National Clinical Guideline for Diagnosis and Management in Primary and Secondary Care.* (National Clinical Guideline Center (UK), 2010).

59. Hoppe, U. C. & Erdmann, E. [Guidelines for the treatment of chronic heart failure. Issued by the Executive Committee of the German Society of Cardiology--Heart and Circulation Research, compiled on behalf of the Commission of Clinical Cardiology in cooperation with Pharmaceutical Commission of the German Physicians' Association]. *Z. Kardiol.* **90**, 218–237 (2001).
60. Jackson, G., Gibbs, C. R., Davies, M. K. & Lip, G. Y. ABC of heart failure. Pathophysiology. *BMJ* **320**, 167–170 (2000).
61. Upadhyya, B., Kitzman, D. W. & Section, C. M. Heart Failure With Preserved Ejection Fraction in Older Adult. *Hear. Fail Clin.* **13**, 485–502 (2018).
62. Pinto, A. R. *et al.* Revisiting Cardiac Cellular Composition. *Circ. Res.* **118**, 400–409 (2016).
63. Hsieh, P. C. H., Davis, M. E., Lisowski, L. K. & Lee, R. T. Endothelial-cardiomyocyte interactions in cardiac development and repair. *Annu. Rev. Physiol.* **1**, 51–66 (2006).
64. Perbellini, F., Watson, S. A., Bardi, I. & Terracciano, C. M. Heterocellularity and Cellular Cross-Talk in the Cardiovascular System. *Front. Cardiovasc. Med.* **5**, 1–11 (2018).
65. Gödecke, A. *et al.* Inotropic response to β -adrenergic receptor stimulation and anti-adrenergic effect of ACh in endothelial NO synthase-deficient mouse hearts. *J. Physiol.* **532**, 195–204 (2001).
66. Warren, J. B. & Williams, J. Nitric oxide attenuates cardiac myocyte contraction. *Am. J. Pathol.* **265**, H176–H182 (1993).
67. Cifarelli, V. *et al.* FOXO1 Mediates the Autocrine Effect of Endothelin-1 on Endothelial Cell Survival. *Mol Endocrinol* **26**, 1213–1224 (2012).
68. Wermuth, P. J., Li, Z., Mendoza, F. A. & Jimenez, S. A. Stimulation of Transforming Growth Factor- Transition and Tissue Fibrosis by Endothelin-1 (ET-1): A Novel Profibrotic Effect of ET-1. *PLoS One* **1**, 1–21 (2016).
69. Kuramochi, Y. *et al.* Cardiac Endothelial Cells Regulate Reactive Oxygen Species-induced Cardiomyocyte Apoptosis through. *J. Biol. Chem.* **279**, 51141–51147 (2004).
70. Narmoneva, D. A., Vukmirovic, R., Davis, M. E., Kamm, R. D. & Lee, R. T. Endothelial Cells Promote Cardiac Myocyte Survival and Implications for Cardiac Regeneration. *Circulation* **110**, 962–968 (2004).
71. Ivey, M. J. & Tallquist, M. D. Defining the Cardiac Fibroblast. *Circ. J.* **80**, (2016).

72. Perbellini, F. *et al.* Investigation of cardiac fibroblasts using myocardial slices. *Cardiovasc. Res.* **114**, 77–89 (2018).
73. Lu, P., Takai, K., Weaver, V. M. & Werb, Z. Extracellular Matrix Degradation and Remodeling in Development and Disease. *Cold Spring Harb Perspect Biol.* **3**, 1–25 (2019).
74. Civitarese, R. A., Kapus, A., Mcculloch, C. A. & Connelly, K. A. Role of integrins in mediating cardiac fibroblast – cardiomyocyte cross talk : a dynamic relationship in cardiac biology and pathophysiology. *Basic Res. Cardiol.* **112**, 1–17 (2017).
75. Fibrillation, A. *et al.* Somatic mutations in the connexin 40 gene (GJA5) in atrial fibrillation. *N. Engl. J. Med.* **354**, 2677–2688 (2006).
76. Hatcher, C. J. & Basson, C. T. Disrupted intercalated discs. Is kindlin-2 required? *Circ. Res.* **102**, 392–394 (2008).
77. Camelliti, P., Devlin, G. P., Matthews, K. G., Kohl, P. & Green, C. R. Spatially and temporally distinct expression of fibroblast connexins after sheep ventricular infarction. *Cardiovasc. Res.* **62**, 415–425 (2004).
78. Quinn, T. A., Camelliti, P., Rog-zielinska, E. A., Siedlecka, U. & Poggioli, T. Electrotonic coupling of excitable and nonexcitable cells in the heart revealed by optogenetics. *PNAS* **113**, 14852–14857 (2016).
79. Porter, K. E. & Turner, N. A. Pharmacology & Therapeutics Cardiac fibroblasts : At the heart of myocardial remodeling. *Pharmacol. Ther.* **123**, 255–278 (2009).
80. Bergmann, O. *et al.* Dynamics of Cell Generation and Turnover in the Article Dynamics of Cell Generation and Turnover in the Human Heart. *Cell* **161**, 1566–1575 (2015).
81. Pinto, A. R., Chandran, A., Rosenthal, N. A. & Godwin, J. W. Isolation and analysis of single cells from the mouse heart. *J. Immunol. Methods* **393**, 74–80 (2013).
82. Kostetskii, I. *et al.* Induced Deletion of the N-Cadherin Gene in the Heart Leads to Dissolution of the Intercalated Disc Structure. *Circ. Res.* **96**, 346–354 (2005).
83. Roy, A, Fields WC, Rocha-Resende C, Resende PR, Guatimosim S, Prado VF, Gros R, P. M. Cardiomyocyte-secreted acetylcholine is required for maintenance of homeostasis in the heart. *FASEB J.* **27**, 5072–5082 (2013).
84. Yamauchi-Takahara K, Ihara Y, Ogata A, Yoshizaki K, Azuma J, K. T. Hypoxic stress induces cardiac myocyte-derived interleukin-6. *Circulation* **91**, 1520–1524 (1995).

85. Yu, X. *et al.* Journal of Molecular and Cellular Cardiology Mechanism of TNF- α autocrine effects in hypoxic cardiomyocytes : Initiated by hypoxia inducible factor 1 α , presented by exosomes. *J. Mol. Cell. Cardiol.* **53**, 848–857 (2012).
86. Jug, B., Guži, B., Vene, N., Šebeštjen, M. & Šabovi, M. Interleukin-6 is a stronger prognostic predictor than high-sensitive C-reactive protein in patients with chronic stable heart failure. *Hear. Vessel.* **24**, 271–276 (2009).
87. Deswal, A. *et al.* Cytokines and cytokine receptors in advanced heart failure: an analysis of the cytokine database from the Vesnarinone trial (VEST). *Circulation* **103**, 2055–2059 (2001).
88. Leucker, T. M. *et al.* Journal of Molecular and Cellular Cardiology Endothelial – cardiomyocyte crosstalk enhances pharmacological cardioprotection. *J. Mol. Cell. Cardiol.* **51**, 803–811 (2011).
89. Giordano, F. J. *et al.* A cardiac myocyte vascular endothelial growth factor paracrine pathway is required to maintain cardiac function. *PNAS* **98**, 5780–5785 (2001).
90. Lindsey, M. L., Yabluchanskiy, A., Zouein, F. A. & Jin, Y. A Novel Collagen Matricryptin Reduces Left Ventricular Dilation Post-Myocardial Infarction by Promoting Scar Formation and Angiogenesis. *JACC* **66**, (2015).
91. Barallobre-barreiro, J., Lynch, M., Yin, X. & Mayr, M. Systems biology — opportunities and challenges : the application of proteomics to study the cardiovascular extracellular matrix. *Cardiovasc. Res.* **44**, 626–636 (2016).
92. Goldsmith, E. C., Bradshaw, A. D., Zile, M. R. & Spinale, F. G. Myocardial fibroblast – matrix interactions and potential therapeutic targets. *J. Mol. Cell. Cardiol.* **70**, 92–99 (2014).
93. Bosman, F. T. & Stamenkovic, I. Functional structure and composition of the extracellular matrix. *J Pathol* **200**, 423–428 (2003).
94. Hägg, P. *et al.* Type XIII collagen : a novel cell adhesion component present in a range of cell-matrix adhesions and in the intercalated discs between cardiac muscle cells. *Matrix Biol.* **19**, 727–742 (2001).
95. Zile, M. R. & Baicu, C. F. Biomarkers of Diastolic Dysfunction and Myocardial Fibrosis : Application to Heart Failure with a Preserved Ejection Fraction. *J Cardiovasc. Trans. Res.* **6**, 501–515 (2013).
96. Casscells, W., Kimura, H., Julian, A., Yu, Z. & Ferranist, V. J. Immunohistochemical Study of Fibronectin in Experimental Myocardial Infarction. *Am. J. Pathol.* **13**, 801–810 (1990).

97. Arslan, F. *et al.* Lack of Fibronectin-EDA Promotes Survival and Prevents Adverse Remodeling and Heart Function Deterioration After Myocardial Infarction. *Circ. Res.* **108**, 582–592 (2011).
98. Aurora, A. B. *et al.* Macrophages are required for neonatal heart regeneration. *JCI* **124**, 1382–1392 (2014).
99. Porrello, E. . R. *et al.* Transient regenerative potential of the neonatal mouse heart. *Science (80-.)*. **331**, 1078–1080 (2011).
100. Frangogiannis, N. G. The inflammatory response in myocardial injury, repair and remodeling. *Nat. Rev. Cardiol.* **11**, 255–265 (2015).
101. Rohani, M. & Parks, W. Matrix remodeling by MMPs during wound repair. *Matrix Biol.* **44–46**, 113–121 (2015).
102. Cleutjens, J., Kandala, J., Guarda, E., Guntaka, R. & Weber, K. Regulation of collagen degradation in the rat myocardium after infarction. *J Mol Cell Cardiol* **27**, 1281–1292 (1995).
103. Saxena, A. *et al.* Regulatory T cells are recruited in the infarcted mouse myocardium and may modulate fibroblast phenotype and function. *Am J Physiol Hear. Circ Physiol* **307**, H1233–H1242 (2014).
104. Heidt, T. *et al.* Differential contribution of monocytes to heart macrophages in steady-state and after myocardial infarction. *Circ. Res.* **115**, 284–295 (2014).
105. Fu, X. *et al.* Specialized fibroblast differentiated states underlie scar formation in the infarcted mouse heart Graphical abstract Find the latest version : Specialized fibroblast differentiated states underlie scar formation in the infarcted mouse heart. *JCI* **128**, 2127–2143 (2018).
106. Gjorevski, N. *et al.* Designer matrices for intestinal stem cell and organoid culture. *Nat. Publ. Gr.* **539**, 560–564 (2016).
107. Partridge, L. & Brüning, J. C. Forkhead transcription factors and ageing. *Oncogene* **27**, 2351–2363 (2008).
108. Critchley DR. Focal adhesions - the cytoskeletal connection. *Curr. Opin. Cell Biol.* **12**, 133–139 (2000).
109. Chrzanowska-Wodnicka, M. & Burridge, K. Rho-stimulated contractility drives the formation of stress fibers and focal adhesions. *J Cell Biol* **133**, 1403–1415 (1996).
110. Adapala, R. *et al.* TRPV4 channels mediate cardiac fibroblast differentiation by integrating mechanical and soluble signals. *J Mol Cell Cardiol* **54**, 45–52 (2013).

111. Kobayashi, K. *et al.* IRAK-M is a negative regulator of Toll-like receptor signaling. *Cell* **110**, 191–202 (2002).
112. Chen, W. *et al.* Endogenous IRAK-M attenuates postinfarction remodeling through effects on macrophages and fibroblasts. *ATVB* **32**, 2598–2608 (2012).
113. Bischof, J. Endothelial-to-Mesenchymal Transition. *Circ. Res.* **124**, 1163–1165 (2019).
114. López-Otín, C., Blasco, M. A., Partridge, L., Serrano, M. & Kroemer, G. The hallmarks of aging. *Cell* **153**, (2013).
115. Barbosa, M. C., Grosso, R. A. & Fader, C. M. Hallmarks of Aging: An Autophagic Perspective. *Front. Endocrinol. (Lausanne)*. **9**, 790 (2018).
116. Disease, C. So! What's aging? Is cardiovascular aging a disease? Edward. *J Mol Cell Cardiol* **8150**, 1–13 (2015).
117. Wahab, A. Theories of Aging. *Int. J. Indian Psychol.* **4**, 15–22 (2017).
118. Lipsky, M. S. & King, M. Biological theories of aging. *Dis. Mon.* **61**, 460–466 (2015).
119. Obas, V. & Vasan, R. S. The aging heart. *Clinical Sci.* **132**, 1367–1382 (2018).
120. McManus, D. D. *et al.* Longitudinal Tracking of Left Atrial Diameter Over the Adult Life Course : Clinical Correlates in the Community. *Circulation* **121**, 667–674 (2010).
121. Volpe, G. J. *et al.* Evaluation of Age-Related Interstitial Myocardial Fibrosis With Cardiac Magnetic Resonance Contrast-Enhanced T 1 Mapping MESA (Multi-Ethnic Study of Atherosclerosis). *J. Am. Coll. Cardiol.* **62**, (2013).
122. Nakayama, H., Nishida, K. & Otsu, K. Macromolecular Degradation Systems and Cardiovascular Aging. *Circ. Res.* **118**, 1577–1592 (2016).
123. Upadhyya, B., Taffet, G. E., Ping, C. & Kitzman, D. W. Heart failure with preserved ejection fraction in the elderly : scope of the problem. *J. Mol. Cell. Cardiol.* **83**, 73–87 (2015).
124. lung, B. & Vahanian, A. Epidemiology of Acquired Valvular Heart Disease. *Can. J. Cardiol.* **30**, 962–970 (2014).
125. Bhatia, N., Basra, S., Skolnick, A. & Wenger, N. Aortic valve disease in the older adult. *J Geriatr Cardiol* **13**, 941–944 (2016).
126. Sud, K. *et al.* Degenerative Mitral Stenosis: Unmet Need for Percutaneous Interventions. *Circulation* **133**, 1594–1604 (2016).

127. Fei, J., Cook, C., Blough, E. & Santanam, N. Age and sex mediated changes in epicardial fat adipokines. *Atherosclerosis* **212**, 488–494 (2010).
128. Nalliah, C. J., Sanders, P., Kottkamp, H. & Kalman, J. M. The role of obesity in atrial fibrillation. *Eur. Heart J.* **37**, 1565–1572 (2016).
129. Jakovljevic, D. G. Physical activity and cardiovascular aging: Physiological and molecular insights. *Exp. Gerontol.* **109**, 67–74 (2018).
130. Rizzoni, D. *et al.* Vascular Aging and Disease of the Small Vessels. *High Blood Press. Cardiovasc. Prev.* **17**, 1–7 (2019).
131. Rivard, A. *et al.* Age-dependent impairment of angiogenesis. *Circulation* **99**, 111–120 (1999).
132. Jiang, F. Autophagy in vascular endothelial cells. *Clin. Exp. Pharmacol. Physiol.* **43**, 1021–1028 (2016).
133. Bjedov, I. *et al.* Mechanisms of life span extension by rapamycin in the fruit fly *Drosophila melanogaster*. *Cell Metab* **11**, 35–46 (2010).
134. Shirakabe, A., Ikeda, Y., Sciarretta, S., Zablocki, D. & Sadoshima, J. Aging and Autophagy in the Heart. *Circ. Res.* **118**, 1563–1576 (2016).
135. Rubinsztein, D., Mariño, G. & Kroemer, G. Autophagy and Aging. *Cell* **146**, 682–695 (2011).
136. Sasaki, Y., Ikeda, Y., Iwabayashi, M., Akasaki, Y. & Ohishi, M. The Impact of Autophagy on Cardiovascular Senescence and Diseases. *Int. Hear. J. Assoc.* **58**, 666–673 (2017).
137. Oyabu, J. *et al.* Autophagy-mediated degradation is necessary for regression of cardiac hypertrophy during ventricular unloading. *Biochem. Biophys. Res. Commun.* **441**, 787–792 (2013).
138. Taneike, M. *et al.* Inhibition of autophagy in the heart induces age-related cardiomyopathy. *Autophagy* **6**, 600–606 (2010).
139. Harman, D. Aging: a theory based on free radical and radiation chemistry. *J Gerontol* **11**, 298–300 (1956).
140. Brown, D. & Griendling, K. Regulation of Signal Transduction by Reactive Oxygen Species in the Cardiovascular System. *Circ. Res.* **116**, 531–549 (2015).
141. Fyhrquist, F., Saijonmaa, O. & Strandberg, T. The roles of senescence and telomere shortening in cardiovascular disease. *Nat. Rev. Cardiol.* **10**, 274–283 (2013).

142. Sack, M., Fyhrquist, F., Saijonmaa, O., Fuster, V. & Kovacic, J. Basic Biology of Oxidative Stress and the Cardiovascular System: Part 1 of a 3-Part Series. *J. Am. Coll. Cardiol.* **70**, 196–211 (2017).
143. North, B. J. & Sinclair, D. A. The intersection between aging and cardiovascular disease. *Circ. Res.* **110**, 1097–1108 (2012).
144. Lee WS, Kim, J. Insulin-like growth factor-1 signaling in cardiac aging. *Biochim. Biophys. - Mol. Basis Dis.* **1864**, 1931–1938 (2018).
145. Milman, S. *et al.* Low insulin-like growth factor-1 level predicts survival in humans with exceptional longevity. *Aging Cell* **13**, 769–771 (2018).
146. Vasan, R. S. *et al.* Serum insulin-like growth factor I and risk for heart failure in elderly individuals without a previous myocardial infarction: the Framingham Heart Study. *Ann. Intern. Med.* **139**, 642–648 (2003).
147. Higashi, Y., Sukhanov, S., Anwar, A., Shai, S.-Y. and Delafontaine, P. Aging, Atherosclerosis, and IGF-1. *J. Gerontol.* **67**, 626–639 (2012).
148. Murtha, L. A. *et al.* The Processes and Mechanisms of Cardiac and Pulmonary Fibrosis . *Frontiers in Physiology* **8**, 777 (2017).
149. Misaka, T. *et al.* Senescence marker protein 30 inhibits angiotensin II-induced cardiac hypertrophy and diastolic dysfunction. *Biochem. Biophys. Res. Commun.* **439**, 142–147 (2013).
150. Noppe, G. *et al.* Reduced scar maturation and contractility lead to exaggerated left ventricular dilation after myocardial infarction in mice lacking AMPKalpha1. *J. Mol. Cell. Cardiol.* **74**, 32–43 (2014).
151. Daskalopoulos, E. P., Dufeys, C., Bertrand, L., Beauloye, C. & Horman, S. AMPK in cardiac fibrosis and repair: Actions beyond metabolic regulation. *J. Mol. Cell. Cardiol.* **91**, 188–200 (2016).
152. Hermida, N. *et al.* HMGCoA reductase inhibition reverses myocardial fibrosis and diastolic dysfunction through AMP-activated protein kinase activation in a mouse model of metabolic syndrome. *Cardiovasc. Res.* **99**, 44–54 (2013).
153. Hardman, S. E., Hall, D. E., Cabrera, A. J., Hancock, C. R. & Thomson, D. The effects of age and muscle contraction on AMPK activity and heterotrimer composition. *Exp. Gerontol.* **55**, 120–128 (2014).

154. Salminen, A. & Kaarniranta, K. AMP-activated protein kinase (AMPK) controls the aging process via an integrated signaling network. *Ageing Res. Rev* **11**, 230–241 (2012).
155. Cieslik, K. *et al.* AICAR-dependent AMPK activation improves scar formation in the aged heart in a murine model of reperfused myocardial infarction. *J Mol Cell Cardiol* **63**, 26–36 (2013).
156. Bujak, M. *et al.* Aging-related defects are associated with adverse cardiac remodeling in a mouse model of reperfused myocardial infarction. *J Am Coll Cardiol*. **51**, 1384–1392 (2008).
157. Yabluchanskiy, A. *et al.* Myocardial Infarction Superimposed on Aging: MMP-9 Deletion Promotes M2 Macrophage Polarization. *J. Gerontol. A. Biol. Sci. Med. Sci.* **71**, 475–483 (2016).
158. Cieslik, K., Trial, J. & Entman, M. Defective myofibroblast formation from mesenchymal stem cells in the aging murine heart rescue by activation of the AMPK pathway. *Am J Pathol* **179**, 1792–1806 (2011).
159. Shimazaki, M. *et al.* Periostin is essential for cardiac healing after acute myocardial infarction. *J Exp Med* **205**, 295–303 (2008).
160. Gabbiani, G., Ryan, G. & Majne, G. Presence of modified fibroblasts in granulation tissue and their possible role in wound contraction. *Experientia* **5**, 549–550 (1971).
161. Michalik, M., Wójcik, K., Paw, M., Wnuk, D. & Koczurkiewicz, P. Fibroblast-to-myofibroblast transition in bronchial asthma. *Cell. Mol. Life Sci.* **75**, 3943–3961 (2018).
162. Hinz, B., Pittet, P., Smith-Clerc, J., Chaponnier, C. & Meister, J. Myofibroblast development is characterized by specific cell-cell adherens junctions. *Mol Biol Cell* **15**, 4310–4320 (2004).
163. Tomasek, J., Gabbiani, G., Hinz, B., Chaponnier, C. & Brown, R. Myofibroblasts and mechano-regulation of connective tissue remodelling. *Nat Rev Mol Cell Biol* **3**, 349–363 (2002).
164. Píera-velázquez, S. & Jimenez, S. A. Endothelial to Mesenchymal Transition: Role in Physiology and in the Pathogenesis of Human Diseases. *Physiol. Rev.* **99**, 1281–1324 (2019).
165. Liu, L., Chen, J., Sun, L. & Xu, Y. Rho1 promotes hypoxia induced endothelial-to-mesenchymal transition by activating WDR5 expression. *J Cell Biochem* **119**, 3384–3393 (2018).
166. Nakao, A. *et al.* Identification of Smad7, a TGFbeta- inducible antagonist of TGF-beta signalling. *Nature* **389**, 631–635 (1997).
167. Imamura, T. *et al.* Smad6 inhibits signalling by the TGF-beta superfamily. *Nature* **389**, 622–626 (1997).

168. Miyazawa, K. & Miyazono, K. Regulation of TGF-beta Family Signaling by Inhibitory Smads. *Cold Spring Harb Perspect Biol* **9**, 1–27 (2017).
169. Nikolova, G., Strilic, B. & Lammert, E. The vascular niche and its basement membrane. *Trends Cell Biol.* **17**, (2006).
170. Sixt, M. *et al.* Roles in T Cell Recruitment Across the Blood – Brain Barrier in Experimental Autoimmune Encephalomyelitis. *J. Cell Biol.* **153**, 933–945 (2001).
171. Ding, B. *et al.* Endothelial-derived inductive angiocrine signals initiate and sustain regenerative lung alveolarization. *Cell* **147**, 539–553 (2012).
172. Aicher, A. *et al.* Essential role of endothelial nitric oxide synthase for mobilization of stem and progenitor cells. *Nat Med* **9**, 1370–1376 (2003).
173. Itkin, T. *et al.* Distinct bone marrow blood vessels differentially regulate haematopoiesis. *Nat. Publ. Gr.* **532**, 323–328 (2016).
174. Ding, B. *et al.* Inductive angiocrine signals from sinusoidal endothelium are required for liver regeneration. *Nature* **468**, 310–315 (2011).
175. Hu, J. *et al.* Endothelial Cell-Derived Angiopoietin-2 Controls Liver Regeneration as a Spatiotemporal Rheostat. *Science (80-.).* **343**, 146–419 (2014).
176. Manavski, Y. *et al.* Endothelial transcription factor KLF2 negatively regulates liver regeneration via induction of activin A. *Proc. Natl. Acad. Sci.* **114**, 3993–3998 (2017).
177. Molenaar, B. & Rooij, E. Van. Time to Dive Deeper Magnifying Our View on Cardiac. *Circ. Res.* **123**, 1033–1035 (2018).
178. Ackers-Johnson, M., Tan, W. L. W. & Foo, R. S.-Y. Following hearts, one cell at a time: recent applications of single-cell RNA sequencing to the understanding of heart disease. *Nat. Commun.* **9**, 4434 (2018).
179. Skelly, D. A. *et al.* Single-Cell Transcriptional Profiling Reveals Cellular Diversity and Intercommunication in the Mouse Heart. *Cell Rep.* **22**, 600–610 (2018).
180. Farbehi, N. *et al.* Single-cell expression profiling reveals dynamic flux of cardiac stromal, vascular and immune cells in health and injury. *Elife* **8**, e43882 (2019).
181. Churko, J. M. *et al.* Defining human cardiac transcription factor hierarchies using integrated single-cell heterogeneity analysis. *Nat. Commun.* **9**, 4906 (2018).

-
182. Hu, P., Liu, J., Zhao, J., Wilkins, B. J. & Lupino, K. Single-nucleus transcriptomic survey of cell diversity and functional maturation in postnatal mammalian hearts. *Genes Dev.* **32**, 1344–1357 (2018).
183. Ramilowski, J. A. *et al.* A draft network of ligand–receptor-mediated multicellular signalling in human. *Nat. Commun.* **6**, 7866 (2015).
184. Iruela-Arispe, M. L., Diglio, C. A. & Sage, E. H. Modulation of extracellular matrix proteins by endothelial cells undergoing angiogenesis in vitro. *Arterioscler. Thromb. A J. Vasc. Biol.* **11**, 805–815 (1991).
185. Frieser, M. *et al.* Cloning of the mouse laminin alpha 4 cDNA. Expression in a subset of endothelium. *Eur. J. Biochem.* **246**, 727–735 (1997).
186. Wagner, J. U. G. *et al.* Switch in Laminin β 2 to Laminin β 1 Isoforms During Aging Controls Endothelial Cell Functions. *Arterioscler. Thromb. Vasc. Biol.* **38**, 1170–1177 (2018).
187. Fleenor, B. S., Marshall, K. D., Rippe, C. & Seals, D. R. Replicative aging induces endothelial to mesenchymal transition in human aortic endothelial cells: potential role of inflammation. *J. Vasc. Res.* **49**, 59–64 (2012).
188. Evrard, S. M. *et al.* Endothelial to mesenchymal transition is common in atherosclerotic lesions and is associated with plaque instability. *Nat. Commun.* **7**, 11853 (2016).
189. Libby, P. & Pasterkamp, G. Requiem for the ‘vulnerable plaque’. *Eur. Heart J.* **36**, 2984–2987 (2015).
190. Carlson, T. R., Hu, H., Braren, R., Kim, Y. H. & Wang, R. A. Cell-autonomous requirement for beta1 integrin in endothelial cell adhesion, migration and survival during angiogenesis in mice. *Development* **135**, 2193–2202 (2008).
191. Zeisberg, E. M. *et al.* Endothelial-to-mesenchymal transition contributes to cardiac fibrosis. *Nat. Med.* **13**, 952–961 (2007).
192. Chen, P. Y. *et al.* Endothelial-to-mesenchymal transition drives atherosclerosis progression. *J. Clin. Invest.* **125**, 4514–4528 (2015).
193. Welch-Reardon, K. M., Wu, N. & Hughes, C. C. W. A role for partial endothelial-mesenchymal transitions in angiogenesis? *Arterioscler. Thromb. Vasc. Biol.* **35**, 303–308 (2015).
194. Chistiakov, D. A., Melnichenko, A. A., Myasoedova, V. A., Grechko, A. V & Orekhov, A. N. Thrombospondins: A Role in Cardiovascular Disease. *Int. J. Mol. Sci.* **18**, 1–29 (2017).

195. Chen, P. Y. *et al.* FGF Regulates TGF- β Signaling and Endothelial-to-Mesenchymal Transition via Control of let-7 miRNA Expression. *Cell Rep.* **2**, 1684–1696 (2012).
196. Miner, J. H. & Yurchenco, P. D. Laminin functions in tissue morphogenesis. *Annu. Rev. Cell Dev. Biol.* **20**, 255–284 (2004).
197. Noakes, P. G., Gautam, M., Mudd, J., Sanes, J. R. & Merlie, J. P. Aberrant differentiation of neuromuscular junctions in mice lacking α -laminin/laminin β 2. *Nature* **374**, 258–262 (1995).
198. Noakes, P. G. *et al.* The renal glomerulus of mice lacking α -laminin/laminin β 2: nephrosis despite molecular compensation by laminin β 1. *Nat. Genet.* **10**, 400–406 (1995).
199. Libby, R. T., Lavalley, C. R., Balkema, G. W., Brunken, W. J. & Hunter, D. D. Disruption of Laminin β 2 Chain Production Causes Alterations in Morphology and Function in the CNS. *J. Neurosci.* **19**, 9399 LP – 9411 (1999).
200. Paneni, F., Diaz Canestro, C., Libby, P., Luscher, T. F. & Camici, G. G. The Aging Cardiovascular System: Understanding It at the Cellular and Clinical Levels. *J. Am. Coll. Cardiol.* **69**, 1952–1967 (2017).
201. Eisenberg, T. *et al.* Cardioprotection and lifespan extension by the natural polyamine spermidine. *Nat. Med.* **22**, 1428–1438 (2016).
202. Ferrari, A. U., Radaelli, A. & Centola, M. Invited review: aging and the cardiovascular system. *J. Appl. Physiol.* **95**, 2591–2597 (2003).
203. Swirski, F. K. & Nahrendorf, M. Cardioimmunology: the immune system in cardiac homeostasis and disease. *Nat. Rev. Immunol.* **18**, 733–744 (2018).
204. van der Maaten, L. & Hinton, G. Visualizing Data using t-SNE. *J. Mach. Learn. Res.* **9**, 2079–2605 (2008).
205. Schaum, N. *et al.* Single-cell transcriptomics of 20 mouse organs creates a Tabula Muris. *Nature* **562**, 367–372 (2018).
206. Chen, W. & Frangogiannis, N. G. The role of inflammatory and fibrogenic pathways in heart failure associated with aging. *Heart Fail. Rev.* **15**, 415–422 (2010).
207. La Manno, G. *et al.* RNA velocity of single cells. *Nature* **560**, 494–498 (2018).
208. Albig, A. R., Neil, J. R. & Schiemann, W. P. Fibulins 3 and 5 Antagonize Tumor Angiogenesis In vivo. *Cancer Res.* **66**, 2621 LP – 2629 (2006).

-
209. Law, R. H. P. *et al.* An overview of the serpin superfamily. *Genome Biol.* **7**, 216 (2006).
210. Pillai, I. C. L. *et al.* Cardiac Fibroblasts Adopt Osteogenic Fates and Can Be Targeted to Attenuate Pathological Heart Calcification. *Cell Stem Cell* **20**, 218–232.e5 (2017).
211. Trial, J., Heredia, C. P., Taffet, G. E., Entman, M. L. & Cieslik, K. A. Dissecting the role of myeloid and mesenchymal fibroblasts in age-dependent cardiac fibrosis. *Basic Res. Cardiol.* **112**, 34 (2017).
212. Vaughan, D. E., Rai, R., Khan, S. S., Eren, M. & Ghosh, A. K. Plasminogen Activator Inhibitor-1 Is a Marker and a Mediator of Senescence. *Arterioscler. Thromb. Vasc. Biol.* **37**, 1446–1452 (2017).
213. Rabieian, R. *et al.* Plasminogen Activator Inhibitor Type-1 as a Regulator of Fibrosis. *J. Cell. Biochem.* **119**, 17–27 (2018).
214. Khan, S. S. *et al.* A null mutation in *SERPINE1* protects against biological aging in humans. *Sci. Adv.* **3**, eaao1617 (2017).
215. Lim, S. L., Lam, C. S. P., Segers, V. F. M., Brutsaert, D. L. & De Keulenaer, G. W. Cardiac endothelium–myocyte interaction: clinical opportunities for new heart failure therapies regardless of ejection fraction. *Eur. Heart J.* **36**, 2050–2060 (2015).
216. Gourdie, R. G., Dimmeler, S. & Kohl, P. Novel therapeutic strategies targeting fibroblasts and fibrosis in heart disease. *Nat. Rev. Drug Discov.* **15**, 620 (2016).
217. del Álamo, J. C. *et al.* High throughput physiological screening of iPSC-derived cardiomyocytes for drug development. *Biochim. Biophys. Acta - Mol. Cell Res.* **1863**, 1717–1727 (2016).
218. Jabs, J. *et al.* Screening drug effects in patient-derived cancer cells links organoid responses to genome alterations. *Mol. Syst. Biol.* **13**, 955 (2017).
219. Toru, O., Hiroshi, A., T., N. A. & Issei, K. Angiogenesis and Cardiac Hypertrophy. *Circ. Res.* **114**, 565–571 (2014).
220. Shiojima, I. *et al.* Disruption of coordinated cardiac hypertrophy and angiogenesis contributes to the transition to heart failure. *J. Clin. Invest.* **115**, 2108–2118 (2005).
221. Daly, C. *et al.* Angiopoietin-2 functions as an autocrine protective factor in stressed endothelial cells. *Proc. Natl. Acad. Sci.* **103**, 15491 LP – 15496 (2006).
222. Y., S. S., Alejandro, B., Juan, M.-S. & R., E. E. Primary Monocytes Regulate Endothelial Cell Survival Through Secretion of Angiopoietin-1 and Activation of Endothelial Tie2. *Arterioscler.*

- Thromb. Vasc. Biol.* **31**, 870–875 (2011).
223. Palmer, R. M. J., Ashton, D. S. & Moncada, S. Vascular endothelial cells synthesize nitric oxide from L-arginine. *Nature* **333**, 664–666 (1988).
224. Dougherty, J. A. *et al.* Extracellular Vesicles Released by Human Induced-Pluripotent Stem Cell-Derived Cardiomyocytes Promote Angiogenesis . *Frontiers in Physiology* **9**, 1794 (2018).
225. Rafii, S., Butler, J. M. & Ding, B.-S. Angiocrine functions of organ-specific endothelial cells. *Nature* **529**, 316 (2016).
226. Augustin, H. G. & Koh, G. Y. Organotypic vasculature: From descriptive heterogeneity to functional pathophysiology. *Science (80-.)*. **357**, eaal2379 (2017).
227. Yosif, M. *et al.* Clonal Expansion of Endothelial Cells Contributes to Ischemia-Induced Neovascularization. *Circ. Res.* **122**, 670–677 (2018).
228. Tang, Y., Nyengaard, J. R., Andersen, J. B., Baandrup, U. & Gundersen, H. J. G. The Application of Stereological Methods for Estimating Structural Parameters in the Human Heart. *Anat. Rec.* **292**, 1630–1647 (2009).
229. Bergmann, O. *et al.* Dynamics of Cell Generation and Turnover in the Human Heart. *Cell* **161**, 1566–1575 (2015).
230. Kim, J. J., Hou, L. & Huang, N. F. Vascularization of three-dimensional engineered tissues for regenerative medicine applications. *Acta Biomater.* **41**, 17–26 (2016).
231. N., H. M., Arne, H. & Thomas, E. Cardiac Tissue Engineering. *Circ. Res.* **114**, 354–367 (2014).
232. Kolesky, D. B., Homan, K. A., Skylar-Scott, M. A. & Lewis, J. A. Three-dimensional bioprinting of thick vascularized tissues. *Proc. Natl. Acad. Sci.* **113**, 3179 LP – 3184 (2016).
233. Oren, C. *et al.* Tissue Engineering of Vascularized Cardiac Muscle From Human Embryonic Stem Cells. *Circ. Res.* **100**, 263–272 (2007).
234. Valarmathi, M. T., Fuseler, J. W., Davis, J. M. & Price, R. L. A Novel Human Tissue-Engineered 3-D Functional Vascularized Cardiac Muscle Construct . *Frontiers in Cell and Developmental Biology* **5**, 2 (2017).
235. Zimmermann, W. H. *et al.* Three-dimensional engineered heart tissue from neonatal rat cardiac myocytes. *Biotechnol. Bioeng.* **68**, 106–114 (2000).
236. Moretti, A., Laugwitz, K.-L., Dorn, T., Sinnecker, D. & Mummery, C. Pluripotent stem cell

- models of human heart disease. *Cold Spring Harb. Perspect. Med.* **3**, (2013).
237. Sekiya, S., Shimizu, T. & Okano, T. Vascularization in 3D tissue using cell sheet technology. *Regen. Med.* **8**, 371–377 (2013).
238. Stoehr, A. *et al.* Spontaneous Formation of Extensive Vessel-Like Structures in Murine Engineered Heart Tissue. *Tissue Eng. Part A* **22**, 326–335 (2016).
239. Masumoto, H. *et al.* Human iPS cell-engineered cardiac tissue sheets with cardiomyocytes and vascular cells for cardiac regeneration. *Sci. Rep.* **4**, 6716 (2014).
240. Chen, T. & Vunjak-Novakovic, G. In Vitro Models of Ischemia-Reperfusion Injury. *Regen. Eng. Transl. Med.* **4**, 142–153 (2018).
241. Jensen, B. C., O’Connell, T. D. & Simpson, P. C. Alpha-1-adrenergic receptors: Targets for agonist drugs to treat heart failure. *J. Mol. Cell. Cardiol.* **51**, 518–528 (2011).
242. Chen, H. *et al.* Adrenergic signaling promotes angiogenesis through endothelial cell-tumor cell crosstalk. *Endocr. Relat. Cancer* **21**, 783–795 (2014).
243. Chalothorn, D., Zhang, H., Clayton, J. A., Thomas, S. A. & Faber, J. E. Catecholamines augment collateral vessel growth and angiogenesis in hindlimb ischemia. *Am. J. Physiol. Circ. Physiol.* **289**, H947–H959 (2005).
244. Nuamnaichati, N., Sato, V. H., Moongkarndi, P., Parichatikanond, W. & Mangmool, S. Sustained β -AR stimulation induces synthesis and secretion of growth factors in cardiac myocytes that affect on cardiac fibroblast activation. *Life Sci.* **193**, 257–269 (2018).
245. Amanfu, R. K. & Saucerman, J. J. Modeling the Effects of β 1-Adrenergic Receptor Blockers and Polymorphisms on Cardiac Myocyte Ca^{2+} Handling. *Mol. Pharmacol.* **86**, 222 LP – 230 (2014).
246. Prichard, B. N. Propranolol and beta-adrenergic receptor blocking drugs in the treatment of hypertension. *Br. J. Clin. Pharmacol.* **13**, 51–60 (1982).
247. Ji, Y. *et al.* The role of β -adrenergic receptor signaling in the proliferation of hemangioma-derived endothelial cells. *Cell Div.* **8**, 1 (2013).
248. Sorriento, D., Trimarco, B. & Iaccarino, G. Adrenergic mechanism in the control of endothelial function. *Transl. Med. @ UniSa* **1**, 213–228 (2011).

5 Permissions to Reprint

Permission for Appendix 1: The review article is submitted to the *Journal of Molecular and Cellular Cardiology* but not published yet. The corresponding author (S. Dimmeler) agreed to include this manuscript into the present dissertation.

Permission for Appendix 2: The permission to reuse the publication “*Wagner, J. U. G. et al. Switch in Laminin β 2 to Laminin β 1 Isoforms During Aging Controls Endothelial Cell Functions. *Arterioscler. Thromb. Vasc. Biol.* 38, 1170–1177 (2018).*” was granted according to the “AHA/ASA Journals permission and rights policies” by the Wolters Kluwer Permissions Team on July 1st 2019 (case #01907912).

Permission for Appendix 3: The manuscript “*Transcriptional heterogeneity of fibroblasts is a hallmark of the aging heart*” is submitted and accepted for publication at the Journal JCI Insights but hasn’t been published yet. The permission to reuse the manuscript (manuscript number: 131092) was granted by the Senior Science Editor Corinne Williams.

Permission for Appendix 4: The manuscript “*Dissection of heterocellular cross-talk in vascularized cardiac tissue mimetics*” is submitted to the Journal JMCC but hasn’t been published yet. On behalf of all contributed authors, as well as the corresponding authors (S. Dimmeler, J. Krishnan) the manuscript was used for this dissertation.

6 Author Contribution

6.1 Author contribution for Appendix 1

1.) Planning and development:

PhD student: **50%**

Stefanie Dimmeler: **50%**

2.) Literature research:

PhD student: **50%**

Stefanie Dimmeler: **50%**

3.) Writing the manuscript:

PhD student: **50%** (+ figures)

Stefanie Dimmeler: **50%**

6.2 Author contribution for Appendix 2

1.) Planning and development:

PhD student: **50%**

Stefanie Dimmeler: **50%**

2.) Conduction the individual investigations and experiments:

PhD student: **82,5%** (Fig. 1 A-B, H-L; Fig. 2 A-I, suppl. Fig. 2 A-B; suppl. Fig. 2-6)

Marion Muhly-Reinholz: **9%** (Fig. 1 C-F suppl. Fig. 2 C)

Reinier Boon: **2,5%** (Suppl. Fig. 1)

Eva-Maria Rogg: **6%** (Fig. 1 A, B, G)

3.) Preparation of data collection and illustrations:

PhD student: **100%** (collecting all data and illustrating all figures)

4.) Data analysis and interpretation:

PhD student: **99%** (Data analysis of all experimental data); **40%** (data interpretation)

Stefanie Dimmeler: **60%** (data interpretation)

David John: **1%** (Data analysis of bulk RNA sequencing results)

5.) Writing the manuscript:

PhD student: **40%**

Stefanie Dimmeler: **60%**

6.3 Author contribution for Appendix 3

1.) Planning and development:

PhD student: 40%	}	Wet-Lab work
Stefanie Dimmeler: 60%		
Ramon Vidal: 40%	}	Bioinformatics
Sascha Sauer: 50%		
Stefaniie Dimmeler: 10%		

2.) Conduction the individual investigations and experiments:

PhD student: **47%** (Establishment of the complete cell culture work as well as cell isolation from mouse hearts and functional analyses + validation of single-nucleus data via RT-qPCR and bulk RNA-Seq + confocal microscope analyses + Fig. 1A; Fig. 3A, B; Fig. 6-7; suppl. Fig. 5, 6, 8, 9A and 11)

Ramon Vidal: **48%** (Generating all bioinformatical data except for the ligand-receptor analysis + Fig. 1-5; Fig. 6D; suppl. Fig. 1-4, 7 and 9B-C)

M. Muhly-Reinholz: **3%** (helped with Fig. 7D-E; suppl. Fig. 9A)

N. Camboa: **1%** (help with Fig. 1 A)

R. Patrick/R. Harvey/S. Dimmeler: **1%** (Fig. 5C)

3.) Preparation of data collection and illustrations:

Promovierender: **43%**

Ramon Vidal: **57%**

4.) Data analysis and interpretation:

PhD student: **20%** (Analysis + Interpretation of all Wet-Lab results + Interpretation of Fig. 1A + 3A)

Stefanie Dimmeler: **40%** (Interpretation of all data)

Ramon Vidal: **20%** (Analysis + Interpretation of bioinformatical data)

Sascha Sauer: **20%** (Interpretation of all data generated by R. Vidal)

5.) Writing the manuscript:

PhD student: 40% (Method section)

Ramon Vidal: 60% (Method section)

S. Sauer: 30% (Main text)

S. Dimmeler: 70% (Main text)

6.4 Author contribution for Appendix 4

1.) Planning and development:

PhD student: **30%**

Minh Duc Pham: **10%**

Stefanie Dimmeler: **30%**

Jaya Krishnan: **30%**

2.) Conduction the individual investigations and experiments:

PhD student: **40%** (Fig. 1A, 2A, B, D, E-G, 3B-D, 4A-G, suppl. Fig. 1, 4-7)

Minh Duc Pham: **25%** (Fig. 1B-J, suppl. Figure 3 + establishment of CTM culture)

Luka Nicin: **25%** (Fig. 2C, E-G, 3A, C-D, 4A, B, suppl. Fig. 4, 5, 7)

M. Muhly-Reinholz/K. Bottermann/J. Madl: **9%** (Imaging)

Martin Hardt: **1%** (TEM imaging)

3.) Preparation of data collection and illustrations:

PhD student: **100%** (collecting all data and illustrating all figures)

4.) Data analysis and interpretation:

PhD student: **15%** (Analysis + interpretation esp. Fig. 2-4, and suppl. Fig. 1, 4-6)

Minh Duc Pham: **15%** (Analysis + interpretation esp. Fig. 1 and suppl. Fig. 3)

Luka Nicin: **10%** (Analysis + interpretation esp. Fig. 2+3 and suppl. Fig. 4+ 5)

S. Dimmeler: **30%** (Interpretation of data esp. Generated by the PhD student and L. Nicin)

J. Krishnan: **30%** (Interpretation of data esp. Generated by Minh Duc Pham)

5.) Writing the manuscript:

PhD student: **30%**

Stefanie Dimmeler **35%**

Jaya Krishnan: **35%**

7 Schriftliche Erklärung

Ich erkläre hiermit ehrenwörtlich, dass ich die dem Fachbereich Biowissenschaften der Johann Wolfgang-Goethe-Universität Frankfurt am Main zur Prüfung eingereichte Dissertation mit dem Titel

Endothelial Cross-Talks in the Aging Heart

im Institut für kardiovaskuläre Regeneration unter Betreuung und Anleitung von Prof. Dr. Stefanie Dimmeler ohne sonstige Hilfe selbst durchgeführt und bei der Abfassung der Arbeit keine anderen als die in der Dissertation angeführten Hilfsmittel benutzt habe. Darüber hinaus versichere ich, nicht die Hilfe einer kommerziellen Promotionsvermittlung in Anspruch genommen zu haben.

Die Grundsätze der Johann Wolfgang-Goethe-Universität Frankfurt am Main zur Sicherung guter wissenschaftlicher Praxis in ihrer gültigen Form liegen mir vor und wurden bei der wissenschaftlichen Arbeit eingehalten.

Die vorliegenden Ergebnisse der Arbeit wurden teilweise in folgendem Publikationsorgan veröffentlicht:

Wagner JUG*, Chavakis E, Rogg EM, Muhly-Reinholz M, Glaser SF, Günther S, John D, Bonini F, Zeiher AM, Schaefer L, Hannocks MJ, Boon RA, Dimmeler S. Switch in Laminin β 2 to Laminin β 1 isoforms during aging controls endothelial cell functions-brief report. **Arterioscler. Thromb. Vasc. Biol.** 2018; 38:1170–77. 10.1161/ATVBAHA.117.310685

(Ort, Datum)

(Unterschrift)

8 Acknowledgments

Abschließend möchte ich all denen, die mich während der Anfertigung dieser Dissertation begleitet haben, meinen Dank aussprechen:

... Im besonderen Maße Frau Prof. Dr. Stefanie Dimmeler für die Bereitstellung der finanziellen, methodischen, räumlichen und intellektuellen Mittel, die nötig waren, um diese Arbeit anzufertigen, sowie für die ausgezeichnete Betreuung während meiner gesamten Doktoranden-Zeit. Ich genoss dabei besonders die inspirierenden Gespräche und Meetings mit ihr, ihre wissenschaftliche sowie personelle Förderung aber auch die Chance diverse nationale und internationale Konferenzen zu besuchen.

... Frau Prof. Dr. Amparo Acker-Palmer, die sich freundlicherweise dazu bereitstellte als Zweitgutachterin für diese Arbeit zu fungieren.

... Herr Prof. Dr. Andreas Zeiher für die sehr angenehmen und stimulierenden Gespräche sowie dem inhaltlichen Input bei den angefertigten Manuskripten.

... Prof. Dr. Reinier Boon besonders für die Einarbeitung in den ersten Monaten.

... meinem Thesis-Komitee bestehend aus Prof. Stefanie Dimmeler, Prof. Reinier Boon und Prof. Liliana Schaefer für den geistigen Input während den jährlichen TAC-Meetings.

... Dr. Nicolas Jaé für die großartige Hilfe im Labor und den wertvollen Gesprächen, sowie dem Korrekturlesen.

... Felix Vetter für die konspirativen Gespräche.

... Caroline Dreis und Marius Klangwart für die vielen kurzweiligen Zugfahrten, inklusive dem „Bahngeflüster“.

... Marion Muhly-Reinholz, Ariane Fischer und Eva-Maria Rogg für die tolle Unterstützung und Einarbeitung im Labor.

... Marco Sachse für die wertvolle Freundschaft, die während des Ski-Retreats 2017 durch einen havarierten Vans entstand.

... dem gesamten Institut für kardiovaskulärer Regeneration für die wunderbare Zusammenarbeit und der herzlichen Aufnahme. Besonders dem Labor 440/441 für die angenehme Zusammenarbeit im vergangenen Jahr.

... dem „Socializing Team“, bestehend aus Lukas Tombor, David John und Luka Nicin, mit dem ich viele kurzweilige Events organisieren durfte.

... Jannis Winckler für das Designen Aquarells.

... den Stiftungen und Förderern des DFG, SFB834, LOEWE CGT, DZHK, ECCPS, CPI, sowie dem CRC1366.

... Dr. Martin Hardt für die angenehmen und fruchtbaren Gespräche.

... und nicht zuletzt meiner Freundin Stefanie Herbel für den starken privaten Rückhalt und dem nötigen Ausgleich abseits des Labors.

9 Appendix

9.2 Appendix 1

Cellular Cross-Talks in the Diseased and Aging Heart

Julian U. G. Wagner^{1, 2, 4} and Stefanie Dimmeler^{1, 2, 3}

¹Institute for Cardiovascular Regeneration, Goethe University, Theodor Stern Kai 7, Frankfurt Germany

²German Center for Cardiovascular Research (DZHK); Frankfurt; Germany

³Cardio-Pulmonary Institute (CPI), Frankfurt; Germany

⁴Faculty for Biological Sciences, Goethe University; Frankfurt; Germany

Corresponding Author:

Prof. Dr. Stefanie Dimmeler
Institute for Cardiovascular Regeneration
Centre of Molecular Medicine
Goethe University Frankfurt
Theodor Stern Kai 7
60590 Frankfurt; Germany
Phone: +49-69-6301-5158
Fax: +49-69-6301-83462
dimmeler@em.uni-frankfurt.de

Abstract

Communication between cells is an important, evolutionarily conserved mechanism which enables the coordinated function of multicellular organisms. Heterogeneity within cell populations drive a remarkable network of cellular cross-talk that allows the heart to function as an integrated unit with distinct tasks allocated to sub-specialized cells. During diseases and aging, cells acquire an overt disordered state that significantly contributes to an altered cellular cross-talk and hence drive cardiac remodeling processes and cardiovascular diseases. However, adaptive mechanisms, and phenotypic changes in subpopulations of cells (e.g. reparative macrophages or fibroblasts) can also contribute to repair and regeneration. In this article, we review the cellular cross-talks between immune cells, endothelial cells, fibroblasts and cardiomyocytes that control heart failure by contributing to cardiac dysfunction and aging, or by mediating repair and regeneration of the heart after injury.

Disorders or diseases of the cardiovascular system are still the primary cause of death globally^{1,2}. Although the heart and the cardiovascular system has been studied for centuries, researchers mainly focused on cardiomyocyte functions and cardiac fibrosis as key mechanisms of heart failure. However, the more recent reports showing that cardiomyocytes only account for up to 35 % of the total cells of the heart³⁻⁵ inspired a more integrated view of cardiac biology. Many cell types including endothelial cells, pericytes, smooth muscle cells, various immune cells, fibroblasts/mesenchymal cells and nerves contribute to the cellular composition of the heart. This diverse set of cells together maintains cardiac function and is the key to control repair and cardiac regeneration. In the present review, we focus on the interplay of immune cells and the three cell populations namely cardiomyocytes (CM), fibroblasts (FB) and endothelial cells (EC) during disease, regeneration and aging. The heterocellular cross-talk in the heart under physiological conditions was recently reviewed by Perbellini, et al⁶. The first two chapters will focus on detrimental and beneficial changes in cellular communication as it occurs during cardiac disease and regeneration, while the last chapter will discuss cellular changes during cardiac aging.

1. Cellular Cross-Talks in the diseased Heart

In the past, cellular cross-talks within hearts have been studied in various animal and disease models including acute myocardial infarction (MI), trans-aortic constriction (TAC), heart failure with preserved ejection fraction and diastolic dysfunction and during aging. During MI, the occlusion of a coronary artery results in a reduced blood and nutrient supply in the underlying tissue causing cell death. This leads to a dramatic change in the cellular composition within the heart tissue: reduced numbers of CMs, ECs and FBs are replaced by various immune cells within the first days upon MI⁷ (Figure 1A). The initial inflammation driven phase is followed by increased EC and FB proliferation, whereas CMs - due to their limited proliferation capacity - remain depleted in the scar tissue of adult mammals. Interestingly, the loss of cells after injury can be counterbalanced in zebrafish^{8,9} or newts¹⁰ as well as in neonatal mice^{11,12}, which are able to regenerate the myocardium after injury. However, unlike the zebrafish heart whose regenerative capacity is preserved throughout the entire lifespan¹³, the regenerative capacity of the murine heart is decreasing after postnatal day 7^{11,12,14,15}. In contrast to MI, the changes of cell compositions upon TAC are less dramatic but also involve invasion of inflammatory cells and an adaptive response of CM-EC communication to cope with the increased oxygen demands of the hypertrophic CM. The interactions occurring in models of HEFpEF and aging are less well studied but certainly involves an increase in fibrosis and extracellular matrix remodeling, which affects other cell types of the heart.

Inflammatory cells in heart disease

Immune cells represent a minor population in the heart under steady state conditions, although all major leukocyte classes are represented including monocyte/macrophages, neutrophils, T- and B- cells and dendritic cells¹⁶. However, invasion of bone marrow-derived inflammatory cells is a hallmark in most if not all cardiac disease models. MI leads to a rapid accumulation of mast cells and neutrophils followed by an activation of tissue resident macrophages and invasion of inflammatory C-C chemokine receptor 2 positive (CCR2⁺), Ly6^{high} monocytes^{17,18} (Figure 1A). Especially tissue resident TIMP4⁺ macrophages were found to proliferate in the peri-infarct zone

and reinforce the macrophage pool in the injured heart¹⁹. In models of pressure overload and HFpEF, CCR2⁺ macrophages also infiltrate the heart^{20,21}. For a detailed description of the various immune cell subsets in cardiac disease, the reader is referred to Swirski & Nahrendorf²².

The inflammatory response has a double-edged role in the regulation of remodeling and heart failure²³: Whereas early stimulation of inflammatory signaling is important for clearance of dead cells from the infarcted tissue, excessive inflammatory injury contributes not only to pathophysiological remodeling of the ventricle but also induces reparative processes. These processes are mediated by a variety of cytokines which interact with non-leukocytes. These include for example mast cell-derived tumor necrosis factor (TNF), which activates endothelial cell²⁴, and T cell-derived IL-17, which stimulates cardiac fibroblasts²⁵. Macrophage and T-cell derived factors can also induce reparative processes (Figure 1B). E.g. transforming growth factor- β (TGF β) and IL-10^{26,27} promote collagen production and resolution of inflammation, whereas vascular endothelial growth factor (VEGF)²⁸ promotes neoangiogenesis (for details see²²). **TGF β** , however, can also have detrimental effects²⁹: It promotes cardiomyocyte death and hypertrophy and mediates cellular differentiations processes, such as fibroblast-to-myofibroblast and endothelial-to-mesenchymal transition (EndoMT)^{30,31}, which both increase the pool of active mesenchymal cells and may contribute to scar formation and detrimental cardiac remodeling³¹.

Endothelial-to-mesenchymal transition (EndoMT) is a complex process by which ECs adopt mesenchymal features such as cellular motility and contractile element. ECs that undergo EndoMT lose the expression of endothelial-specific genes including vascular-endothelial cadherin and CD31 but acquire mesenchymal transcriptomic signatures by expressing –among others– SM22 α , S100A4, fibronectin, EDA, N-cadherin, type I and III collagen³². The process is induced by many different stimuli. In the injured and diseased heart, mostly inflammatory or pro-fibrotic factors such as TGF β and hypoxia drive EndoMT³³. During cardiac development EndoMT plays a critical role. While it has been shown that about 10% of ECs in human fetal cardiac valves undergo EndoMT, only 1% remain in adult valves³⁴. However, in adulthood EndoMT can also be maladaptive and displays a role in valvular diseases³⁵. Furthermore, EndoMT was shown to occur during MI³⁶, in atherosclerotic lesions and was associated with plaque erosions³⁷. For a detailed description of EndoMT in development and disease, the reader is referred elsewhere^{32,35}.

IL-10 reduces the ratio of pro-inflammatory M1 to M2 macrophages in MI models thereby eliciting an anti-inflammatory effect^{38,39} (Figure 1B). Consistently, IL-10-deficient mice have increased infarct size and enhanced myocardial necrosis with increased neutrophil infiltration⁴⁰. Although its role as anti-inflammatory mediator, which improves cardiac function after injury in the MI model is well established, a recent study suggest that it may have mild, but adverse effects if released by macrophages in a model of diastolic dysfunction²¹. A common effect observed in diastolic dysfunction²¹ and post-infarction remodeling³⁹ is that IL-10 activates FBs. Since FBs play an important role in wound healing and cardiac remodeling their activation may contribute to the beneficial effect of IL-10 in acute injury models, whereas a long term chronic activation of FBs may be detrimental to the heart. In this regard, Hulsmans et al.²¹ examined cardiac macrophages in two different approaches to study diastolic dysfunction by using first a combination of salty drinking water, unilateral nephrectomy as well as chronic exposure to

aldosterone and second a mouse model of physiological aging. They documented that the density of myocardial macrophages and IL-10 expression increased upon diastolic dysfunction, whereas IL-10 expression shifted macrophages in an autocrine manner to a more pro-fibrotic subset, and additionally activated FBs resulting in increased FB proliferation and elevated collagen deposition and thereby to ventricular wall stiffness. By contrast, a macrophage-specific IL-10 depletion improved cardiac filling during diastole²¹.

Endothelial cross-talks

Cardiac ECs form the inner surface of the heart chambers, as well as the inner lining of the entire macro- and microvasculature supplying the myocardium with blood. To fulfil the high oxygen demands, a capillary ratio of > 1 capillary/myocyte is required and hence it is not surprising that ECs outnumber CMs by a ratio of 3:1⁴¹. However, the total EC content has not been uniformly defined yet since it varies depending on the methodology that were used. For example, Pinto et al. reported by immune fluorescence staining that ECs make up 60% of the non-myocytes in the murine heart¹⁶, while using histological techniques, Perbellini et al. described that ECs account for 48% of the entire heart⁴². On the other extreme, Banerjee and co-workers showed via FACS studies that the EC content of the entire mouse heart is only 7%⁴³. Admittedly, one has to keep in mind, that tissue dissection can be very harsh and might digest even membrane surface proteins such as CD144 or CD31 on ECs preventing capturing these cells in flow cytometry studies. However, various studies have consistently reported changes in EC numbers and functions within the heart upon injury. After an initial decline in EC after infarction which is caused by cell death, new blood vessels growth between 7-14 days after injury. In models of pressure overload, adaptive angiogenesis and neovascularization is augmented to fulfill the increased oxygen demand of the hypertrophic CM⁴⁴. A failure of angiogenesis in both models leads to the progression of HF⁴⁵.

In the heart, EC closely interact with CMs already during development, e.g. by releasing neuregulin, neurofibromatosis type-1 (NF1) and platelet-derived growth factor β (PDGFB)^{6,46-48}. After cardiac injury, a major function of ECs was attributed to the control of immune cell invasion⁴⁹ via up-regulation of P-selectin⁵⁰ as well as MCP-1⁵¹ and the restoration of the vascular network to provide oxygen to the ischemic or hypertrophic cardiac tissue. Several studies, however, suggest that EC have important functions beyond acting as inflammatory gate keeper or oxygen pipelines^{52,53}. In other organs, such as the liver or lung, a paracrine activity of ECs (so called "angiocrine" mediators) was shown to control regeneration^{54,55}. In the heart, EC can release many factors that control FB and CM functions but a direct pro-regeneration activity has not yet been reported.

Important insights into CM-EC communication paths were provided by studies showing that hypertrophic CM secrete pro-angiogenic factors such as VEGF or angiopoietin-1 to promote adaptive vessel growth. Inhibition of VEGF prevented increased capillary density and induced heart failure^{44,56}. But EC can also signal back to CM: For example, EC derived endothelin-1 acts in a paracrine manner on CMs (via the ET_A receptor) and induces hypertrophy as well as remodeling in the diseased heart⁶. Other EC-derived factors were shown to elicit protective effects on CM. For example, apelin, which is mainly expressed by ECs, protects against the progression of heart failure in mice⁵⁷. Likewise, nitric oxide, which is mainly produced by the endothelial nitric oxide synthase under baseline conditions, is known to inhibit CM hypertrophy⁵⁸. However, disease or cardiac stress-related uncoupling of eNOS can promote

oxidative stress and result in pathological cardiac remodeling⁵⁹. EC also express transporters of glutathione (such as the ATP-binding cassette transporter ABCG2), which enriches the extracellular space with this important antioxidant and reduces reactive oxygen species that mediate CM damage⁶⁰ (Figure 1C).

Since the interpretation of *in vivo* studies targeting ECs are often hampered by potential confounding effects of increased or diminished perfusion, co-culture studies have been used to gain insights into direct EC-CM interactions. Such a study demonstrates that EC promote CM survival by reducing apoptosis and necrosis and promoted spatial remodeling as well as synchronized contraction of CMs by augmenting connexin 43 expression⁶¹. A cardiac protective role of ECs was further described by Kuramochi et al, showing that EC-derived neuregulin reduces apoptosis of CMs in a co-culture system⁶².

Cardiomyocytes

CMs are the contractile element of the myocardium. Their synchronized contraction maintains a proper cardiac strain that is needed to pump blood through the circulatory system. To maintain cardiac contraction throughout a whole lifespan, CMs are equipped with a very large cytoplasm that is crammed with sarcomeres, the contractile unit of myocytes and mitochondria to meet their high energy demand⁶. The main interaction partners of CMs are neighboring CMs. The connection is established by specific gap junctions, so-called intercalated disks that are usually formed by connexins⁶. These junction proteins allow the direct exchange of ions, small molecules as well as small peptides between CMs and also electrically couple the entire myocardium⁶.

CM also communicate with other cells, via secretion of various chemokines. For instance, CM-derived VEGF-A plays a crucial role during cardiac development by controlling the formation of capillaries⁶³. In addition to the bidirectional interplay of CM with EC and inflammatory cells described above, CM death itself can contribute to the pro-inflammatory extracellular milieu. Thus, CM death or stimulation of CMs by immune cells cause the secretion of pro-inflammatory chemokines and cytokines, which further aggravates inflammation and activates neighboring EC or FB. For example, CM-derived IL-6, TNF α and IL-1 β activates neutrophils and augment adhesion as well as invasion into the damaged tissue via expression of intercellular adhesion molecule 1⁶⁴. Dying CMs and degraded ECM both further release danger-associated molecular patterns that promote additional inflammatory reactions via toll-like receptor (TLR) signaling⁶⁵. Reactive oxygen species that additionally trigger the immune response, are increasingly formed and released by CMs upon hypoxic conditions⁶⁴. However, deciphering the role of the innate immune system in myocardial diseases turned out to be challenging, because of conflicting observations that were made in ischemic heart diseases indicating both a beneficial and a detrimental role of cardiomyocyte TLRs upon cardiac injury. Whereas a short-term activation of TLRs was found to have a cytoprotective effect within the heart, long-term activation of TLRs is maladaptive resulting in increased pro-inflammatory cytokine release and adhesion molecule expression leading to the recruitment of neutrophils, dendritic cells and monocytes into the myocardium and adverse cardiac remodeling^{66,67}. In the murine heart, at least six TLRs are expressed including TLR2, TLR3, TLR4, TLR5, TLR7 and TLR9⁶⁸, of which TLR2 and TLR4 are best studied⁶⁹⁻⁷¹. Interestingly, both TLR2 and TLR4 seem to have an anti-apoptotic effect in CMs upon serum-deprivation and LPS-stimulation^{72,73}. TLR4 further mediates iNOS induction in CMs leading to an increased NO production that was documented to inhibit caspase-3 activity^{74,75}.

Frantz et al. demonstrated that the blocking of TLR2 in neonatal rat CMs oxidative stress-induced apoptosis and cell injury⁷⁶. However, as mentioned above, TLR signaling may also be detrimental to heart including adverse cardiac remodeling. For instance, studies reported a reduced infarct size, neutrophil recruitment and ROS as well as cytokine release and augmented contractile performance and recovery in TLR2-deficient mice^{77,78}. Similar findings were shown after deletion of TLR4^{79,80}.

Fibroblasts

Cardiac FBs are small elongated spindle-shaped cells with a strong secretory phenotype. They display a granular cytosol containing a pronounced rough endoplasmic reticulum. Unlike CMs, that are organized in a defined structure within the heart, FBs are roughly distributed throughout the entire myocardium and are located in the interstitial space between CMs⁸¹. Studies on fibroblasts have been hampered by the lack of specific marker, since many of the proteins which are highly expressed on FBs such as vimentin or fibroblast-specific protein 1 (FSP1) are also expressed on other cells⁸². More recent studies used platelet-derived growth factor receptor α (PDGFR α), TCF21 or DDR2, which are considered to be more specific for FBs⁸². FBs derive from multiple origins including the epicardium, the endocardium and neuronal crest derived cells, which all give rise to FB during development. The origin of FBs that is responsible for cardiac fibrosis in the diseased adult heart has been controversial but most recent lineage tracing studies suggest a predominant contribution of tissue resident FBs⁸². FBs may directly interact with other cells via connexins possibly allowing an electric coupling with CMs⁸³.

Cardiac injury and subsequent inflammation induces dramatic changes in FB resulting in increased proliferation, differentiation and matrix production⁸⁴. FBs thereby respond to many factors (e.g. IL-6, IL-10) provided by inflammatory cells, EC and CM but also can signal back to these cells. For example, fibroblast-derived granulocyte–macrophage colony-stimulating factor (GM-CSF) was shown to induce the production and recruitment of myeloid cells⁸⁵. Moreover, bioinformatic assessment of single cell sequencing data sets suggest that FB are cells with a high expression of “outgoing” signals representing extracellular factors that can putatively interact with receptors expressed on other cardiac cells⁷ (Figure 1D). Such a view of FBs being major determinants of the microenvironment is consistent with findings in other tissues or pathologies demonstrating that FBs drive the microenvironment e.g. in cancer⁸⁶.

FBs are major producers of extracellular matrix components and modifying enzymes e.g. Lys oxidases or proteases. Since CMs are physically linked to the ECM via integrin molecules⁸⁷, regulation of the ECM by FBs indirectly influences CMs. Of the numerous additional factors released by FBs (but also other cells), TGF β , IL-6, and endothelin 1 have significant effects on CMs. FBs also secrete miRNA-loaded exosomes; here miR-21* loaded exosomes were shown to induce CM hypertrophy⁸⁸. Recent studies also suggest that a FB subset can produce Wnt inhibitory factors, which may have autocrine or paracrine functions⁷. Interestingly, this FB subset was shown to be reduced after MI⁷. While these examples highlight the interaction of FBs with CM, bioinformatics analysis of single cell sequencing data sets suggest that the main interacting cell type of fibroblasts in the heart may be endothelial cells, which may trigger further research to elucidate the interactions between these two cell types^{7,89}.

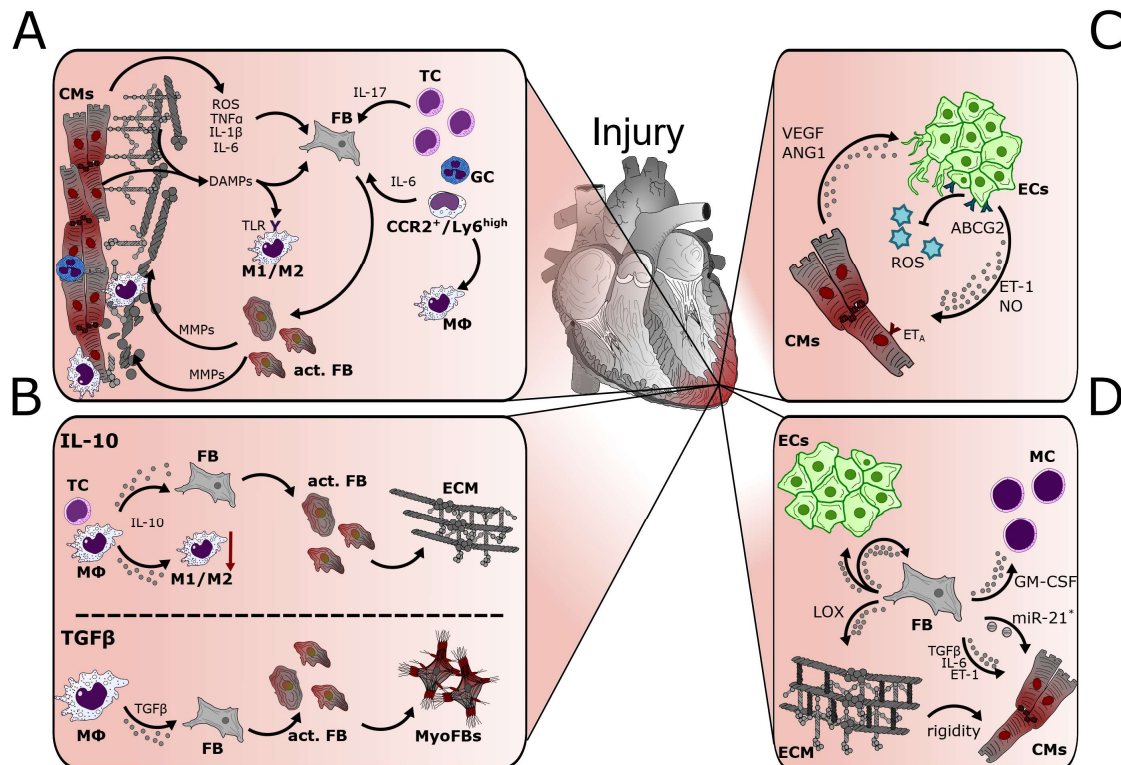


Figure 1: Cellular cross-talk in the injured heart. (A) Cardiac injury and thereby the lack of oxygen stimulates cardiomyocytes (CMs) in the injured heart to release pro-inflammatory factors (ROS, TNF α , IL-6 and IL-1 β) into the extracellular space. T cells (TC), granulocytes (GC) and CCR2⁺/Ly6^{high} monocytes infiltrate the injured area and release further pro-inflammatory factors (IL-6, IL-17). The released factors stimulate fibroblasts (FBs) to become activated FBs (act. FBs). Damaged extracellular matrix (ECM) components and hypoxic CMs additionally release danger-associated molecular patterns (DAMPs) that further activate FBs and also stimulate M1 and M2 macrophages (M Φ) via toll-like receptors (TLR). Activated FBs secrete matrix metalloproteases (MMPs) that degrade the ECM and enables the infiltration of phagocytes to remove cell and matrix debris. (B) TC- and M Φ -derived IL-10 reduces the ratio of pro-inflammatory M1 to M2 macrophages thereby eliciting an anti-inflammatory effect. IL-10 further activate FBs to produce ECM components in order to form the scar tissue in infarcted hearts. (C) Hypoxic CMs release pro-angiogenic factors (VEGF, ANG1) to induce revascularization, whereas endothelial cells (ECs) interacts with CMs by releasing ET-1 and nitric oxide (NO). To neutralize ROS concentration, ECs transporters of glutathione (such as the ATP-binding cassette transporter ABCG2). (D) FBs cross-talks with a variety of cardiac cells. By secreting granulocyte–macrophage colony-stimulating factor (GM-CSF), FBs recruit monocytes, but also signals to ECs via paracrine and autocrine factors. CM hypertrophy is induced by FB-derived TGF β , IL-6 and ET-1 as well as exosomes loaded with miR-21*.

2. Cellular cross-talks in regeneration

In contrast to model organisms such as zebrafish or newts, the adult mammalian heart has a limited capacity for regeneration. Recent studies, however, demonstrated that mice hearts can regenerate during the first week after birth^{11,12,14,15}. The regenerative capacity has been mainly attributed to an increase in CM proliferation, which is lost during adulthood^{14,15}. However, several studies are providing evidence that other cell populations are required as well to allow a successful regeneration of the cardiac tissue.

Inflammatory cells during cardiac regeneration: Pro-angiogenic macrophages can play an active role in cardiac regeneration by promoting vessel growth⁹⁰. Macrophage subpopulations are also required for regeneration of hearts in salamander⁹¹. In contrast to the transient extracellular matrix that normally accompanies regeneration in salamander hearts, macrophage depletion resulted in a permanent, highly cross-linked extracellular matrix scar derived from alternative fibroblast activation and lysyl-oxidase enzymes⁹¹. Interestingly, cardiac resident macrophage-derived cytokines can promote CM proliferation in hypoxic neonates⁹² suggesting an additional potential role of macrophages in CM replacement. However, in salamander hearts, macrophage depletion did not interfere with CM proliferation⁹¹ indicating that CM replacement may be controlled by a macrophage-independent mechanism in this setting (Figure 2A). In zebrafish models, Bevan et al.⁹³ recently demonstrated that both *tnfa*⁺ and *tnfa*⁻ macrophage subsets manipulate cardiac regeneration. While *tnfa*⁺ macrophages facilitate a pro-inflammatory response and promote scar formation via *Csf1ra* upon cryoinjury, *tnfa*⁻ macrophages contribute to scar removal and resolution of the inflammatory response during regeneration⁹³. For a more detailed description of the regenerative capacity of macrophages, the reader is referred to further review articles^{94,95}.

The important role of immune cells is further underlined by findings showing that T-cells are important players in regeneration⁹⁶⁻⁹⁸. Thus, zebrafish Treg-like (Treg) cells modulated inflammation and stimulated regeneration in different organs including the heart⁹⁹. Interestingly, the pro-regenerative activity was mediated through interleukin-10-independent secretion of organ-specific regenerative factors, namely Neuregulin 1, which rescued the regeneration defects associated with Treg cell depletion⁹⁹. In addition, Treg conditioned medium or overexpression of Treg secreted factors (*Cst7*, *Tnfsf11*, *Il33*, *Fgl2*, *Matn2*, and *Igf2*) reduced infarct size and augmented CM proliferation in infarcted mouse hearts¹⁰⁰ (Figure 2B).

Fibroblasts during cardiac regeneration: Increasing evidence suggests that also specific FB populations may support CM growth and maturation through the secretion of specific ECM components. Therefore, it is not surprising that regenerated cardiac tissue in zebrafish and in neonatal mice is characterized by a fibroblast-rich scar tissue⁸². In line with this, embryonic cardiac FB were shown to induce CM proliferation *in vitro*, whereas adult cardiac FB rather promoted myocyte hypertrophy¹⁰¹. Fibronectin, collagen and heparin-binding EGF-like growth factor were identified as embryonic cardiac fibroblast-specific signals that collaboratively promoted via integrin beta 1 CM proliferation in a paracrine fashion¹⁰¹. The responsible FB (sub) population that promotes regeneration in adult hearts remains to be identified. They may be remnants of embryonic FBs, epicardial-derived cells or other pro-regenerative fibroblast population described in the adult heart⁸¹ (Figure 2A).

Endothelial cells during cardiac regeneration: A rapid restoration of oxygen supply by growth of new capillaries and vessels is key to regeneration. Besides re-establishing perfusion, ECs express a number of cardio-affective paracrine factors to restore CM survival and function. Bassat et al. recently reported that ECs express the extracellular matrix protein agrin, which enhances CM proliferation in mouse- and human-derived iPS cells *in vitro* and improve cardiac repair *in vivo* upon MI¹⁰². ECs also synthesize nitric oxide (NO) by the endothelial NO-synthase, which has a protective role during cardiac damage¹⁰³. Whether NO also affects cardiac regeneration, however, is unclear.

Cholinergic nerves during cardiac regeneration: Since 1950 we know that nerves play an important role during tissue regeneration: limb regeneration is impaired, if the intervening nerve is severed prior to or shortly after limb amputation¹⁰⁴. These results were further confirmed in 1960s and the regenerative effect was linked to cholinergic nerves^{105,106}. Interestingly, Mahmoud et al. transferred these regenerative effects to the cardiovascular field and showed that pharmacological inhibition of sympathetic nerves reduces CM proliferation in zebrafish and neonatal mice after MI^{107,108}. The reduction in CM proliferation was rescued by using nerve growth factor and neuregulin-1¹⁰⁸.

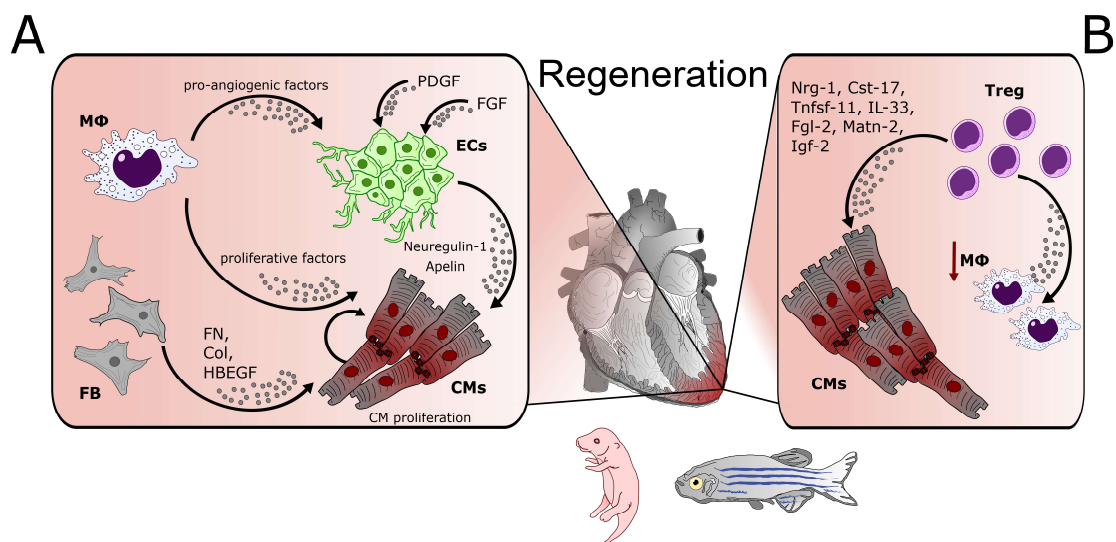


Figure 2: Cellular cross-talk during regeneration. In contrast to adult mammalian heart, newts and zebrafishes are capable to regenerate their hearts. **(A)** Macrophage- (MΦ-) derived pro-angiogenic factors as well as FGF and PDGF stimulate endothelial cell (EC) sprouting to induce revascularization. Cardiomyocyte (CM) proliferation is driven by fibroblast- (FB-) derived FN, Col and HBEGF, EC-derived neuregulin-1 and apelin as well as MΦ-derived proliferative factors. **(B)** Regulatory T cells (Treg) further induce CM proliferation by releasing Nrg-1, Cst7, Tnfsf11, Il33, Fgl2, Matn2, and Igf2 and attenuate MΦ activation.

3. Changes in Cellular Cross-Talks during Aging

Aging is the major risk factor for decline in cardiovascular physiological functions and development of cardiovascular diseases. On macroscopic level, characteristic cardiac remodeling processes can be observed that mostly affect the cardiac chamber geometry, including age-related dilation of the left atrium accompanied by myocardial fibrosis¹⁰⁹. Further structural alterations can be found in the left ventricle that undergoes cardiac hypertrophy, increased wall thickness and chamber dilation, as well as interstitial fibrosis¹¹⁰. Apart from chamber abnormalities, age-related valve diseases also occur with aortic valve stenosis being the most prevalent one¹¹¹. Furthermore, diastolic function also declines with advanced age, whereas concomitant systolic dysfunction was not reported¹¹². However, Feridooni et al. noted that the ability to augment ventricular function is disturbed under high demand situation, such as exercise, in old adults, while the systolic function at rest is not affected¹¹². Cellular and molecular processes that underlie these cardiac alterations can be quite diverse. Replicative senescence caused by shortening of telomeres^{113–115}, increased oxidative stress¹¹⁶ and DNA damage¹¹⁷, deregulation of genes and proteins, impaired cell-cell communication, and an altered systemic and local environment cause the eventual demise of cells¹¹⁸. Many of these changes are described in the aging heart. In cardiomyocytes, however, telomere shortening likely is caused by telomere erosion¹¹⁹.

Senescent cells and SASP in the aging heart: Cellular senescence is characterized by a growth arrest and is part of a physiological process that maintains tissue homeostasis and limits tumor progression. However, it has also been implicated as a major cause of age-related disease in part mainly because senescent cells release a pro-inflammatory senescent associated secretory phenotype (SASP)¹²⁰ (Figure 3A). The secretome of senescent cells include soluble signaling molecules, secreted proteases as well as insoluble / extracellular matrix components. Examples are inflammatory cytokines (e.g. IL-1, IL-6, IL-8), ROS, matrix metalloproteases and urokinases, or FB-derived collagens (e.g. Collagen type 1a), which can all act in an auto- or paracrine fashion on neighboring cardiac cells (for review see^{121,122}). The aged human heart was shown to contain an increased proportion of senescent cardiac progenitor cells that displayed high levels of the senescent biomarkers SA- β -gal, γ H2AX and p16^{Ink4a}. As described for other senescent cells, these cells expressed also high amounts of SASP factors such as PAI-1, IL-8, IL-1 β , MMP-3, GM-CSF and IL-6 that negatively impacted surrounding cells and promoted senescence of other cells to switch to a senescent phenotype, thereby reducing cardiac repair during aging¹²³. Also FB of the aged heart secrete SASP associated factors. Single nucleus sequencing revealed that cardiac FBs of the aging heart highly express the SASP factor PAI-1. PAI-1 was further identified as one of the crucial factors in conditioned medium from age-heart derived FB, which interferes with endothelial cell angiogenesis⁸⁹. In addition, mesenchymal stromal cells display senescence and SASP in the aging heart, which contributes to the recruitment of CCR-2-dependent monocytes. The recruited monocytes were associated with increased inflammatory macrophage-derived IL-1 β , which in turn promoted further cardiac mesenchymal stromal cell senescence¹²⁴. Interestingly, also systemic interactions control cardiac senescence. In parabiosis models it was shown that young mice can provide cardiac protection for aged mice¹²⁵. While the origins of the cardioprotective effectors are not fully understood, a recent study suggests a contribution of adipose tissue¹²⁶. Visceral adipose tissue was reported to increase osteopontin (OPN) expression during aging, which was associated with cardiac fibrosis and reduced cardiac function. Both the removal of visceral adipose tissue and OPN-deficiency in aged mice restored

cardiac function and reduced cardiac fibrosis. Interestingly, conditioned medium of OPN deficient adipocytes promoted FB senescence thereby limiting their expansion, indicating that FB senescence might also be a mechanism to protect from cardiac fibrosis¹²⁶. But overall, targeting senescent cells in the aging heart might be a promising therapeutic strategy. In this respect, genetic removal of p16^{Ink4a+} senescent cells by a *INK-ATTAC* transgenic mouse line extended lifespan and attenuated cardiac deterioration¹²⁷. To be applied to patients, a new class of drugs was identified targeting specifically senescent cells, the so-called **senolytics**. These class of agents including dasatinb and quercetin and the anti-cancer drug ABT263 has been used in various experimental models^{128–130} and is being tested in proof-of-concept clinical trials to clear senescent cells from the aging tissue¹³¹. In a small Phase I study with patients with idiopathic pulmonary fibrosis, hints of improved physical functions were reported after treatment with dasatinb and quercetin, but the treatment was also associated with adverse events¹³¹.

Immune cells in the aging heart: Ageing is additionally associated with major alterations of the immune system, referred to as “**inflamm-aging**” (Figure 3B). This is reflected by alterations in the relative numbers and proportions of cardiac leukocytes: old hearts have proportionally more monocyte-derived cardiac macrophages and an increased population of granulocytes²¹. Moreover, aged mouse hearts have more CD8⁺ T-cells than other lymphocytes, but the potential implications of these specific changes remain unclear (for review see²²). In addition, hematopoietic stem cells can acquire mutations that lead to the expansion of mutated clones (so called clonal hematopoiesis of indeterminate potential, CHIP) leading to changes in the inflammatory properties of the mutated cell^{132,133}. Such mutations predominantly occur in epigenetic regulators (such as *DNMT3a* or *TET2*) and are associated with detrimental effects of heart function in mice injury models^{133,134} and prognosis of patients with aortic stenosis¹³⁵ or heart failure¹³⁶. To what extent and how these mutations affect the local paracrine pattern and influence cardiac cells remains to be investigated.

Cardiomyocytes in the aging heart: With advancing age, the myocardium undergoes degenerative alterations¹²¹. This includes in particular a decrease in β -adrenergic receptor (β -AR) response that has been described by a process called “ β -adrenergic receptor desensitization” by which phosphorylation of receptor structures results in a reduction in β -AR density and their internalization in the cell membrane^{137,138}. Since β -AR stimulation triggers intercellular Ca²⁺ release from the sarcoplasmic reticulum and thereby the activation of contractile proteins, the age-related decrease in β -AR density has a negative inotropic effect that leads to a reduced ventricular function¹³⁷. Cardiac aging is also associated with mitochondrial dysfunction with an increased ROS generation and release causing mitochondria DNA damage and hence further mitochondria dysfunction^{139,140}. Furthermore, elevated levels of angiotensin II has been shown to induce CM hypertrophy, apoptosis as well as cardiac fibrosis directly¹⁴¹. The long-term inhibition of the angiotensin II converting enzyme and the angiotensin II receptor were both shown to prevent age-related cardiac pathologies and prolonged rodent survival¹⁴².

Further factors, which are involved in cardiac aging include (but are not limited to) IGF-1 and GDF-11 which are both decreased on circulating level. GDF-11 (= growth differentiation factor-11, a member of the TGF β family) shows a decreased blood level in cardiac aging. By combining

young and aged mice in a parabiosis study, Loffredo et al. restored circulating GDF-11 blood levels that prevented age-related cardiac hypertrophy and a reduced expression of the hypertrophy-related marker genes ANP and BNP in CMs¹²⁵. In humans, low circulating levels of GDF-11 were associated with increased ventricular hypertrophy¹⁴³. However, the findings have been controversial. Smith et al. injected recombinant GDF-11 in 24-months-old mice to restore circulating GDF-11 levels and were unable to reverse cardiac hypertrophy. Cardiac structure and function were also not restored. By using phenylephrine-treated neonatal rat CM, GDF-11 did not prevent but rather promoted hypertrophy *in vitro*¹⁴⁴. Likewise, IGF-1 appears to have also a controversial role in cardiac aging: both protective and detrimentally effects have been described in the aging heart. Several studies demonstrated that IGF-1 acts anti-inflammatory and has a cardio-protective functions¹⁴⁵. In addition, IGF-1 deficient mice showed an increased life expectancy and the same association was seen in human^{146,147}. However, some studies show contradicting results. Whereas IGF-1 overexpression in mouse hearts showed reduced CM death after MI and reduced ventricular dilation, hypertrophy, as well as diabetic cardiomyopathy¹⁴⁸⁻¹⁵⁰, other studies demonstrated that IGF-1 overexpression causes cardiac hypertrophy and heart failure and worsen recovery upon MI^{151,152}. Additionally, age-dependent increased expression of the inflammatory mediator ANGPTL2 (angiopoietin-like protein 2) is associated with cellular senescence (so far only proven in the skeletal muscle¹⁵³) and its overexpression in the heart impairs cardiac function by decreasing myocardial energy metabolism and inactivation of Akt as well as sarco(endo)plasmic reticulum Ca²⁺-ATPase (SERCA)2a signalling¹⁵⁴ suggesting that it might also contribute to cardiac dysfunction in the aging heart.

Fibroblasts in the aging heart: Cardiac aging is associated with an increase in fibroblasts relative to other cell types of the heart¹⁵⁵. Cardiac fibrosis is a reactive phenomenon that is associated with left ventricular hypertrophy¹⁵⁶. However, the underlying mechanisms mediating fibrosis during aging are still not fully understood. It is known that elevated angiotensin II levels and chronic inflammation can increase FB activation, proliferation, matrix protein production and hypertrophy¹⁵⁶. Furthermore, aged cardiac FB were demonstrated to increase the expression of prolyl hydroxylases and lysyl oxidase that promote ventricular stiffness by cross-linking matrix protein chains^{157,158}.

Additionally, aging is generally associated with an impairment of receptor-mediated functions, because of the loss of receptors or their uncoupling from their specific signaling pathways¹⁵⁹. This is true for FBs, which show an impaired TGF β and EGF response^{160,161} and ECs, which are characterized by compromised VEGF signaling¹⁶² in aging (Figure 3C-D). One may speculate that a more general decline in receptor-mediated signaling may compromise the cellular interactions and fine tuning of communication in the heart.

Endothelial cells in the aging heart: Aging plays a major role in vascular and cardiac remodeling. With advancing age, endothelial senescence and inflammation is mediated via the above mentioned pathways including oxidative stress, telomere erosion and mitochondrial dysfunction¹⁶³. FOXO and SIRT are two major regulators that control endothelial function¹⁶⁴. Whereas overexpression of FOXO1 in mice shows reduced angiogenesis through a so far unclear mechanism¹⁶⁵, FOXO3 and SIRT1 were described to regulate the expression of genes involved in mitochondrial antioxidant defense (MnSOD, catalase, sestrins, and selenoprotein P) and DNA

repair (GADD45a), thus, opposing the age-related effects of ROS in ECs^{166–168}. Since both FOXO and SIRT are downstream targets of IGF-1 and given that FOXO and SIRT play a protective role in maintaining health and function of ECs, they could be potential players in the age-related decline of endothelial function.

Similar to FBs, aging may also control extracellular matrix production in ECs. A dysregulation of the laminin β 1 and β 2 chain expression in aged cardiac mouse ECs was previously described. In the aging heart, ECs shift the expression from laminin β 2 to β 1 and thereby modulate cell-matrix adhesion, cell migration and EndoMT in an autocrine manner that may impair vessel integrity¹⁶⁹. Endothelial integrity is further disturbed by the age-related increase in ROS in the vasculature that leads to a Src-dependent degradation and loss of vascular-endothelial (VE)-cadherin from adherens junctions which impairs the ability to amplify endothelial dilation¹⁷⁰.

Advanced age is also associated with deteriorations of the arterial system that contribute to organ and tissue dysfunction¹⁷¹. Aging central arterial ECs display a decreased NO production^{172,173}, impaired barrier function¹⁷⁴ and are more prone to apoptosis¹⁷⁵. They additionally have a pro-inflammatory phenotype which includes the expression of various pro-inflammatory mediators such as ET-1¹⁷⁶, angiotensin II¹⁷⁷, TGF β , TNF α and IL-6¹⁷⁸. This pro-fibrotic and pro-inflammatory environment can be permissive for EndoMT and hence contribute to pathophysiologic alterations of the arterial wall like neointima formation and atherosclerosis. Evidences are given by studies showing that aged arterial ECs reduce internalization but increase degradation of VE-cadherin^{170,179}. Furthermore, aging arterial ECs reveal a prominent intimal fibrous lesion with expression of rigid proteins such as collagen and fibronectin. Vascular stiffness is further promoted by reduced compliance of elastic fibers and extensive cross-linking of collagen and fibronectin chains^{180–182}. The expression of the pro-fibrotic and pro-inflammatory factors mediating these processes can be localized to ECs and smooth muscle cells (SMC). *In vitro* assays showed that SMCs from aged arteries have increased proliferative and migratory capacities as well as higher NF κ B activity and expression of pro-fibrotic and pro-inflammatory mediators compared to young arterial SMCs. In contrast, mature contractile SMCs might have a reduced viability in aging arteries^{180–183}. As the aged arterial wall provides a pro-inflammatory environment that might support EndoMT, ECs undergoing EndoMT and not solely SMCs might contribute to arterial stiffness and fibrosis and hence promote arterial dysfunction¹⁷¹.

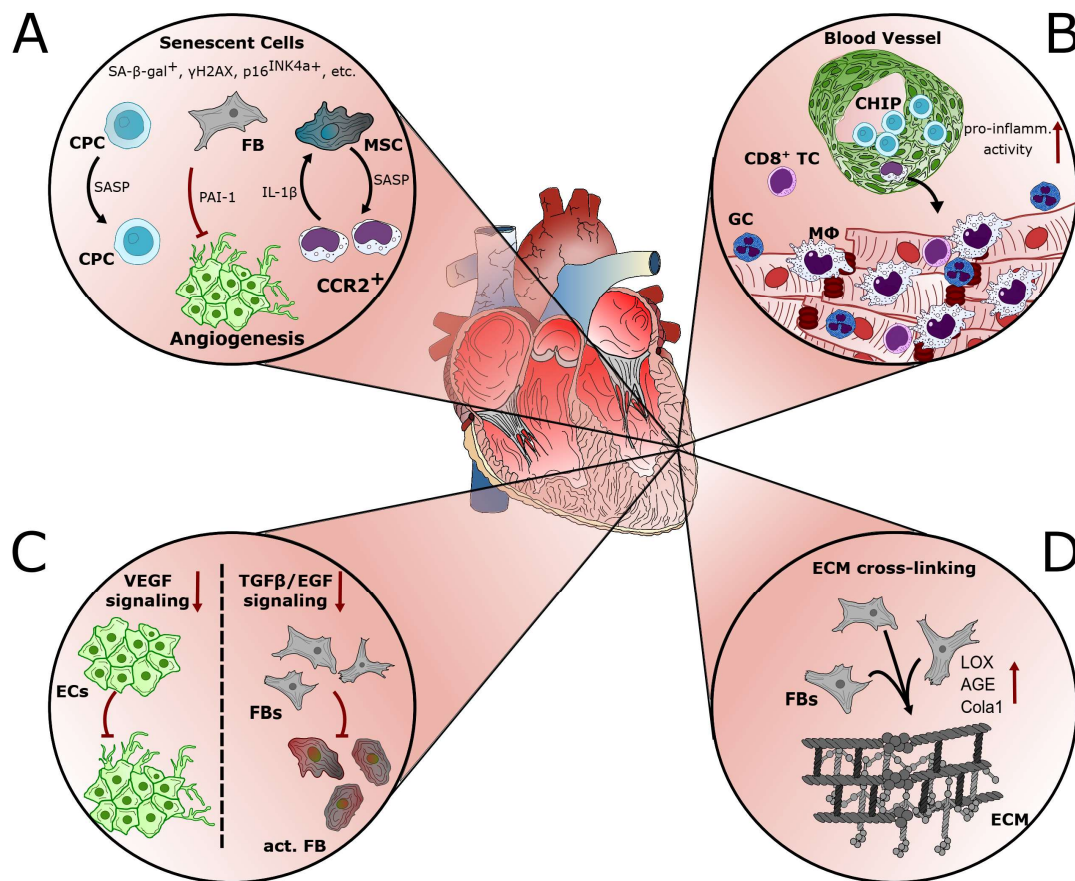


Figure 3: Cellular cross-talk in the aging heart. (A) Cellular senescence is characterized by the presence of various biomarkers such as high senescence-associated β-galactosidase activity (SA-β-gal⁺), γH2AX, p16^{INK4a} expression (p16^{INK4a}⁺), etc. Senescent cardiac progenitor cells (CPC) release SASP factors like PAI-1, IL-1, IL-6 and IL-8 and render senescence in otherwise healthy CPC. Aged cardiac fibroblasts (FB) secrete the SASP factor PAI-1 to inhibit angiogenesis and senescent mesenchymal stromal cells (MSC) release SASP factors that recruit CCR2⁺ monocytes that release IL-1 β and further render senescence in MSC. (B) Ageing is associated with major alterations of the immune system, referred to as “inflamm-aging”. This is reflected by alterations in the relative numbers of cardiac leukocytes: old hearts have proportionally more monocyte-derived cardiac macrophages (MΦ) and an increased population of granulocytes (GC). Moreover, aged mouse hearts have more CD8⁺ T cells (TC) than other lymphocytes. (C) In addition, aging is generally associated with an impairment of receptor-mediated functions, because of the loss of receptors or their uncoupling from their specific signaling pathways. This is true for FBs, which show an impaired TGFβ and EGF response and endothelial cells, which are characterized by compromised VEGF signaling. (D) Aging FBs display increased extracellular matrix (ECM) production and an increased expression of lysyl oxidase (LOX) as well as advanced glycation end-products (AGE) that excessively cross-link collagens and thereby promote ventricular rigidity.

4. Perspectives

The presented examples illustrate many facets of intracellular communication, which can be essential for maintenance of tissue homeostasis, repair and regeneration but may also contribute to pathological processes in the heart. Most studies so far focused on the elucidation of well-known mediators of cellular communication, mainly connexins, soluble cytokines or

growth factors which act on receptor expression in other cell types or other ligand-receptor interaction. Other ways of communication, e.g. microRNAs or other RNAs by exosomes, have also been studied, but mainly as therapeutic vehicles; their role as natural communication tools in physiological settings in tissues is less clear. Advanced technologies are likely to provide novel insights into small metabolites or lipids which can control cell-cell communication and influence cardiac physiology and disease. Finally, we are just at the beginning to understand the cellular heterogeneity within given cell types. Here single cell technologies likely will provide insights into the changes of cellular phenotypes under disease setting and may help to gain a deeper understanding of the impact of disease and aging on cellular phenotypes. All of these new insights may provide targets for controlling pathologically relevant alterations of cellular communication pathways in the future.

References

1. Benjamin, E. J. *et al.* Heart Disease and Stroke Statistics-2017 Update: A Report From the American Heart Association. *Circulation* **135**, e146–e603 (2017).
2. Timmis, A. *et al.* European Society of Cardiology: Cardiovascular Disease Statistics 2017. *Eur. Heart J.* **39**, 508–579 (2017).
3. Bergmann, O. *et al.* Dynamics of Cell Generation and Turnover in the Article Dynamics of Cell Generation and Turnover in the Human Heart. *Cell* **161**, 1566–1575 (2015).
4. Pinto, A. R., Chandran, A., Rosenthal, N. A. & Godwin, J. W. Isolation and analysis of single cells from the mouse heart. *J. Immunol. Methods* **393**, 74–80 (2013).
5. Perbellini, F. *et al.* Investigation of cardiac fibroblasts using myocardial slices. *Cardiovasc. Res.* **114**, 77–89 (2018).
6. Perbellini, F., Watson, S. A., Bardi, I. & Terracciano, C. M. Heterocellularity and Cellular Cross-Talk in the Cardiovascular System. *Front. Cardiovasc. Med.* **5**, 1–11 (2018).
7. Farbehi, N. *et al.* Single-cell expression profiling reveals dynamic flux of cardiac stromal, vascular and immune cells in health and injury. *Elife* **8**, e43882 (2019).
8. Poss, K. D., Wilson, L. G. & Keating, M. T. Heart Regeneration in Zebrafish. *Science (80-.)*. **298**, 2188 LP – 2190 (2002).
9. Raya, Á. *et al.* Activation of Notch signaling pathway precedes heart regeneration in zebrafish. *Proc. Natl. Acad. Sci.* **100**, 11889 LP – 11895 (2003).
10. Witman, N., Murtuza, B., Davis, B., Arner, A. & Morrison, J. I. Recapitulation of developmental cardiogenesis governs the morphological and functional regeneration of adult newt hearts following injury. *Dev. Biol.* **354**, 67–76 (2011).
11. Porrello, E. . R. *et al.* Transient regenerative potential of the neonatal mouse heart. *Science (80-.)*. **331**, 1078–1080 (2011).
12. Porrello, E. R. *et al.* Regulation of neonatal and adult mammalian heart regeneration by the miR-15 family. *Proc. Natl. Acad. Sci.* **110**, 187 LP – 192 (2013).

13. Itou, J., Kawakami, H., Burgoyne, T. & Kawakami, Y. Life-long preservation of the regenerative capacity in the fin and heart in zebrafish. *Biol. Open* **1**, 739 LP – 746 (2012).
14. Jesty, S. A. *et al.* c-kit+ precursors support postinfarction myogenesis in the neonatal, but not adult, heart. *Proc. Natl. Acad. Sci. U. S. A.* **109**, 13380–13385 (2012).
15. Strungs, E. G. *et al.* Cryoinjury models of the adult and neonatal mouse heart for studies of scarring and regeneration. *Methods Mol. Biol.* **1037**, 343–353 (2013).
16. Pinto, A. R. *et al.* Revisiting Cardiac Cellular Composition. *Circ. Res.* **118**, 400–409 (2016).
17. Molawi, K. *et al.* Progressive replacement of embryo-derived cardiac macrophages with age. *J. Exp. Med.* **211**, 2151 LP – 2158 (2014).
18. Epelman, S. *et al.* Embryonic and Adult-Derived Resident Cardiac Macrophages Are Maintained through Distinct Mechanisms at Steady State and during Inflammation. *Immunity* **40**, 91–104 (2014).
19. Dick, S. A. *et al.* Self-renewing resident cardiac macrophages limit adverse remodeling following myocardial infarction. *Nat. Immunol.* **20**, 29–39 (2019).
20. Patel, B. *et al.* CCR2+ Monocyte-Derived Infiltrating Macrophages Are Required for Adverse Cardiac Remodeling During Pressure Overload. *JACC Basic to Transl. Sci.* **3**, 230–244 (2018).
21. Hulsmans, M. *et al.* Cardiac macrophages promote diastolic dysfunction. *J. Exp. Med.* **215**, 423–440 (2018).
22. Swirski, F. K. & Nahrendorf, M. Cardioimmunology: the immune system in cardiac homeostasis and disease. *Nat. Rev. Immunol.* **18**, 733–744 (2018).
23. Frangogiannis, N. G. The inflammatory response in myocardial injury, repair, and remodelling. *Nat. Rev. Cardiol.* **11**, 255 (2014).
24. Zhang, J. *et al.* Regulation of Endothelial Cell Adhesion Molecule Expression by Mast Cells, Macrophages, and Neutrophils. *PLOS ONE* **6**, 17–19 (2011).
25. Xiaoxiang, Y. *et al.* Deleterious Effect of IL-23/IL-17A Axis and $\gamma\delta$ T Cells in Left Ventricular Remodeling after Myocardial Infarction in Rodent. *Circulation* **126**, A14348–A14348 (2012).
26. Ulrich, H. *et al.* Activation of CD4+ T Lymphocytes Improves Wound Healing and Survival After Experimental Myocardial Infarction in Mice. *Circulation* **125**, 1652–1663 (2012).
27. Johannes, W. *et al.* Foxp3+ CD4+ T Cells Improve Healing After Myocardial Infarction by Modulating Monocyte/Macrophage Differentiation. *Circ. Res.* **115**, 55–67 (2014).
28. Nahrendorf, M. *et al.* The healing myocardium sequentially mobilizes two monocyte subsets with divergent and complementary functions. *J. Exp. Med.* **204**, 3037 LP – 3047 (2007).
29. Euler, G. Good and bad sides of TGF β -signaling in myocardial infarction. *Frontiers in Physiology* **6**, 66 (2015).

30. Bischof, J. Endothelial-to-Mesenchymal Transition. *Circ. Res.* **124**, 1163–1165 (2019).
31. Trial, J. & Cieslik, K. A. Extracellular Matrix in Cardiovascular Pathophysiology Changes in cardiac resident fibroblast physiology and phenotype in aging. *J Physiol Hear.* **315**, H754–H755 (2018).
32. Piera-velazquez, S. & Jimenez, S. A. Endothelial to Mesenchymal Transition: Role in Physiology and in the Pathogenesis of Human Diseases. *Physiol. Rev.* **99**, 1281–1324 (2019).
33. Joyce, B. Endothelial-to-Mesenchymal Transition. *Circ. Res.* **124**, 1163–1165 (2019).
34. Paruchuri, S. *et al.* Human pulmonary valve progenitor cells exhibit endothelial/mesenchymal plasticity in response to vascular endothelial growth factor-A and transforming growth factor-beta2. *Circ. Res.* **99**, 861–869 (2006).
35. Kovacic, J. C. *et al.* Endothelial to Mesenchymal Transition in Cardiovascular Disease. *J. Am. Coll. Cardiol.* **73**, 190 LP – 209 (2019).
36. Bayoumi, A. S. *et al.* MicroRNA-532 protects the heart in acute myocardial infarction, and represses prss23, a positive regulator of endothelial-to-mesenchymal transition. *Cardiovasc. Res.* **113**, 1603–1614 (2017).
37. Evrard, S. M. *et al.* Endothelial to mesenchymal transition is common in atherosclerotic lesions and is associated with plaque instability. *Nat. Commun.* **7**, 11853 (2016).
38. Krishnamurthy, P. *et al.* IL-10 Inhibits Inflammation and Attenuates Left Ventricular Remodeling After Myocardial Infarction via Activation of STAT3 and Suppression of HuR. *Circ. Res.* **104**, 9–18 (2009).
39. Jung, M. *et al.* IL-10 improves cardiac remodeling after myocardial infarction by stimulating M2 macrophage polarization and fibroblast activation. *Basic Res. Cardiol.* **112**, 33 (2017).
40. Yang, Z., Zingarelli, B. & Szabo, C. Crucial role of endogenous interleukin-10 production in myocardial ischemia/reperfusion injury. *Circulation* **101**, 1019–1026 (2000).
41. Anversa, P., Olivetti, G., Melissari, M. & Loud, A. V. Stereological measurement of cellular and subcellular hypertrophy and hyperplasia in the papillary muscle of adult rat. *J. Mol. Cell. Cardiol.* **12**, 781–795 (1980).
42. Perbellini, F. *et al.* Investigation of cardiac fibroblasts using myocardial slices. *Cardiovasc. Res.* **114**, 77–89 (2017).
43. Banerjee, I., Fuseler, J. W., Price, R. L., Borg, T. K. & Baudino, T. A. Determination of cell types and numbers during cardiac development in the neonatal and adult rat and mouse. *Am. J. Physiol. Circ. Physiol.* **293**, H1883–H1891 (2007).
44. Sano, M. *et al.* p53-induced inhibition of Hif-1 causes cardiac dysfunction during pressure overload. *Nature* **446**, 444–448 (2007).
45. Hein, S. *et al.* Progression from compensated hypertrophy to failure in the pressure-overloaded human heart: structural deterioration and compensatory mechanisms. *Circulation* **107**, 984–991 (2003).
46. Leucker, T. M. *et al.* Endothelial–cardiomyocyte crosstalk enhances pharmacological

- cardioprotection. *J. Mol. Cell. Cardiol.* **51**, 803–811 (2011).
47. Wen, C. *et al.* Endothelial Actions of ANP Enhance Myocardial Inflammatory Infiltration in the Early Phase After Acute Infarction. *Circ. Res.* **119**, 237–248 (2016).
 48. Wan, A. & Rodrigues, B. Endothelial cell–cardiomyocyte crosstalk in diabetic cardiomyopathy. *Cardiovasc. Res.* **111**, 172–183 (2016).
 49. Lai, S.-L., Marín-Juez, R. & Stainier, D. Y. R. Immune responses in cardiac repair and regeneration: a comparative point of view. *Cell. Mol. Life Sci.* **76**, 1365–1380 (2019).
 50. Weyrich, A. S., Ma, X., Lefer, D. J., Albertine, K. H. & Lefer, A. M. In Vivo Neutralization of P-Selectin Protects Feline Heart and Endothelium in Myocardial Ischemia and Reperfusion Injury. *J. Clin. Invest.* **91**, 2620–2629 (1993).
 51. Kumar, A. G. *et al.* Induction of monocyte chemoattractant protein-1 in the small veins of the ischemic and reperfused canine myocardium. *Circulation* **95**, 693–700 (1997).
 52. Manavski, Y., Boon, R. A. & Dimmeler, S. Vascular niche controls organ regeneration. *Circ. Res.* **114**, 1077–1079 (2014).
 53. Colliva, A., Braga, L., Giacca, M. & Zacchigna, S. Endothelial cell–cardiomyocyte crosstalk in heart development and disease. *J. Physiol.* **597**, 1–17 (2019).
 54. Hu, J. *et al.* Endothelial Cell-Derived Angiopoietin-2 Controls Liver Regeneration as a Spatiotemporal Rheostat. *Science (80-.)*. **343**, 146–419 (2014).
 55. Manavski, Y. *et al.* Endothelial transcription factor KLF2 negatively regulates liver regeneration via induction of activin A. *Proc. Natl. Acad. Sci.* **114**, 3993–3998 (2017).
 56. Shiojima, I. *et al.* Disruption of coordinated cardiac hypertrophy and angiogenesis contributes to the transition to heart failure. *J. Clin. Invest.* **115**, 2108–2118 (2005).
 57. Kuba, K. *et al.* Impaired heart contractility in Apelin gene-deficient mice associated with aging and pressure overload. *Circ. Res.* **101**, e32–42 (2007).
 58. Li, W. *et al.* Premature death and age-related cardiac dysfunction in male eNOS-knockout mice. *J. Mol. Cell. Cardiol.* **37**, 671–680 (2004).
 59. Takimoto, E. *et al.* Oxidant stress from nitric oxide synthase-3 uncoupling stimulates cardiac pathologic remodeling from chronic pressure load. *J. Clin. Invest.* **115**, 1221–1231 (2005).
 60. Yasutomi, H. *et al.* The ATP-Binding Cassette Transporter ABCG2 Protects Against Pressure Overload–Induced Cardiac Hypertrophy and Heart Failure by Promoting Angiogenesis and Antioxidant Response. *Arterioscler. Thromb. Vasc. Biol.* **32**, 654–661 (2012).
 61. Narmoneva, D. A., Vukmirovic, R., Davis, M. E., Kamm, R. D. & Lee, R. T. Endothelial Cells Promote Cardiac Myocyte Survival and Implications for Cardiac Regeneration. *Circulation* **110**, 962–968 (2004).
 62. Kuramochi, Y. *et al.* Cardiac Endothelial Cells Regulate Reactive Oxygen Species-induced Cardiomyocyte Apoptosis through. *J. Biol. Chem.* **279**, 51141–51147 (2004).
 63. Giordano, F. J. *et al.* A cardiac myocyte vascular endothelial growth factor paracrine

- pathway is required to maintain cardiac function. *PNAS* **98**, 5780–5785 (2001).
64. Frangogiannis, N. G. The inflammatory response in myocardial injury, repair and remodeling. *Nat. Rev. Cardiol.* **11**, 255–265 (2015).
 65. Fatih, A. *et al.* Myocardial Ischemia/Reperfusion Injury Is Mediated by Leukocytic Toll-Like Receptor-2 and Reduced by Systemic Administration of a Novel Anti-Toll-Like Receptor-2 Antibody. *Circulation* **121**, 80–90 (2010).
 66. Mann, D. L. The emerging role of innate immunity in the heart and vascular system: for whom the cell tolls. *Circ. Res.* **108**, 1133–1145 (2011).
 67. Chao, W. Toll-like receptor signaling: a critical modulator of cell survival and ischemic injury in the heart. *Am. J. Physiol. Circ. Physiol.* **296**, H1–H12 (2009).
 68. Boyd, J. H., Mathur, S., Wang, Y., Bateman, R. M. & Walley, K. R. Toll-like receptor stimulation in cardiomyocytes decreases contractility and initiates an NF- κ B dependent inflammatory response. *Cardiovasc. Res.* **72**, 384–393 (2006).
 69. Frantz, S. *et al.* Toll4 (TLR4) expression in cardiac myocytes in normal and failing myocardium. *J. Clin. Invest.* **104**, 271–280 (1999).
 70. Pascal, K. *et al.* CD14-Deficient Mice Are Protected Against Lipopolysaccharide-Induced Cardiac Inflammation and Left Ventricular Dysfunction. *Circulation* **106**, 2608–2615 (2002).
 71. Pascal, K. *et al.* Toll-Like Receptor 2 Mediates Staphylococcus aureus-Induced Myocardial Dysfunction and Cytokine Production in the Heart. *Circulation* **110**, 3693–3698 (2004).
 72. Chao, W. *et al.* Lipopolysaccharide improves cardiomyocyte survival and function after serum deprivation. *J. Biol. Chem.* **280**, 21997–22005 (2005).
 73. Zhu, X. *et al.* MyD88 and NOS2 are essential for Toll-like receptor 4-mediated survival effect in cardiomyocytes. *Am. J. Physiol. Circ. Physiol.* **291**, H1900–H1909 (2006).
 74. Maejima, Y., Adachi, S., Morikawa, K., Ito, H. & Isobe, M. Nitric oxide inhibits myocardial apoptosis by preventing caspase-3 activity via S-nitrosylation. *J. Mol. Cell. Cardiol.* **38**, 163–174 (2005).
 75. Dimmeler, S., Haendeler, J., Nehls, M. & Zeiher, A. M. Suppression of apoptosis by nitric oxide via inhibition of interleukin-1 β -converting enzyme (ICE)-like and cysteine protease protein (CPP)-32-like proteases. *J. Exp. Med.* **185**, 601–607 (1997).
 76. Frantz, S., Kelly, R. A. & Bourcier, T. Role of TLR-2 in the activation of nuclear factor kappaB by oxidative stress in cardiac myocytes. *J. Biol. Chem.* **276**, 5197–5203 (2001).
 77. Sakata, Y. *et al.* Toll-like receptor 2 modulates left ventricular function following ischemia-reperfusion injury. *Am. J. Physiol. Heart Circ. Physiol.* **292**, H503–9 (2007).
 78. Favre, J. *et al.* Toll-like receptors 2-deficient mice are protected against postischemic coronary endothelial dysfunction. *Arterioscler. Thromb. Vasc. Biol.* **27**, 1064–1071 (2007).
 79. Oyama, J. *et al.* Reduced myocardial ischemia-reperfusion injury in toll-like receptor 4-deficient mice. *Circulation* **109**, 784–789 (2004).

80. Chong, A. J. *et al.* Toll-like receptor 4 mediates ischemia/reperfusion injury of the heart. *J. Thorac. Cardiovasc. Surg.* **128**, 170–179 (2004).
81. Ivey, M. J. & Tallquist, M. D. Defining the Cardiac Fibroblast. *Circ. J.* **80**, 2269–2276 (2016).
82. Moore-Morris, T., Cattaneo, P., Puceat, M. & Evans, S. M. Origins of cardiac fibroblasts. *J. Mol. Cell. Cardiol.* **91**, 1–5 (2016).
83. Quinn, T. A., Camelliti, P., Rog-zielinska, E. A., Siedlecka, U. & Poggioli, T. Electrotonic coupling of excitable and nonexcitable cells in the heart revealed by optogenetics. *PNAS* **113**, 14852–14857 (2016).
84. Fu, X. *et al.* Specialized fibroblast differentiated states underlie scar formation in the infarcted mouse heart Graphical abstract Find the latest version : Specialized fibroblast differentiated states underlie scar formation in the infarcted mouse heart. *JCI* **128**, 2127–2143 (2018).
85. Anzai, A. *et al.* The infarcted myocardium solicits GM-CSF for the detrimental oversupply of inflammatory leukocytes. *J. Exp. Med.* **214**, 3293–3310 (2017).
86. Liu, T., Zhou, L., Li, D., Andl, T. & Zhang, Y. Cancer-Associated Fibroblasts Build and Secure the Tumor Microenvironment. *Front. cell Dev. Biol.* **7**, 60 (2019).
87. Critchley DR. Focal adhesions - the cytoskeletal connection. *Curr. Opin. Cell Biol.* **12**, 133–139 (2000).
88. Bang, C. *et al.* Cardiac fibroblast-derived microRNA passenger strand-enriched exosomes mediate cardiomyocyte hypertrophy. *J. Clin. Invest.* **124**, 2136–2146 (2014).
89. Vidal, R. *et al.* Transcriptional heterogeneity of fibroblasts is a hallmark of the aging heart. *J. Clin. Investig. Insights in press*, (2019).
90. Aurora, A. B. *et al.* Macrophages are required for neonatal heart regeneration. *J. Clin. Invest.* **124**, 1382–1392 (2014).
91. Godwin, J. W., Debuque, R., Salimova, E. & Rosenthal, N. A. Heart regeneration in the salamander relies on macrophage-mediated control of fibroblast activation and the extracellular landscape. *NPJ Regen. Med.* **2**, 1–11 (2017).
92. Liu, B. *et al.* Cardiac resident macrophages are involved in hypoxia-induced postnatal cardiomyocyte proliferation. *Mol. Med. Rep.* **15**, 3541–3548 (2017).
93. Bevan, L. *et al.* Specific macrophage populations promote both cardiac scar deposition and subsequent resolution in adult zebrafish. *Cardiovasc. Res.* (2019). doi:10.1093/cvr/cvz221
94. Wynn, T. A. & Vannella, K. M. Macrophages in Tissue Repair, Regeneration, and Fibrosis. *Immunity* **44**, 450–462 (2016).
95. Saclier, M., Cuvellier, S., Magnan, M., Mounier, R. & Chazaud, B. Monocyte/macrophage interactions with myogenic precursor cells during skeletal muscle regeneration. *FEBS J.* **280**, 4118–4130 (2013).
96. Dobaczewski, M., Xia, Y., Bujak, M., Gonzalez-Quesada, C. & Frangogiannis, N. G. CCR5 signaling suppresses inflammation and reduces adverse remodeling of the infarcted

- heart, mediating recruitment of regulatory T cells. *Am. J. Pathol.* **176**, 2177–2187 (2010).
97. Stefan, F. *et al.* Regulatory T cells improve healing after myocardial infarction. *Circ. Res.* **113**, A211–A211 (2013).
 98. Zouggari, Y. *et al.* Regulatory T cells modulate postischemic neovascularization. *Circulation* **120**, 1415–1425 (2009).
 99. Hui, S. P. *et al.* Zebrafish Regulatory T Cells Mediate Organ-Specific Regenerative Programs. *Dev. Cell* **43**, 659–672.e5 (2017).
 100. Zacchigna, S. *et al.* Paracrine effect of regulatory T cells promotes cardiomyocyte proliferation during pregnancy and after myocardial infarction. *Nat. Commun.* **9**, 2432 (2018).
 101. Ieda, M. *et al.* Cardiac fibroblasts regulate myocardial proliferation through beta1 integrin signaling. *Dev. Cell* **16**, 233–244 (2009).
 102. Bassat, E. *et al.* The extracellular matrix protein agrin promotes heart regeneration in mice. *Nature* **547**, 179 (2017).
 103. Bolli, R. Cardioprotective function of inducible nitric oxide synthase and role of nitric oxide in myocardial ischemia and preconditioning: an overview of a decade of research. *J. Mol. Cell. Cardiol.* **33**, 1897–1918 (2001).
 104. Singer, M. The Influence of the Nerve in Regeneration of the Amphibian Extremity. *Q. Rev. Biol.* **27**, 169–200 (1952).
 105. Drachman, D. B. Atrophy of Skeletal Muscle in Chick Embryos Treated with Botulinum Toxin. *Science (80-)*. **145**, 719 LP – 721 (1964).
 106. Singer, M., Davis, M. H. & Scheuing, M. R. The influence of atropine and other neuropharmacological substances on regeneration of the forelimb in the adult urodele, *Triturus*. *J. Exp. Zool.* **143**, 33–45 (1960).
 107. A., W. I., Julie, G., Wayne, B. & M., H. J. Sympathetic Reinnervation Is Required for Mammalian Cardiac Regeneration. *Circ. Res.* **117**, 990–994 (2015).
 108. Mahmoud, A. I. *et al.* Nerves Regulate Cardiomyocyte Proliferation and Heart Regeneration. *Dev. Cell* **34**, 387–399 (2015).
 109. McManus, D. D. *et al.* Longitudinal Tracking of Left Atrial Diameter Over the Adult Life Course : Clinical Correlates in the Community. *Circulation* **121**, 667–674 (2010).
 110. Volpe, G. J. *et al.* Evaluation of Age-Related Interstitial Myocardial Fibrosis With Cardiac Magnetic Resonance Contrast-Enhanced T 1 Mapping MESA (Multi-Ethnic Study of Atherosclerosis). *J. Am. Coll. Cardiol.* **62**, (2013).
 111. Lung, B. & Vahanian, A. Epidemiology of Acquired Valvular Heart Disease. *Can. J. Cardiol.* **30**, 962–970 (2014).
 112. Feridooni, H. A., Dibb, K. M. & Howlett, S. E. How cardiomyocyte excitation, calcium release and contraction become altered with age. *J. Mol. Cell. Cardiol.* **83**, 62–72 (2015).

113. Blasco, M. A. Telomere length, stem cells and aging. *Nat. Chem. Biol.* **3**, 640–649 (2007).
114. Blackburn, E. H., Greider, C. W. & Szostak, J. W. Telomeres and telomerase: the path from maize, Tetrahymena and yeast to human cancer and aging. *Nat. Med.* **12**, 1133–1138 (2006).
115. Olovnikov, A. M. Telomeres, telomerase, and aging: origin of the theory. *Exp. Gerontol.* **31**, 443–448 (1996).
116. Hekimi, S., Lapointe, J. & Wen, Y. Taking a “good” look at free radicals in the aging process. *Trends Cell Biol.* **21**, 569–576 (2011).
117. Edgar, D. *et al.* Random Point Mutations with Major Effects on Protein-Coding Genes Are the Driving Force behind Premature Aging in mtDNA Mutator Mice. *Cell Metab.* **10**, 131–138 (2009).
118. López-Otín, C., Blasco, M. A., Partridge, L., Serrano, M. & Kroemer, G. The hallmarks of aging. *Cell* **153**, (2013).
119. Boon, R. A. *et al.* MicroRNA-34a regulates cardiac ageing and function. *Nature* **495**, 107–110 (2013).
120. Tchkonina, T., Zhu, Y., van Deursen, J., Campisi, J. & Kirkland, J. L. Cellular senescence and the senescent secretory phenotype: therapeutic opportunities. *J. Clin. Invest.* **123**, 966–972 (2013).
121. Siddiqi, S. & Sussman, M. A. Cardiac Hegemony of Senescence. *Curr. Transl. Geriatr. Exp. Gerontol. Rep.* **2**, 1–12 (2013).
122. Postmus, A. C. *et al.* Senescent cells in the development of cardiometabolic disease. *Curr. Opin. Lipidol.* **30**, 177–185 (2019).
123. Lewis-McDougall, F. C. *et al.* Aged-senescent cells contribute to impaired heart regeneration. *Aging Cell* **18**, e12931 (2019).
124. Martini, H. *et al.* Aging induces cardiac mesenchymal stromal cell senescence and promotes endothelial cell fate of the CD90 + subset. *Aging Cell* **18**, e13015 (2019).
125. Loffredo, F. S. *et al.* Growth differentiation factor 11 is a circulating factor that reverses age-related cardiac hypertrophy. *Cell* **153**, 828–839 (2013).
126. Sawaki, D. *et al.* Visceral Adipose Tissue Drives Cardiac Aging Through Modulation of Fibroblast Senescence by Osteopontin Production. *Circulation* **138**, 809–822 (2018).
127. Baker, D. J. *et al.* Naturally occurring p16Ink4a-positive cells shorten healthy lifespan. *Nature* **530**, 184 (2016).
128. Lehmann, M. *et al.* Senolytic drugs target alveolar epithelial cell function and attenuate experimental lung fibrosis ex vivo. *Eur. Respir. J.* **50**, (2017).
129. Xu, M. *et al.* Senolytics improve physical function and increase lifespan in old age. *Nat. Med.* **24**, 1246–1256 (2018).
130. Chang, J. *et al.* Clearance of senescent cells by ABT263 rejuvenates aged hematopoietic stem cells in mice. *Nat. Med.* **22**, 78–83 (2016).

131. Justice, J. N. *et al.* Senolytics in idiopathic pulmonary fibrosis: Results from a first-in-human, open-label, pilot study. *EBioMedicine* **40**, 554–563 (2019).
132. Jaiswal, S. *et al.* Clonal Hematopoiesis and Risk of Atherosclerotic Cardiovascular Disease. *N. Engl. J. Med.* **377**, 111–121 (2017).
133. Sano, S. *et al.* CRISPR-Mediated Gene Editing to Assess the Roles of Tet2 and Dnmt3a in Clonal Hematopoiesis and Cardiovascular Disease. *Circ. Res.* **123**, 335–341 (2018).
134. Sano, S. *et al.* Tet2-Mediated Clonal Hematopoiesis Accelerates Heart Failure Through a Mechanism Involving the IL-1beta/NLRP3 Inflammasome. *J. Am. Coll. Cardiol.* **71**, 875–886 (2018).
135. Mas-Peiro, S. *et al.* Clonal haematopoiesis in patients with degenerative aortic valve stenosis undergoing transcatheter aortic valve implantation. *Eur. Heart J.* (2019). doi:10.1093/eurheartj/ehz591
136. Dorsheimer, L. *et al.* Association of Mutations Contributing to Clonal Hematopoiesis With Prognosis in Chronic Ischemic Heart Failure. *JAMA Cardiol.* **4**, 25–33 (2019).
137. Ferrara, N. *et al.* β -adrenergic receptor responsiveness in aging heart and clinical implications. *Frontiers in Physiology* **4**, 396 (2014).
138. Giuseppe, R. *et al.* Targeting the β -Adrenergic Receptor System Through G-Protein–Coupled Receptor Kinase 2: A New Paradigm for Therapy and Prognostic Evaluation in Heart Failure. *Circ. Hear. Fail.* **5**, 385–391 (2012).
139. Dai, D.-F. & Rabinovitch, P. S. Cardiac Aging in Mice and Humans: The Role of Mitochondrial Oxidative Stress. *Trends Cardiovasc. Med.* **19**, 213–220 (2009).
140. Dai, D.-F. *et al.* Overexpression of catalase targeted to mitochondria attenuates murine cardiac aging. *Circulation* **119**, 2789–2797 (2009).
141. A., D. A. *et al.* Angiotensin II–Mediated Phenotypic Cardiomyocyte Remodeling Leads to Age-Dependent Cardiac Dysfunction and Failure. *Hypertension* **46**, 426–432 (2005).
142. Basso, N. *et al.* Protective effect of long-term angiotensin II inhibition. *Am. J. Physiol. Circ. Physiol.* **293**, H1351–H1358 (2007).
143. Olson, K. A. *et al.* Association of growth differentiation factor 11/8, putative anti-ageing factor, with cardiovascular outcomes and overall mortality in humans: analysis of the Heart and Soul and HUNT3 cohorts. *Eur. Heart J.* **36**, 3426–3434 (2015).
144. C., S. S. *et al.* GDF11 Does Not Rescue Aging-Related Pathological Hypertrophy. *Circ. Res.* **117**, 926–932 (2015).
145. Vinciguerra, M., Santini, M. P., Claycomb, W. C., Ladurner, A. G. & Rosenthal, N. Local IGF-1 isoform protects cardiomyocytes from hypertrophic and oxidative stresses via SirT1 activity. *Aging (Albany, NY)*. **2**, 43–62 (2009).
146. Milman, S. *et al.* Low insulin-like growth factor-1 level predicts survival in humans with exceptional longevity. *Aging Cell* **13**, 769–771 (2018).
147. North, B. J. & Sinclair, D. A. The intersection between aging and cardiovascular disease. *Circ. Res.* **110**, 1097–1108 (2012).

148. Li, Q. *et al.* Overexpression of insulin-like growth factor-1 in mice protects from myocyte death after infarction, attenuating ventricular dilation, wall stress, and cardiac hypertrophy. *J. Clin. Invest.* **100**, 1991–1999 (1997).
149. Kajstura, J. *et al.* IGF-1 Overexpression Inhibits the Development of Diabetic Cardiomyopathy and Angiotensin II–Mediated Oxidative Stress. *Diabetes* **50**, 1414 LP – 1424 (2001).
150. Li, Q. *et al.* Cardiac-specific overexpression of insulin-like growth factor 1 attenuates aging-associated cardiac diastolic contractile dysfunction and protein damage. *Am. J. Physiol. Circ. Physiol.* **292**, H1398–H1403 (2007).
151. Delaughter, M. C., Taffet, G. E., Fiorotto, M. L., Entmann, M. L. & SCHWARTZ, R. J. Local insulin-like growth factor I expression induces physiologic, then pathologic, cardiac hypertrophy in transgenic mice. *FASEB J.* **13**, 1923–1929 (1999).
152. Prêle, C. M. *et al.* Insulin-like growth factor-1 overexpression in cardiomyocytes diminishes ex vivo heart functional recovery after acute ischemia. *Cardiovasc. Pathol.* **21**, 17–27 (2012).
153. Zhao, J. *et al.* Age-dependent increase in angiopoietin-like protein 2 accelerates skeletal muscle loss in mice. *J. Biol. Chem.* **293**, 1596–1609 (2018).
154. Tian, Z. *et al.* ANGPTL2 activity in cardiac pathologies accelerates heart failure by perturbing cardiac function and energy metabolism. *Nat. Commun.* **7**, 13016 (2016).
155. Gramley, F. *et al.* Age-related atrial fibrosis. *Age (Omaha)*. **31**, 27–38 (2009).
156. Murtha, L. A. *et al.* The Processes and Mechanisms of Cardiac and Pulmonary Fibrosis. *Frontiers in Physiology* **8**, 777 (2017).
157. Stephens, E. H. & Grande-Allen, K. J. Age-related changes in collagen synthesis and turnover in porcine heart valves. *J. Heart Valve Dis.* **16**, 672–682 (2007).
158. Rohrbach, S., Simm, A., Pregla, R., Franke, C. & Katschinski, D. M. Age-dependent increase of prolyl-4-hydroxylase domain (PHD) 3 expression in human and mouse heart. *Biogerontology* **6**, 165–171 (2005).
159. Robert, L. & Fulop, T. Aging of cell communication: loss of receptor function. *Interdiscip. Top. Gerontol.* **39**, 142–162 (2014).
160. Shiraha, H., Gupta, K., Drabik, K. & Wells, A. Aging fibroblasts present reduced epidermal growth factor (EGF) responsiveness due to preferential loss of EGF receptors. *J. Biol. Chem.* **275**, 19343–19351 (2000).
161. Cieslik, K., Trial, J. & Entman, M. Defective myofibroblast formation from mesenchymal stem cells in the aging murine heart rescue by activation of the AMPK pathway. *Am J Pathol* **179**, 1792–1806 (2011).
162. Rivard, A. *et al.* Age-dependent impairment of angiogenesis. *Circulation* **99**, 111–120 (1999).
163. Münzel, T. *et al.* Impact of Oxidative Stress on the Heart and Vasculature. *J. Am. Coll. Cardiol.* **70**, 212 LP – 229 (2017).
164. F., O. M., Michael, P., David, S. & Brian, N. FOXOs and Sirtuins in Vascular Growth,

- Maintenance, and Aging. *Circ. Res.* **110**, 1238–1251 (2012).
165. Potente, M. *et al.* Involvement of Foxo transcription factors in angiogenesis and postnatal neovascularization. *J. Clin. Invest.* **115**, 2382–2392 (2005).
 166. Brunet, A. *et al.* Stress-Dependent Regulation of FOXO Transcription Factors by the SIRT1 Deacetylase. *Science (80-.)*. **303**, 2011 LP – 2015 (2004).
 167. Kops, G. J. P. L. *et al.* Forkhead transcription factor FOXO3a protects quiescent cells from oxidative stress. *Nature* **419**, 316–321 (2002).
 168. Tran, H. *et al.* DNA Repair Pathway Stimulated by the Forkhead Transcription Factor FOXO3a Through the Gadd45 Protein. *Science (80-.)*. **296**, 530 LP – 534 (2002).
 169. Wagner, J. U. G. *et al.* Switch in Laminin β 2 to Laminin β 1 Isoforms During Aging Controls Endothelial Cell Functions. *Arterioscler. Thromb. Vasc. Biol.* **38**, 1170–1177 (2018).
 170. Chang, F., Flavahan, S. & Flavahan, N. A. Superoxide inhibition restores endothelium-dependent dilatation in aging arteries by enhancing impaired adherens junctions. *Am. J. Physiol. Heart Circ. Physiol.* **314**, H805–H811 (2018).
 171. Flavahan, N. A. In Development-A New Paradigm for Understanding Vascular Disease. *J. Cardiovasc. Pharmacol.* **69**, 248–263 (2017).
 172. Anna, C. *et al.* Aging-Induced Phenotypic Changes and Oxidative Stress Impair Coronary Arteriolar Function. *Circ. Res.* **90**, 1159–1166 (2002).
 173. Sun, D. *et al.* Reduced release of nitric oxide to shear stress in mesenteric arteries of aged rats. *Am. J. Physiol. Circ. Physiol.* **286**, H2249–H2256 (2004).
 174. Belmin, J., Corman, B., Merval, R. & Tedgui, A. Age-related changes in endothelial permeability and distribution volume of albumin in rat aorta. *Am. J. Physiol. Circ. Physiol.* **264**, H679–H685 (1993).
 175. Csiszar, A., Ungvari, Z., Koller, A., Edwards, J. G. & Kaley, G. Proinflammatory phenotype of coronary arteries promotes endothelial apoptosis in aging. *Physiol. Genomics* **17**, 21–30 (2004).
 176. Goel, A. *et al.* Increased endothelial exocytosis and generation of endothelin-1 contributes to constriction of aged arteries. *Circ. Res.* **107**, 242–251 (2010).
 177. Wang, M. *et al.* Angiotensin II Activates Matrix Metalloproteinase Type II and Mimics Age-Associated Carotid Arterial Remodeling in Young Rats. *Am. J. Pathol.* **167**, 1429–1442 (2005).
 178. Csiszar, A., Ungvari, Z., Koller, A., Edwards, J. G. & Kaley, G. Aging-induced proinflammatory shift in cytokine expression profile in coronary arteries. *FASEB J.* **17**, 1183–1185 (2003).
 179. Chang, F., Flavahan, S. & Flavahan, N. A. Endothelial Adherens Junctions and Endothelial Dysfunction in Aging Arteries. *FASEB J.* **30**, 1276.5-1276.5 (2016).
 180. Miller, S. J. *et al.* Development of progressive aortic vasculopathy in a rat model of aging. *Am. J. Physiol. Circ. Physiol.* **293**, H2634–H2643 (2007).

181. Zhihe, L., Jeffrey, F., S., G. Z. & G., L. E. Increased Expression of Matrix Metalloproteinase-2 in the Thickened Intima of Aged Rats. *Hypertension* **33**, 116–123 (1999).
182. Mingyi, W. *et al.* Matrix Metalloproteinase 2 Activation of Transforming Growth Factor- β 1 (TGF- β 1) and TGF- β 1–Type II Receptor Signaling Within the Aged Arterial Wall. *Arterioscler. Thromb. Vasc. Biol.* **26**, 1503–1509 (2006).
183. Wang, M., Khazan, B. & Lakatta, E. G. Central Arterial Aging and Angiotensin II Signaling. *Curr. Hypertens. Rev.* **6**, 266–281 (2010).

9.3 Appendix 2

Switch in Laminin $\beta 2$ to Laminin $\beta 1$ Isoforms During Aging Controls Endothelial Cell Functions—Brief Report

Julian U.G. Wagner, Emmanouil Chavakis, Eva-Maria Rogg, Marion Muhly-Reinholz, Simone F. Glaser, Stefan Günther, David John, Francesca Bonini, Andreas M. Zeiher, Liliana Schaefer, Melanie-Jane Hannocks, Reinier A. Boon,* Stefanie Dimmeler*

Objective—Endothelial cells play important roles in tissue homeostasis and vascularization, a function that is impaired by aging. Here, we aim to decipher the role of the microenvironment underlying the impairment of endothelial cell functions by aging.

Approach and Results—RNA sequencing of isolated cardiac endothelial cells derived from young and 18-month-old mouse hearts revealed that aging affects the endothelial expression of genes encoding extracellular matrix proteins, specifically the laminin $\beta 1$ (*Lamb1*) and laminin $\beta 2$ (*Lamb2*) chains. Whereas *Lamb1* was upregulated, *Lamb2* was decreased in endothelial cells in old mice compared with young controls. A similar change in expression patterns was observed after induction of acute myocardial infarction. Mimicking aging and injury conditions by plating endothelial cells on laminin $\beta 1$ -containing laminin 411 matrix impaired endothelial cell adhesion, migration, and tube formation and augmented endothelial-to-mesenchymal transition and endothelial detachment compared with laminin 421, which contains the laminin $\beta 2$ chain. Because laminins can signal via integrin receptors, we determined the activation of ITGB1 (integrin $\beta 1$). Laminin 421 coating induced a higher activation of ITGB1 compared with laminin 411. siRNA-mediated silencing of ITGB1 reduced laminin $\beta 2$ -dependent adhesion, suggesting that laminin $\beta 2$ more efficiently activates ITGB1.

Conclusions—Mimicking age-related modulation of laminin $\beta 1$ versus $\beta 2$ chain expression changes the functional properties and phenotype of endothelial cells. The dysregulation of the extracellular matrix during vascular aging may contribute to age-associated impairment of organ function and fibrosis.



Visual Overview—An online [visual overview](#) is available for this article. (*Arterioscler Thromb Vasc Biol.* 2018;38:1170-1177. DOI: 10.1161/ATVBAHA.117.310685.)

Key Words: aging ■ endothelial cell ■ extracellular matrix ■ laminin ■ integrin

Downloaded from <http://ahajournals.org> by on December 10, 2018

Risk factors for coronary artery disease, including aging, are associated with impaired endothelial cell (EC) functions in conductance vessels leading to atherosclerotic lesion progression and subsequently myocardial infarction. Aging is additionally associated with impaired EC functions at the level of the microcirculation and reduced neovascularization after ischemia.¹ Microcirculatory dysfunction also occurs in patients with dilated cardiomyopathy.² Under certain conditions, ECs can undergo morphological and functional changes, thereby acquiring a mesenchymal phenotype. This process named endothelial-to-mesenchymal transition (EndoMT) can occur in many pathological conditions^{3,4,5} and is increased in senescent ECs in vitro.⁶ EndoMT leads to the formation of mesenchymal cells such as fibroblasts and is additionally associated with a proinflammatory phenotype of ECs.⁷ The induction of EndoMT is tightly controlled by several stimuli, such as

the prototypic inducer TGF- β (transforming growth factor- β), but can be antagonized by angiogenic growth factors (eg, FGF [fibroblast growth factor]).⁸ Extracellular matrix is critical for the function and integrity of blood vessels. ECs synthesize various extracellular matrix proteins, which control adhesion and motility, particularly during angiogenesis.⁹ Laminins comprise a large family of extracellular heterotrimeric matrix proteins that contain an α -chain, a β -chain, and a γ -chain and are important regulators of cell differentiation, migration, and adhesion.^{9,10} Eleven genetically distinct laminin chains exist, combining to form distinct heterotrimeric molecules,¹² which are named according to their chain composition; for example, laminin 411, a well-known endothelial basement membrane component consists of laminin $\alpha 4$, $\beta 1$, and $\gamma 1$ chains.¹³ Genetic deletion of many laminins leads to embryonic lethality, but conditional deletion studies indicate that laminins

Received on: September 19, 2017; final version accepted on: March 6, 2018.

From the Institute for Cardiovascular Regeneration (J.U.G.W., E.-M.R., M.M.-R., S.F.G., D.J., F.B., R.A.B., S.D.) and Institute of Pharmacology and Toxicology (L.S.), Goethe University, Frankfurt am Main, Germany; Internal Medicine III, Department of Cardiology, Goethe University Hospital, Frankfurt am Main, Germany (E.C., A.M.Z.); Max Planck Institute for Heart and Lung Research, Bad Nauheim, Germany (S.G.); German Center of Cardiovascular Research (DZHK), Frankfurt am Main (J.U.G.W., S.F.G., A.M.Z., R.A.B., S.D.); and Institute of Physiological Chemistry and Pathobiochemistry and Cells-in-Motion Cluster of Excellence, University of Münster, Germany (M.-J.H.).

*These authors contributed equally to this article.

The online-only Data Supplement is available with this article at <http://atvb.ahajournals.org/lookup/suppl/doi:10.1161/ATVBAHA.117.310685/-/DC1>.

Correspondence to Stefanie Dimmeler, PhD, Institute for Cardiovascular Regeneration, Goethe University, Frankfurt am Main, Theodor Stern Kai 7, Frankfurt 60590, Germany. E-mail dimmeler@em.uni-frankfurt.de

© 2018 American Heart Association, Inc.

Arterioscler Thromb Vasc Biol is available at <http://atvb.ahajournals.org>

DOI: 10.1161/ATVBAHA.117.310685

Nonstandard Abbreviations and Acronyms	
AMI	acute myocardial infarction
EBM	endothelial basal medium
EC	endothelial cells
EndoMT	endothelial-to-mesenchymal transition
HUVEC	human umbilical vein endothelial cell
ITGB1	integrin β 1
Lamb1	laminin β 1
Lamb2	laminin β 2
PECAM-1	platelet EC adhesion molecule-1
TGF-β	transforming growth factor β
VE-cadherin	vascular endothelial cadherin

play crucial roles in the functional integrity and regeneration of various tissues, including skeletal muscle tissue^{11,14,15} and endothelium.^{16–18} In addition, laminins have been implicated in cardiovascular functions and, in particular, in the synthetic versus contractile phenotype of smooth muscle cells.¹⁹

In this study, we aimed to determine the influence of aging and injury on EC matrix production. We observed a switch in the expression of laminins: the β 1 chain gene (*Lamb1*) was upregulated, whereas the β 2 chain gene (*Lamb2*) tended to be downregulated in cardiac ECs from old mice. Therefore, we performed in vitro studies using recombinant laminin 411 (containing *Lamb1*) and laminin 421 (containing *Lamb2*) and showed that the 2 laminin isoforms exhibit distinct effects on EC adhesion and phenotype.

Materials and Methods

In Vivo Studies

C57BL/6 mice were obtained from Charles River (Sulzfeld, Germany) and Janvier (Le Genest Saint-Isle, France). Acute myocardial infarction (AMI) was induced in male mice (8–10 weeks old) by ligation of the left anterior coronary artery under anesthesia with isoflurane and analgesia with Temgesic (0.1 mg/kg body weight) and Bupivacaine (1–2 mg/kg body weight). Postoperative care was maintained by a daily check-up and by Ampicillin (2 mg in 250 mL drink water), Carprofen (5 mg/kg body weight), and Temgesic (0.1 mg/kg body weight) application at the first 2 days after surgery. At day 3, Temgesic (0.05 mg/kg body weight) was used. Three days after AMI, ECs from the hearts' ventricle were isolated as described below.

Cardiac EC Isolation

Cardiac ECs were isolated from male old (18 months) versus young (12–15 weeks) mice after perfusion with isolectin by using a commercial service (Angiocrine Biosciences, San Diego, CA) isolating Cdh5+isolectin+ cells.²⁰ For analysis of ECs after AMI, mice hearts were harvested, cut into small pieces, and washed with Hanks buffered saline solution (+Ca²⁺/+Mg²⁺). Tissue dissociation was performed in 5 mL of Hanks buffered saline solution (+Ca²⁺/+Mg²⁺) containing 600 U/mL Collagenase Type II (Gibco by Life Technologies). To dissociate the solid heart tissue, genteMACS Dissociator (Miltenyi) with the pre-programmed program *m_neoheart_01_01* was used after 30, 20, and 10 minutes of digestion at 37°C. In a first step, cardiomyocytes were depleted by centrifugation (80g, 1 minute, 4°C), and ECs were isolated using Dynabeads (Invitrogen by Life Technologies) coated with anti-CD144 antibodies (BD Pharmingen) by magnetic separation (Miltenyi).

RNA Sequencing

RNA was isolated from isolated cardiac ECs using the miRNeasy micro Kit (Qiagen) combined with on-column DNase digestion (DNase-Free

DNase Set; Qiagen) to avoid contamination by genomic DNA. RNA and library preparation integrity were verified with a BioAnalyzer 2100 (Agilent) or LabChip Gx Touch 24 (Perkin Elmer). Four hundred nanograms of total RNA (control cardiac EC versus AMI cardiac EC) and 10 ng of total RNA (young cardiac EC versus aged cardiac EC) were used as input for ribosomal depletion with RiboGone-Mammalian (Clontech) followed by library preparation using SMARTer Stranded Total RNA Sample Prep Kit (Clontech). Sequencing was performed on the NextSeq500 instrument (Illumina) using v2 chemistry, resulting in 27 to 35 million reads per library with 2×75 bp paired-end setup. The resulting raw reads were assessed for quality, adapter content, and duplication rates with FastQC. *Fastx_trimmer* was used to trim the first 5 bp. Trimmed and filtered reads were aligned versus the Ensembl mouse genome version mm10 (GRCm38) using STAR 2.4.0a with the standard parameters.²¹ The number of reads aligning to genes was counted and compared with Cuffdiff version 2.2.1.²² The Ensembl annotation was enriched with UniProt data (release 06.06.2014) based on Ensembl gene identifiers (Activities at the Universal Protein Resource [UniProt]).

Immunostaining of Laminin β 1, Laminin β 2, and Isolectin B4

To determine laminin β 1 versus laminin β 2 expressions at the protein level, fluorescence immunostaining was performed in 3 young (12–15 weeks) and 3 aged (18 months) mouse heart cryosections. In some cases, heart sections were fixed for 2 minutes with ice-cold acetone or methanol and dried. Before antibody incubation, sections were washed once in 0.1% Triton X-100 in PBS for 5 minutes at room temperature (RT) and blocked in PBS containing 1% BSA for 1 hour at RT. Subsequently, sections were incubated with primary antibodies at RT for 60 minutes or overnight at 4°C. After washing in PBS containing 0.1% Triton X-100, incubations with secondary antibodies were performed at RT for 60 minutes. Primary antibodies used included rat antimouse laminin β 1 (3A4; conditioned medium, undiluted²³), rabbit antimouse laminin β 2 (489; 1:300²⁴), rat antimouse laminin α 2 (4H8-2),²⁵ rabbit antimouse laminin α 2 (401²⁶), and biotinylated isolectin B4 (diluted 1:100; number B-1205; Vector). Secondary antibodies included goat antirat Alexa Fluor 555 (number A21434; Invitrogen), goat antirabbit Alexa Fluor 488 (number A11008; Invitrogen), and streptavidin Alexa Fluor 647 (number S32357; Invitrogen) for isolectin B4. Nuclei were stained with Hoechst 33342 (number AS-83218; AnaSpec, Inc). To quantify laminin β 2 chain expression, fluorescence intensity per area was measured using the National Institutes of Health ImageJ software. To distinguish between the myocardial basement membrane staining and that of blood vessels, sections were double-stained for laminin α 2 (using 401²⁵ to mark myogenic basement membranes and laminin β 1 (3A4) or laminin α 2 (using 4H8-2) and laminin β 2 (489).

In Vitro Studies

Cell Culture

Human umbilical vein ECs (HUVECs) were purchased from Lonza and cultured with endothelial basal medium (EBM, Lonza) supplemented with 10% fetal calf serum (Invitrogen), amphotericin-B, ascorbic acid, bovine brain extract, endothelial growth factor, gentamycin sulfate, and hydrocortisone (EGM-singleQuots, Lonza) at a humidified atmosphere at 37°C and 5% CO₂. The described supplemented medium is referred as full EBM. Cells were detached with 0.25% trypsin (Life Technologies), which was incubated for 5 minutes at 37°C and 5% CO₂. Trypsin was neutralized by adding full medium, and the cell number was determined by using the cell counter NucleoCounter (ChemoMetec), as described in the manufacturer's protocol.

Coating of Cell Culture Dishes

Coating of cell culture dishes was performed by using 10.6 nmol/L of the human recombinant laminin 411 and 421 (BioLamina) or fibronectin (Sigma-Aldrich) diluted in PBS containing Ca²⁺ and Mg²⁺ (Sigma-Aldrich). Matrix proteins were incubated in cell culture dishes either for 2 hours at 37°C and 5% CO₂ or overnight at 4°C before seeding cells.

5×10⁴ HUVECs were seeded in 2 mL full EBM per coated 12-well plate well and were cultured for 10 days at 37°C and 5% CO₂ before performing functional assays. After 5 days, a replat was performed.

Proliferation Assay

The Click-IT EdU Microplate assay kit (Thermo Fisher Scientific) was used to analyze the cell proliferation of HUVECs cultured for 10 days on the different matrices.

Caspase 3/7 Activity Assay

The Apo-ONE Homogeneous Caspase 3/7 assay (Promega) was used to determine caspase 3/7-dependent apoptosis of HUVECs cultured for 10 days on the different matrices.

Tube-Formation Assay

In vitro tube formation was performed with 1.5×10^5 HUVECs cultured in 12-well plates (Greiner Bio-One GmbH) that had been coated with 250 μ L Matrigel (number 356234; Corning) containing 5 μ g laminin 421 or laminin 411. Matrigel without laminin served as control. Tube formation was determined after 24 hours by counting the branch points within the tube networks and by measuring the cumulative tube length in 3 randomly chosen microscopic fields with a computer-assisted microscope using Axiovision 4.5 (Zeiss).

HUVEC Matrix Adhesion Assay

Specific HUVEC adhesion to laminin 411, 421, or fibronectin was measured by performing cell adhesion assays. Four wells of a clear 96-well plate (Greiner Bio-One GmbH) were coated with laminin 421, laminin 411, or fibronectin as control. To determine nonspecific adhesion, additional 4 wells were coated with 10.6 nmol/L heat-inactivated BSA. Next, each well was blocked with 3% heat-inactivated BSA for 1 hour at RT. HUVECs were labeled with BCECF-AM (2', 7'-bis-(2-carboxyethyl)-5-(and-6)-carboxyfluorescein, acetoxymethyl ester; number B1150; Thermo Fisher Scientific) in EBM without any supplements for 30 minutes at 37°C. After labeling, a concentration of 1×10^6 HUVECs per 1 mL was adjusted in 0% EBM+0.05% BSA. 5×10^5 HUVECs were seeded as triplicate in the coated 96-well plate, which was washed twice with 200 μ L of 0% EBM+0.05% BSA and was pre-filled with 50 μ L of prewarmed 0% EBM+0.05% BSA. Wells filled with 50 μ L of 0% EBM+0.05% BSA only served as blank controls. HUVECs were allowed to adhere for 1 hour at 37°C and 5% CO₂. The initial fluorescence intensity of the labeled cells was measured using the microplate reader device Synergy HT Fluorometer (BioTek). After removal of nonadherent cells by washing, adherent cells were quantified. To receive the matrix-specific adhesion, the BSA blank values were subtracted from the matrix values. The results were represented as percentage of matrix-specific adhesion after washing against initial cell input.

Cell Migration Assay

Cell migration on laminin matrices was assessed by Boyden chamber assays. The assays were conducted in 24-well plates (Corning). Boyden chamber (FluoroBlok, Corning) inserts with 8- μ m pores were coated with laminin 421, laminin 411, and fibronectin (as positive control) overnight at 4°C as described above. The bottom chamber was loaded with 800 μ L full EBM. 5×10^4 HUVECs were adjusted in 200 μ L and added to the upper chamber. The cells were incubated for 3 hours at 37°C and 5% CO₂ in a humidified atmosphere, and the filters were fixed in 4% HistoFix (Carl-Roth GmbH & Co KG) and stained with 4',6-diamidino-2-phenylindole (Carl-Roth GmbH & Co KG). The number of cells that migrated through the filter was determined by counting the cells in 5 randomly chosen images in the center of the filter at $\times 10$ magnification using a Zeiss Axio Observer.Z1 microscope.

Induction of EndoMT

To determine the degree of EndoMT, 5×10^4 HUVECs were seeded in full EBM in 12-well plates coated with the different laminin isoforms or fibronectin, as described above. Cells were cultured for 7 days by performing a replate at day 5. After 7 days, the cells were split into 2 matrix-coated 12-well dishes. After 24 hours, EndoMT was induced by treating cells with endothelial basal medium supplemented with 10% fetal calf serum, amphotericin-B, ascorbic acid, gentamycin sulfate, and hydrocortisone (referred to hereafter as differentiation medium) without TGF β 2 or by treating cells with differentiation medium with 10 ng/mL human recombinant TGF β 2 (R&D Systems), which promotes EndoMT. After 48 hours, cells were

treated again with differentiation medium with or without TGF- β 2 and were incubated for additional 24 hours. To determine the degree of EndoMT on mRNA level, the expression of vascular endothelial cadherin (VE-cadherin) and endothelial NO synthase (as endothelial marker) and calponin and SM22 α (as smooth muscle marker) against P0 as reference gene were measured. Results are represented as fold change relative to the values measured in cells plated on laminin 421.

Detachment Assay

Cell-matrix detachment was assessed by seeding human coronary artery ECs (Lonza) in 50% confluence in 12-well plates coated with LM421 or LM411. To remove nonadhering or dead cells, the medium was changed after 1 hour of attachment. After further 24 and 48 hours, medium was changed, and cells in supernatants were quantified using a Neubauer chamber.

RNA Isolation and Quantification

Total RNA was purified from cells using the miRNeasy kits (Qiagen), combined with on-column DNase digestion (DNase-Free DNase Set, Qiagen) according to the manufacturer's instruction. The RNA concentration was determined by measuring absorption at 260 and 280 nm with the NanoDrop ND 2000-spectrophotometer (PeqLab).

cDNA Synthesis

To quantify mRNA expression by quantitative polymerase chain reaction (qPCR), 100 ng to 1 μ g of total RNA were reverse transcribed using the reverse transcriptase MuLV (Life Technologies). The cDNA synthesis was performed in a reaction volume of 20 μ L using 1 \times PCR Buffer II (10 \times) with magnesium (Thermo Fisher Scientific), 5 mmol/L of MgCl₂ (Applied Biosystems), 0.5 μ g of random hexamer primer (Thermo Fisher Scientific), 0.5 mmol/L of dNTP mix (Fermentas), 20 U of RNase inhibitor (Thermo Fisher Scientific), and 50 U of MuLV reverse transcriptase. The reaction was incubated at 43°C for 75 minutes followed by 5 minutes of heat inactivation at 95°C. The synthesized cDNA was diluted with RNase/DNase-free water (Invitrogen) to prevent any interferences during qPCR caused by the ion strength present in the cDNA reaction.

Real-Time qPCR

Real-time qPCR was performed using Fast SYBR Green master mix (Applied Biosystems) and an Applied Biosystems StepOnePlus machine. The synthesized cDNA served as template. Primer sequences were designed using the NCBI Primer-BLAST online tool and were purchased from Sigma-Aldrich. Primer sequences can be found in the Table. The real-time qPCR was performed in a volume of 20 μ L containing 5 μ L of cDNA template, 10 μ L of 2 \times Fast SYBR Green master

Table. Primer Sequences

Species	Gene	Primer	Sequence (5'–3')
Human	<i>Calponin</i>	Sense	CTGGCTGCAGCTTATTGATG
		Antisense	CTGAGAGAGTGGATCGAGGG
Human	<i>eNOS</i>	Sense	CACTCCCATGACTTTGGTGT
		Antisense	GTCGCGGTAGAGATGGTCAA
Human	<i>ITGB1</i>	Sense	ATTCCCTTCTCAGAAAGTC
		Antisense	TTTTCTTCCATTTCCCTCG
Human	<i>RPLP0</i>	Sense	TCGACAATGGCAGCATCTAC
		Antisense	ATCCGTCTCCACAGACAAGG
Human	<i>SM22α</i>	Sense	AAGAATGATGGGCACTACCG
		Antisense	ATGACATGCTTCCCTCCTCG
Human	<i>VE-cadherin</i>	Sense	ACGCCTCTGTCATGTACCAA
		Antisense	ACGATCTCATACCTGGCCTG

eNOS indicates endothelial NO synthase; ITGB1, integrin β 1; RPLP0, ribosomal P0; and VE-cadherin, vascular endothelial cadherin.

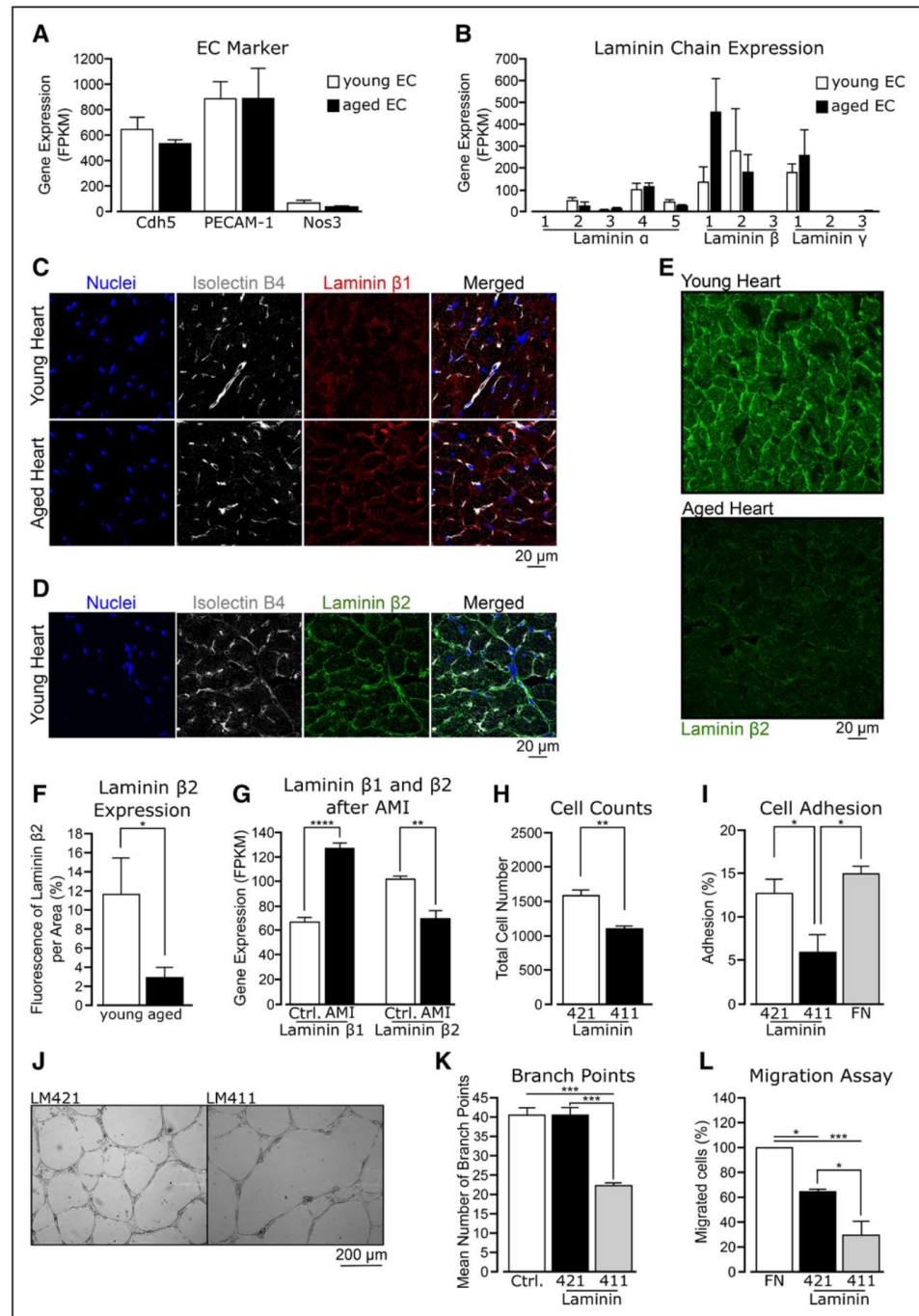


Figure 1. Laminin β1 and laminin β2 expression in aging and myocardial ischemia. **A** and **B**, Cdh5⁺ Isolectin⁺ cardiac endothelial cells (ECs) were isolated from the heart of 12 to 15 wks vs 18-mo-old mice, and RiboMinus RNA deep sequencing was performed to screen for gene expression differences. Whereas expression of endothelial markers (Cdh5, PECAM-1 [platelet endothelial cell adhesion molecule-1], and Nos3 [endothelial NO synthase]) was not altered (**A**), a dysregulation in laminin β1 and laminin β2 chain was found (**B**), but no changes in expression of laminin α (laminin α 1–5) or γ (laminin γ 1–3) chains were observed (n=3). **C**, Histological analysis of laminin β1 (detected by rat anti-*Lamb1* antibody, red) revealed a change in expression and localization with aging. ECs were stained with isolectin B4 (white). Nuclei were stained with Hoechst 33342 (blue). A representative image of >10 sections from 3 animals per group is shown. **D**, The colocalization of laminin β2 (detected by rabbit anti-*Lamb2* antibody) expression with isolectin B4–positive ECs in young hearts. **E**, Representative overviews of laminin β2 stainings in young vs old hearts. Quantification of laminin β2 expression is shown in **F**. For statistical analysis, n=9 (3 images per 6 animals) were used. **G**, Laminin β1 and laminin β2 RNA expression was analyzed using RNA deep sequencing data from ECs isolated at d 3 after acute myocardial infarction (AMI; n=4 control vs n=3 AMI). **H**, In vitro experiments revealed a reduced cell number after culturing human umbilical vein ECs (HUVEC) for 10 d on the laminin β1 matrix (laminin 411) compared with the laminin β2 matrix (laminin 421). Cell numbers were determined by counting total cell number of 10 randomly chosen view fields taken with the Zeiss Axiovert 100 microscope (n=4). **I**, Matrix adhesion (1 h) on laminin 421, laminin 411, or fibronectin (FN). Data (*Continued*)

mix (Applied Biosystems), 3 μ L of water, and 1 μ L of the sense and antisense primer (stock concentration of 10 μ mol/L each). Human ribosomal P0 (RPLP0) mRNA served as endogenous control. The real-time qPCR was performed in duplicates, and the analysis was performed with the formula $2^{-\Delta\Delta CT}$, with $\Delta\Delta CT = CT_{\text{target gene}} - CT_{\text{endogenous control}}$.

Immunostaining: VE-Cadherin and SM22 α

To determine EndoMT at the protein level, immunostaining against VE-cadherin and SM22 α were performed. 2×10^5 HUVECs were cultured in 8-well chamber glass slide (Nunc) coated with laminin 411 and laminin 421. Before culturing on the slides, HUVECs were preincubated 7 days on laminin 411 or 421. EndoMT was induced as described above. After EndoMT induction, cells were stained with goat anti-SM22 α antibody (number ab10135; Abcam) and anti-VE-cadherin antibody (number 2500S; Cell Signaling Technology). For primary antibody detection, the secondary anti-goat antibody, conjugated with Alexa Fluor 555 (number ab150130; Abcam) and antirabbit antibody, conjugated with Alexa Fluor 488 (number A-21206; Life Technology) were used. Nuclei were stained with 4',6-diamidino-2-phenylindole (number 6335.1; Carl-Roth GmbH & Co KG). Five random images per condition were taken using the Core LSM Leica microscope and the LASX software (Leica). To determine the degree of EndoMT, SM22 α -positive and VE-cadherin-positive cells were represented as percentage of the total cell number per image.

Immunostaining: Integrin β 1

Active ITGB1 (integrin β 1) was determined by immunostaining with an antibody recognizing the active conformations of ITGB1.²⁷ The wells of 8-well chamber glass slides (Nunc) were coated with 10.6 nmol/L of laminin 411, laminin 421, or fibronectin. 4×10^4 HUVECs per well were cultured for 24 hours at 37°C and 5% CO₂. After removing the media, cells were stained using the primary anti-ITGB1 antibody (clone: 12G10; number MAB2247; Merck Millipore) to detect active ITGB1. The primary antibody was detected with the secondary antimouse antibody (number A-11029; Thermo Fisher Scientific), conjugated with Alexa Fluor 488. Cytoskeleton was stained with phalloidin (number A22287; Thermo Fisher Scientific), conjugated with Alexa Fluor 647, whereas nuclei were labeled with 4',6-diamidino-2-phenylindole (number 6335.1; Carl-Roth GmbH & Co KG). Between 5 and 10 random images per condition were taken using the Core LSM Leica microscope and the LASX software (Leica). Signal intensities were evaluated using the National Institutes of Health ImageJ software. Data were normalized relative to the mean fluorescence signal detected in cells plated on laminin 421.

siRNA Transfection

HUVECs were transfected with siRNA purchased from Qiagen and Dharmacon. In brief, 1.8×10^5 HUVECs were seeded in 6-well plates and incubated at 37°C and 5% CO₂ for 24 hours. Cells were transfected using the Lipofectamine RNAiMax (Invitrogen) according to the manufacturer's protocol. Predesigned siRNA pool anti-hs_Integrin beta 1 SMARTpool (number M-004506-00-0005; Dharmacon) was used for siRNA-mediated silencing of ITGB1. AllStar Negative Control siRNA (number 1027280; Qiagen) were used as controls. Cells were cultured for 48 hours after transfection.

Secretome Analysis

Secreted proteins were detected in supernatants of HUVECs, which were cultured for 24 hours on LM421 or LM411. Supernatants were centrifuged (1500 rpm, 5 minutes) and were concentrated using 3K centrifugal filter units (Amicon Ultra-4, UFC800324; Merck Millipore; 6-fold). Then, cytokines and growth factors were detected using the Proteome Profiler Angiogenesis Array (ARY007; R&D Systems) according to the manufacturer's protocol.

Pathway Analysis and Heat Map Generation

Pathway analysis was performed with RNA deep sequencing data derived from isolated ECs of aged versus young mice hearts and from post-AMI versus control hearts. Significantly regulated genes were used for the analysis by using the metascapereg online tool. A heat map of RNA deep sequencing data derived from ECs isolated from aged versus young mice hearts was generated using the Morpheus online tool.

Statistical Analysis

Data are represented as mean, and error bars indicate SEM. Data were assessed statistically (D'Agostino and Kolmogorov–Smirnov test) for normality, and statistical power was determined, using 2-sided, unpaired *t* test for 2-group comparisons. For comparisons of >2 groups, multiple-group ANOVA with a post hoc Bonferroni test was used. **P*<0.05; ***P*<0.01; ****P*<0.001, and *****P*<0.0001.

Results

Aging and Injury Regulates Endothelial Laminin Isoform Expression

To elucidate the effect of aging on ECs, we isolated ECs from hearts of young (12–15 weeks) and 18-month-old mice using a previously established protocol.²⁰ Whereas EC marker genes such as Cdh5 (also known as VE-cadherin), endothelial NO synthase (Nos3), and CD31 (also known as PECAM-1 [platelet EC adhesion molecule-1]) were equally expressed (Figure 1A), several genes clustered in old versus young mice (Figure 1 in the [online-only Data Supplement](#)). Specifically, we observed a switch in the expression of the genes encoding laminin β chains (Figure 1B). *Lamb1* mRNA expression was increased, whereas *Lamb2* was decreased (Figure 1B). Expression of α and γ chains was not changed (Figure 1B). Histological analysis of *Lamb1* confirmed the dysregulation during aging (Figure 1C). Interestingly, the localization of the laminin β 1 and β 2 proteins was also changed. In young hearts, laminin β 1 was preferentially localized to the myocardial basement membrane, which was visualized by costaining for laminin α 2 (Figure IIA in the [online-only Data Supplement](#)), whereas in old mice hearts, laminin β 1 staining was increased in and around ECs (Figure 1C). By contrast, the laminin β 2 chain was highly expressed in vessels of the young hearts (Figure 1D; Figure IIB in the [online-only Data Supplement](#)) but was significantly reduced in old hearts (Figure 1E and 1F).

To determine whether the dysregulation of laminin β -isoforms is specific for aging or might also occur after injury, we measured *Lamb1* and *Lamb2* expression in ECs isolated from hearts 3 days after AMI (Figure 1G). Myocardial infarction resulted in significantly augmented *Lamb1* expression, whereas *Lamb2* mRNA expression was reduced. Histological analysis confirmed an upregulation of *Lamb1* and downregulation of *Lamb2* in the infarct zone (Figure IIC in the [online-only Data Supplement](#)). These data demonstrate that aging and injury control the expression of *Lamb1* and *Lamb2*.

Figure 1 Continued. were represented as percentage of matrix-specific adhesion after washing against initial cell input (n=4). **I**, Tubeformation assay of 1.5×10^5 HUVEC cultured 24 h on Matrigel (Corning) supplemented with 5- μ g laminin 421 or laminin 411. **K**, The quantification of branch points counted in 3 randomly chosen microscope images taken with the Zeiss Axiovert 100 microscope (n=4). **L**, Migration assay of 5×10^4 HUVEC cultured for 3 h in Boyden chambers that were coated with FN, laminin 421, or laminin 411. Cells that migrated through the chamber were stained with 4',6-diamidino-2-phenylindole and monitored with the Zeiss Axiovert microscope. Migration was determined by counting cells in 5 randomly chosen images (n=3). Data are expressed as mean \pm SEM. Statistical significance was determined, using the 2-sided, unpaired *t* test for 2-group comparisons (**A**, **B**, and **F** through **H**). For comparisons of >2 groups, multiple-group ANOVA with a post hoc Bonferroni test was used (**I** through **L**). **P*<0.05; ***P*<0.01; ****P*<0.001; and *****P*<0.0001.

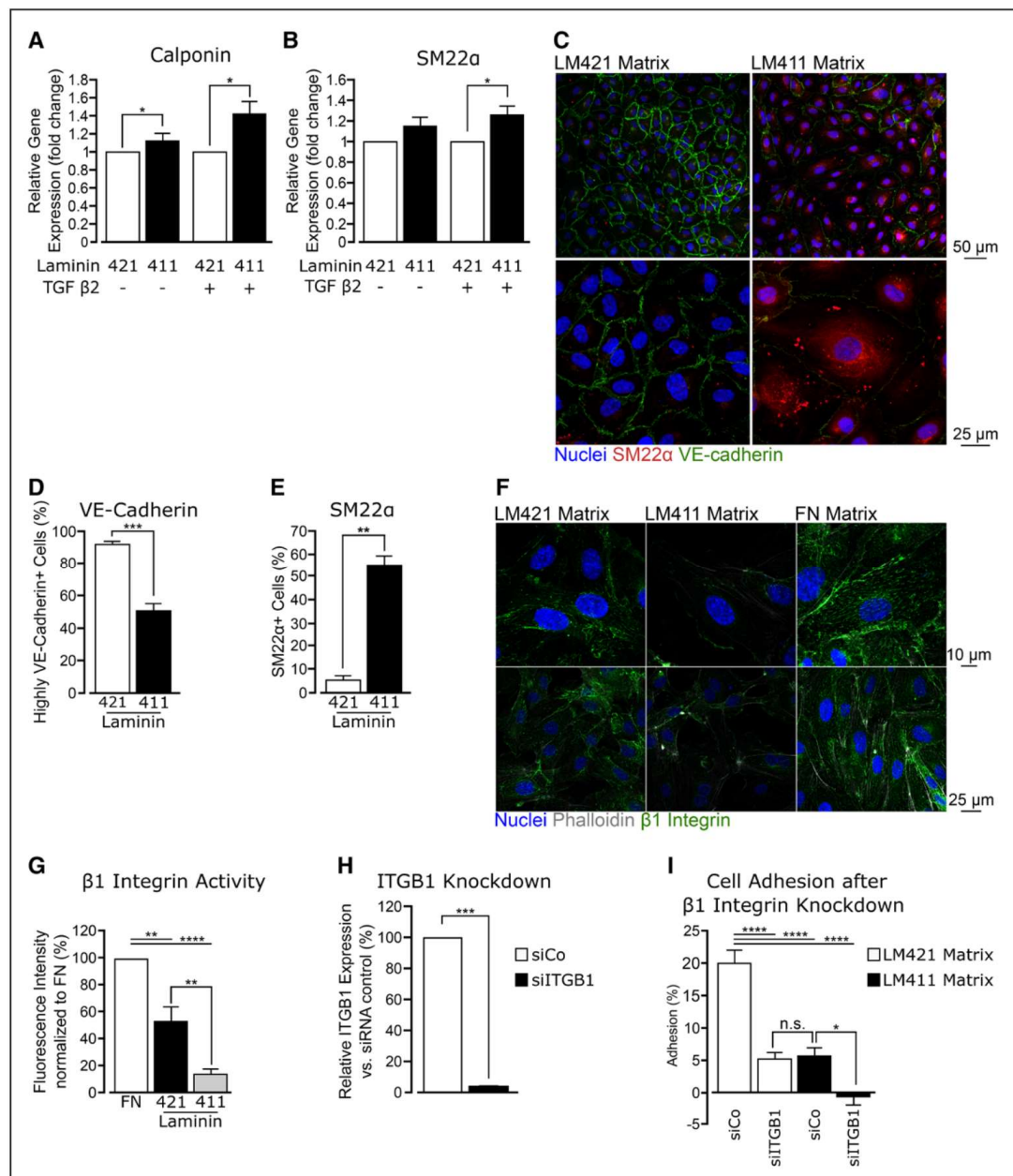


Figure 2. Laminin β 1 promotes endothelial-to-mesenchymal transition (EndoMT) and decreases integrin β 1 activity in endothelial cells compared with laminin β 2. **A** and **B**, Laminin β 1 (laminin 411) matrix augments expression of mesenchymal markers (calponin and SM22 α) on RNA level in the presence and absence of TGF β 2 (transforming growth factor β ; R&D Systems GmbH), compared with laminin β 2 (laminin 421) matrix. Before EndoMT induction, cells incubated 7 d on the respective laminin matrix. On day 9 and 11, cells were treated with medium conditioned either with or without 10 ng/mL TGF β 2 ($n=4$). **C**, Histological analysis of vascular endothelial cadherin (VE-cadherin; green) as endothelial marker (detected by rabbit anti-VE-cadherin antibody; Abcam) and SM22 α (red) as mesenchymal marker (detected by goat anti-SM22 α antibody; Cell Signaling Technology) shows morphological differences in size and shape of cells incubated on the laminin β 1 matrix in the presence of TGF β 2 compared with cells incubating on the laminin β 2 matrix. Nuclei stained with DAPI (4',6-diamidino-2-phenylindole; blue) served as counterstaining. The quantification of proteins is provided in **D** and **E** ($n=3$). **F** and **G**, Histological analysis of cells cultured for 24 h on the laminin β 2 (laminin 421), laminin β 1 (laminin 411), and fibronectin (FN) matrices revealed a decrease in ITGB1 (integrin β 1, green) activity in cells cultured on the laminin β 1 matrix compared with cells cultured on the laminin β 2 or FN matrices. Phalloidin-stained F-actin (gray) and DAPI-stained nuclei (blue) served as counterstaining ($n=4$). A representative example is shown in **F** and quantification is shown in **G**. **H** and **I**, After siRNA-mediated silencing of ITGB1 using 25 nmol/L siRNA (Dharmacon) for 48 h (**H**), cell-matrix adhesion assay was determined (**I**, $n=6$). Matrix adhesion was quantified as percentage of matrix-specific adhesion after washing (background was subtracted). Data are expressed as mean \pm SEM. Statistical analysis was done using 2-sided, unpaired t test for 2-group comparisons (**A** through **E** and **H**). For comparisons of >2 groups, multiple-group ANOVA with a post hoc Bonferroni test was used (**G** and **I**). * $P<0.05$; ** $P<0.01$; *** $P<0.001$ and **** $P<0.0001$.

Cultivation of ECs on Laminin β 1 Versus Laminin β 2 Affects Adhesion and EndoMT

Because laminin β 1 and β 2 differ by 49.8% in amino acid sequence in mouse and 50.8% in human, we questioned whether laminins carrying these chains have distinct functions in ECs. To mimic the *in vivo* situation, we cultured human umbilical cord vein ECs on the laminin isoforms carrying the major endothelial laminin α chain, laminin α 4,¹³ coupled with either laminin β 1 or β 2 chains, and the γ 1 chain, ie, laminin 411 or 421, respectively. After 10 days of culture, significantly lower numbers of ECs were observed on laminin 411 versus 421 matrices (Figure 1H). To determine whether reduced cell number was because of an effect on cell proliferation or cell death, we measured EC proliferation and apoptosis by microplate assays. However, neither apoptosis (as assessed by caspase 3/7 activity) nor cell proliferation was affected by the different matrices (Figure IIIA and IIIB in the [online-only Data Supplement](#)). To elucidate whether the reduced cell numbers observed on the laminin 411 matrix might be caused by an impaired adhesion, we measured short-term adhesion on laminin 411 versus laminin 421. Indeed, EC adhesion was significantly lower on laminin 411 versus laminin 421 or fibronectin matrix (Figure 1I). Moreover, laminin 411 matrix reduced EC migration and tube formation (Figure 1J through 1L; Figure IIIC and IIID in the [online-only Data Supplement](#)). Similar effects were observed when assessing migration of human coronary artery ECs (Figure IIIE in the [online-only Data Supplement](#)).

Because cellular senescence was shown to augment EndoMT *in vitro*⁶ and EndoMT markers were elevated in ECs isolated from aged and infarcted mice hearts (Figure IV in the [online-only Data Supplement](#)), we next investigated the effects of laminin 411 and laminin 421 on EndoMT by measuring expression of mesenchymal/smooth muscle markers. Laminin 411 matrix augmented basal and TGF- β 2-induced calponin, SM22 α , and vimentin mRNA expression compared with laminin 421-cultured ECs (Figure 2A and 2B; Figure VA in the [online-only Data Supplement](#)). In addition, SM22 α protein expression and morphological changes consistent with EndoMT were higher in laminin 411-cultured ECs in the presence of TGF- β 2 (Figure 2C through 2E). Although EC markers were not affected at the mRNA level (Figure VB in the [online-only Data Supplement](#)), VE-cadherin protein expression was lower in laminin 411-cultured cells (Figure 2C and 2D). The localization of VE-cadherin at the EC junctions was also less pronounced in laminin 411-cultured ECs (Figure 2C), suggesting that laminin 411 augments EndoMT. Because EndoMT was recently reported in ECs in human atherosclerotic lesions,⁵ where plaque erosion may trigger acute events,²⁸ we assessed the impact of the matrix on EC detachment. EC cultured on laminin 411 matrix showed significantly higher detachment compared with laminin 421 matrix (Figure IIIF in the [online-only Data Supplement](#)). Together, these data provide evidence that a switch in laminin β 1 to laminin β 2 affects EC functions and phenotypes *in vitro*.

Laminin 411 Versus 421 Isoforms Differentially Regulate Integrin Activation

Laminins bind to integrins to regulate cellular functions.²⁹ Among the known interaction partners of laminin 411 and 421, ITGB1 is highly expressed and functionally important in

ECs.³⁰ Therefore, we determined the effect of laminin 411 versus 421 on ITGB1 activation by using antibodies that specifically detect the active form of ITGB1. Culturing EC on laminin 421 resulted in a significantly higher activation of ITGB1 compared with EC cultured on laminin 411 (Figure 2F and 2G). Silencing of ITGB1 by siRNA reduced EC adhesion on laminin 421 matrix to levels measured on laminin 411 matrix and abolished adhesion on laminin 411 matrix (Figure 2H and 2I).

Discussion

In summary, the data of the present study demonstrate that endothelial extracellular matrix proteins are dysregulated by aging. The switch from *Lamb2*, which is highly expressed in ECs of young hearts, to *Lamb1* gene expression in aged hearts modulates EC functions and phenotype. EC adhesion was higher on laminin 421 matrix, probably because of higher ITGB1 activation elicited by laminin 421 compared with laminin 411 matrix. Importantly, laminin 411 sensitizes EC to lose their endothelial identity and acquire mesenchymal features. EndoMT was shown to contribute to cardiac fibrosis³ and atherosclerosis,^{4,5} both of which are prototypic age-associated diseases. The age-associated switch in *Lamb2* to *Lamb1* may, thus, facilitate these pathophysiological processes. However, we cannot exclude that this switch might be a compensatory mechanism because myocardial injury also induced a similar change in *Lamb1/Lamb2* expression and a transient, incomplete induction of EndoMT, which may even promote sprouting angiogenesis.³¹ Moreover, because ECs were shown to provide extracellular factors that determine the balance between regeneration versus fibrosis in other tissues such as lung or liver,³² one may speculate that a dysfunction of ECs matrix protein synthesis might not only impair EC intrinsic functions but also change the paracrine environment, thereby contributing to age-associated tissue dysfunction. Interestingly, we observed profound changes in cytokines and growth factors in supernatants obtained from EC that were cultured on laminin 411 versus 412 matrix (Figure VI in the [online-only Data Supplement](#)). Thus, laminin 411-cultured cells secrete less thrombospondin-2, a cytokine with multiple and complex effects on the cardiovascular system,³³ and FGF2, a well-established inhibitor of EndoMT.³⁴ Further *in vivo* studies are needed to confirm our *in vitro* studies and will need to address the relevance of endothelial *Lamb1* and *Lamb2* in injury and aging.

Acknowledgments

We thank Ariane Fischer for help with the animal experiments and Dr Lydia Sorokin (University Münster) for conceptual advice. The study is supported by the Deutsche Forschungsgemeinschaft SFB834 (Project B5), the DFG Clusters of Excellence Cardiopulmonary Systems and Cells-in-Motion, and the LOEWE Center for Cell- and Gene Therapy (state of Hessen).

Disclosures

None.

References

- Rivard A, Fabre JE, Silver M, Chen D, Murohara T, Kearney M, Magner M, Asahara T, Isner JM. Age-dependent impairment of angiogenesis. *Circulation*. 1999;99:111–120.

2. Neglia D, Michelassi C, Trivieri MG, Sambucetti G, Giorgetti A, Pratali L, Gallopin M, Salvadori P, Sorace O, Carpeggiani C, Poddighe R, L'Abbate A, Parodi O. Prognostic role of myocardial blood flow impairment in idiopathic left ventricular dysfunction. *Circulation*. 2002;105:186–193.
3. Zeisberg EM, Tarnavski O, Zeisberg M, Dorfman AL, McMullen JR, Gustafsson E, Chandraker A, Yuan X, Pu WT, Roberts AB, Neilson EG, Sayegh MH, Izumo S, Kalluri R. Endothelial-to-mesenchymal transition contributes to cardiac fibrosis. *Nat Med*. 2007;13:952–961. doi: 10.1038/nm1613.
4. Chen PY, Qin L, Baeyens N, Li G, Afolabi T, Budatha M, Tellides G, Schwartz MA, Simons M. Endothelial-to-mesenchymal transition drives atherosclerosis progression. *J Clin Invest*. 2015;125:4514–4528. doi: 10.1172/JCI82719.
5. Evrard SM, Lecce L, Michelis KC, et al. Endothelial to mesenchymal transition is common in atherosclerotic lesions and is associated with plaque instability. *Nat Commun*. 2016;7:11853. doi: 10.1038/ncomms11853.
6. Fleenor BS, Marshall KD, Rippe C, Seals DR. Replicative aging induces endothelial to mesenchymal transition in human aortic endothelial cells: potential role of inflammation. *J Vasc Res*. 2012;49:59–64. doi: 10.1159/000329681.
7. Pérez L, Muñoz-Durango N, Riedel CA, Echeverría C, Kalergis AM, Cabello-Verrugio C, Simon F. Endothelial-to-mesenchymal transition: cytokine-mediated pathways that determine endothelial fibrosis under inflammatory conditions. *Cytokine Growth Factor Rev*. 2017;33:41–54. doi: 10.1016/j.cytogfr.2016.09.002.
8. Dejana E, Hirschi KK, Simons M. The molecular basis of endothelial cell plasticity. *Nat Commun*. 2017;8:14361. doi: 10.1038/ncomms14361.
9. Iruela-Arispe ML, Diglio CA, Sage EH. Modulation of extracellular matrix proteins by endothelial cells undergoing angiogenesis in vitro. *Arterioscler Thromb*. 1991;11:805–815.
10. Domogatskaya A, Rodin S, Tryggvason K. Functional diversity of laminins. *Annu Rev Cell Dev Biol*. 2012;28:523–553. doi: 10.1146/annurev-cellbio-101011-155750.
11. Yao Y. Laminin: loss-of-function studies. *Cell Mol Life Sci*. 2017;74:1095–1115. doi: 10.1007/s00018-016-2381-0.
12. Aumailley M. The laminin family. *Cell Adh Migr*. 2013;7:48–55. doi: 10.4161/cam.22826.
13. Frieser M, Nöckel H, Pausch F, Röder C, Hahn A, Deutzmann R, Sorokin LM. Cloning of the mouse laminin alpha 4 cDNA. Expression in a subset of endothelium. *Eur J Biochem*. 1997;246:727–735.
14. Riederer I, Bonomo AC, Mouly V, Savino W. Laminin therapy for the promotion of muscle regeneration. *FEBS Lett*. 2015;589:3449–3453. doi: 10.1016/j.febslet.2015.10.004.
15. Yao Y, Norris EH, Mason CE, Strickland S. Laminin regulates PDGFR β (+) cell stemness and muscle development. *Nat Commun*. 2016;7:11415. doi: 10.1038/ncomms11415.
16. Thyboll J, Kortessmaa J, Cao R, Soininen R, Wang L, Iivanainen A, Sorokin L, Risling M, Cao Y, Tryggvason K. Deletion of the laminin alpha4 chain leads to impaired microvessel maturation. *Mol Cell Biol*. 2002;22:1194–1202.
17. Wu C, Ivars F, Anderson P, Hallmann R, Vestweber D, Nilsson P, Robenek H, Tryggvason K, Song J, Korpos E, Loser K, Beissert S, Georges-Labouesse E, Sorokin LM. Endothelial basement membrane laminin alpha5 selectively inhibits T lymphocyte extravasation into the brain. *Nat Med*. 2009;15:519–527. doi: 10.1038/nm.1957.
18. Di Russo J, Luik AL, Yousif L, Budny S, Oberleithner H, Hofschröder V, Klingauf J, van Bavel E, Bakker EN, Hellstrand P, Bhattacharya A, Albinsson S, Pincet F, Hallmann R, Sorokin LM. Endothelial basement membrane laminin 511 is essential for shear stress response. *EMBO J*. 2017;36:183–201. doi: 10.15252/embj.201694756.
19. Yousif LF, Di Russo J, Sorokin L. Laminin isoforms in endothelial and perivascular basement membranes. *Cell Adh Migr*. 2013;7:101–110. doi: 10.4161/cam.22680.
20. Nolan DJ, Ginsberg M, Israely E, et al. Molecular signatures of tissue-specific microvascular endothelial cell heterogeneity in organ maintenance and regeneration. *Dev Cell*. 2013;26:204–219. doi: 10.1016/j.devcel.2013.06.017.
21. Dobin A, Davis CA, Schlesinger F, Drenkow J, Zaleski C, Jha S, Batut P, Chaisson M, Gingeras TR. STAR: ultrafast universal RNA-seq aligner. *Bioinformatics*. 2013;29:15–21. doi: 10.1093/bioinformatics/bts635.
22. Liao Y, Smyth GK, Shi W. featureCounts: an efficient general purpose program for assigning sequence reads to genomic features. *Bioinformatics*. 2014;30:923–930. doi: 10.1093/bioinformatics/btt656.
23. Sixt M, Hallmann R, Wendler O, Scharffetter-Kochanek K, Sorokin LM. Cell adhesion and migration properties of beta 2-integrin negative polymorphonuclear granulocytes on defined extracellular matrix molecules. Relevance for leukocyte extravasation. *J Biol Chem*. 2001;276:18878–18887. doi: 10.1074/jbc.M010898200.
24. Sasaki T, Mann K, Miner JH, Miosge N, Timpl R. Domain IV of mouse laminin beta1 and beta2 chains. *Eur J Biochem*. 2002;269:431–442.
25. Schuler F, Sorokin LM. Expression of laminin isoforms in mouse myogenic cells *in vitro* and *in vivo*. *J Cell Sci*. 1995;108(pt 12):3795–3805.
26. Ringelmann B, Röder C, Hallmann R, Maley M, Davies M, Grounds M, Sorokin L. Expression of laminin alpha1, alpha2, alpha4, and alpha5 chains, fibronectin, and tenascin-C in skeletal muscle of dystrophic 129ReJ dy/dy mice. *Exp Cell Res*. 1999;246:165–182. doi: 10.1006/excr.1998.4244.
27. Manavski Y, Carmona G, Bennewitz K, Tang Z, Zhang F, Sakurai A, Zeiher AM, Gutkind JS, Li X, Kroll J, Dimmeler S, Chavakis E. Brag2 differentially regulates β 1- and β 3-integrin-dependent adhesion in endothelial cells and is involved in developmental and pathological angiogenesis. *Basic Res Cardiol*. 2014;109:404. doi: 10.1007/s00395-014-0404-2.
28. Libby P, Pasterkamp G. Requiem for the 'vulnerable plaque'. *Eur Heart J*. 2015;36:2984–2987. doi: 10.1093/eurheartj/ehv349.
29. Nishiuchi R, Takagi J, Hayashi M, Ido H, Yagi Y, Sanzen N, Tsuji T, Yamada M, Sekiguchi K. Ligand-binding specificities of laminin-binding integrins: a comprehensive survey of laminin-integrin interactions using recombinant alpha3beta1, alpha6beta1, alpha7beta1 and alpha6beta4 integrins. *Matrix Biol*. 2006;25:189–197. doi: 10.1016/j.matbio.2005.12.001.
30. Carlson TR, Hu H, Braren R, Kim YH, Wang RA. Cell-autonomous requirement for beta1 integrin in endothelial cell adhesion, migration and survival during angiogenesis in mice. *Development*. 2008;135:2193–2202. doi: 10.1242/dev.016378.
31. Gerhardt H, Golding M, Fruttiger M, Ruhrberg C, Lundkvist A, Abramsson A, Jeltsch M, Mitchell C, Alitalo K, Shima D, Betsholtz C. VEGF guides angiogenic sprouting utilizing endothelial tip cell filopodia. *J Cell Biol*. 2003;161:1163–1177. doi: 10.1083/jcb.200302047.
32. Manavski Y, Boon RA, Dimmeler S. Vascular niche controls organ regeneration. *Circ Res*. 2014;114:1077–1079. doi: 10.1161/CIRCRESAHA.114.303452.
33. Chistiakov DA, Melnichenko AA, Myasoedova VA, Grechko A V, Orekhov AN. Thrombospondins: a role in cardiovascular disease. *Int J Mol Sci*. 2017;18:E1540. doi: 10.3390/ijms18071540.
34. Chen PY, Qin L, Barnes C, Charisse K, Yi T, Zhang X, Ali R, Medina PP, Yu J, Slack FJ, Anderson DG, Kotelianski V, Wang F, Tellides G, Simons M. FGF regulates TGF- β signaling and endothelial-to-mesenchymal transition via control of let-7 miRNA expression. *Cell Rep*. 2012;2:1684–1696. doi: 10.1016/j.celrep.2012.10.021.

Highlights

- The study reports that aging and injury induce a switch in endothelial expression of the β chain isoforms of laminins, which comprise important extracellular matrix proteins.
- Mimicking age-related modulation of laminin β 1 versus β 2 chain expression changes the functional properties and phenotype of endothelial cells.
- Thus, the laminin β 1-containing matrix impaired endothelial cell adhesion, migration, and tube formation and augmented endothelial-to-mesenchymal transition and endothelial detachment *in vitro*.
- The dysregulation of the extracellular matrix during vascular aging may contribute to age-associated impairment of organ function and fibrosis.

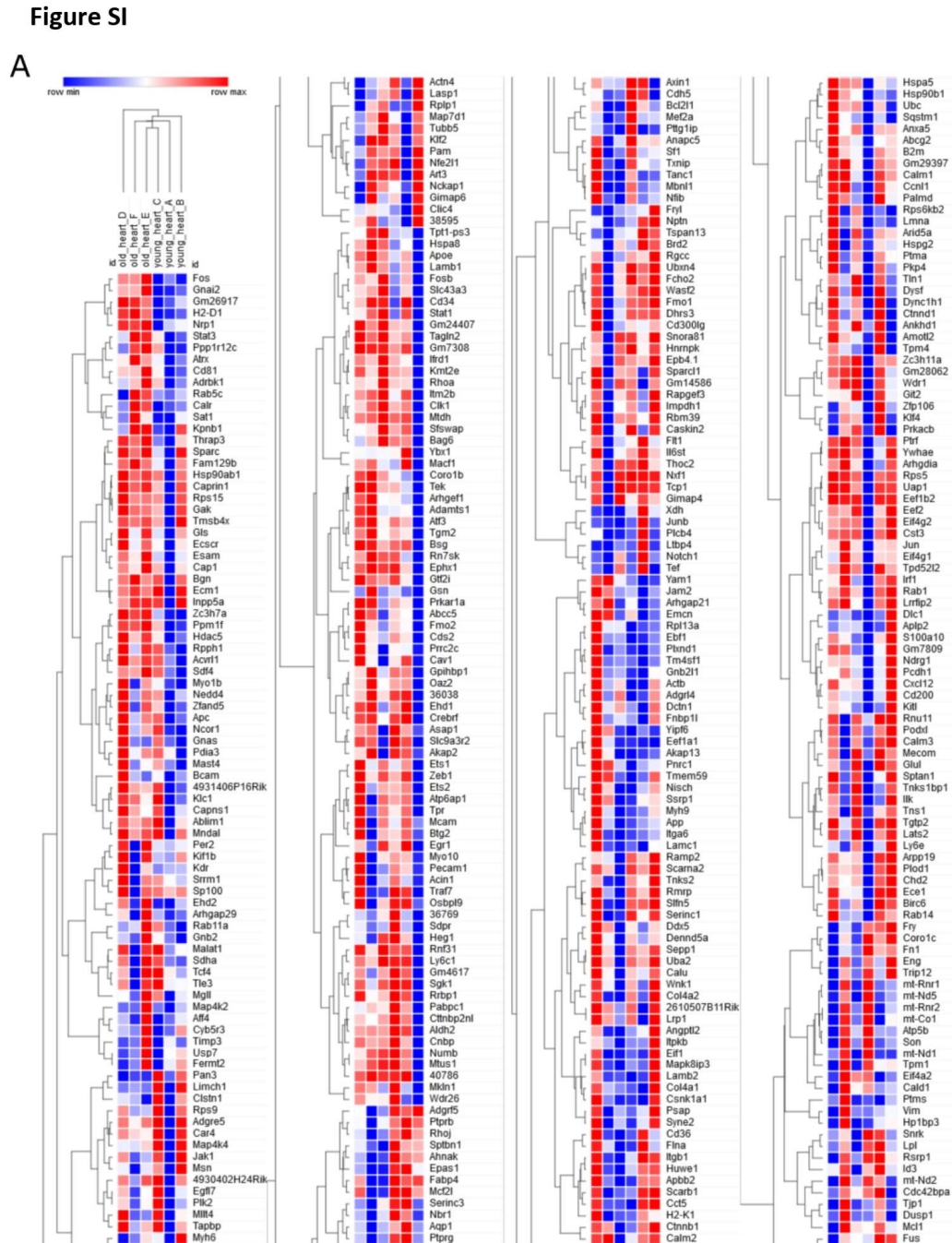


Figure S1: Visualization and analysis of RNA sequencing data. (A) Hierarchical clustering with the 408 most consistently expressed genes identified by RNA sequencing (FPKM sum of all samples > 400 and standard deviation within the group < 0.5 x mean expression in the group). Based on these genes, endothelial cells from young and old mouse hearts cluster together. Figure shows one continuous analysis in four parts. **(B)** Volcano plot of the endothelial RNA sequencing results. Y-axis depict p-value. X-axis shows expression ratio in old vs. young mouse heart endothelial cells (n = 3).

Figure SII

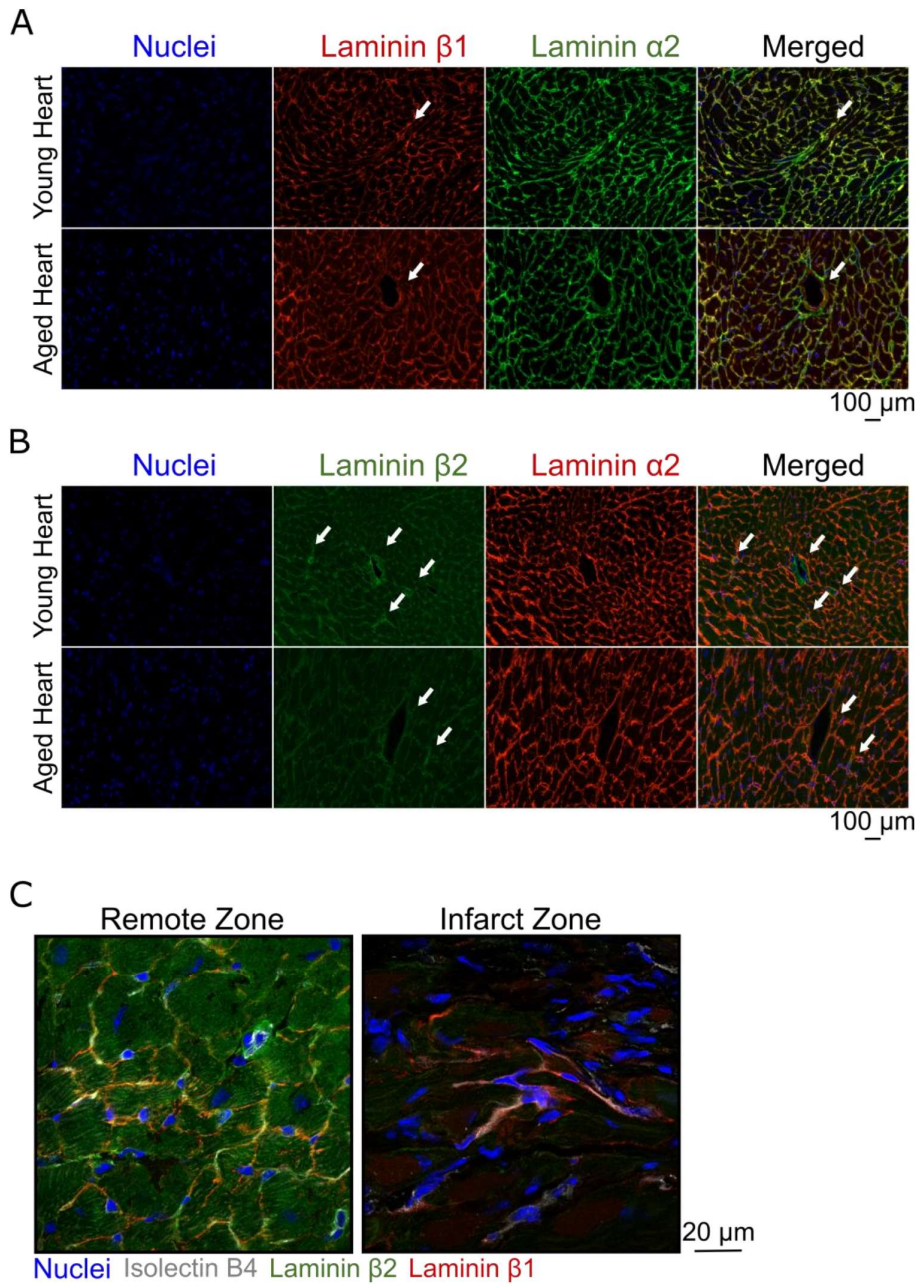


Figure SII: (A) Histological analysis of laminin β 1 (detected by rat anti-Lamb1 antibody, red) and laminin α 2 (detected by rabbit anti-Lama2 antibody, green) in 3 young (15 weeks) versus 3 aged (18 months) mice hearts. Nuclei were stained (blue) as counterstaining ($n = 3$). (B) Immunostaining of laminin β 2 (rabbit anti-Lamb2 antibody, green) and laminin α 2 (detected by rat anti-Lama2 antibody, red) and nuclei (blue) as counterstaining in young (15 weeks) and aged (18 months) mice hearts. Arrows indicate blood vessels. (C) Sections of remote and infarcted (apex) zone of hearts of 8-10 weeks old mice 3 days after AMI ($n = 4$). Representative stainings of laminin β 1 (detected by rat anti-Lamb1 antibody, red), laminin β 2 (rabbit anti-Lamb2 antibody, green) and nuclei (blue).

Figure SIII

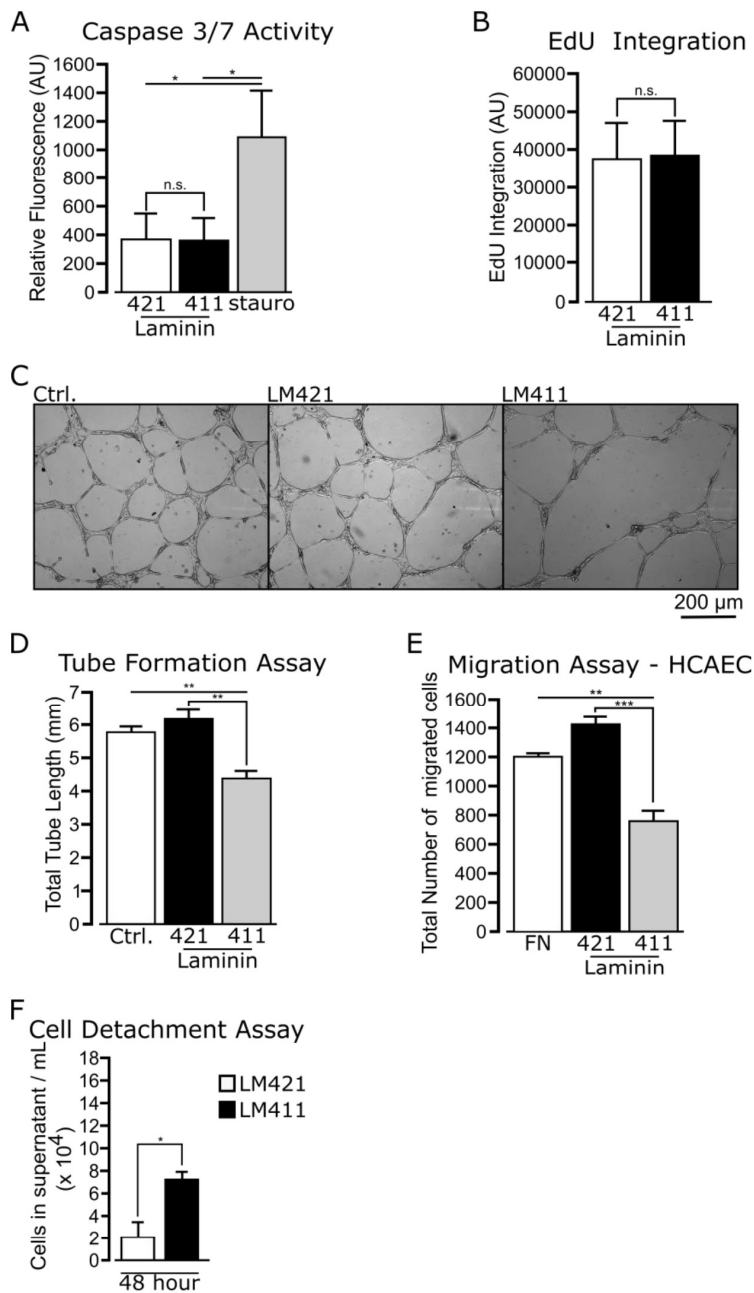


Figure SIII: (A) Cells were incubated on laminin β 2 (laminin 421) or laminin β 1 (laminin 411) matrix and apoptosis was measured by determining caspase 3 and caspase 7 activity after 10 days' incubation on each laminin matrix using the "Apo-ONE[®] Homogenous Caspase 3/7 assay kit" (Promega). (n = 5). Cells treated for 4 hours with 200 nM staurosporine (stauro) served as positive control. (B) Cell proliferation was determined by EdU integration (after 4 hours of 10 μ M EdU application using the Click-IT[®] EdU Microplate assay kit, Thermo Fisher Scientific) in cells incubating 10 days on both laminin (laminin 421 or 411) matrices (n = 3). (C) Tube formation assay of 1.5×10^5 HUVEC cultured 24h on Matrigel (Corning) supplemented with 5 μ g laminin 421 or laminin 411 or no laminin (Ctrl.). Panel D shows the cumulative tube length in three randomly chosen microscope images taken with the Zeiss Axiovert 100 microscope (n = 4). (E) Migration Assay of 5×10^4 HCAEC cultured for 3 hours in Boyden chambers that were coated with fibronectin (FN), laminin 421 or laminin 411. Cells that migrated through the chamber were stained with DAPI and monitored with the Zeiss Axiovert microscope. Migration was determined by counting cells in 5 randomly chosen images (n = 3). (F) Cell-matrix detachment was assessed by seeding human coronary artery EC (HCAEC) in 50% confluency in 12-well plates coated with LM421 or LM411. To remove culture supernatant from not adhering or dead cells, medium was changed after 1 hour. After a second change of medium at 24h, supernatants were removed at 48 h and cells were quantified using the Neubauer chamber (n = 3). Data are expressed as mean \pm SEM. Statistical analysis was performed using the unpaired, two-sided T-test (B and F). Multiple-group ANOVA with a post-hoc Bonferroni was used for panel A, D and E. *p < 0.05; **p < 0.01 and ***p < 0.001.

Figure SIV

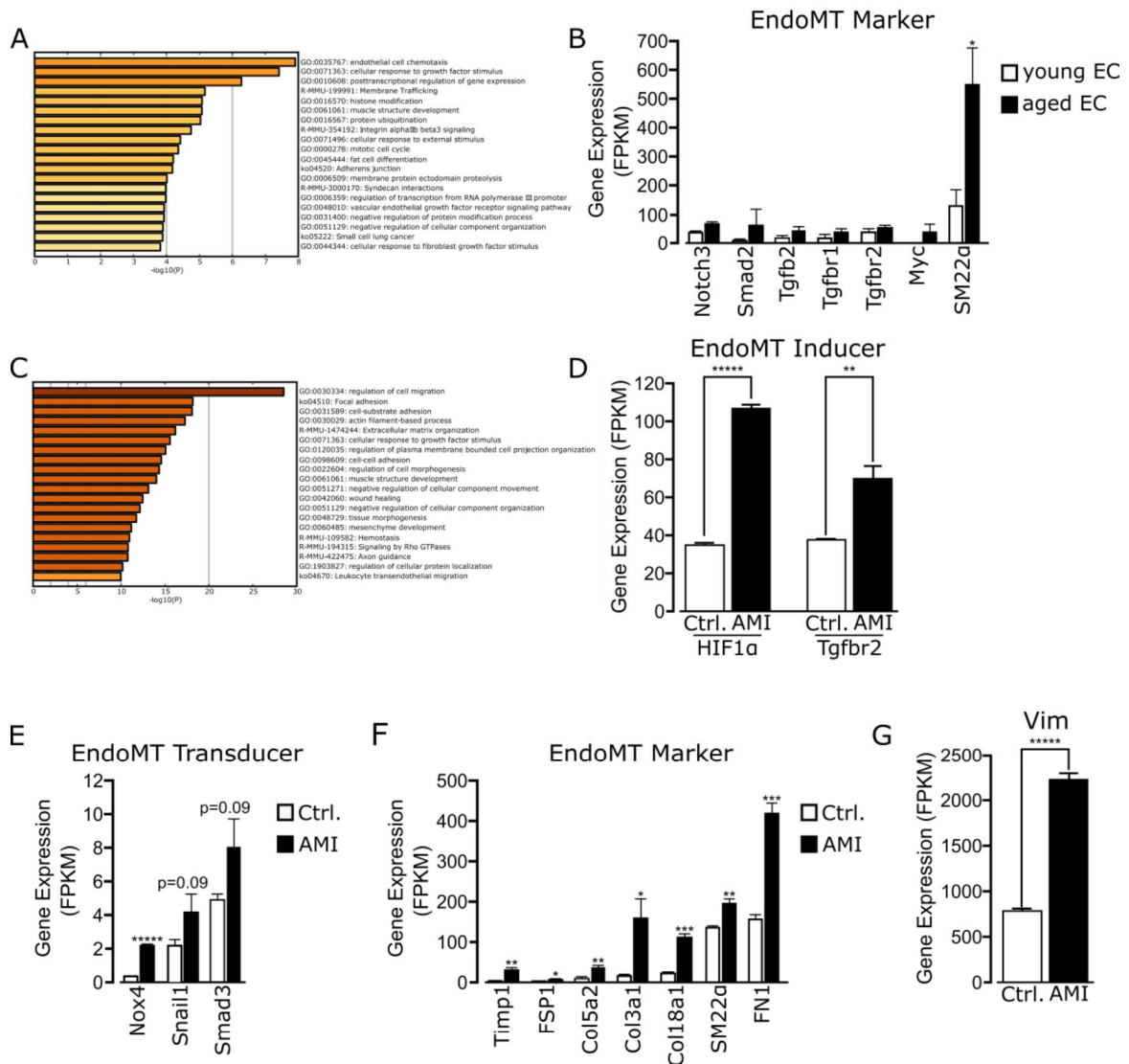


Figure SIV: Pathway analysis. (A/B) Pathway analysis after RNA deep sequencing data from cardiac endothelial cells, derived from 12-15 weeks versus 18 months old mice. Significantly ($p < 0.05$) regulated genes were used for the analysis. Panel B shows common EndoMT markers identified in the RNA deep sequencing data set ($n = 3$). **(C-G)** Pathway analysis after RNA deep sequencing from cardiac endothelial cells 3 days after acute myocardial infarction (AMI) versus control (Ctrl.). Significantly regulated genes ($p < 0.05$) with an average FPKM of >60 were used for analysis. **(D-G)** Expression of common EndoMT inducers (HIF1 α , Tgfr2), EndoMT transducers (Nox4, Snail1 and Smad3) and EndoMT markers 3 days after AMI versus control ($n = 3$ AMI vs. 4 Ctrl.). Data are expressed as mean \pm SEM. Statistical analysis was performed using the unpaired, two-sided T-test (B and F). * $p < 0.05$; ** $p < 0.01$; *** $p < 0.001$ and **** $p < 0.00001$.

Figure SV

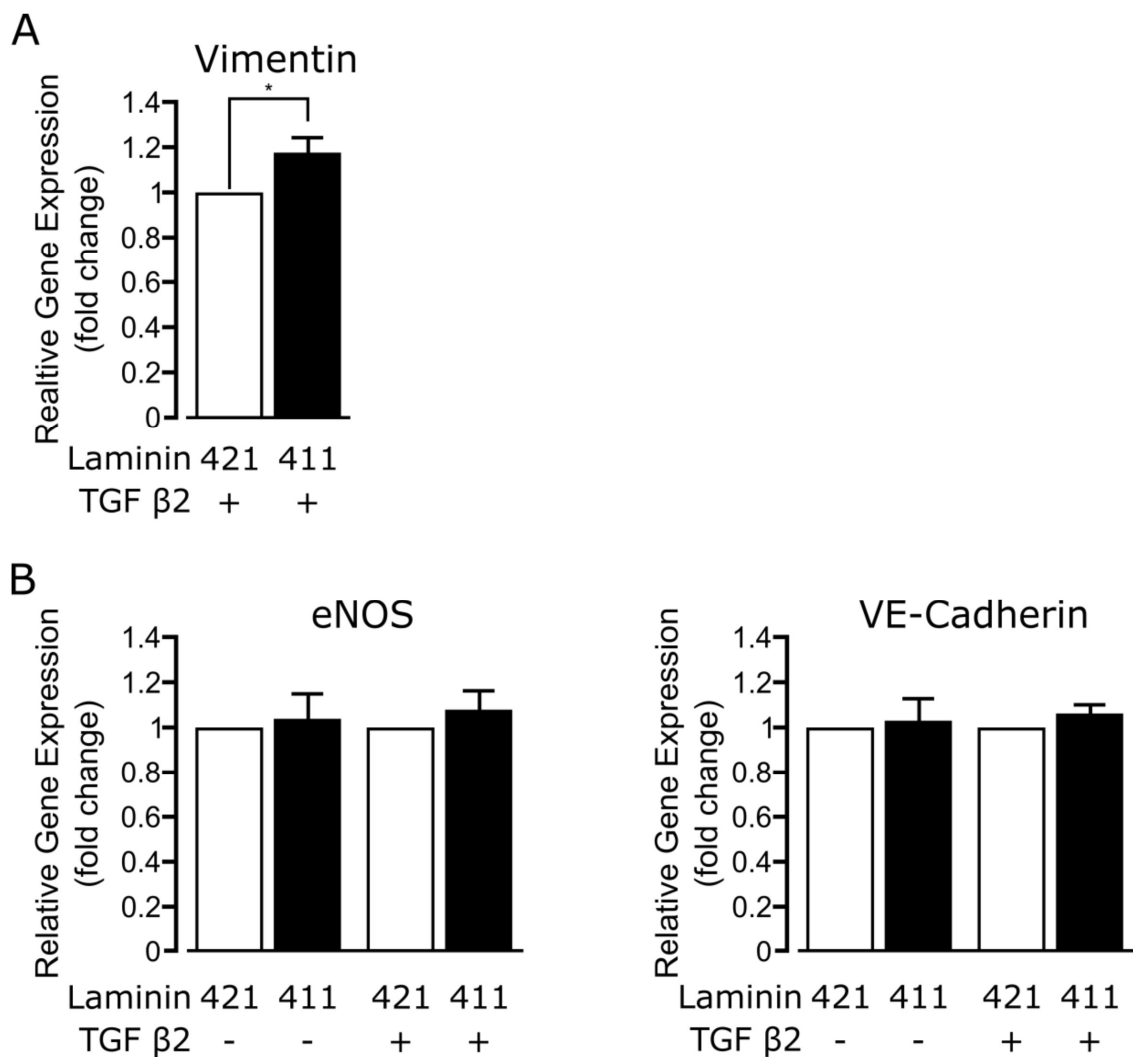


Figure SV: TGF β 2 induced EndoMT in HUVEC cultured on laminin 421 and laminin 411. (A) Expression of the mesenchymal marker vimentin was augmented by the laminin 411 matrix upon TGF β 2 treatment (n=4). **(B)** Laminin β 1 (laminin 411) matrix does not affect expression of endothelial markers (eNOS and VE-cadherin) on RNA level in the presence and absence of TGF β 2 (R&D Systems GmbH), compared to laminin β 2 (laminin 421) matrix. Prior to EndoMT induction, cells incubated 7 days on the respective laminin matrix. On day 9 and 11, cells were treated with medium conditioned either with or without 10ng/mL TGF β 2. Data are expressed as the mean \pm SEM. Statistical analysis was performed using the unpaired, two-sided T-test *p < 0.05.

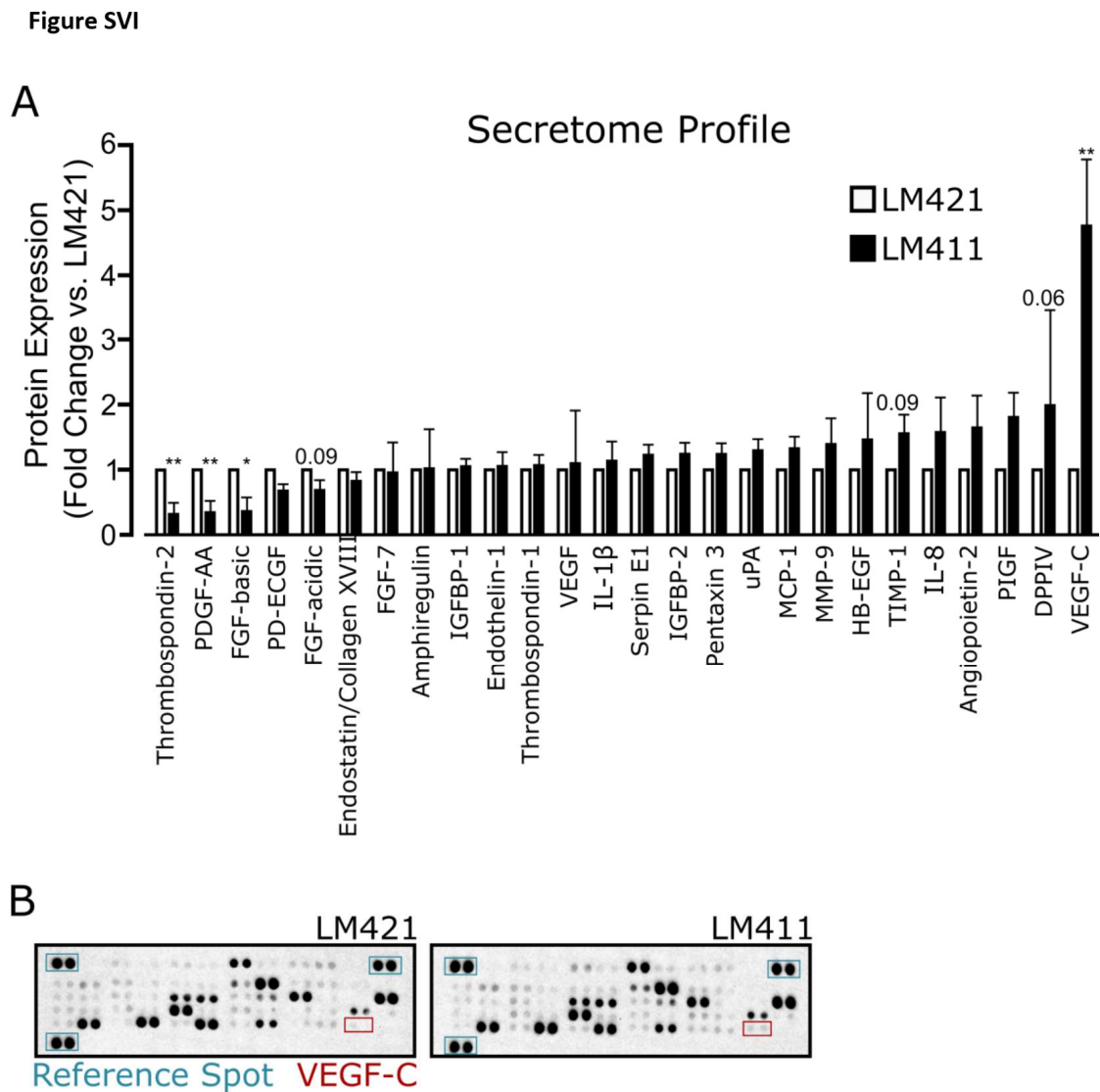


Figure SVI: Secretome analysis of HUVEC cultured on laminin 421 and laminin 411. (A) Quantification of the detectable proteins present in the supernatant of HUVECs cultured 24h on LM421 and LM411. Protein expression was determined using the Proteome Profiler Angiogenesis Array (ARY007; R&D Systems GmbH, in $n = 4$). (B) Representative images of the Proteome Profiler membranes used for protein detection. Reference spots are highlighted in blue and VEGF-C—as example—is highlighted in red. The left membrane was used for the cell culture supernatant of HUVECs incubating on LM421. The right membrane was used for the supernatant of HUVECs cultured on LM411. Data are expressed, as the mean \pm SEM. Statistical analysis was performed using the unpaired, two-sided T-test. * $p < 0.05$ and ** $p < 0.01$.

9.4 Appendix 3

Transcriptional heterogeneity of fibroblasts is a hallmark of the aging heart

Ramon Vidal^{1,2,†}, Julian Uwe Gabriel Wagner^{3,4,†}, Caroline Braeuning¹, Cornelius Fischer¹,
Ralph Patrick^{5,6}, Lukas Tombor⁴, Marion Muhly-Reinholz⁴, David John⁴, Magdalena Kliem^{1,2},
Thomas Conrad¹, Nuno Guimarães-Camboa^{4,8}, Richard Harvey^{5,6,7}, Stefanie Dimmeler^{3,5,8,††,*},
Sascha Sauer^{1,2,9,††,*}

¹ Max Delbrück Center for Molecular Medicine, Berlin, Germany

² Berlin Institute of Health, Berlin, Germany

³ Faculty for Biological Sciences, Goethe University; Frankfurt; Germany

⁴ Institute for Cardiovascular Regeneration, Goethe University Frankfurt, Germany

⁵ Developmental and Stem Cell Biology Division, Victor Chang Cardiac Research Institute,
Darlinghurst, Australia

⁶ St. Vincent's Clinical School, UNSW Sydney, Kensington, Australia.

⁷ School of Biotechnology and Biomolecular Science, UNSW Sydney, Kensington, Australia

⁸ Cardiopulmonary Institute, Frankfurt, Germany

⁹ German Center for Cardiovascular Research DZHK, Berlin, Germany

† and ††: these authors contributed equally

*Correspondence to: Dimmeler@em.uni-frankfurt.de, sascha.sauer@mdc-berlin.de

Address of corresponding authors:

Prof. Stefanie Dimmeler
Institute for Cardiovascular Regeneration
Goethe University Frankfurt
Theodor Stern Kai 7
60590 Frankfurt
Germany
Phone: +49-69-6301-6667

Dr. Sascha Sauer
Max Delbrück Center for Molecular Medicine
Robert-Rössle-Straße 10
13092 Berlin
Germany
Phone: +49-30-9406-2995

Abstract

Aging is a major risk factor for cardiovascular disease. Although the impact of aging has been extensively studied, little is known regarding the processes in cells of the heart. Here we analyzed the transcriptomes of hearts of 12 weeks and 18 months old mice by single-nucleus RNA-sequencing. Among all cell types, aged fibroblasts showed most significant differential gene expression, increased RNA dynamics and network entropy. Aged fibroblasts exhibited most significantly changed expression patterns of inflammatory, extra-cellular matrix organization angiogenesis- and osteogenic genes. Functional analyses indicated deterioration of paracrine signatures between fibroblasts and endothelial cells in old hearts. Aged heart-derived fibroblasts impaired endothelial cell angiogenesis and autophagy but augmented the pro-inflammatory response. In particular, expression of *Serpine1* and *Serpine2* were significantly increased and secreted by old fibroblasts to exert anti-angiogenic on endothelial cells, an effect that could be significantly prevented by using neutralizing antibodies. Moreover, we found an enlarged subpopulation of aged fibroblasts expressing osteoblast genes in the epicardial layer associated with increased calcification. Taken together this study provides system-wide insights and identifies molecular changes of aging cardiac fibroblasts, which may contribute to declined heart function.

Introduction

In general, aging increases the incidence of cardiovascular disease and significantly alters cardiac structure and function (1). Intervention with cardioprotective substances has been proposed to extend life span (2). Cardiovascular aging is associated with increased vascular and ventricular stiffness, interstitial cardiac fibrosis, augmented left ventricular wall thickness and reduced neovascularization abilities after ischemia (1, 3). Fibrotic remodeling of the aging ventricle plays an important role in the pathogenesis of diastolic heart failure and fibrosis of the conduction system contributes to the development of arrhythmias and conduction abnormalities (4, 5). On a cellular level, replicative senescence caused by shortening of telomeres, increased oxidative stress and DNA damage, deregulation of genes and proteins, impaired cell-cell communication, and an altered systemic and local environment are hallmarks of aging (6). In the heart, aging is associated with increased fibroblast activation, impaired angiogenesis and increased cardiomyocyte hypertrophy together contributing to the above described cardiac phenotypes (7). In addition, relative numbers and proportions of cardiac leukocytes are altered: old hearts have proportionally more monocyte-derived cardiac macrophages and an increased population of granulocytes (8). However, we still know surprisingly little about the fundamental effects of aging on cellular heterogeneity of cardiac parenchymal, mural and vascular cells.

Here we describe a first mammalian transcriptional cell atlas of the aging heart. This data allows for both understanding the healthy state and the causal effects of intrinsic cardiac aging.

Results

Single-nucleus RNA-sequencing reveals cellular heterogeneity of cardiac cells in aging

To comprehensively decipher the expected cellular responses to intrinsic cardiac aging, we applied micro-droplet based single-nucleus RNA-sequencing (9) of cross-sections of snap-frozen heart samples from syngeneic 3 young male mice (12 weeks old) and 3 aged male mice (18 months old). In total, we analyzed 14,827 nuclei from young hearts and 12,981 nuclei from old hearts were used (Supplemental Table 1). Using t-distributed stochastic neighbor embedding (t-SNE) (10) global dimension reduction was constructed from all samples to visualize clusters that were defined by cell-specific gene markers (Figure 1A and Supplemental Table 2). Alignment of samples indicated high reproducibility across samples (Supplemental Figure 1). Most of the cells were in G1 phase and no influence of aging on cell cycle activity was observed (Supplemental Figure 2).

Unsupervised clustering revealed a total of 15 distinct gene expression patterns (Figure 1A, Supplemental Figure 3). Using cell type specific gene markers (Supplemental Table 2) and published mouse single-cell gene expression data (11, 12), 7 major cell types could be annotated including fibroblasts (A, B), cardiomyocytes (A, B, C), endothelial cells (A, B, C), immune cells (A, B, C), pericytes, epicardial cells, and adipocytes (Figure 1A and Supplemental Figure 3). In particular, for fibroblasts, the unsupervised clustering revealed two main clusters (fibroblast A (79.42%) and fibroblast B (20.58%). Separation of these two clusters was not significant (Supplemental Figure 3B) and gene markers were very similar (Supplemental Table 2); moreover, these two clusters were almost equally populated by young and old cells. Analysis of

the cell numbers in clusters of other cell types than fibroblasts showed in part trends for changes during aging (Supplemental Figure 4), but did not reveal statistically significant differences.

In general, 128 differentially expressed non-redundant genes (DEGs) were found between young and aged hearts (Figure 1B and Supplemental Table 3). Considering the DEGs in all cell clusters, a total of 107 genes showed significantly increased expression ($p_{adj} < 0.1$) and 21 genes showed significantly decreased expression ($p_{adj} < 0.1$) in aged versus young hearts (Supplemental Table 3). Interestingly, aging predominantly affected gene expression patterns in fibroblasts (Figure 1B). Several highly differentially expressed genes could be confirmed by qRT-PCR of isolated cardiac fibroblasts (Supplemental Figure 5).

GO analysis of differentially expressed genes revealed a cell type specific enrichment of genes associated with various pathways such as angiogenesis, chemotaxis/migration, inflammation/immune response and cell/matrix association (Figure 1C). Only few co-expression networks and significantly regulated genes were shared between the main cell types. Among them, the expression of the components of the complement system were commonly augmented in all cell types (Figure 1D), which is consistent with the finding of a general cardiac aging promoting effect of the complement system (13).

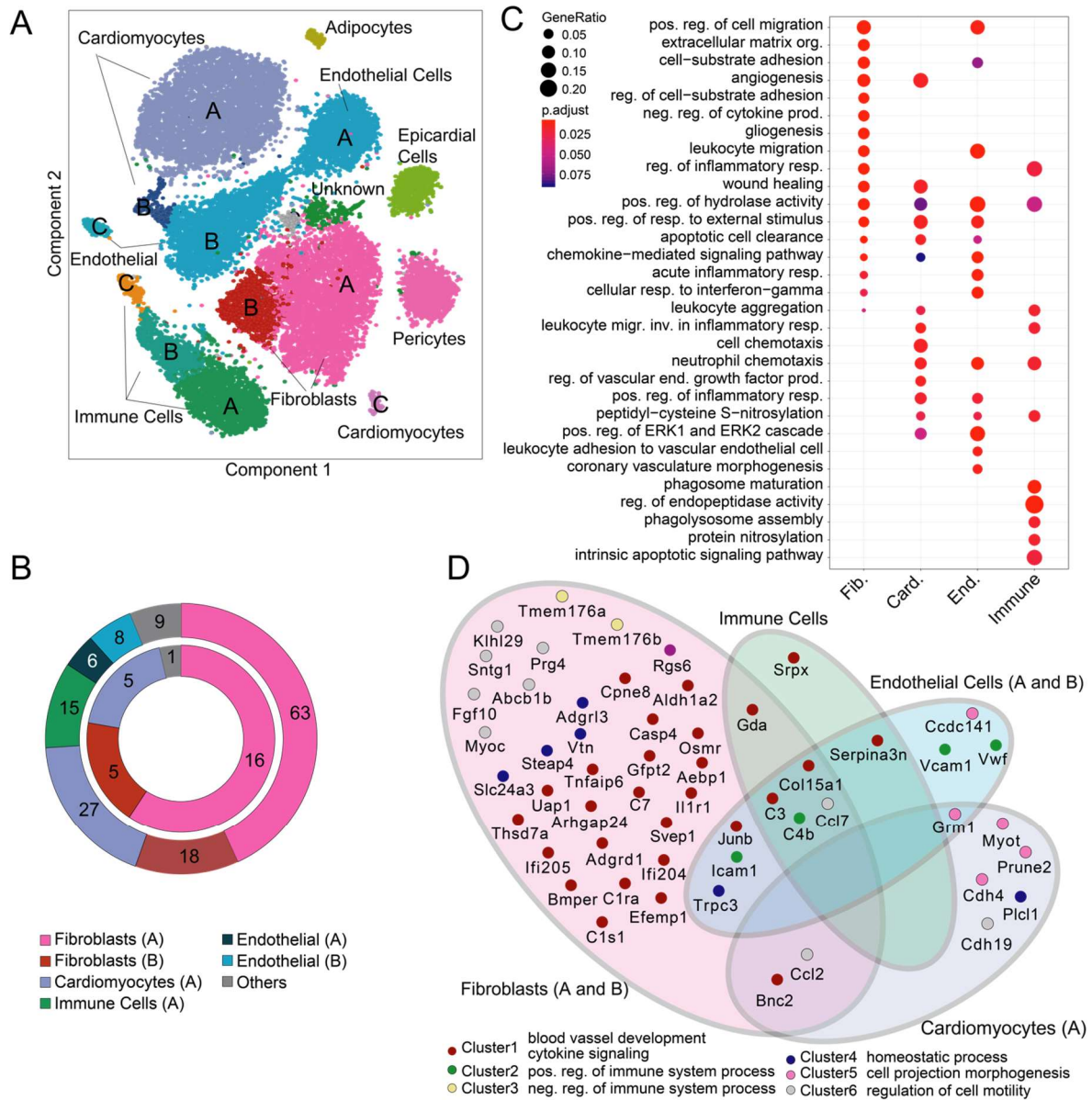


Figure 1: Cell type-specific composition of the heart in young and old mice. (A) t-SNE representation of all cells and cell-clusters from all 6 samples. Clusters were annotated according to their detected gene markers. Details about each cell population can be found in Supplemental Figure 3 and Supplemental Table 2. Most cell clusters could be separated with high confidence; however, in this initial analysis fibroblasts remained difficult to distinguish from each other. (B) A total of 128 unique differentially expressed genes (DEG) (adj. p-value < 0.1) were found between young and old samples among all detected clusters. Outer circle represents up-regulated genes in old samples and inner circle represents the down-regulated genes in old. (C) GO enrichment comparison (hypergeometric test) of the DEGs between young and old samples in the cell populations with at least one significant result (adjusted p-value < 0.1). Up and down-regulated genes were analyzed together. Subpopulations were analyzed together. (D) The differentially expressed genes were grouped into co-expressed networks and represented as different color; these networks were functionally annotated according to their genes. These genes were spatially organized in a Venn diagram for easy access of same DEGs in multiple cell types

Single-nucleus RNA-sequencing identifies specific fibroblast subpopulations involved in cardiac aging

Since our data suggest that aging has the most profound impact on cardiac fibroblasts (Figure 1, B and D), we focused our attention on these cells. To gain insights into age-associated fibroblast populations, we applied sub-clustering techniques to sort and group cells using the 85 unique genes that were differentially expressed in fibroblasts during aging. Sub-clustering identified 13 fibroblast subpopulations (Figure 2, A and B), of which sub-clusters 1, 5, 10 and 11 were mostly populated by young cells, whereas sub-clusters 2, 3, 4, 7, 8 and 12 were mostly populated by old cells (Figure 2C). All gene markers for the sub-clusters are listed in Supplemental Table 5.

The different age-dependent sub-clusters showed profound alterations in gene pathways (Figure 2D, Supplemental Table 6). GO terms that were enriched in sub-clusters of young fibroblasts were connected to regulation of muscle system process and generation of metabolites (sub-cluster 11) (Figure 2D). Angiogenesis was in general found to be enriched in all sub-clusters that were mainly populated by old fibroblasts. Moreover, sub-clusters 2, 4 and 8, also mainly populated by old cells, associated with genes involved in regulation of endothelial cell proliferation and migration. Genes associated with osteoblasts were also prominently augmented in sub-clusters 2 and 4. Immune response genes were mainly found in sub-cluster 3 (Figure 2D, Supplemental Table 6), which was predominant for cells from old mice. The increase in pro-inflammatory phenotypes resembles the response of fibroblasts during cardiac injury or remodeling (4, 5). The age-associated phenotypes of sub-cluster 2 showing an induction of epithelial cell proliferation is consistent with an expansion of fibroblasts and increased interstitial fibrosis in the aging heart (4) (Supplemental Figure 6). However, it was unknown that cardiac fibroblasts elicit cell-specific individual changes in vascular/angiogenesis profiles during aging (as observed in sub-clusters 2, 3, 4, 7 and 8) or may acquire more cells with osteogenic phenotypes (as in sub-clusters 2 and 4).

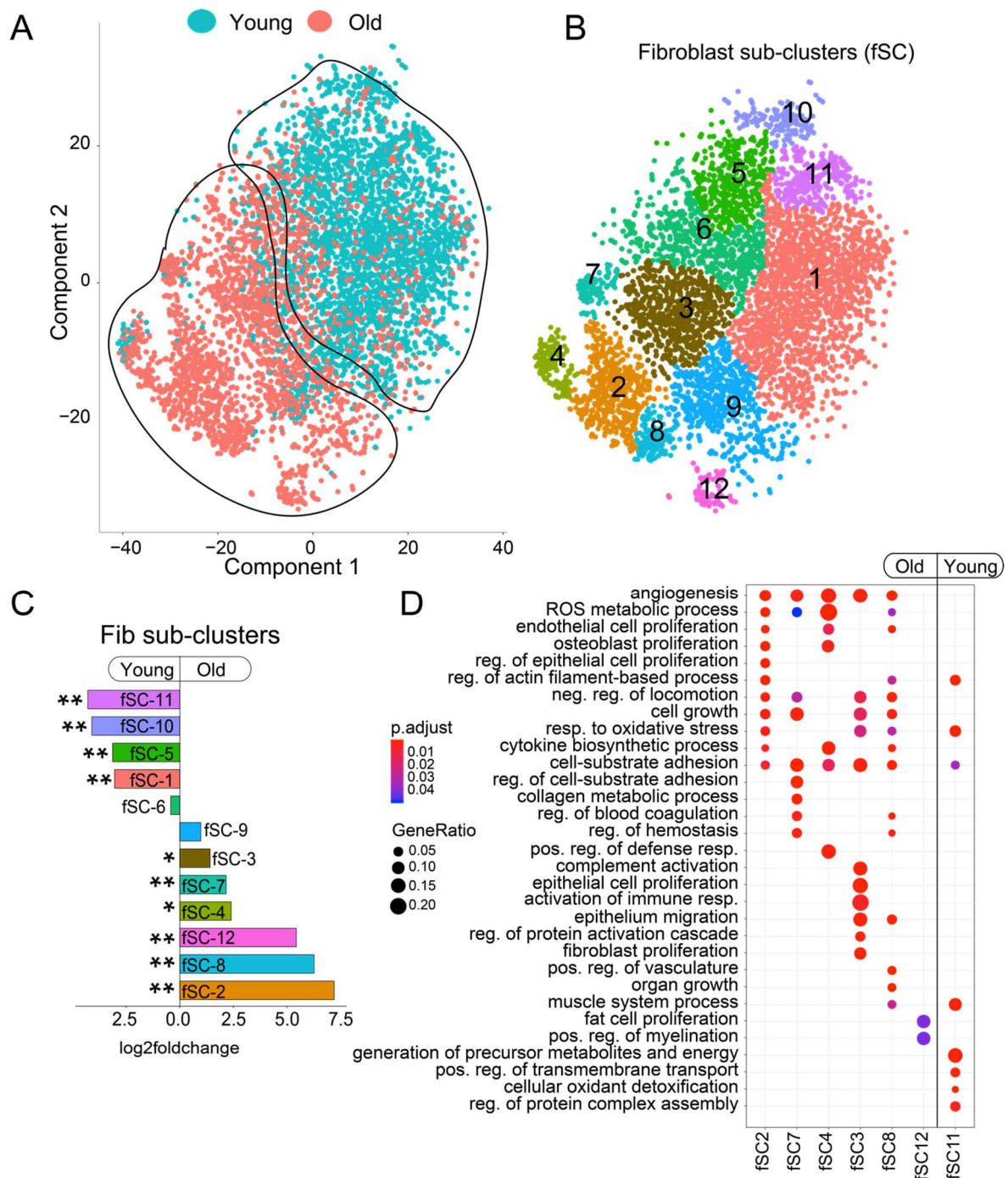


Figure 2: Aging fibroblasts sub-clusters. (A) Old and young fibroblasts were clustered using differentially expressed genes as anchors. (B) Sub-clusters of fibroblasts were found using Louvain algorithm implemented in Monocle2 (see Materials and Methods). (C) Differences in cell numbers between old and young in all sub-clusters were calculated by comparing the normalized means and the significance by fisher exact test (*p-value < 0.05 and **p-value < 0.01). (D) GO enrichment (hypergeometric test with adjust p-value cutoff of 0.1) comparison between all fibroblast sub-clusters (if any).

Single-nuclei RNA sequence reveals dynamic states of fibroblasts and entropy increase change during aging

Next, we applied the DDRTree algorithm from Monocle2 to sort and plot cells in a linear order. The linear representation of the cells shows the dynamic states of fibroblasts during the aging process (Figure 3A, B, Supplemental Figure 7). Here, states of the right end (states a, b, and d) were dominantly populated by young fibroblasts, which showed increased expression of genes required for heart fibroblast functions such as extracellular structure organization. States of the left end (states h, j and l) were predominantly populated by aged fibroblasts, which were enriched with genes required for cell proliferation (j), inflammatory response (h, j, l), angiogenesis (j, l) and osteoblast differentiation (j, l) (Figure 3, A and C, Supplemental Table 7 and Supplemental Table 8).

Interestingly, analyzing the entire single-nucleus mRNA expression data of cardiac fibroblasts, we observed highest amounts of unspliced RNAs (increased transcriptional activity or so-called “RNA velocity” (14)) in the fibroblast states j, l and h (Figure 3D); these most dynamic states were in particular populated by old cells (Figure 3, A, B, C and D).

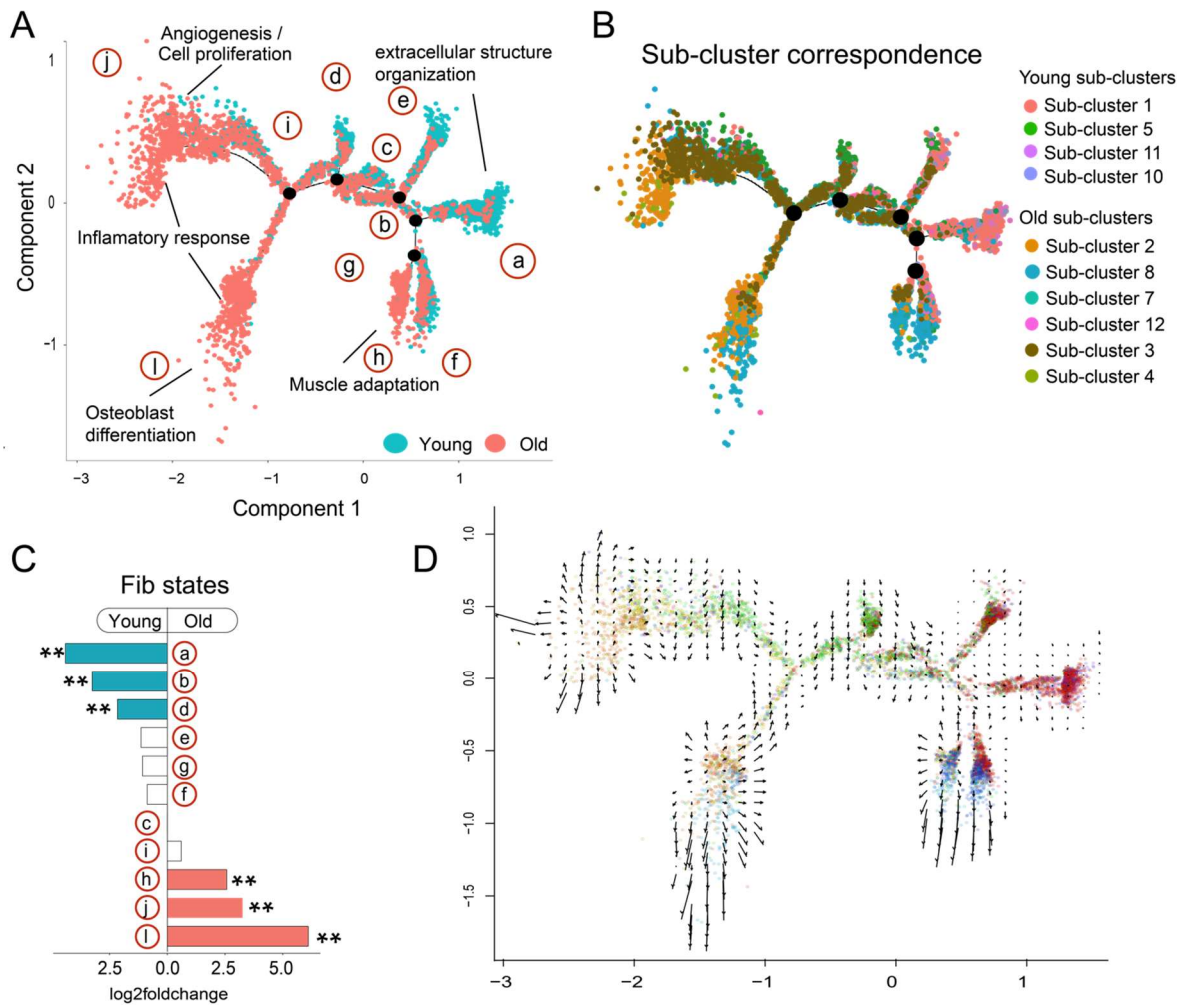


Figure 3: Transcriptional activity in aging cardiac fibroblasts. (A) Fibroblasts were sorted using DDRTree algorithm and using the DEGs between old and young in order to define different cell development states during in aging. (B) Projection of sub-clusters into the different cell states, same colors from Figure 2B were used. (C) Differences in cell numbers between old and young of all fibroblast states were calculated by comparing the normalized means. Significance was calculated by Fisher exact test (*p-value < 0.05 and **p-value < 0.01). (D) Transcriptional activity is estimated by measuring the ratio between unspliced and spliced mRNAs. This so-called RNA velocity is represented by high-dimensional vectors; the longer the arrow in the plot, the higher the transcriptional activity as seen in the extremities of states h, j and l plot containing mostly old cells.

Furthermore, we observed a consistent age-related increase of entropy in all fibroblasts when comparing young and old (Figure 4A). Subpopulations that were mainly populated by old cells showed higher entropy than subpopulations that were rather populated by young cells (Figure 4B). Of note, genes related to the cell-specific functions of fibroblasts such as extracellular matrix organization showed increased entropy in aged versus young fibroblasts (Figure 4C). These results indicate a higher transcriptional heterogeneity of aged heart fibroblasts, which could lead to a decline of efficient, synchronous expression of fibroblast-specific genes, eventually resulting in decreased molecular network stability.

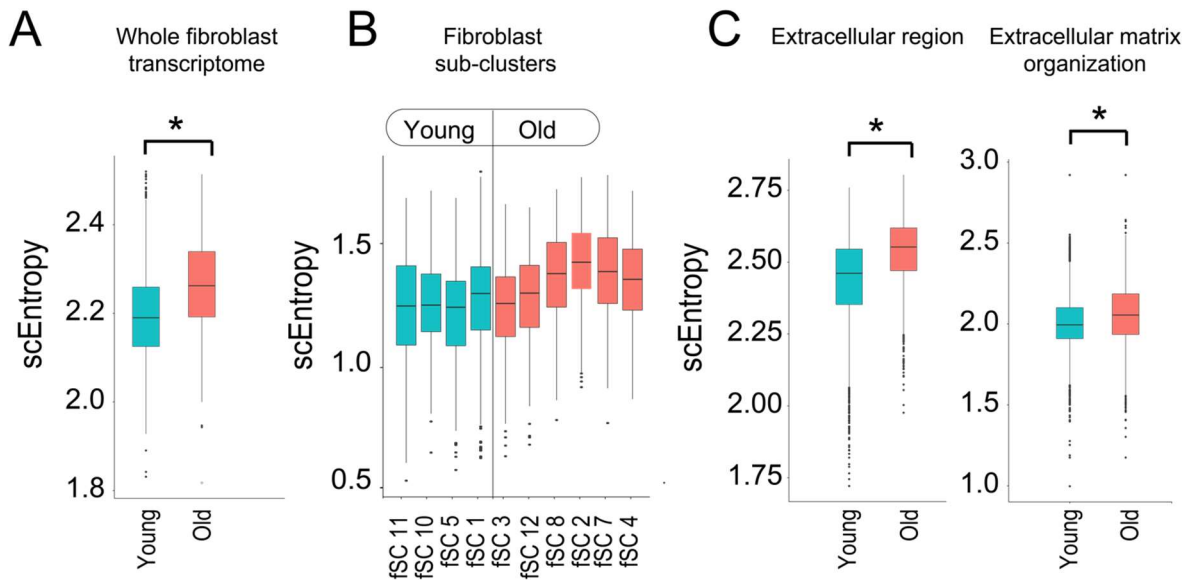


Figure 4: Single-cell entropy (scEntropy). (A) Single-cell entropy observed in old and young fibroblasts cells. (B) Single-cell entropy (transcriptional “disorder”) detected in fibroblast sub-clusters. Highest entropy was found in sub-clusters (2, 4, 7 and 8), which were mostly populated by aged fibroblast cells. (C) Single-cell entropy observed in overall old and young fibroblasts cells for selected gene sets. Mann-Whitney-Wilcoxon Test was applied in the pairwise comparisons (young versus old) in order to calculate statistical significance between young and old cell entropy means (*p-value < 2.2e-16).

Aging alters fibroblast-endothelial interactions

To analyze potential functional consequences of the observed transcriptional changes, we first assessed the differentially expressed angiogenesis-related genes found in fibroblast cell clusters 2, 3, 4, 7 and 8 (Figure 2, B and D). Interestingly, many of these genes are known from endothelial-mesenchymal transition (EndMT), which refers to the process leading to the phenotypic change of endothelial cells into mesenchymal cells (15) (Figure 5A). Therefore, we speculated that endothelial cell-derived fibroblasts might have accumulated during aging. However, no significant increase of endothelial markers was found in old fibroblasts, suggesting that the EndMT-associated regulated genes (e.g. *Klf4*, *Tgfb2*, *Sulf1*, *Loxl2*; Figure 5B) represent the activation of a transcriptional transition program in cardiac fibroblasts but are not related to the transition of the endothelial lineage.

Some of the observed angiogenesis-related genes associated with aging are also known to encode for extracellular proteins, suggesting that a paracrine cross talk of cardiac fibroblasts with cardiac endothelial cells may be affected during aging. Indeed, weighted analysis of the ligand-receptor interactions indicated that fibroblasts were the most “out-bound” cells, whereas endothelial cells were the most “receiving” cells in the aging heart (Figure 5, C and D). To address whether the paracrine activity of fibroblasts is altered in aging, we generated conditioned medium from aged and young mice cardiac fibroblasts and determined the angiogenesis regulatory activity in vitro (Figure 6A). Conditioned medium derived from aged fibroblasts showed a reduced angiogenic property compared to medium of young heart-derived fibroblasts demonstrating an impaired cross talk during aging (Figure 6B). Consistently, capillary

density was profoundly reduced in fibrotic regions of aged hearts (Figure 6C and Supplemental Figure 8A).

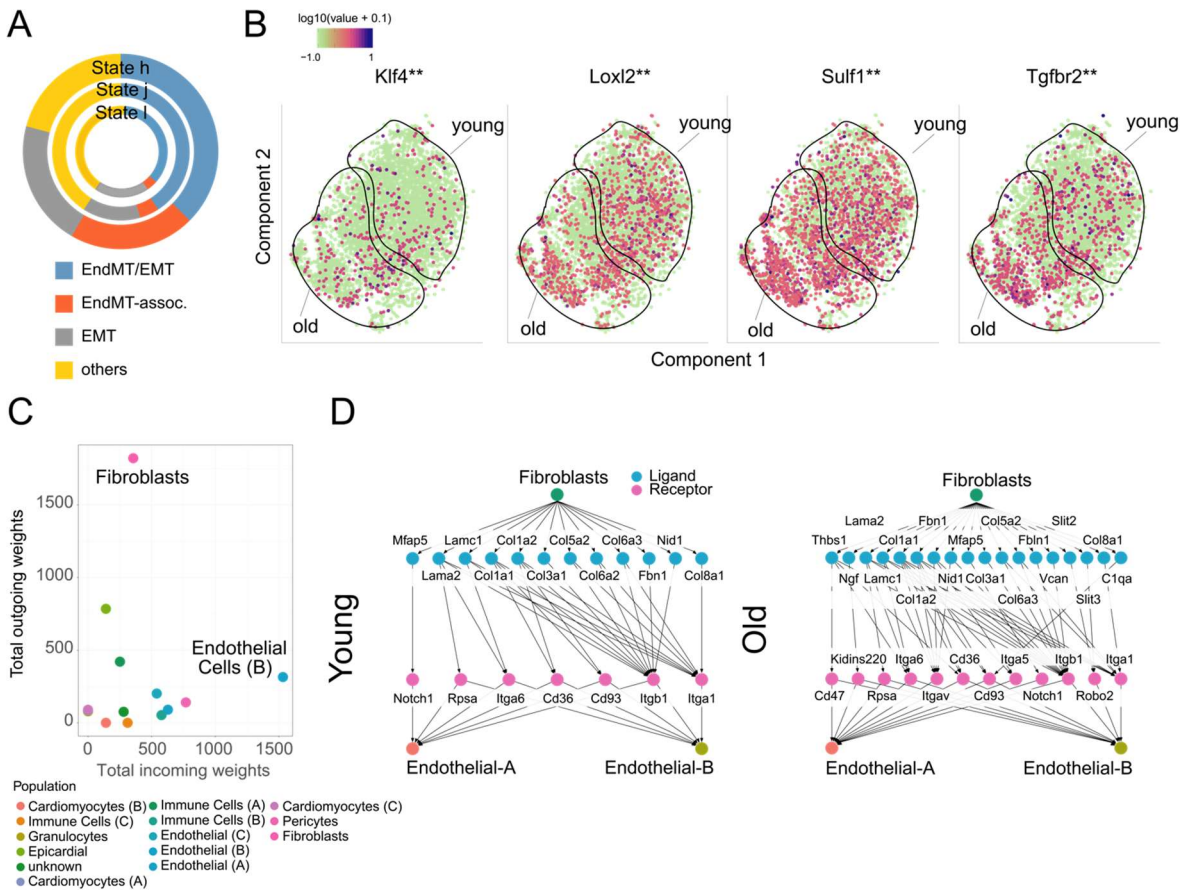


Figure 5: Fibroblast and endothelial interaction (A) Genes associated with endothelial-mesenchymal transition (EndMT) and epithelial-mesenchymal transition (EMT) expressed in fibroblasts states l, j and h. **(B)** Expression of Klf4, Loxl2, Sulf1 and Tgfbr2 in fibroblast sub-clusters. **(C)** Interaction network of each annotated cluster showing the total outgoing weights (secreted/paracrine / autocrine signals) and total incoming weights (ligand binding / receptor activation) signals among the clusters. **(D)** Ligand receptor interaction analysis. Connections found between fibroblasts and endothelial cells are shown for young and old mouse hearts.

Aged fibroblasts expressed various candidates that might mediate anti-angiogenic effects including Efemp1 (also known as Fibulin 3), a gene that is known to inhibit tumor angiogenesis (16), and several members of the anti-angiogenic serpins such as Serpine1 (also known as PAI1) and Serpine2 (alias Nexin) (17) (Figure 6D). Using a screen for angiogenesis-related proteins we detected increased levels of Serpine1 in the medium of aged fibroblasts (Figure 6E). Next, we tested the effect of recombinant Serpine1 and Serpine2, which both reduced tube formation (Supplemental Figure 8B/C). To determine their contribution to the anti-angiogenic activity of aged fibroblast supernatants on endothelial cells, we used neutralizing antibodies which block both serpins (Supplemental Figure 8B/C). Inhibition of serpins significantly rescued the impaired angiogenesis induced by conditioned medium from aged fibroblasts (Figure 6F), whereas Efemp1 antibodies had no effect on endothelial cells (Supplemental Figure 8D). These data

suggest that increased expression of serpins in fibroblasts during aging mediates an anti-angiogenic effect on endothelial cells.

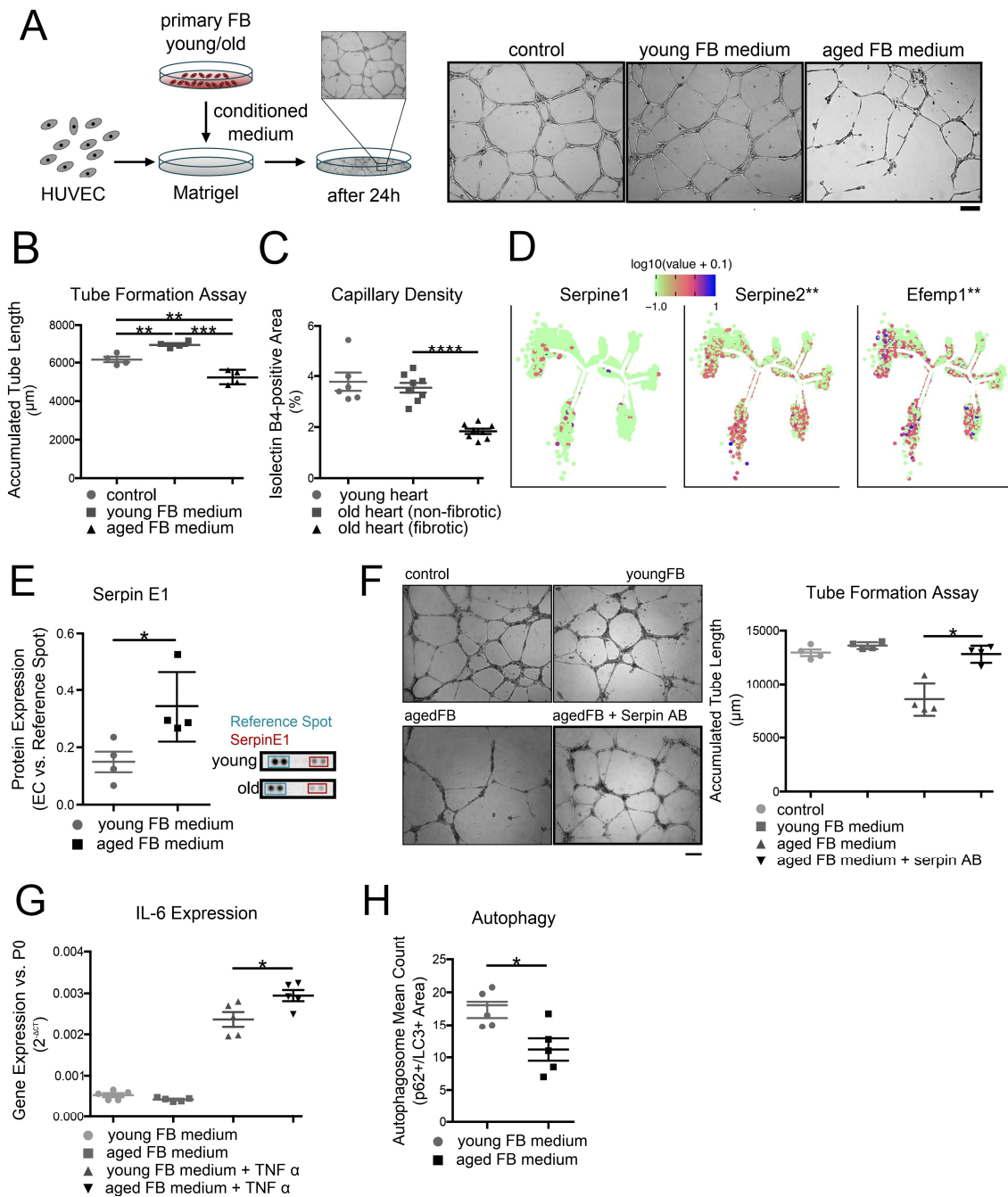


Figure 6: Age-dependent changes of fibroblast function on endothelial cells. (A-B) Experimental outline and tube formation assay of human umbilical vein endothelial cells (HUVEC) that were cultured in conditioned medium received from young (12 weeks) and aged (20 months) cardiac mouse fibroblasts. Accumulated tube length was measured in five randomly chosen microscopic fields with a computer-assisted microscope using Axiovision 4.5 (Zeiss) (scale bar: 100 μm ; n=4). **(C)** Capillary density of random areas of young (12 weeks; n=6) and old (n=8) heart section vs. capillary density of fibrotic (n=8) areas of aged hearts (20 months). Shown is the quantification of the Isolectin B4-positive area vs. the total area (%). **(D)** Expression of Serpine 1, Serpine 2 and Efemp1 in fibroblasts displayed in log scale in trajectory plots. **(E)** Secretion of SerpinE1 in isolated

young and aged cardiac fibroblasts cultured for 24h in serum-free medium. Data were derived using a mouse angiogenesis array (R&D Systems) of culture supernatants of isolated cardiac fibroblasts (n=4). **(F)** Tube formation assay of human umbilical vein endothelial cells (HUVEC) that were cultured in conditioned medium received from young (12 weeks) and aged (20 months) cardiac mouse fibroblasts. The aged phenotype was rescued by supplementing the aged fibroblast medium with 4 μ g of an anti-Serpin antibody. Accumulated tube length was measured in five randomly chosen microscopic fields with a computer-assisted microscope using Axiovision 4.5 (Zeiss) (scale bar: 200 μ m; n=4). **(G)** RNA expression of IL-6 in HUVECs cultured in conditioned medium received from young (12 weeks) and aged (18 months) cardiac mouse fibroblasts and in the presence and absence of 10 ng/mL TNF α for 24h (n=5). **(H)** Quantification of autophagosomes in HUVEC cultured with conditioned medium received from young (12 weeks) and aged (18 months) cardiac mouse fibroblasts. Autophagosomes were detected by immunostainings against p62 and LC3, whereby autophagosomes were considered to be p62/LC3-double positive (n=5). Data are shown as mean \pm SEM **(B, C, E, F, G and H)**. After passing Gaussian distribution, statistical analysis was performed using the unpaired, two-sided T-test **(C, E, G and H)**. For comparisons of >2 groups, multiple-group one-way ANOVA with a post hoc Bonferroni test was used **(B and F)**, indicated as follows: *P<0.05; **P<0.01; ***P<0.001 and ****P<0.0001.

Effect of fibroblasts on age-associated signatures of endothelial cells

To determine if aged heart-derived fibroblasts may further promote an aging phenotype of endothelial cells, we tested the effect of conditioned medium on hallmarks of aged endothelial cells. Conditioned medium of aged heart-derived fibroblasts did not affect proliferation of endothelial cells (Supplementary Figure 8E) suggesting that it does not influence replicative senescence. However, aged fibroblast conditioned medium enhanced the pro-inflammatory activation of endothelial cells (Figure 6G) and reduced endothelial cell autophagy (Figure 6H), which both are typical features of impaired endothelial cells (18, 19) These data suggest that aged heart fibroblasts impair endothelial cell pro-angiogenic functions and promote age-associated changes in endothelial cells.

Aging fibroblasts adopt osteogenic fates

Finally, we addressed the relevance of the observed augmented and more entropic expression of osteogenic genes in fibroblasts of sub-clusters 2 and 4 (Figure 2D, Supplemental Table 6 and Figure 7A). Cardiac fibroblasts were shown to adopt osteogenic fates in conditions of pathological heart remodeling (20); however, whether such transitions occur during aging remained unclear. Therefore, we further explored these findings by analyzing the expression of genes associated with osteogenesis. Various genes involved in osteoblast differentiation and functions (e.g. Ddr2, Runx2, Gpm6b, Junb, Cebpb) were all expressed at higher levels in sub-cluster 2, which was populated by old fibroblasts (Figure 7A and Supplemental Table 5). Some of these genes such as Runx2 were also significantly elevated in the total fibroblast population (Figure 7B). Histological assessment confirmed the occurrence of a subset of osteocalcin-expressing fibroblasts in the aging heart (Figure 7C), which were mainly located in the epicardial layer (Figure 7D and E). Consistently, calcification was increased in the aging heart, particularly in the epicardium (Supplemental Figure 9A). To determine if epicardial cells may acquire an osteogenic state, we determined the expression of the osteoblast genes in the epicardial cell cluster (Supplemental Figure 9B/C). The epicardial cell cluster is characterized by high expression of epicardial markers Wt1 and Upk3b but only weakly expresses fibroblast marker

genes such as *Pdgfra* (Supplemental Figure 9B). However, this cluster did not show any changes in the expression of osteogenic genes such as *Cebpb* or *Runx2* (Supplemental Figure 9C) suggesting that the acquisition of the osteogenic state may preferentially occurring in *Pdgfra*-positive fibroblastic populations within the epicardial layer.

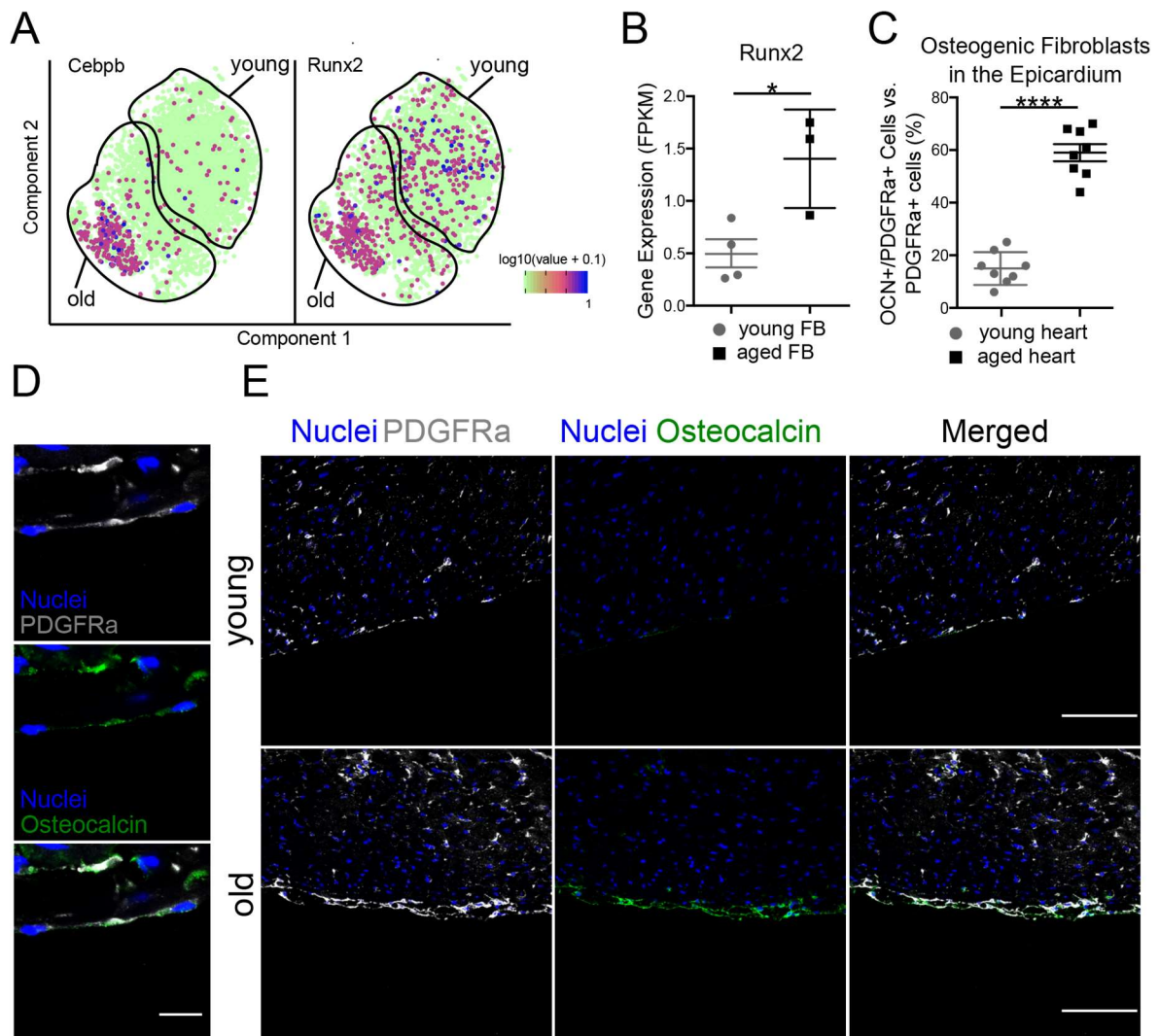


Figure 7: Aging alters fibroblasts to adopt osteogenic fates. (A) Expression of *Cebpb* and *Runx2* in fibroblasts displayed in log scale in sub-cluster analysis plot. Young and old enriched sub-clusters are separated by lines and as displayed in Fig. 2A-B (B) Expression of *Runx2* in young and aged cardiac fibroblasts. Data were derived from bulk RNA sequencing of isolated cardiac fibroblasts (4 young vs. 3 old samples). (C-E) Histological analysis of heart sections derived from young (12 weeks old) and old (>18 months old) mice. Immunostaining was performed against osteocalcin (OCN, green) as osteogenic marker and PDGFRa (grey) as fibroblast marker. Nuclei were stained with Hoechst 33342 (blue) (n=8; 4-6 images per heart). Quantification of OCN+/PDGFRa+ double-positive cells vs. PDGFRa+ single-positive cells is shown in C. Representative examples are shown in D (scale bar: 10 μm) and E (scale bar: 100 μm). Images were monitored using the Leica TCS SP8 confocal microscope. Data are shown as mean \pm SEM (B, C). After passing Gaussian distribution, statistical analysis was performed using the unpaired, two-sided T-test, indicated as follows: * $P < 0.05$ and **** $P < 0.0001$.

Discussion

Here we analyzed transcriptional changes of major cell types of the aging mouse heart at single-cell resolution. Of note, fibroblasts showed most profound heterogeneity and the highest number of differentially expressed genes. In particular, in cardiac fibroblasts we observed more fuzzy and diverse transcriptional profiles in old versus young heart cells, as evidenced by increased entropy of cell-type specific, functionally relevant genes and pathways, indicating quantitative loss of systemic function of fibroblasts during cardiac aging. These results suggest a general age-associated change in cellular heterogeneity of cardiac fibroblasts, which is in line with previous studies showing an age-dependent increase in cell-to-cell transcriptional variability after immune stimulation of CD4⁺ T-cells in mice (21). Possibly, the increased RNA velocity of fibroblasts may relate to resolution of cell specific boundaries associated with de-differentiation or acquirement of interim cellular phenotypes.

Fibroblasts are well known to contribute to interstitial fibrosis, which is a pathological process that increases the stiffness of the heart and contributes to age-associated decline in diastolic heart function. Interstitial fibrosis is associated with deregulation of resident mesenchymal fibroblasts, which acquire a pro-inflammatory state (22). This finding is recapitulated in our trajectory analysis demonstrating immune/inflammatory activation in the fibroblasts, in particular in states j and l, which are preferentially populated by cells from old heart-derived fibroblasts.

Various previous studies suggest that fate changes between endothelial cells and fibroblasts can occur in both ways under pathological conditions. Both EndMT and mesenchymal-endothelial transitions (MEndT) were described after pathological activation of the heart e.g. after infarction. The incidence of EndMT in aging seems largely unknown, but senescent endothelial cells were shown to acquire mesenchymal properties in vitro (23). However, we could not find evidence for an increase of cells co-expressing mesenchymal and endothelial markers, which is compatible with recent lineage tracing studies, suggesting that also the extent to which endothelial cells contribute to heart fibroblasts after myocardial infarction is rather limited (24).

Our comprehensive single-cell transcriptome data and weighted analysis of the ligand-receptor interactions suggested interaction of fibroblasts and “receiving” endothelial cells in the aging. Single-nucleus RNA-seq data indicated deregulation of angiogenesis-related genes with known paracrine functions in the aging fibroblast cell populations. In line with this, our functional tests revealed a disturbed cross talk of aged cardiac fibroblasts with endothelial cells during aging. Fibroblasts may contribute to the change of the microenvironment in the aged heart to control the functional response of endothelial cells. Specifically, we identified fibroblast-derived serpins as mediators of endothelial dysfunction. Serpine1 expression is well known to be increased in senescent cells in the aging heart (25). A null mutation of SERPINE1 in humans protects against aging (26). In combination with its anti-angiogenic activity (17), the induction of this pleiotropic gene in aging fibroblasts may contribute to the reduced capillary density observed in the fibrotic regions of the aging hearts. The impaired microcirculation observed in the aging heart may further aggravate fibrosis, cardiac hypertrophy and cardiac dysfunction. In addition, we showed that conditioned medium increased the pro-inflammatory activation of endothelial cells and

reduced endothelial cell autophagy. While the mechanism by which aged fibroblasts may interfere with endothelial cell autophagy is unclear, one may speculate that Serpine1, which was shown to exhibit a pro-inflammatory activity (27), may also affect endothelial inflammatory responses. Enhanced vascular inflammation may potentially lead to tissue invasion of inflammatory bone marrow-derived cells, which may replace tissue resident macrophages and further enhance the aging process. Interestingly, conditioned medium from aged fibroblasts had no significant effect on cellular proliferation suggesting that aged fibroblasts do not contribute to endothelial cell replicative senescence. Together, our data suggest that fibroblasts of the aging heart induce some but not all of the signatures of aging endothelial cells. In addition to serpins many other cytokines and extracellular matrix genes are dysregulated in the aging fibroblast, many of which are predicted to interact with endothelial cells. Therefore, it is likely the interaction of aging fibroblasts with endothelial cells in vivo is more complex than could be mimicked by mechanistic experimental intervention.

In addition, we found that old fibroblasts of the heart acquired osteogenic traits. Interestingly, a very recent study showed that aged skin fibroblasts appear to gain adipogenic traits (28), suggesting a tissue-specific impact of aging on fibroblast identity. Aging is well known to augment vascular calcification, but a fate change of fibroblast to osteogenic cells in the heart has only recently been described under pathological stress conditions (20). Our data suggest that natural aging is also associated with such a change in fibroblast fates leading to an increasing, but low number of osteocalcin gene expressing cells in the heart. Previous published single-cell datasets of young mice hearts (11, 29) showed mostly cells with gene expression profiles resembling here-shown young fibroblast sub-clusters (Supplemental Figure 10). Very few cells from these public datasets have transcriptional profiles related to fibroblast sub-clusters 2, 4 or 8 (enriched with genes involved in epithelial cell proliferation and osteoblast). Histological staining suggested that osteocalcin expressing cells were located in the epicardial layer, in which calcification was in particular observed. Our in silico analysis of the epicardial cell cluster suggested that aged heart epicardial cells do not show an increase in osteoblast genes, but we cannot rule out that a subset of Pdgfra expressing epicardial cells of the aging heart may cluster within the fibroblast population. The consequences of these fate changes on cardiac function need to be further explored.

In this study we focused on the discovery of cell-type specific effects of aging under well-defined conditions. Our single-nucleus transcriptome data revealed systemic responses of cardiac cells to aging, in particular with respect to the heterogeneity and specific age-related changes of fibroblast sub-populations (Supplemental Figure 11). Of note, beyond shedding light on mechanistic processes of aging with unprecedented resolution, transcriptome analyses of individual cells can be leveraged to discover entry points of physiological disorder, resulting from the effects of intrinsic aging.

Material and Methods

Laboratory animals

Isogenic male C57BL/6JRj inbred mice were obtained from Janvier (Le Genest Saint-Isle, France). C57BL/6JRj strain. Homozygosity of these inbred mice was controlled by Janvier using exome

sequencing (<https://www.janvier-labs.com/461.html>). To obtain hearts, mice were sacrificed by cervical dislocation under anesthesia with isoflurane. The obtained hearts were either snap frozen with liquid nitrogen for nuclei isolation or freshly used for cell isolation.

Nuclei isolation

Whole mouse hearts (derived from three 12 weeks old and from three 18 months old mice) were dissociated in liquid nitrogen using a mortar. The sample was then transferred into a Dounce homogenizer. For isolation of nuclei we strictly followed the experimental steps that are detailed in (30). Samples were homogenized and lysed to release the nuclei, followed by FACS (Aria III, BD Genomics) of DAPI stained high quality nuclei to sort out any residual cell debris. Integrity and purity of the nuclei was inspected visually using a Leica DMI8 inverted microscope. Yield of nuclei was quantified by using a Neubauer chamber.

(Single-nucleus) cDNA library preparation and Illumina short-read sequencing

Generation of libraries for single-cell mRNA sequencing was done using the Chromium Single Cell 3' protocol (10X Genomics). Briefly, we applied droplet based nuclei encapsulation, lysis, as well as individual transcript (UMI) and nuclei barcoding for generation of 3' end-counting mRNA sequencing libraries, using the Single Cell 3' v2 Reagent Kits from 10X Genomics. The libraries were sequenced using a HiSeq 4000 sequencer (Illumina). Bulk transcriptome data of fibroblasts generated by applying conventional TruSeq library preparation (Illumina) and Illumina sequencing were used to validate single-nucleus sequencing results.

Quality control and read mapping

The Cell Ranger suite version 2.1.0 was used to perform barcode processing and single cell gene UMI (unique molecular index) counting (<http://software.10xgenomics.com/single-cell/overview/welcome>).

Reads were aligned to GRCm38 reference genome and gene annotation was extracted from gencode vM12. Intronic mapped reads were assumed to be part of pre-mRNAs; therefore, they were also assigned to the respective gene. Since Cell Ranger counts only those reads that map to exons, we created a modified GTF (gene transfer format) file, which denotes each gene transcript locus as one exon and rebuilt cellranger reference (cellranger mkref). This step was necessary due to high number of pre-mRNA in nuclei. Final results of the Cell Ranger analysis contain the count values of UMIs assigned to each gene in each of the cells for each respective sample using all mapped reads. The summary of all statistics for each sample can be found in Table S1. Data is accessible through The full raw and processed data was submitted to the ArrayExpress database of the European Bioinformatics Institute (EBI); accession number: E-MTAB-7869

Cell cycle analysis

Cell cycle states were established using cyclone implemented in scran package (v1.6.6) and the mouse model, available in the package (mouse_cycle_markers.rds). Cells were classified into G1, S and G2M phase, based on their normalized gene count (31).

Data normalization, clustering and cell population definition

Cell Ranger raw result tables were merged and analyzed using Seurat suite version 2.2.0 (32). Only genes expressed in at least 40 different nuclei and nuclei with a minimum of 200 genes were generally kept for analysis. For some specific analysis below, we partly applied more restricted values. Gene expression (in UMI) was log-normalized and scaled. Variable genes for each of the 6 samples were detected by Seurat “FindVariableGenes” function using default options. Clustering was done using only variable genes. In order to obtain a global set of variable genes, we combined the set of variable genes from all 6 samples using the union of the top 1000 variable genes in each one. To align all 6 samples and remove potential batch effects derived from sample preparation and sequencing, we first run a canonical correlation analysis (CCA) using a diagonal implementation of CCA on each sample. Then we aligned the subspaces across all selected variables on this CCA.

To explore transcriptional heterogeneity and to undertake initial cell clustering, we reduced dimensionality using the aligned CCAs. We used CCA loadings as input for a graph-based approach to cluster cells by cell type and as input for t-distributed stochastic neighbor embedding (t-SNE) for reduction to two dimensions for visualization purposes. For the overall dataset, we selected the first 20 dimensions that explained more variability than expected by chance using a permutation-based test as implemented in Seurat. For further clustering of cells within primary clusters (sub-clustering), we selected variable numbers of CCAs for dimensionality reduction using either a permutation-based test or heuristic methods implemented in Seurat. Clusters were identified using the function “FindClusters” from Seurat using default parameters. The robustness of the clusters was calculated using the function “AssessNodes” from Seurat. For each cluster, a phylogenetic tree based on the distance matrix in gene expression space is computed. Next, it computes an out of bag error for a random forest classifier trained on each internal node split of the tree.

Cluster annotation to heart cell types

To identify specific markers to each cluster and consequently annotate them with the respective heart cell type, we applied Seurat “FindAllMarkers” function using the area-under-the-curve-based scoring classifier with default parameters. We used the default Wilcoxon rank sum test for the specific cell type analysis.

The assignment of each cluster to a specific cell type was done manually by making use of published gene expression data and by single cell profile projection using scmap. We projected heart single-cells from Tabula Muris consortium (12) set onto our single-nuclei in order to identify the similar cell types and show the reproducibility from both approaches. All default parameters were used; the numbers of selected features were defined as the top 40.

Differential expression using DESeq2

To identify differentially expressed genes (DEGs) between the old and the young hearts we used the DESeq2 (v. 1.20) in order to explore the statistical power of the replicates (33). Differential expression analysis was conducted separately for each cluster. Data were filtered for quality; for each sub cell-type we allowed only cells/nuclei with more than 1000 UMIs (for cardiomyocytes we used 2000 as minimum due to the high number of nuclei from this type), 500 detected genes and maximum 0.05% of mitochondrial reads. Only clusters with more than 500 cells after filtering were analyzed. Clusters were summarized by total counts for each gene in order to generate an in silico bulk RNA-seq data set. This way we could access fold changes and adjusted p-values for differentially expressed genes between young and old samples, containing 3 replicates each sub-type. The test for significance was computed by the nbinomLRT DESeq2 function and the significantly differentially expressed genes selected using Independent hypothesis weighting (IHW) (34).

Gene enrichment analysis

We used ClusterProfile (R package; v. 3.8) and ConsensusPathDB (<http://cpdb.molgen.mpg.de/CPDB>) for pathway analysis of age-associated transcripts. In ClusterProfile, all gene names were first converted into Entrez IDs and then enriched for both KEGG and GO-terms. Benjamini & Hochberg FDR was used for multiple testing corrections. The significant threshold 0.05 after correction for multiple testing was applied. We further used the online tool Metascape (<http://metascape.org/gp/index.html#/main/step1>) for gene ontology analysis of genes enriched and differentially expressed in fibroblast population A and B.

Co-expression networks

WGNCA (35) was used to build co-expression networks from DEGs profiles. Each cluster was analyzed independently, as well as up (higher expression on old heart) and down regulated genes. Cells were extra filtered for quality as described in item "Differential expression using DESeq2". The soft-threshold power parameter was selected when "scale-free topology r-squared" reached a value higher than 0.7. Minimum module size was set to 5.

Sub-clustering based on DEGs

Differentially expressed genes between old and young fibroblasts were used for sub-clustering and detecting cell populations of fibroblasts based on the signal produced by these genes. We used Monocle2 sorting cell functions and set up the differentially expressed genes as ordering genes for reducing dimensions. Seurat objects were converted into Monocle (v2.4) (36) objects using the "importCDS" function. Two different dimension reduction algorithms were used for graphical representation of the data, the tSNE and DDRTree. For tSNE we used the following parameters: num_dim=15, max_components=2, norm_method=log. The clustering was performed using the following parameters: rho_threshold=2, delta_threshold=5. For DDRTree we used as parameter: auto_param_selection=T.

The DDRTree graph representation help us to visualize the progress of possible cells transitions within the cell types using aging as sorting factor. We plotted the sub-clusters split by age and states split by sub-cluster and age.

RNA velocity

We run `velocity.py` (14) annotator for each mapped bam file using the default parameters for 10X Genomics technology and gencode vM12 gtf file for intron-exon annotation. The resulting loom object for each sample was loaded and processed in R using the `velocity.R` (v. 0.17) package. We used the embedding from monocle DDRTree representation for cell-cell distance calculation and final velocity plots. The estimation of RNA velocity was done with the grouping of 10 cells; the other parameters were set to default.

Entropy calculation

We used SLICE (v0.99.0) (37) package to calculate entropy values of groups of cells/nuclei based on a set of genes. The Seurat objects were sliced according to this set of genes and to the group of cells/nuclei to be analyzed. Entropy was calculated by using the `getEntropy` function from SLICE package applying a bootstrap calculation of size 1000, 100 iterations and random seed "201602".

Ligand-receptor interactions

Ligand-receptor interaction analysis was performed according to the approach described previously (29). Briefly, a weighted directed graph with 4 layers of nodes was built linking source cell types (layer 1), defined by expression of a ligand (layer 2), to target cell types (layer 4) expressing a corresponding receptor (layer 3), after reference to a curated map of ligand-receptor pairs (38) . Source-ligand and receptor-target edges were weighted according to expression fold-change in ligands and receptors, respectively. Ligand-receptor edges were further weighted by mouse-specific association scores from the STRING database (39). Permutation testing (100,000 permutations) of randomized network connections was applied to determine significant source-target network connections following Benjamini-Hochberg multiple-testing correction (adjusted $P < 0.01$).

Cardiac Fibroblast Cell Isolation

Cardiac fibroblasts were isolated from male old (20 months) versus young (12 weeks) mice. After sacrificing the mice, hearts were harvested, cut into small pieces and washed with Hank's buffered saline solution (+Ca²⁺/+Mg²⁺). Tissue dissociation was performed in 2.5 mL of a commercial enzyme mix (Neonatal Heart Dissociation Kit, mouse and rat by Miltenyi Biotec GmbH). To dissociate the solid heart tissue, gentleMACSTM Dissociator (Miltenyi Biotec GmbH) with the pre-programmed program `m_neoheart_01_01` was used after 25 minutes, three times

15 minutes of digestion at 37°C. The cellular components of the digested heart suspension were pelleted by centrifugation (80x g, 5 minutes, 4°C) and then resuspended in 3 mL DMEM High Glucose GlutaMAX (Invitrogen by Lifetechnologies) containing 10% FCS (Invitrogen by Lifetechnologies) and penicillin/streptomycin (Roche). Fibroblasts were isolated via plating the cell suspension for 2 hours at 37°C and 5% CO₂ in a humidified atmosphere. After plating, the non-fibroblast cells were removed by three washing steps using PBS (Invitrogen).

RNA isolation and quantification

Total RNA was purified from cells using the miRNeasy kits (Qiagen), combined with on-column DNase digestion (DNase Set, Qiagen) according to the manufacturer's instruction. The RNA concentration was determined by measuring absorption at 260 nm and 280 nm with the NanoDrop[®]ND 2000-spectrophotometer (PeqLab).

Bulk RNA sequencing

RNA was isolated from isolated cardiac fibroblasts using the miRNeasy micro Kit (Qiagen) combined with on-column DNase digestion (DNase-Free DNase Set, Qiagen) to avoid contamination by genomic DNA. RNA and library preparation integrity were verified with a BioAnalyzer 2100 (Agilent) or LabChip Gx Touch 24 (Perkin Elmer). 200ng of total RNA was used as input for Truseq Stranded Total RNA Library preparation following the low sample protocol (Illumina). Sequencing was performed on the NextSeq500 instrument (Illumina) using v2 chemistry, resulting in minimum of 30M reads per library with 1x75bp single end setup. Demultiplexing and adapter removal was performed by bcl2fastq software (Illumina) and resulting raw reads were assessed for quality, adapter content and duplication rates with FastQC. Fastx_trimmer was used to trim the first 5 bp. Trimmed and filtered reads were aligned versus the Ensembl mouse genome version mm10 (GRCm38) using STAR 2.4.0a with the standard parameters (40). The number of reads aligning to genes was counted and compared with Cifffdiff version 2.2.1 (41). The Ensembl annotation was enriched with UniProt data (release 06.06.2014) based on Ensembl gene identifiers (Activities at the Universal Protein Resource (UniProt)).

cDNA synthesis

To quantify mRNA expression by qPCR, 100 ng - 1 µg of total RNA were reverse transcribed using the reverse transcriptase MuLV (Life Technologies) as previously described (42). The cDNA synthesis was performed in a reaction volume of 20 µL using 1x PCR Buffer II (10x) with magnesium (Thermo Fisher Scientific), 5 mM of MgCl₂ (Applied Biosystems), 0.5 µg of random hexamer primer (Thermo Fisher Scientific), 0.5 mM of dNTP mix (Fermentas), 20 units of RNase inhibitor (Thermo Fisher Scientific) and 50 units of MuLV reverse transcriptase. The reaction was incubated at 43 °C for 75 minutes followed by 5 minutes of heat-inactivation at 95 °C. The synthesised cDNA was diluted with RNase-/DNase-free water (Invitrogen) to prevent any interference during qPCR caused by the ion strength present in the cDNA reaction.

Real-time quantitative polymerase chain reaction (RT-qPCR)

RT-qPCR was performed using Fast SYBR Green master mix (Applied Biosystems) and an Applied Biosystems StepOnePlus machine as described previously (42). The synthesised cDNA served as template. Primer sequences were designed using the NCBI Primer-BLAST online tool and were purchased from Sigma-Aldrich (a full list can be found in the Supplemental Table 9). The RT-qPCR was performed in a volume of 20 μ L containing 5 μ L of cDNA template, 10 μ L of 2x Fast SYBR Green master mix (Applied Biosystems), 3 μ L water and 1 μ L of the sense and antisense primer (stock concentration of 10 μ M each). Mouse or human ribosomal P0 (RPLP0) mRNA served as endogenous control. The RT-qPCR was performed in duplicates and the analysis was carried out with the formula $2^{-\Delta\text{CT}}$, with $\Delta\text{CT} = \text{CT target gene} - \text{CT endogenous control}$.

Cell culture of endothelial cells

Human umbilical vein endothelial cells (HUVEC) were purchased from Lonza and cultured with endothelial basal medium (EBM, Lonza) supplemented with 10 % fetal calve serum (FCS; Invitrogen), Amphotericin-B, ascorbic acid, bovine brain extract (BBE), endothelial growth factor (EGF), gentamycin sulphate and hydrocortisone (EGM-singleQuots, Lonza) at 37°C and 5% CO₂, at humidified atmosphere. Isolated cardiac mouse fibroblasts were cultured with DMEM high glucose GlutaMAX (Invitrogen) supplemented with 10% FCS (Invitrogen) and penicillin / streptomycin (Roche) at 37°C and 5% CO₂ at a humidified atmosphere. Cells detachment was performed with 0.25% trypsin (Life Technologies), which was incubated for 2 minutes at 37 °C and 5% CO₂ and neutralised with fully supplemented medium. The cell number was determined using the cell counter NucleoCounter (ChemoMetec), as described in the manufacturer's protocol.

Fibroblast-conditioned medium

To obtain fibroblast-conditioned medium for endothelial cell – fibroblast interaction studies, isolated cardiac fibroblasts from young and old mice were cultured 24 hours after cell isolation in 12-well cell culture plates (Greiner Bio-One GmbH) with 1.5 mL of fully supplemented endothelial basal medium (EBM) per well at 37°C and 5% CO₂ at humidified atmosphere. After 24 hours, cell culture supernatants were centrifuged (500x g, 5 minutes) to deplete dead cells and stored at -80°C.

Tube formation assay

In vitro tube formation was performed with 1.5×10^5 HUVECs cultured in 1 mL of fibroblast-conditioned EBM in 12-well plates or with 2×10^4 HUVECs cultured in 100 μ L of conditioned medium in 96 well plates (Greiner Bio-One GmbH) that had been coated with 200 or 100 μ L Matrigel (#356234, Corning). Tube formation was determined after 24 hours by measuring the accumulated tube length in five randomly chosen microscopic fields with a computer-assisted microscope using Axiovision 4.5 (Zeiss).

For rescue experiments, medium of aged fibroblasts were supplemented with 4 µg of a serpin (AF3828, R&D Systems) or Efemp1 (LS-B11500; LifeSpan Biosciences) neutralizing antibody.

For the recombinant serpin study, HUVECs were cultured in medium supplemented with 10 ng/mL serpin E1 (Cusabio, CSB-EP021081MO) or serpin E2 (R&D Systems, 2175-PI-010) for 24 hours.

Inflammation study

We seeded 80,000 HUVECs in 24-well plates and cultured in conditioned medium of fibroblasts derived from young and aged mouse hearts in the presence and absence of 10 ng/mL TNFα. After 24 hours, IL-6 expression was determined using RT-qPCR.

Autophagy

We seeded 40,000 HUVECs in 8-well chamber slides that had been coated with fibronectin before. HUVECs were cultured for 24 hours and stained as follows: HUVECs were fixed for 10 minutes with 4% HistoFix, permeabilized with 0.1% Triton X-100 and blocked in 10% donkey serum for 30 minutes. Primary mouse anti-p62 (Novus Biologicals, H00008878-M01) and rabbit anti-LC3 (Novus Biologicals, NB100-2220SS) antibodies incubated in 10% donkey serum overnight at 4°C. DAPI (1:1000) as well as the secondary anti-rabbit Alexa488 (Invitrogen, A21206) and anti-mouse Alexa568 (Invitrogen, 498389) antibodies incubated for one hour. Autophagosomes were identified as p62/LC3-double-positive areas and counted in four images per condition.

Proliferation

We seeded 40,000 HUVECs in 8-well chamber slides that were coated with fibronectin. HUVECs were cultured for 24 hours and stained with DAPI. Cell were counted in four randomly chosen images.

Secretome Analysis

Secreted proteins were detected in supernatants of isolated fibroblasts, which were cultured for 24 hours in DMEM without any supplements. Supernatants were centrifuged (1500 rpm, 5 minutes) to remove cell debris and stored at -80°C. Cytokines and growth factors were detected using the Proteome Profiler Mouse Angiogenesis Array (ARY015; R&D Systems) according to the manufacturer's protocol.

Picrosirius red staining

Picrosirius red staining was used to determine collagen deposition and fibrosis in paraffin sections of young versus aged mice hearts. In a first step, the paraffin sections were deparaffinised with xylene (twice 10 minutes) and an ethanol series of 100%, 95%, 80%, 70% and 50% ethanol (5 minutes each step), before washing the sections with water and PBS (5 minutes each step). In a second step, a 0.1% Picrosirius Red solution was prepared by solving 0.5 g Sirius Red (Waldeck GmbH) in 500 mL picric acid (Sigma-Aldrich) that incubated with the deparaffinised sections for 1 hour. After washing two times with acidified water, the sections were dehydrated with 100% ethanol, cleared with xylene and mounted with Pertex (Meditex)

Von Kossa staining

Cardiac calcification was detected on paraffin section (10 μ m) of young (12 weeks) and aged (18-20 months) mouse hearts by using the Silver plating kit acc. to von Kossa (1.00362.0001; Merck). In a first step, the paraffin sections were deparaffinised with xylene (twice 10 minutes) and an ethanol series of 100%, 95%, 80%, 70% and 50% ethanol (5 minutes each step), before washing the sections with water and PBS (5 minutes each step). In a second step, silver nitrate solution incubated for 20 minutes with the sections. After washing with water, sodium thiosulfate solution was used and incubated for 5 minutes with the sections. Sections were washed with water and nuclei were stained with Kernechtrot. After washing again with water, sections were dehydrated with an ascending ethanol series (70%, 96%, 100%: 1 minute each), cleared with xylene and mounted with Pertex (Meditex).

Immunostaining of PDGFR α and osteocalcin

To validate single-nucleus RNA sequencing clustering, fluorescence immunostaining was performed in young (12 weeks) and aged (18-20 months) mouse heart paraffin sections. Hearts were fixed immediately in 4% HistoFix overnight, embedded in paraffin, sectioned at 4 μ m thickness using a microtome and placed on adhesive glass slides. Next, slides were incubated at 60 °C for 1 h and deparaffinised with xylene (twice 10 minutes) and an ethanol series of 100%, 95%, 80%, 70% and 50% ethanol (5 minutes each step), before washing the sections with water and PBS (5 minutes each step). Sections were unmasked with 0.01 M citrate buffer (pH = 6), washed for 5 minutes with PBS, 0.1% Triton X-100 and blocked for 1 hour with PBS containing 1% BSA, 2% donkey serum and 0.1% Triton X-100. The primary antibodies anti-osteocalcin (ab93876; Abcam) and anti-Pdgfra (AF1062; R&D Systems) were diluted 1:100 in Pblec buffer (1mM MgCl₂, 1 mM CaCl₂, 0,1 mM MnCl₂, 1% Triton X-100 in PBS; pH=6.9) and incubated at 4°C overnight (or for 1 hour at room temperature) on the sections. Sections were washed three times with PBS, 0.1% Triton X-100 and the secondary antibodies donkey anti-rabbit Alexa Fluor 488 (A21206; Invitrogen) and donkey anti-goat Alexa Fluor 647 (A21447; Invitrogen) incubated for 1 hour at room temperature (dilution: 1:300) on the slides. After washing slides again three times with 0.1% Triton X-100, slides were mounted with mounting medium containing Hoechst 33342.

Immunostaining for capillary density

Capillary density was determined in 4µm thick paraffin-embedded sections from young (12 weeks) and aged (18-20 months) mouse hearts. Sections were dried over night at 37°C, incubated at 60 °C for 1 hour and deparaffinised with xylene (twice 10 minutes). An ethanol series of 100%, 95%, 80%, 70% and 50% ethanol (5 minutes each step) was applied, before washing the sections with water. Sections were unmasked with 0.01 M citrate buffer (pH = 6), washed for 5 minutes with PBS, 0.1% Triton X-100 and blocked for 1 hour with PBS containing 1% BSA and 0.1% Triton X-100. Biotinylated Isolectin B4 (Vector #B1205) was diluted 1:50 and incubated over night at 4°C. Next, 1:200 streptavidin Alexa Fluor 488 (Invitrogen #S32354) and 1:400 wheat germ agglutinin Alexa Fluor 647 (molecular probes #W32466) incubated for 1 hour at room temperature. Nuclei were stained with Hoechst 33342. Capillary density was determined in Isolectin B4-positive area per total area in four images per condition.

Statistical analysis of molecular and cell biological assays

Data of targeted molecular and cell biological procedures described above are represented as mean and error bars indicate standard error of the mean (SEM). After passing Gaussian distribution as assessed by Kolmogorov-Smirnov or D'Agostino-Pearson normality test, statistical power was determined, using two-sided, unpaired T-test for two-group comparison. For comparisons of more than two groups, multiple group ANOVA with a post hoc Bonferroni test was used.

Study approval

All animal experiments were approved by the Regional Board of the State of Hessen, Germany.

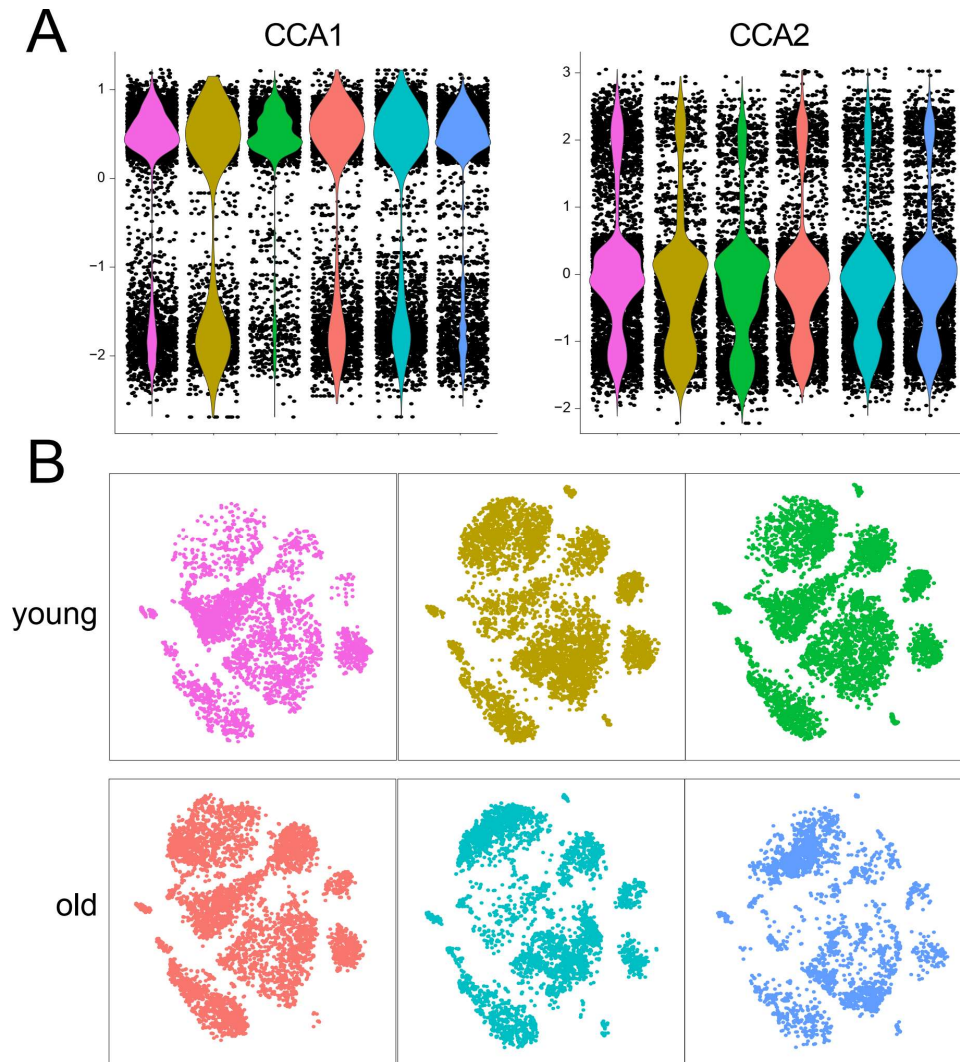
Author contributions

SD, SS designed research studies; JUGW performed the wet lab experiments with technical support of CB, CF, MMR, and TC; RV, CF, SS acquired sequence data. JUGW, RV, LT, DJ, MK, SD and SS analyzed sequence and other experimental data; RV, JUGW, SD and SS wrote the manuscript with input from all other authors. NGC and RH provided conceptual advice. Shared co-authorship was granted according to individual workload and impact on the study.

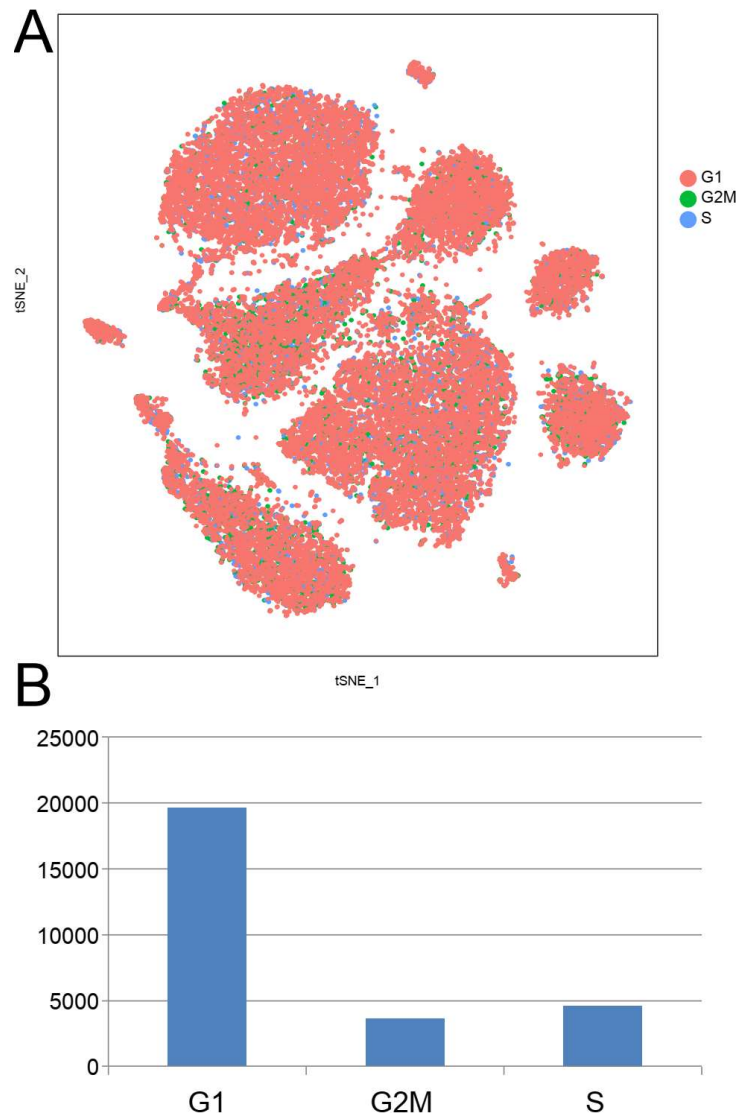
Acknowledgements

The study was supported by the Helmholtz Association of German Research Centers (MDC), Berlin Institute of Health (S.S.), the European Union (FP-7, grant agreement 262055, ESGI (to S.S.), BMBF (grant 01EA1604) to S.S.; DZHK (German Centre for Cardiovascular Research)) and the BMBF (German Ministry of Education and Research) shared expertise program to S.D. and S.S.; CRC1366, Exc2026, the Robert Schwiете Foundation and the Australian Academy of Science (Selby Foundation) to S.D.

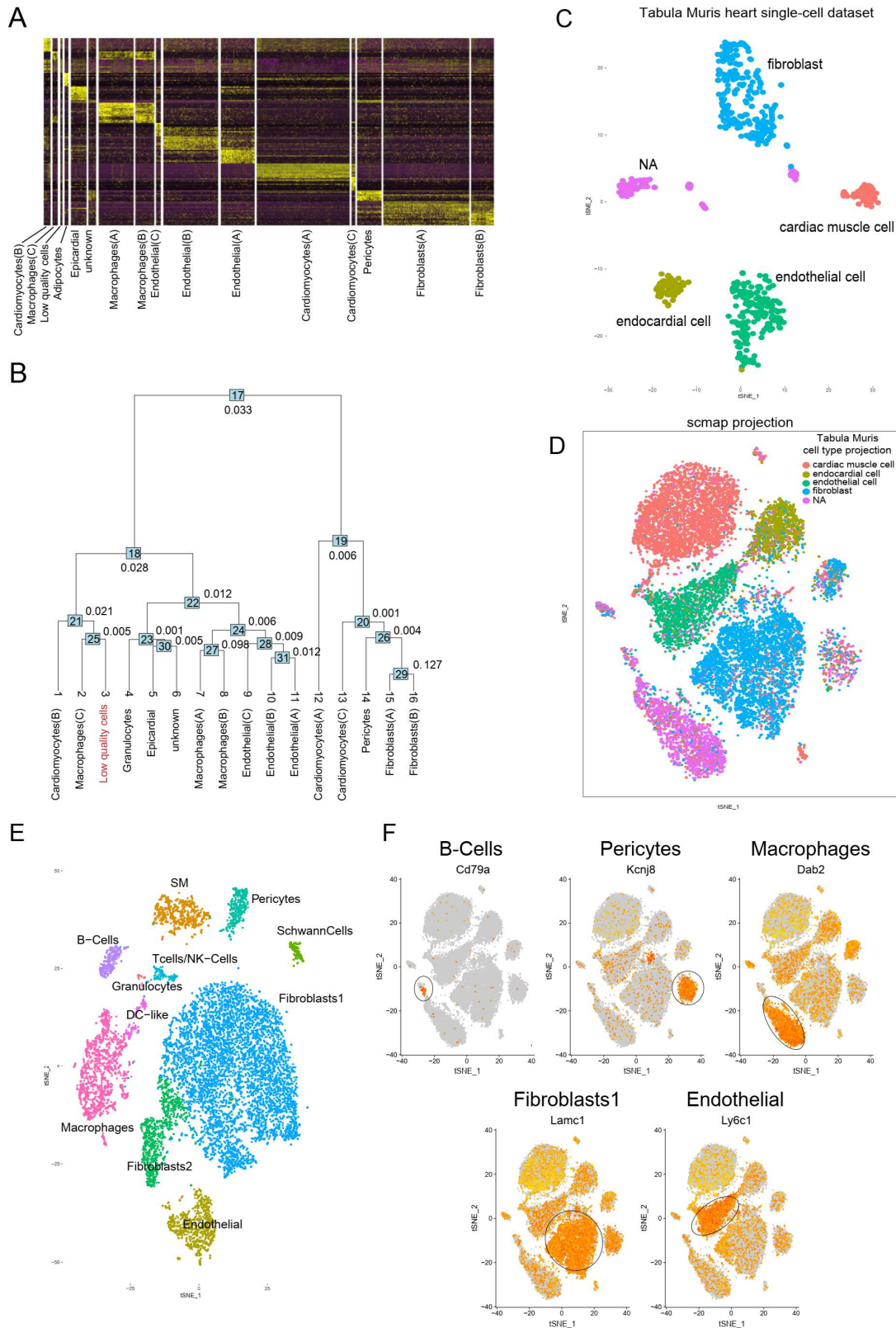
We thank Dr. Nicolas Socci for evaluation of the statistical analyses of this study.



Supplemental Figure 1: Alignment of all samples. All 6 samples from young and old mice were aligned together in order to allow for inter-sample comparisons. **(A)** A canonical correlation analysis (CCA) was applied to identify common sources of variation between the datasets; the top 1000 variable genes of all samples were used to align the CCA subspaces of all samples in a new dimensional reduction (*cca.aligned*). **(B)** Using these aligned dimensions; it was possible to run a single integrated analysis on all cells. t-SNE plots show a complete overlap of all samples and no library preparation or sequencing batch effects.

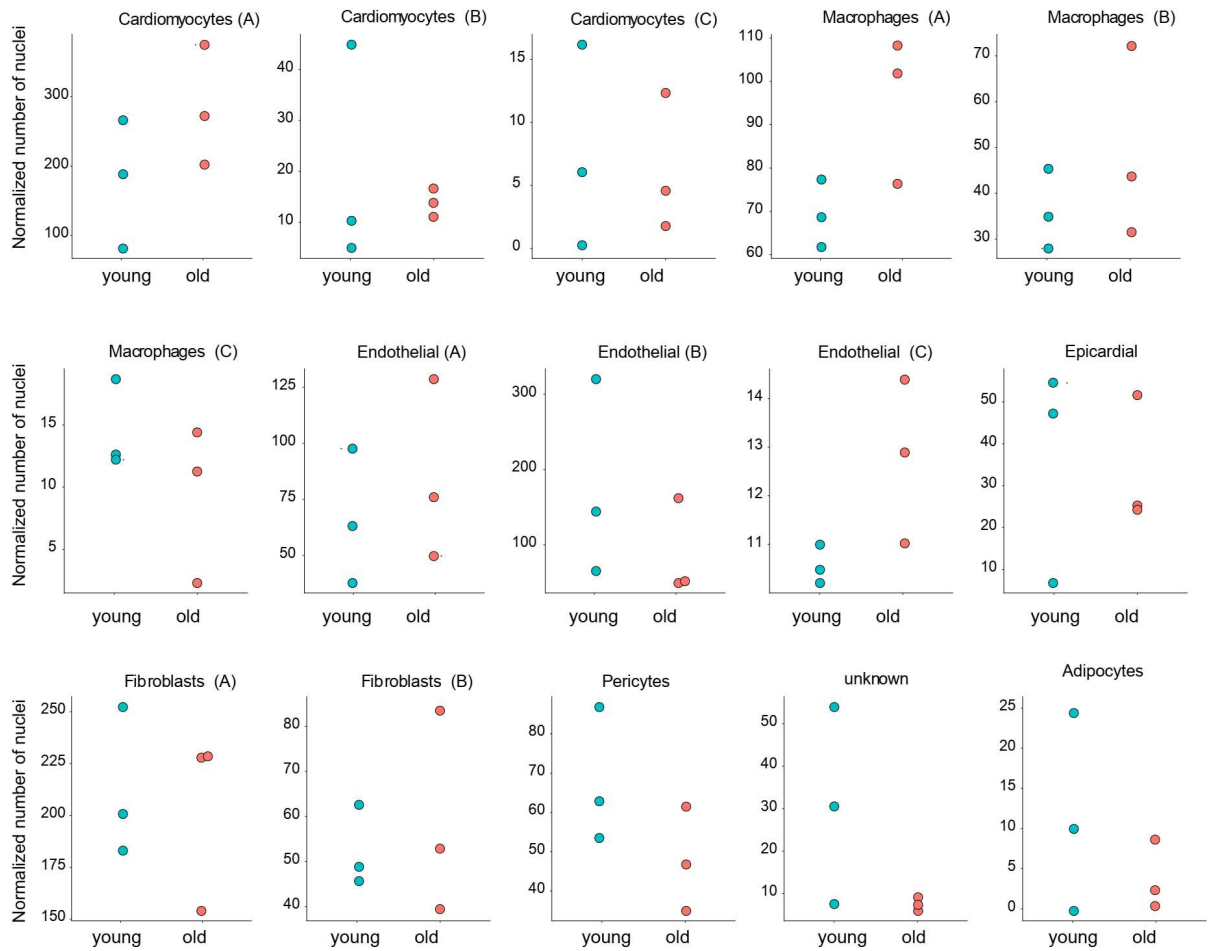


Supplemental Figure 2: (A) Quality control. Cell cycle distribution of all cells was predicted using mouse-trained model (see Materials and Methods). (B) t-SNE colored by cell stage. This quality control shows that data was homogeneous. Most of the cells were synchronized in G1 phase.

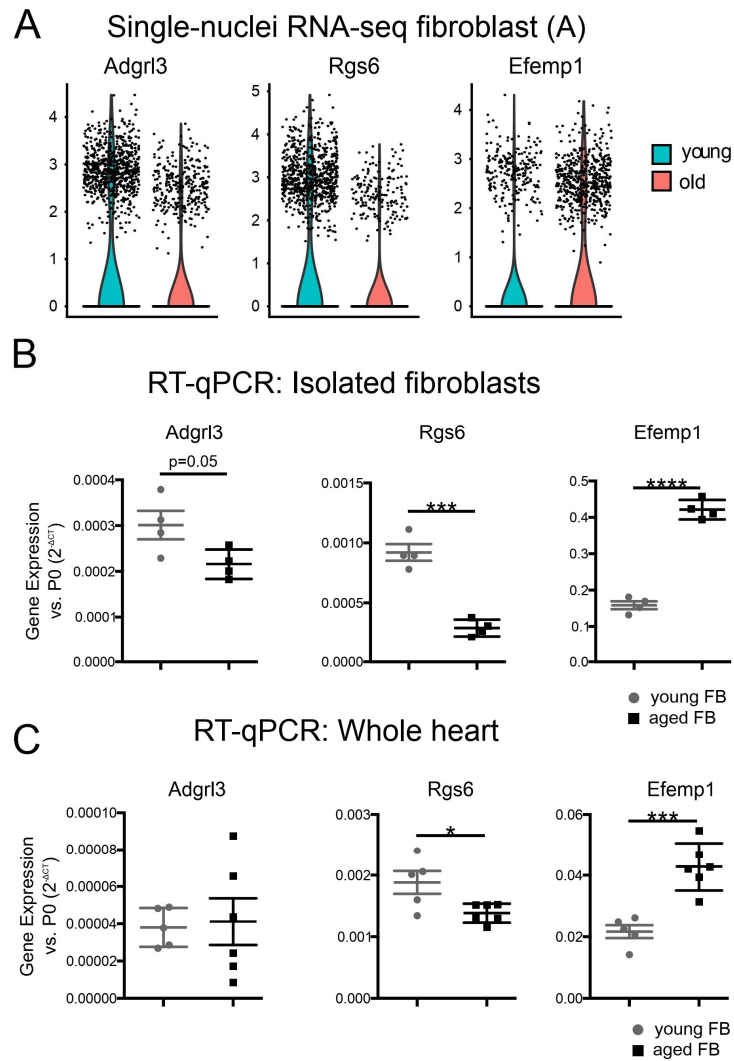


Supplemental Figure 3: (A) Cluster analysis. Genes enriched in each cluster were identified using a “ROC” test in Seurat (see Supplemental Table 2), comparing cells assigned to each cluster to all other cells. A heat-map was constructed using these genes found to define each cluster. The cluster labeled as “Low quality cells” in red showed excessive enrichment of mitochondrial genes; this one was not considered in further analysis as these nuclei likely represented low quality or dying cells.

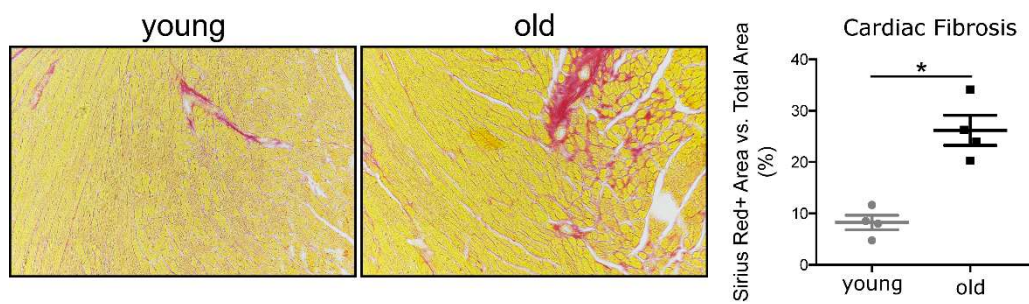
(B) We built a phylogenetic tree based on the distance matrix in gene expression of each cluster and we computed an out of bag error for each internal node of the tree. All values below 0.1 show a high confidence for all clusters. Of note, fibroblasts A and B are within this threshold, so that these two different cell clusters can be separated with less confidence. **(C)** Heart cell type annotation derived from data of the Tabula Muris consortium (see Materials and Methods). **(D)** Projection of these RNA expression profiles to our single-nuclei RNA expression data. According to Tabula Muris consortium data, our endothelial A cluster should be considered endocardial cells. Cardiomyocyte B cells represent a merged cell type between endothelial cells and cardiomyocytes. Of note, cardiomyocytes may contain more than one nucleus, potentially in different states, which may complicate the assignment of such multinuclear cell types. In general, Tabula Muris data do not comprise many of our cell populations resulting in unidentified cells or cells with mixed signals, as was the case for pericytes, neuronal like cells and immune cells. **(E)** Heart cell type annotation derived from alternative single-cell heart data of Daniel et al. 2018 (see Materials and Methods). **(F)** Expressed gene markers of main cell types described in Daniel et al. 2018 in our cell populations (see Materials and Methods).



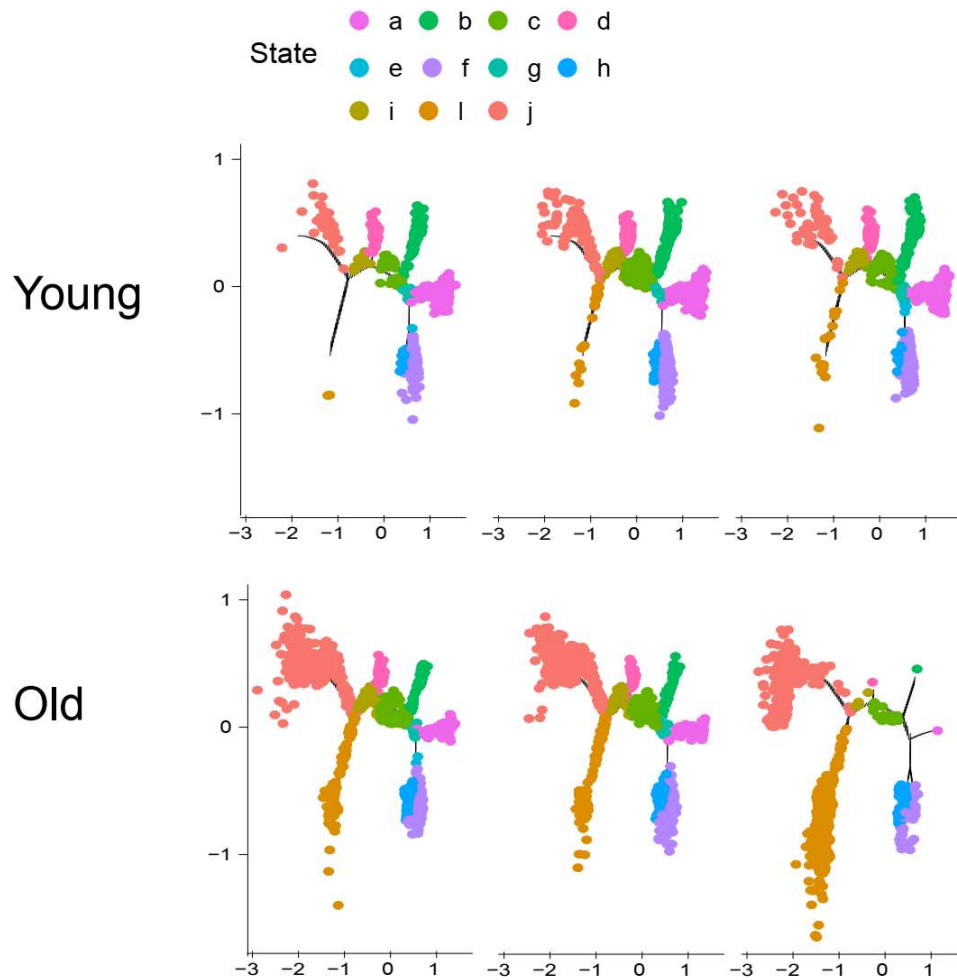
Supplemental Figure 4: Cell numbers. Comparison of number of nuclei on each cluster (normalized per 1000) between young and old samples detected by single-nucleus RNA-sequencing. In line with expectations we observed in particular for (multinucleate) cardiomyocyte A cells a trend for higher numbers of nuclei in old versus young samples. Due to too few numbers of samples, no statistical test could be reasonably applied to test potential mean differences significances. Although we observed some trends we do not have statistical power to find any significant change in cell (nuclei) population numbers.



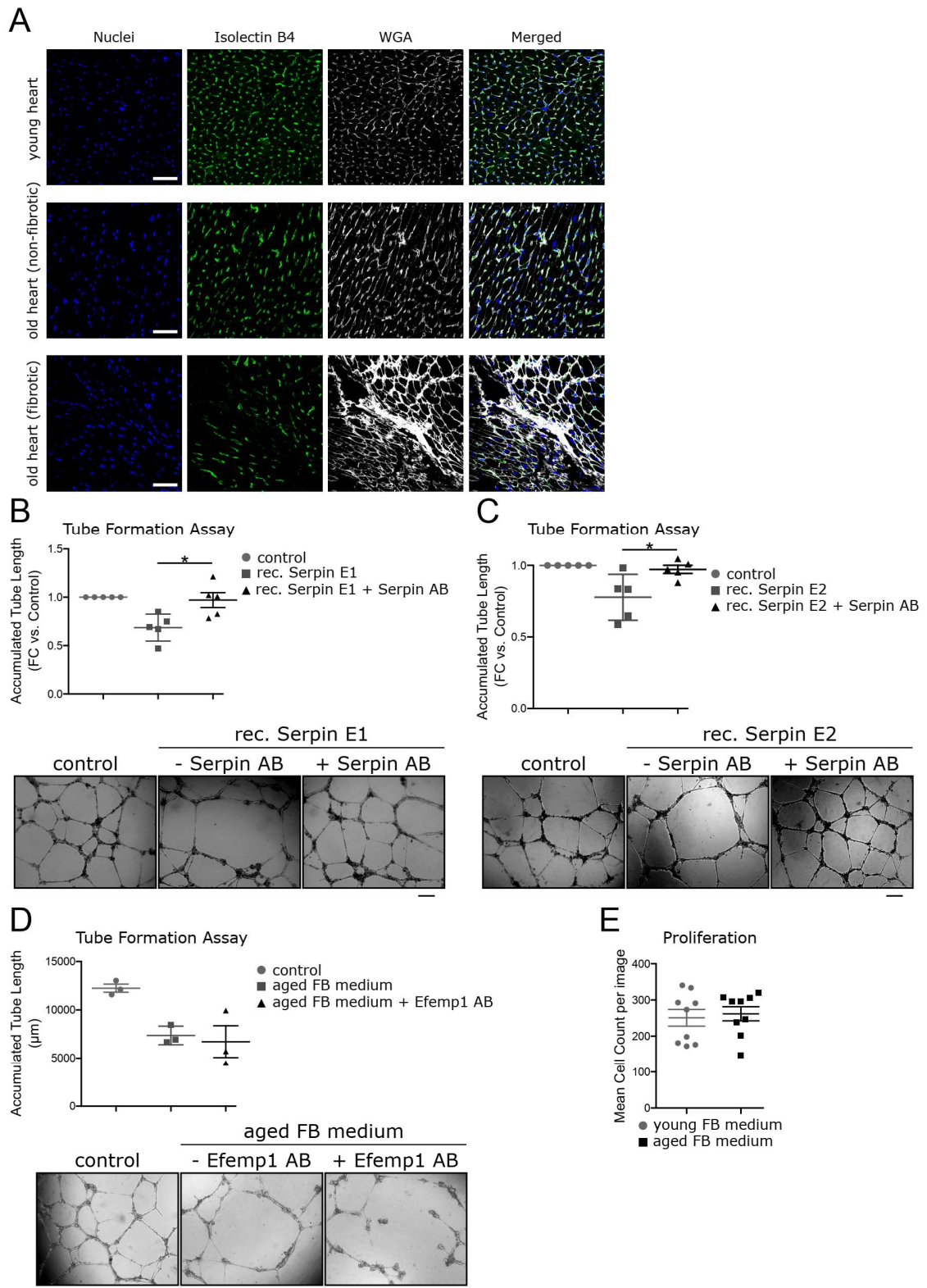
Supplemental Figure 5. Validation of fibroblast genes regulated by aging. (A) Violin plots of *Adgrl3*, *Rgs6* and *Efemp1* expressed in fibroblast population A derived from the single-nucleus sequencing data set. The validation of these genes was done via RT-qPCR with RNA derived from isolated cardiac fibroblasts (B) and RNA derived from whole mouse hearts (C). Data are shown as mean \pm SEM (B, C). Statistical analysis was performed using the unpaired, two-sided T-test (B, C), indicated as follows: * $P < 0.05$; *** $P < 0.001$ and **** $P < 0.0001$.



Supplemental Figure 6: Fibrosis in aged mice hearts. Fibrosis was determined via picrosirius red staining of young (12 weeks) and aged (20 months) mouse heart sections. Shown are 2 representative images of 24 images (n=4). Images were monitored using the Nikon Eclipse Ci microscope system and fibrosis was determined using the imageJ software. Data are shown as mean \pm SEM. Statistical analysis was performed using the unpaired, two-sided T-test, indicated as follows: *P<0.05.

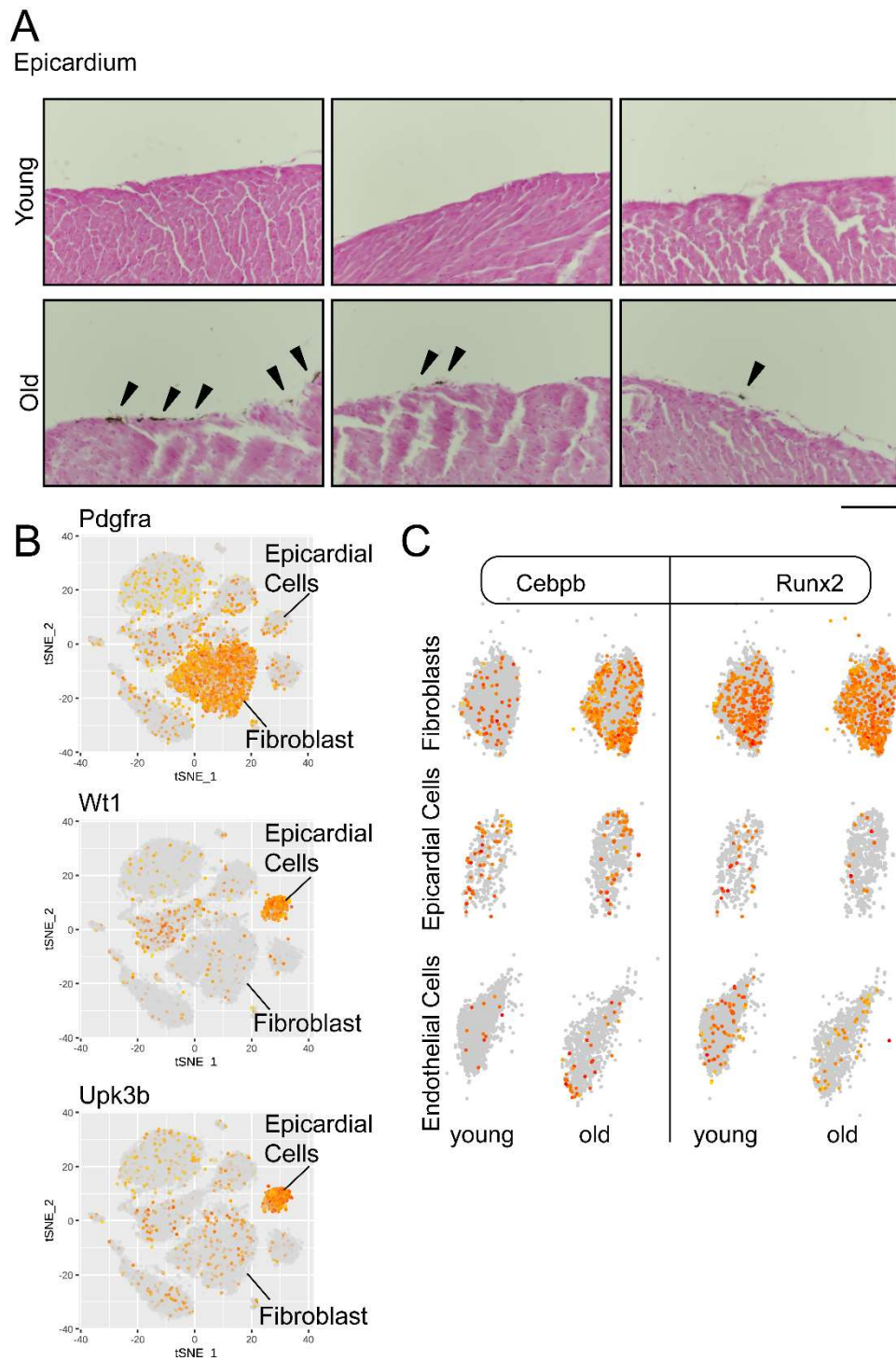


Supplemental Figure 7: Fibroblasts cell states in young and old mouse hearts. Samples feature a very similar cell state profile, showing data reproducibility. States are represented by different colours, enriched genes on each state is described in Supplemental Table 7. Each state can aggregate one or more fibroblast sub-cluster as shown in Figure 3B.

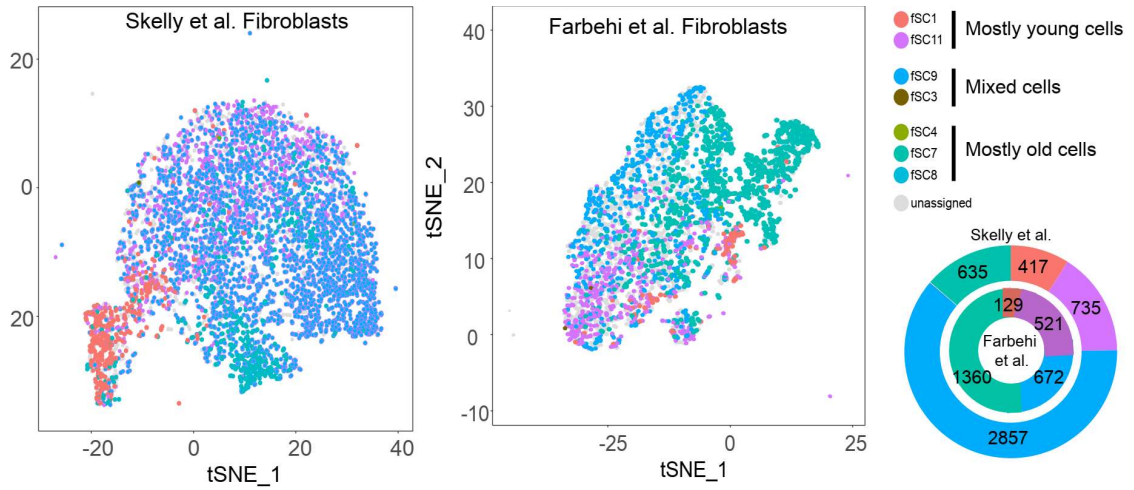


Supplemental Figure 8. Effect of fibroblast secretome on endothelial cells. (A) Capillary density of healthy young and healthy old, as well as fibrotic old heart sections. Capillaries were stained isolectin b4 (green), cell membranes with WGA (white) and nuclei (blue) with Hoechst 33342 (scale bar: 50 µm). (B) Tube formation assay of human umbilical vein endothelial cells (HUVEC) that were cultured

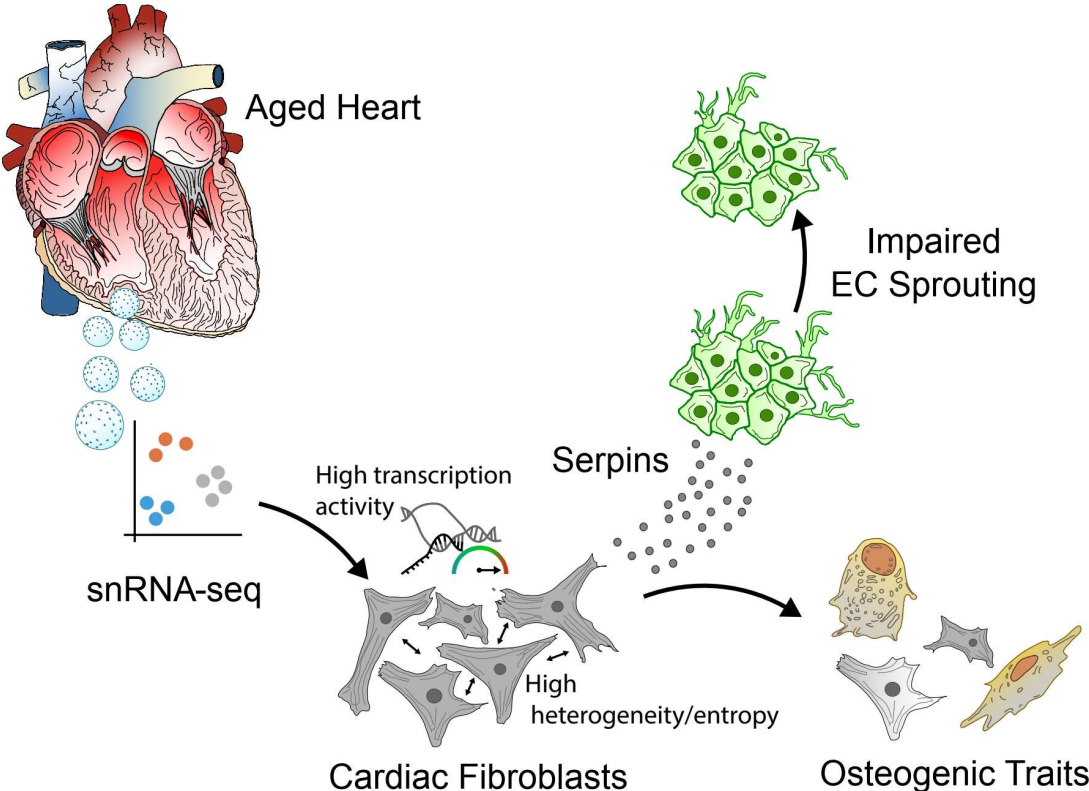
in medium without any supplements (control), 10 ng/mL recombinant Serpin E1 (rec. Serpin E1) or 10 ng/mL recombinant Serpin E1 + 4 μ g anti-serpin antibody (rec. Serpin E1 + Serpin AB). Accumulated tube length was measured in five randomly chosen microscopic fields with a computer-assisted microscope using Axiovision 4.5 (Zeiss) (scale bar: 200 μ m; n=5). (C) Tube formation assay. HUVECs that were cultured in medium without any supplements (control), 10 ng/mL recombinant Serpin E2 (rec. Serpin E2) or 10 ng/mL recombinant serpin E2 + 4 μ g anti-serpin antibody (rec. Serpin E2 + Serpin AB). Accumulated tube length was measured in five randomly chosen microscopic fields with a computer-assisted microscope using Axiovision 4.5 (Zeiss) (scale bar: 200 μ m; n=5). (D) Tube formation assay of HUVECs that were cultured in conditioned medium received from young (12 weeks) and aged (20 months) cardiac mouse fibroblasts. The aged phenotype was rescued by supplementing the aged fibroblast medium with 4 μ g of an anti-Efemp1 antibody. Accumulated tube length was measured in five randomly chosen microscopic fields with a computer-assisted microscope using Axiovision 4.5 (Zeiss) (n=3). (E) Proliferation of HUVECs cultured with conditioned medium received from young (12 weeks) and aged (18 months) cardiac mouse fibroblasts (n=9). Data are shown as mean \pm SEM. Statistical analysis was performed using an unpaired, two-sided T-test, indicated as follows: *P<0.05.



Supplemental Figure 9: Calcification in the aged epicardium. (A) Exemplary images of the epicardium in young (12 weeks) and old (20 months) mouse hearts. Calcification (dark spots, indicated by black arrows) is stained using the von Kossa staining method, whereas nuclei are stained with Kernechtrot (scale = 100 μ m). (B) Expression of *Pdgfra*, *Wt1* and *Upk3b* in young versus old nuclei cluster of the entire snRNA seq data set as shown in Figure 1A. (C) Expression of the osteogenic marker genes *Cebpb* and *Runx2* in young versus old endothelial cell, fibroblast and epicardial cell clusters



Supplemental Figure 10: Comparison of transcriptional profile from published fibroblast data. Using scmap (see methods), we mapped the fibroblast sub-cluster transcriptional profiles into already published datasets.



Supplemental Figure 11. (A) Summary visual description of the aging heart by single cell analysis.

References

1. Paneni F, Diaz Cañestro C, Libby P, Lüscher TF, Camici GG. The Aging Cardiovascular System: Understanding It at the Cellular and Clinical Levels. *J. Am. Coll. Cardiol.* 2017;69(15):1952–1967.
2. Eisenberg T et al. Cardioprotection and lifespan extension by the natural polyamine spermidine. *Nat. Med.* 2016;22:1428.
3. Lakatta EG. So! What's aging? Is cardiovascular aging a disease? *J. Mol. Cell. Cardiol.* 2015;83:1–13.
4. Chen W, Frangogiannis NG. The role of inflammatory and fibrogenic pathways in heart failure associated with aging. *Heart Fail. Rev.* 2010;15(5):415–422.
5. Gourdie RG, Dimmeler S, Kohl P. Novel therapeutic strategies targeting fibroblasts and fibrosis in heart disease. *Nat. Rev. Drug Discov.* 2016;15(9):620–638.
6. López-Otín C, Blasco MA, Partridge L, Serrano M, Kroemer G. The hallmarks of aging. *Cell* 2013;153(6):1194–1217.
7. Ferrari AU, Radaelli A, Centola M. Invited review: aging and the cardiovascular system. *J. Appl. Physiol.* 2003;95(6):2591–2597.
8. Swirski FK, Nahrendorf M. Cardioimmunology: the immune system in cardiac homeostasis and disease. *Nat. Rev. Immunol.* 2018;18(12):733–744.
9. Habib N et al. Massively parallel single-nucleus RNA-seq with DroNc-seq. *Nat. Methods* 2017;14:955–958.
10. Van Der Maaten L, Hinton G. Visualizing Data using t-SNE. *J. Mach. Learn. Res.* 2008;9:2579–2605.
11. Skelly DA et al. Single-Cell Transcriptional Profiling Reveals Cellular Diversity and Intercommunication in the Mouse Heart. *Cell Rep.* 2018;22(3):600–610.
12. Schaum N et al. Single-cell transcriptomics of 20 mouse organs creates a Tabula Muris. *Nature* 2018;562:367–372.
13. Naito AT et al. Complement C1q activates canonical Wnt signaling and promotes aging-related phenotypes. *Cell* 2012;149(6):1298–1313.
14. La Manno G et al. RNA velocity of single cells. *Nature* 2018;560(7719):494–498.
15. Dejana E, Hirschi KK, Simons M. The molecular basis of endothelial cell plasticity. *Nat. Commun.* 2017;8:14361.
16. Albig AR, Neil JR, Schiemann WP. Fibulins 3 and 5 antagonize tumor angiogenesis in vivo. *Cancer Res.* 2006;66(5):2621–2629.
17. Law RHP et al. An overview of the serpin superfamily. *Genome Biol.* 2006;7(5):216.

18. Vion A-C et al. Autophagy is required for endothelial cell alignment and atheroprotection under physiological blood flow. *Proc. Natl. Acad. Sci.* 2017;114(41):E8675–E8684.
19. Torisu K et al. Intact endothelial autophagy is required to maintain vascular lipid homeostasis. *Aging Cell* 2016;15(1):187–191.
20. Pillai ICL et al. Cardiac Fibroblasts Adopt Osteogenic Fates and Can Be Targeted to Attenuate Pathological Heart Calcification. *Cell Stem Cell* 2017;20(2):218–232.
21. Martinez-Jimenez CP et al. Aging increases cell-to-cell transcriptional variability upon immune stimulation. *Science* 2017;355(6332):1433–1436.
22. Trial J, Heredia CP, Taffet GE, Entman ML, Cieslik KA. Dissecting the role of myeloid and mesenchymal fibroblasts in age-dependent cardiac fibrosis. *Basic Res. Cardiol.* 2017;112(4):34.
23. Fleenor BS, Marshall KD, Rippe C, Seals DR. Replicative aging induces endothelial to mesenchymal transition in human aortic endothelial cells: potential role of inflammation. *J. Vasc. Res.* 2012;49(1):59–64.
24. Fu X et al. Specialized fibroblast differentiated states underlie scar formation in the infarcted mouse heart. *J. Clin. Invest.* 2018;128(5):2127–2143.
25. Vaughan DE, Rai R, Khan SS, Eren M, Ghosh AK. Plasminogen Activator Inhibitor-1 Is a Marker and a Mediator of Senescence. *Arterioscler. Thromb. Vasc. Biol.* 2017;37(8):1446–1452.
26. Khan SS et al. A null mutation in SERPINE1 protects against biological aging in humans. *Sci. Adv.* 2017;3(11):1617.
27. Rabieian R et al. Plasminogen Activator Inhibitor Type-1 as a Regulator of Fibrosis. *J. Cell. Biochem.* 2018;119(1):17–27.
28. Salzer MC et al. Identity Noise and Adipogenic Traits Characterize Dermal Fibroblast Aging. *Cell* 2018;175(6):1575–1590.
29. Farbehi N et al. Single-cell expression profiling reveals dynamic flux of cardiac stromal, vascular and immune cells in health and injury. *Elife* 2019;8.
30. Krishnaswami SR et al. Using single nuclei for RNA-seq to capture the transcriptome of postmortem neurons. *Nat. Protoc.* 2016;11:499.
31. Scialdone A et al. Computational assignment of cell-cycle stage from single-cell transcriptome data. *Methods* 2015;85:54–61.
32. Butler A, Hoffman P, Smibert P, Papalexi E, Satija R. Integrating single-cell transcriptomic data across different conditions, technologies, and species. *Nat. Biotechnol.* 2018;36:411–420.
33. Love MI, Huber W, Anders S. Moderated estimation of fold change and dispersion for RNA-seq data with DESeq2. *Genome Biol.* 2014;15(12):550.
34. Ignatiadis N, Klaus B, Zaugg JB, Huber W. Data-driven hypothesis weighting increases detection power in genome-scale multiple testing. *Nat. Methods* 2016;13:577.

35. Langfelder P, Horvath S. WGCNA: an R package for weighted correlation network analysis. *BMC Bioinformatics* 2008;9(1):559.
36. Trapnell C et al. The dynamics and regulators of cell fate decisions are revealed by pseudotemporal ordering of single cells. *Nat. Biotechnol.* 2014;32(4):381–386.
37. Guo M, Bao EL, Wagner M, Whitsett JA, Xu Y. SLICE: Determining cell differentiation and lineage based on single cell entropy. *Nucleic Acids Res.* 2017;45(7):e54.
38. Ramilowski JA et al. A draft network of ligand–receptor-mediated multicellular signalling in human. *Nat. Commun.* 2015;6:7866.
39. Roth A et al. The STRING database in 2017: quality-controlled protein–protein association networks, made broadly accessible. *Nucleic Acids Res.* 2016;45(D1):D362–D368.
40. Dobin A et al. STAR: Ultrafast universal RNA-seq aligner. *Bioinformatics* 2013;29(1):15–21.
41. Liao Y, Smyth GK, Shi W. FeatureCounts: An efficient general purpose program for assigning sequence reads to genomic features. *Bioinformatics* 2014;30(7):923–930.
42. Wagner JUG et al. Switch in Laminin β 2 to Laminin β 1 Isoforms During Aging Controls Endothelial Cell Functions—Brief Report/Highlights. *Arterioscler. Thromb. Vasc. Biol.* 2018;38(5):1170–1177.

9.5 Appendix 4

Dissection of heterocellular cross-talk in vascularized cardiac tissue mimetics

Julian Uwe Gabriel Wagner^{1,4,*}, Minh Duc Pham^{1,7,*}, Luka Nicin^{1,*}, Marie Hammer¹, Katharina Bottermann¹, Ting Yuan¹, Rahul Sharma^{1,7}, David John¹, Marion Muhly-Reinholz¹, Lukas Tombor¹, Martin Hardt², Josef Madl³, Stefanie Dimmeler^{1,5,6,#}, Jaya Krishnan^{1,6,7,#}

¹Institute for Cardiovascular Regeneration, Goethe University Frankfurt, Germany

²Imaging Unit, Justus-Liebig University Giessen, Germany

³Institute for Experimental Cardiovascular Medicine, University Heart Center Freiburg · Bad Krozingen, and Faculty of Medicine, University of Freiburg, Germany

⁴Faculty for Biological Sciences, Goethe University; Frankfurt; Germany

⁵German Center for Cardiovascular Research DZHK, Berlin, Germany

⁶Cardiopulmonary Institute, Frankfurt, Germany

⁷Genome Biologics, Frankfurt, Germany

*contributed equally; #contributed equally

Address of corresponding author:

Jaya Krishnan

Institute of Cardiovascular Regeneration, Centre for Molecular Medicine

Building 25B, Rm. 550, Goethe-University Frankfurt,

Theodor-Stern-Kai 7, 60590 Frankfurt am Main, Germany

krishnan@med.uni-frankfurt.de, +49 (0) 69 / 6301-87949

Short title: Heterocellular cross-talk in cardiac mimetics

Abstract

Cellular specialization and interaction with other cell types in cardiac tissue is essential for the coordinated function of cell populations in the heart. The complex interplay between cardiomyocytes, endothelial cells and fibroblasts is necessary for adaptation but can also lead to pathophysiological remodeling. To understand this complex interplay, we developed 3D vascularized cardiac tissue mimetics (CTM) to study heterocellular cross-talk in hypertrophic, hypoxic and fibrogenic environments. This 3D platform responds to physiologic and pathologic stressors and mimics the microenvironment of diseased tissue. In combination with endothelial cell fluorescence reporters, these cardiac tissue mimetics can be used to precisely visualize and quantify cellular and functional responses upon stress stimulation.

Utilizing this platform, we demonstrate that stimulation of α/β -adrenergic receptors with phenylephrine (PE) promotes cardiomyocyte hypertrophy, metabolic maturation and vascularization of CTMs. Increased vascularization was promoted by conditioned medium of PE-stimulated cardiomyocytes and blocked by inhibiting VEGF or upon β -adrenergic receptor antagonist treatment, demonstrating cardiomyocyte-endothelial cross-talk. Pathophysiological stressors such as severe hypoxia reduced angiogenic sprouting and increased cell death, while TGF β 2 stimulation increased collagen deposition concomitant to endothelial-to-mesenchymal transition. In sum, we have developed a cardiac 3D culture system that reflects native cardiac tissue function, metabolism and morphology - and for the first time enables the tracking and analysis of cardiac vascularization dynamics in physiology and pathology.

Keywords: cardiac 3D culture; intercellular cross-talk; EndMT

Introduction

The heart comprises of several different cell types including cardiomyocytes (CM), endothelial cells (EC) and fibroblasts (FB), which closely interact during tissue homeostasis and in pathophysiological conditions [1, 2]. In spite of this, *in vitro* models largely rely on 2D CM monocultures for disease modeling and drug screening [3]. However, 2D monocultures lack cellular maturity and cannot accurately mimic native tissue response to pharmacological agents [4]. To circumvent these issues, 3D CM culture methods have been developed. While an improvement over 2D cultures, 3D CM monocultures do not recapitulate the inter-cellular cross-talk between CMs, FBs and EC that is typical of the native myocardium [1, 2]. This is particularly striking considering FBs and ECs make up 70-80% of the heart by cell number [5, 6]. Thus, studying the response of 3D CM monocultures to pathologic stress or drug stimuli ignores the interaction and impact of resident cardiac FBs and ECs. For example, pathologic stimuli are shown to induce adaptive growth of ECs to satisfy the increased oxygen demands of the enlarged heart, and inhibition or impairment of this adaptive pro-angiogenic mechanism results in heart failure [7, 8]. Mechanistically, the adaptive response of ECs in pathology has been shown to occur in part in response to secretion of pro-angiogenic factors such as the vascular endothelial growth factor (VEGF) [9], angiopoietins [10, 11], pro-angiogenic extracellular vesicles [12] and nitric oxide [13] secreted by CMs. In turn, ECs and blood vessels, initially thought being exclusively responsible for providing oxygen to the tissue, release a variety of “angiocrine” cytokines and matrix proteins to control CM growth, regeneration and fibrosis in various organs [14-16]. Hence, communication between ECs and CMs is bi-directional [17].

In vitro 3D models that accurately recapitulate this complex heterocellular interplay are necessary to bridge the gap between existing *in vitro* and *in vivo* models. Several groups have generated cardiac 3D tissue constructs using various types of biodegradable matrixes, scaffolds and different types of strategies to form such constructs [18-20]. The addition of cultured primary or stem cell-derived ECs has also led to reports of vascularized 3D tissues [21-27]. However, due to the lack of vascular network development, EC maturation and fibroblasts in these models, they provide limited insight into the dynamics and heterocellular interplay of the angiogenic response to physiologic or pathologic stimuli. Thus, 3D cardiac tissue models that attempt to mimic heterocellular interactions under pathophysiological conditions are sparse and largely fail to accurately mimic native tissue cellular composition, morphology, metabolism and function, and stress response [28].

Here, we used a 3D cardiac triculture approach to study heterocellular cross-talk in the context of physiologic and pathophysiologic (hypoxia, pro-fibrotic/-inflammatory) stimulation. These cardiac tissue mimetics (CTMs) comprise of CMs, ECs and FBs and display cellular maturation and well-developed tissue vascularization. CTMs generated using our methodology respond to cardiac stressors and display changes in metabolism, growth and vascularization resembling, in part, native tissue response. In this setting, we further explored the intercellular cross-talk between CM, EC and FB evoked by pathophysiologic stimuli. Taken together, our studies demonstrate the utility of CTMs as a robust *in vitro* model for heterocellular cross-talk studies in the settings of myocardial tissue homeostasis and disease, including studies of drug cardiotoxicity.

Materials and Methods

Cell isolation

Mated female Sprague Dawley rats were obtained from Charles River (Sulzfeld, Germany) and Janvier (Le Genest Saint-Isle, France). Rats were sacrificed by cervical dislocation and hearts were obtained from P1 and P2 rat pups. The obtained hearts were then transferred into Hank's buffered saline solution (-Ca²⁺/-Mg²⁺) containing 0.2% 2,3-Butanedione monoxime (short BDM; Sigma-Aldrich; B0753-25G) and were cut into small pieces. Tissue dissociation was performed in 5 mL of a commercially available enzyme mix (Neonatal Heart Dissociation Kit, mouse and rat by Miltenyi Biotec GmbH). To dissociate the solid heart tissue, genteMACS™ Dissociator (Miltenyi Biotec GmbH) with the pre-programmed program m_neoheart_01_01 was used after four times 15 minutes of digestion at 37°C. Cardiomyocytes and fibroblasts of the digested heart suspension were pelleted by centrifugation (80x g, 5 minutes), resuspended in plating medium (DMEM high glucose, M199 EBS (both without L-Glutamine by BioConcept), 10% horse serum, 5% fetal calf serum, 2% L-glutamine and penicillin/streptomycin) and plated for 1 hour and 40 minutes in 6 cm cell culture dishes (Greiner Bio-One GmbH) at 37°C and 5% CO₂ at humidified atmosphere [29, 30]. The fact that fibroblasts are able to attach to uncoated culture dishes, allowed taking cardiomyocytes from the culture supernatant while fibroblasts attached to the culture dish.

Cell culture

Human umbilical vein endothelial cells (HUVEC) were purchased from Lonza and cultured with endothelial basal medium (EBM, Lonza) supplemented with 10% fetal calf serum (FCS; Invitrogen), Amphotericin-B, ascorbic acid, bovine brain extract (BBE), endothelial growth factor (EGF), gentamycin sulphate and hydrocortisone (EGM-singleQuotes, Lonza) at 37°C and 5% CO₂, at humidified atmosphere.

HEK293T cells were cultured with DMEM high glucose GlutaMAX (Invitrogen) supplemented with 10% FCS (Invitrogen) and penicillin / streptomycin (Roche) at 37°C and 5% CO₂, at humidified atmosphere. Isolated cardiac rat fibroblasts and cardiomyocytes were cultured with maintenance medium (DMEM high glucose, M199 EBS (both without L-Glutamine by BioConcept), 1% horse serum, 2% L-glutamine and penicillin/streptomycin) at 37°C and 5% CO₂ at a humidified atmosphere. Before culturing cardiomyocytes, cell culture dishes had been coated with collagen (AdvanceMatrix; 5005-100ML) for 10 minutes at 37°C. Cell detachment was performed with 0.25% trypsin (Life Technologies), which was incubated for 2 minutes at 37°C and 5% CO₂ and neutralised with fully supplemented EBM medium or plating medium. The cell number was determined using the cell counter NucleoCounter (ChemoMetec), as described in the manufacturer's protocol or by using Neubauer improved hemocytometer (Peqlab).

Lentiviral GFP expression

Lentiviral particles were generated by transfecting HEK293T cells with the packing plasmids pCMVΔR8.91 and pMD2.G as well as the plasmid SEW carrying the GFP-ORF. To generate the SM22α-GFP reporter virus, a SEW plasmid carrying an SM22α-GFP-ORF was used as previously described [31]. In brief, HEK293T cells were cultured in a T175 flask (Greiner Bio-One GmbH)

until reaching a confluence of 70%. A transfection mix of 100 μ L Opti-MEM (Life Technologies GmbH) containing 6 μ g of pCMV Δ R8.91, 2 μ g of pMD2.G and 8 μ g of SEW was prepared that pre-incubated for 20 minutes at room temperature before adding to the HEK293T culture. After 4 days of culturing, culture supernatant was cleared from cellular debris by centrifugation (500x g, 5 minutes, 4°C) and concentrated 40x using the Amicon Ultra-15 centrifugal units 100 KD (4 times, 2500x g, 30 minutes, 4°C) by Millipore (UCF910024). For GFP expression, 300,000 HUVECs were seeded in a T25 flask (Greiner Bio-One GmbH) and virus-containing supernatants were titrated on HUVECs for 24 hours to determine the titres needed to transduce >95% of the cells. After 7 days of culturing, GFP expression was confirmed by fluorescence microscopy.

CTM formation

Primary rat cardiomyocytes (CM), cardiac rat fibroblasts (FB) and HUVEC were used for CTM formation. In brief, droplets of 30 μ L plating medium containing 32,000 CMs and 6,400 FBs were cultured as hanging drops at 37°C and 5% CO₂ at humidified atmosphere to form cardiac spheroids. After 4 days, cardiac spheroids were collected and coated in plating medium supplemented with either no additional matrix proteins, 1:500 fibronectin (Sigma-Aldrich; F0895) or 1:10 growth factor reduced matrigel (Corning; 356230) for 1 hour at 4°C. The coated spheroids were then singularized in 96-well plates (ultra-low attachment U-bottom plate by Corning; 7007) with 50 μ L plating medium per well. At least 4 hours after spotting, 10,000 HUVECs in 50 μ L fully supplemented EBM were added to each well. HUVECs were allowed for 24 hours to attach to the cardiac spheroids (spheroids containing CM, FB and HUVEC are referred as CTMs from here after) and medium was changed to maintenance medium containing fully supplemented EBM (50%:50%) containing either no treatment, 200 μ M phenylephrine (short PE; Sigma-Aldrich; P6126-5G), PE + 0.1% DMSO, PE + 1 μ M propranolol (Sigma-Aldrich; P0884-5G), PE + 50 μ M metoprolol (Sigma-Aldrich; 80337-100MG), PE + 100 nM ICI 118.551 (Sigma-Aldrich; I127-5MG) or PE + 1:50 neutralizing VEGF antibody (R&D Systems; AF564). CTMs were cultured for 10 days by refreshing the medium with the respective stimulus (no stimulus, PE, antibodies or β -blockers) every second day. Vascularisation was determined using the Leica TCS SP8 confocal microscope and the LAS X software by measuring the accumulated HUVEC-sprout length, mean HUVEC-sprout thickness and mean number of branch points within the vascular network.

Contractility measurement

Spontaneous CTM contraction: Spontaneous CTM contraction was determined by counting the number of beats per minute of at least 6 CTMs per condition using a computer-assisted microscope using Axiovision 4.5 (Zeiss).

Paced CTMs: For pacing experiment, every single CTM was transferred into a 35/10 mm cell culture dish (Greiner Bio-One) and incubated at 37°C and 5% CO₂ for 30 min. The CTM was then electrically paced at 1 Hz and 15 V with a Myopacer field stimulator (IonOptix). Changes in cell dimension which were observed using the Myocyte Calcium and Contractility system (IonOptix) were taken as readouts for contractility measurements. In brief, high speed digital imaging was performed with MyoCam-S to record CTM shortening. Units/pixels were determined by calibrating the system with a micrometer. The IonOptix CTM spacing algorithm

was used to record CTM shortening and connected to Fast Fourier Transformation (FFT) to determine the average CTM movement edge spacing of the region of interest in one or more lines of a video image.

Size measurement

CTM size: CTM diameter was measured after 10 days of culturing using a computer-assisted bright field microscope with the Axiovision 4.5 software (Zeiss).

Cardiomyocyte size: Cryo-sections of CTMs were stained with DAPI, anti- α -Actinin and Alexa Flour conjugate of Wheat-Germ-Agglutinin (WGA). Surface area quantification was performed using ImageJ (Fiji). 100-150 cells of each condition, exhibiting clear α -actinin signal and distinct cell boundary demarcation as marked by Wheat Germ Agglutinin (WGA) staining, were manually selected and outlined using the Wacom freehand tool. Marked areas were then quantified by ImageJ.

Seahorse assay

The Agilent Seahorse XFe96 spheroid microplate was coated with Poly-D Lysine 100 $\mu\text{g}/\text{mL}$ following the manual instruction. 1X KHB medium (111 mM NaCl, 4.7 mM KCl, 2 mM MgSO_4 , 1.2 mM Na_2HPO_4 , 2.5 mM D-Glucose, 0.5 mM carnitine) supplemented with 6 mM D-Glucose was prepared prior the experiment. CTMs were washed twice with KHB medium and every single CTM was then transferred directly into each well of XFe96 spheroid microplate containing 175 μL of KHB medium. CTMs were centered into the micro-chamber and incubated at 37°C in non- CO_2 incubator for 1 hour. The Seahorse XF Cell Mito Stress Test was performed using sequential injection of Oligomycin (2.5 μM , Sigma, O4876), FCCP (2.0 μM , Sigma, C2920) and Antimycin A (0.5 μM , Sigma, A8674) following a 3-min-mixing and 3-min-measuring cycles for up to 3 hours. Oxygen consumption rate (OCR) and Extracellular acidification rate (ECAR) were measured and calculated using Seahorse XFe96 Analyzers (Agilent Technologies).

Fluorescence immunohistochemistry

CTMs were collected and fixed with 4% Histofix (Carl-Roth GmbH & Co. KG) for 1 hour at room temperature. Whole CTMs as well as cryo-sections of CTMs were used for fluorescence immunohistochemistry.

In case of whole mount stainings, CTMs were permeabilized with 0.2% Triton X-100 in PBS for 1 hour at room temperature followed by blocking with 5% horse serum (Sigma-Aldrich) in PBS for 30 minutes at room temperature. Primary antibodies (see Table 1) were diluted 1:200 in 5% horse serum and incubated over night at 4°C. Before using the secondary antibody (see table below), CTMs were washed three times with PBS containing 1% Tween 20 and 0.002% Triton X-100 (referred as PBT from here after) for 20 minutes at room temperature. Secondary antibodies (1:500) and DAPI (1:1000; Carl-Roth GmbH & Co. KG) were diluted in 5% horse serum together and incubated for 4 hours at room temperature in the dark. After washing CTMs again three times with PBT, CTMs were mounted with ProLong Gold Antifade Mountant (Thermo Fisher Scientific; P36934) and analysed using the Leica TCS SP8 confocal microscope.

Cryo-sections were prepared by embedding fixed spheroids in O.C.T medium (Tissue-Tek), snap-freezing them in liquid nitrogen and cutting them in 10 μm thick sections. Sections were permeabilized and blocked for one hour in 0.1% Triton X100 (in PBS + BSA). Primary antibody incubated with the sections diluted 1:50-1:100 in 1mM MgCl_2 , 1 mM CaCl_2 , 0,1 mM MnCl_2 , 1% Triton X-100 or 0.2% saponin over night at 4°C. The next day, sections were washed trice with 0.1% Triton X100/PBS or 0.2 saponin (five minutes each) and incubated with the secondary antibody diluted 1:200 in 0.1% Triton X100 or 0.2% saponin (in PBS) for one hour at room temperature in the dark. Finally, sections were washed again trice with 0.1% Triton X100 /PBS or 0.2% saponin and mounted with mounting medium containing DAPI or Hoechst 33342. Endothelial cells were stained with Isolectin B4.

In case of neonatal CM staining, cells were cultured overnight and then fixed with PFA 4% for 30 minutes at room temperature. After that cells were permeabilized with 0.2% Triton X-100 for 15 minutes at room temperature following by blocking with 5% horse serum in PBS for 15 minutes at room temperature. Primary antibodies were diluted 1:200 in 2% horse serum and incubated over night at 4°C. Cells were then washed for five time with PBS for 5 minutes at room temperature. Secondary antibodies (1:500), DAPI (1:1000) and Phalloidin (1:50) were diluted in 2% horse serum together and incubated for 2 hours at room temperature in the dark. After washing cells five times with PBS for 5 minutes, cells were mounted with ProLong Gold Antifade Mountant and analysed using an inverted fluorescence microscope (Nikon Eclipse Ti2 fluorescence microscope).

Second-harmonics generation

The second-harmonics generation imaging was performed on an upright spectral multiphoton microscope (Leica TCS SP8 DIVE, non-descanned spectral detectors, objective HC IRAPO L 25x/1.00 W) using 10 μm thick CTM sections. A 1045nm laser was used for SHG and the signal was detected with a PMT and a detection window from 517nm to 527nm. A second detection window was used to record autofluorescence for comparison (552nm to 565nm).

Sirius red staining

Sirius red staining was used to determine collagen deposition and fibrosis in CTM cryo-sections sections. In a first step, sections were washed with water and PBS (5 minutes each). In a second step, a 0.1% Picosirius Red solution was prepared by solving 0.5 g Sirius Red (Waldeck GmbH) in 500 mL picric acid (Sigma-Aldrich) that incubated with the deparaffinised sections for 1 hour. After washing two times with acidified water, the sections were dehydrated with 100% ethanol, cleared with xylene and mounted with Pertex (Medite).

Transmission electron microscopy

Mature CTMs were washed once with PBS and fixed in 4% formaldehyde in 0.1 M phosphate buffer over night at 4°C. After postfixing with 1% osmium tetroxide for 1 hour at room temperature, CTMs were washed twice with 0.1 M phosphate buffer and incubated over night at 4°C in 2% aqueous uranyl acetate (Polysciences). CTMs were washed twice with water and dehydrated in an ethanol series (30, 50, 70, 80, 90, 96, and 99% [vol/vol], 10 minutes each)

and embedded in Epon (Serva). Ultrathin sections were inspected in the transmission electron microscope (EM 912a/b; Zeiss) and images were recorded at a slight underfocus using a cooled 2,000- by 2,000-pixel slow-scan charge-coupled device (CCD) camera (SharpEye/TRS) and the iTEM package (Olympus Soft Imaging Solutions).

Generating cardiomyocyte-/fibroblast-conditioned media

To obtain cardiomyocyte- and fibroblast-conditioned medium, 200,000 isolated cardiac fibroblasts and 250,000 isolated cardiomyocytes were seeded in 24-well plates (Greiner Bio-One GmbH) and cultured with 0.5 mL of maintenance medium containing no further supplement, 200 μ M PE, PE+0.1% DMSO, PE+1 μ M propranolol, PE + 100 nM ICI 118.551 or PE+50 μ M metoprolol. After 72 hours, cell culture supernatants were centrifuged (500x g, 5 minutes) to deplete dead cells and stored at -80°C.

VEGF ELISA

The rat VEGF Quantikine ELISA kit (RRV00, R&D Systems) was used to quantify VEGF in the supernatants of cardiomyocyte monocultures.

Spheroid-based angiogenic sprouting Assay

Endothelial cell sprouting was studied by *in vitro* spheroid-based angiogenesis assays. In brief, HUVECs were trypsinized and transferred into a mixture of fully supplemented EBM and methylcellulose (80%:20%). 400 HUVEC in 100 μ L per well were distributed to a U-bottom 96-well plate (Greiner Bio-One GmbH) and cultured at 37°C and 5% CO₂ at humidified atmosphere. After 24 hours, spheroids were collected, pelleted (200x g, 3 minutes), resuspended in methylcellulose supplemented with FCS (80%:20%) and embedded in a collagen Type-I gel (Corning; 354236). HUVEC spheroids were then either cultured with fully supplemented EBM (+/- VEGF (50 ng/mL; BioLegend; 583702) or +/- PE (200 μ M)), maintenance medium or conditioned cell culture medium. After 24 hours, sprouting was determined by measuring the cumulative sprout length of ten randomly chosen spheroids using a computer-assisted microscope using Axiovision 4.5 (Zeiss).

Network Formation Assay

Vascular endothelial cell network formation assay was performed as previously described [32]. Briefly, *in vitro* network formation was performed with 2×10^4 HUVECs cultured in 100 μ L of fully supplemented EBM in 96-well plates (Greiner Bio-One GmbH) that had been coated with 100 μ L matrigel (Corning; 356234,). Network formation was determined after 24 hours by measuring the accumulated tube length in three randomly chosen microscopic fields with a computer-assisted microscope using Axiovision 4.5 (Zeiss).

RNA Isolation and quantification

CTMs, heart tissues of neonatal pups and adult rats were collected into Lysing Matrix D tubes (MP Biomedical; 6913-500) and 700 μ L of TriFast (VWR; 3010-100ML) was added. Cells and tissues were homogenized 3 times for 20s following by 5 min. pause on ice. Total RNA was purified with the Direct-zol™ RNA MicroPrep kit (Zymo Research; R2060). The RNA concentration was determined by measuring absorption at 260 nm and 280 nm with the NanoDrop®ND 2000-spectrophotometer (PeqLab).

cDNA synthesis and quantitative Polymerase chain reaction (qPCR)

cDNA was synthesized from 500 ng of total RNA with EcoDry Premix RNA to cDNA (Random Hexamers) (Clontech; 639546). qPCR was performed using 10 μ L of iTaq™ Universal SYBR® Green Supermix (Bio-Rad; 172-5124), 1 μ L of 10 μ mol/L forward and reverse primer each, 1 μ L of cDNA template and 7 μ L of H₂O in a Bio-Rad CFX96 Connect Real-Time PCR system. Primers using to quantify mRNA expression were ordered from Metabion (Table 2).

Bulk RNA Sequencing

Bulk RNA sequencing was performed as previously described [32]. In brief, RNA and library preparation integrity were verified with a BioAnalyzer 2100 (Agilent) or LabChip Gx Touch 24 (Perkin Elmer). 100-200 ng of total RNA was used as input for Truseq Stranded Total RNA Library preparation following the low sample protocol (Illumina). Sequencing was performed on the NextSeq500 instrument (Illumina) using v2 chemistry, resulting in minimum of 30M reads per library with 1x75bp single end setup. Demultiplexing and adapter removal was performed by bcl2fastq software (Illumina) and resulting raw reads were assessed for quality, adapter content and duplication rates with FastQC. Fastx_trimmer was user to trim the first 5 bp. Trimmed and filtered reads were aligned versus the Ensembl mouse genome version mm10 (GRCm38) using STAR 2.4.0a with the standard parameters [33]. The number of reads aligning to genes was counted and compared with Cifffdiff version 2.2.1 [34]. The Ensemble annotation was enriched with UniProt data (release 06.06.2014) based on Ensembl gene identifiers (Activities at the Universal Protein Resource (UniProt)).

Lactate Dehydrogenase assay

Media of CTMs were replaced completely with fresh medium 24h before performing the assays. After 24h, supernatants were collected and in maximum 50 μ L of each supernatant was used for every measurement with the Lactate Dehydrogenase Activity Kit (Sigma; MAK066). To determine enzyme activity, the absorbance at 450 nm (A_{450}) was measured with the CLARIOstar plate reader (BMG Labtech). LDH activity were calculated following the manufacturer's instruction.

Toxicity assay

CTMs that incubated with 0.2% H₂O₂ in medium for 30 minutes at 37°C served as positive control. In the second step, CTMs were washed three times with PBS, fixed with 4% Histofix (Carl-Roth GmbH & Co. KG) for 1 hour at room temperature and stained against phospho-Histone H2A.X following immunohistochemistry staining procedure (please see section *Fluorescence immunohistochemistry*).

Injury assay

CTMs (generated with GFP-HUVEC or SM22 α -GFP-HUVEC) were cultured as described in the section *CTM formation* in the presence of PE to reach full maturation. After 10 days of PE-treatment, inflammation was mimicked using culture medium with 10 ng/mL transforming growth factor β 2 (short: TGF β 2; R&D Systems; 302-B2) and PE as well as FGF-, EGF- and BBE-depleted EBM instead of fully supplemented EBM for 72 hours at 37°C and 5% CO₂. Culturing mature CTMs at 0.1 % O₂ for 72 hours was used as ischemic model. Mature CTMs that were kept in PE-supplemented medium only, were used as control condition. After culturing mature CTMs under both injury model conditions, CTM cryo-sections or whole CTMs were used for immunofluorescence staining or SHG.

Statistical Analysis

Data are represented as mean and error bars indicate standard deviation (SD). Data were assessed statistically (Shapiro-Wilk and Kolmogorov–Smirnov test) for normality and statistical power was determined for Gaussian distributed data, using two-sided, unpaired T-test for two-group comparison. For comparisons of more than two groups, multiple group ANOVA with a post hoc Bonferroni test was used. For data that were not Gaussian distributed, a Kruskal-Wallis test with a multiple group Dunn's correction was used for multiple group comparison. For comparing two groups, a Mann-Whitney test was used. n.s. = not significant; *p < 0.05; **p < 0.01; ***p < 0.001 and **** p < 0.0001.

Results

Establishment of vascularized 3D CTMs

To establish the 3D culture, cardiomyocytes (CM) and cardiac fibroblasts (FB) were isolated from neonatal rat hearts. The respective fractions were separated by pre-plating and thereafter mixed at a ratio of CM:FB 5:1. The mixed cells were left to form spheroids in hanging drops containing 32000 CMs and 6400 FBs for 4 days. The spheroids were then collected and distributed individually into wells of Ultra-low-attachment (ULA) plates. GFP-transduced human umbilical vein endothelial cells (HUVEC) were added into each well with the ratio of CM:HUVEC of 3:1 to allowing monitoring of vessel growth. The cardiac tissue mimetics (CTMs) were subsequently treated with phenylephrine (PE) every second day and harvested 10 days after for further assays. A schematic overview of the protocol is shown (**Fig. 1A**).

We assessed if CTMs respond to physiologic hypertrophic stimuli with PE, an α -adrenergic receptor agonist [35]. Indeed, stimulation with PE significantly increased CTM growth (**Fig. 1B**), CM maturation and hypertrophy as evidenced by increased sarcomeric α -actinin staining, enhanced sarcomere organization and density, and the shift towards adult-type titin isoform expression [36, 37] (**Fig. 1C-E**). Consistent with the physiologic effects of short term cardiac PE stimulation [35], a significant increase in contractile amplitude was detected in paced CTMs (**Fig. 1F**). Further, as observed in native myocardium, PE stimulation led to increased oxidation metabolism, mitochondrial function and mitochondrial density, concomitant with a reduction in glycolysis (**Fig. 1G-J, Fig. S1A and B**). These phenotypic changes in CTM adrenergic signaling response, metabolism and contractility are further reflected in the enrichment and elevated expression of these KEGG gene sets upon PE stimulation (**Fig. S2A-D**).

To ascertain that our culture conditions with PE did not cause general cell death, we stained PE treated and untreated CTMs for phosphorylated histone H2AX (γ H2AX), a DNA double strand break marker of genomic instability and apoptosis (**Fig. S3A**) [38]. In parallel, detection of extracellular lactate dehydrogenase (LDH), as a marker of necrosis [39], failed to reveal differences compared to control untreated CTMs (**Fig. S3B**). Taken together, our data demonstrates that CTMs generated with our platform are viable, functional, metabolically active and responsive to physiologic stimuli.

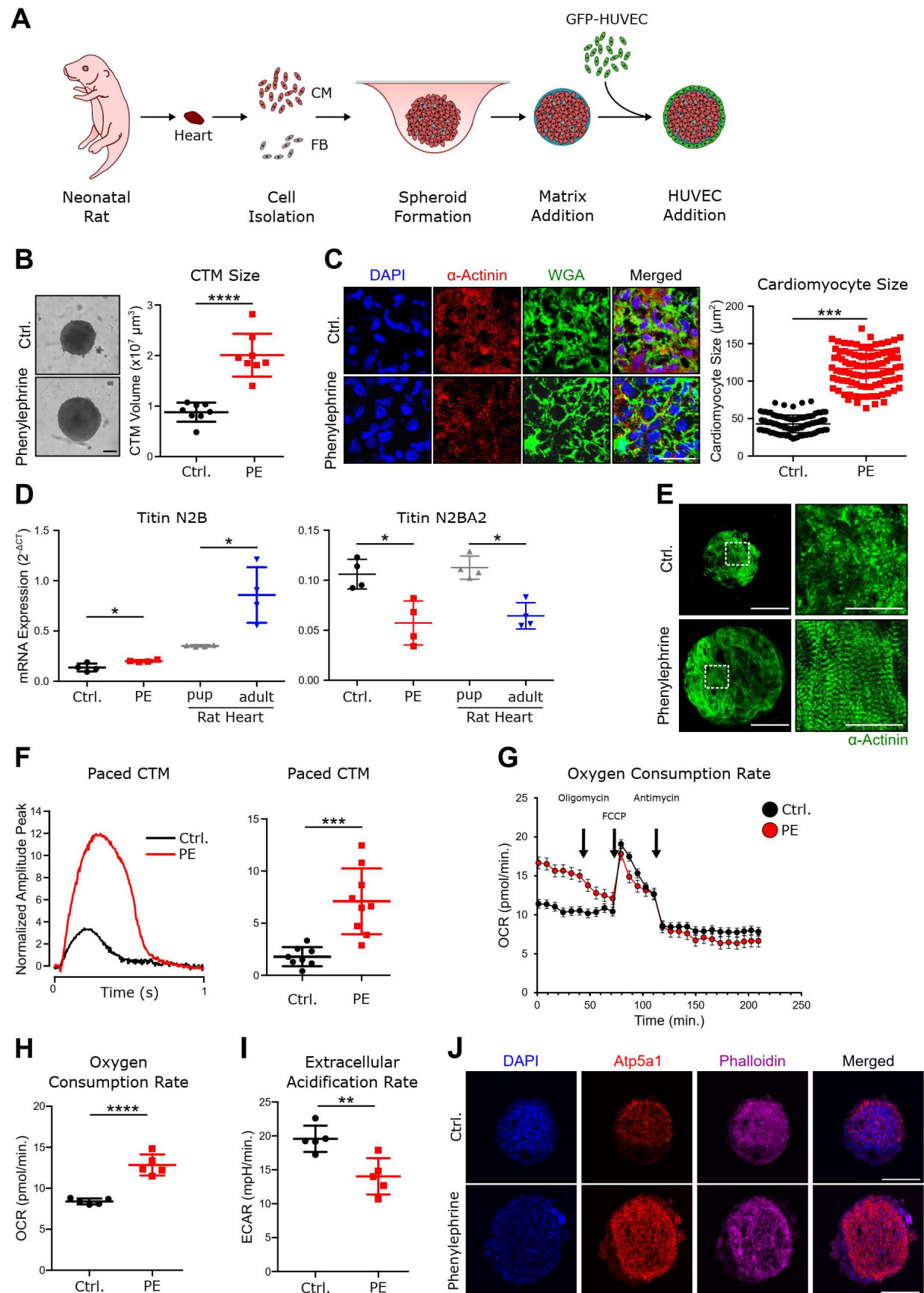


Figure 1: Establishment of a vascularized 3D CTM culture. (A) Schematic presentation of CTM formation. Cardiomyocytes (CM) and fibroblasts (FB) were isolated from neonatal rat hearts and cultured in hanging drops to allow spheroid formation. After 4 days, cardiac spheroids were

harvested, matrix proteins were added to optimize cells adhesion and human umbilical vein endothelial cells (HUVEC) that had been transduced with green fluorescence protein (GFP) were seeded on top of the cardiac spheroid. CTMs were cultured for 10 days. **(B)** Size of CTMs without treatment (control, Ctrl.) or treated for 10 days with 200 μ M phenylephrine (PE). CTM size is shown as volume (scale bar = 100 μ m; n = 8). **(C)** Size of CM within CTMs cultured for 10 days under no PE or PE. CM were stained with WGA (green) and α -actinin (red). Nuclei were stained with DAPI (blue). Scale bar = 20 μ m (n = 100 cells per condition). **(D)** mRNA expression of Titin N2B and N2BA2 in control and PE-treated CTMs, as well as in whole hearts from postnatal (pup) and adult rats (n = 4). **(E)** Immunofluorescence imaging of CTMs cultured for 10 days with no PE (Ctrl.) or PE. Cardiomyocyte maturation was monitored by striation formation seen by α -actinin staining (green). Scale bar = 100 μ m and 30 μ m. **(F)** CTM contractility upon electric pacing with 1 Hz. Contractility was determined by determining the amplitude peak of contracting CTMs (8 control vs. 9 PE-treated CTMs were used). One representative normalized amplitude trace per condition is shown on the right site. **(G, H)** Assessment of oxygen consumption rate (OCR) as a measure of glucose oxidation in CTMs treated with oligomycin, carbonyl cyanide-4 (trifluoromethoxy)-phenylhydrazone (FCCP) and antimycin as indicated. Depicted are rates expressed as OCR. (*P < 0.05 compared to control treated CTMs, paired t-test). **(I)** Assessment of basal extracellular acidification rate (ECAR) as a measure of glycolysis in CTMs treated as indicated (n = 5). **(J)** To study if phenylephrine has a toxic effect on mitochondrial density, mature control vs. PE CTMs were stained against Atp5a1 (red). Nuclei were stained with DAPI (blue) and cytoskeletal with phalloidin (magenta). A representative image is shown (scale bar = 100 μ m). Data are shown as mean \pm SD. Statistical power was determined using the unpaired, two-sided T-test (B, C, F, G, H and I) and the nonparametric Mann-Whitney test (D), indicated as follows: *p < 0.05, **p < 0.01, ***p < 0.001 and ****p < 0.0001.

PE stimulation augments vascularization of CTMs

Consistent with previous reports of increased capillary density after *in vivo* PE stimulation [40, 41], treatment of CTMs with PE led to significantly augmented vascularization, increased tube length, branch points and tube thickness (**Fig. 2A, B, Fig. S4A**). Furthermore, indicative of active neoangiogenesis, more filopodia were detected in PE-stimulated CTMs (**Fig. 2A**). To determine if increased vascularization was mediated by direct action of PE on the ECs, we generated 3D monocultures of HUVECs and treated these spheroids with an identical concentration of PE. Surprisingly, PE stimulation did not impact EC spheroid sprouting, while stimulation with the pro-angiogenic Vascular endothelial growth factor (VEGF) as positive control, significantly increased vascular network growth and branching (**Fig. 2C**). These data suggest that increased vascularization induced by PE in the 3D triculture CTM is likely a consequence of cross-talk between cells contained within the CTM (**Fig. 2D**), and not due to direct function of PE on ECs. To test this hypothesis, we collected conditioned medium of cardiac CMs or FBs monocultures and applied them to HUVEC spheroids (**Fig. 2E, Fig. S4B and C**). CM-conditioned and FB-conditioned medium displayed a tendency for increased EC sprout formation at baseline by about 1.5 (CM) and 3-fold (FB), but the difference failed to achieve statistical significance (**Fig. 2E, Fig. S4C**). However, additional stimulation of CM cultures with PE prior to conditioned medium collection did significantly increase the capacity for EC growth and sprouting (**Fig. 2E**), whereas no effect was observed from conditioned medium of PE stimulated FB (**Fig. S4C**). As pro-hypertrophic stimulation of CMs has been shown to induce VEGF release and can mediate an adaptive response of ECs [41], we tested the contribution of VEGF by adding neutralizing antibodies to the CM-conditioned medium. Indeed, neutralizing VEGF antibodies reduced the pro-angiogenic effects of conditioned medium from PE-stimulated CMs (**Fig. 2F**). Consistent with this finding, treatment of 3D CTMs with neutralizing VEGF antibodies also significantly reduced vascularization (**Fig. 2G**). These data suggest that our *in vitro* 3D CTM model recapitulates previous *in vivo* studies demonstrating a cross-talk between CMs and ECs via VEGF [12, 42]. This hypothesis is further strengthened

as levels of VEGF were found to be increased in culture supernatants of PE stimulated CM monocultures compared to untreated CMs cultures (**Fig. S4D**).

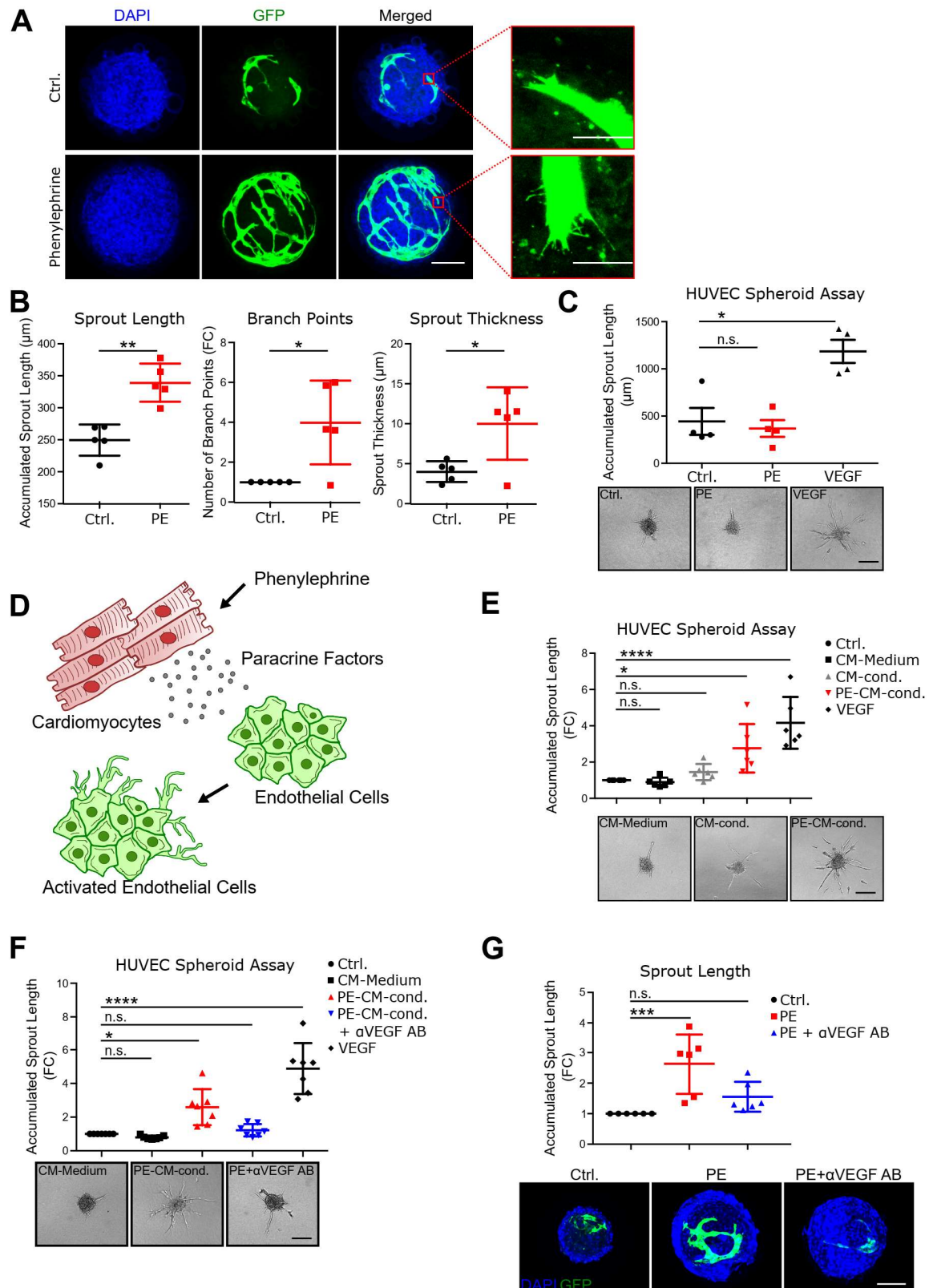


Figure 2: Phenylephrine induces CTM sprouting via paracrine signaling. (A-B) In comparison to control (Ctrl.) conditions, 200 μ M phenylephrine (PE) treatment for 10 days induces

angiogenesis (scale bar = 100 μm) and filopodia (scale bar = 12.5 μm) formation (A) as assessed by determining the accumulated sprout length, number of branch points and tube thickness in control vs. PE treated CTMs (B, n = 5) using the Leica TCS SP8 confocal microscope and the LAS X software. (C) To see if PE is influencing vessel growth directly, a spheroid-based angiogenic sprouting assay was performed using approx. 400 HU-VEC per spheroid. HUVEC spheroids were embedded in a collagen matrix and treated with no stimulus (Ctrl.), 200 μM PE or 50 ng/mL vascular endothelial growth factor (VEGF) for 24 hours. Sprouting was determined by measuring the cumulative sprout length of ten randomly chosen spheroids using a computer-assisted microscope using Axiovision 4.5 (Zeiss) (scale bar = 100 μm ; n = 4). (D) A schematic presentation is used to illustrate the hypothesis that phenylephrine stimulates cardiomyocytes to secrete pro-angiogenic factors that activate the neighboring endothelial cells. (E) To assess whether PE-treated cardiomyocytes secrete pro-angiogenic factors, a further HUVEC spheroid-based angiogenic sprouting assay was performed by stimulating the HUVEC spheroids with blank maintenance medium, 50 ng/mL VEGF or cell culture supernatants of neonatal rat cardiomyocytes that were treated either with no PE or PE for 72 hours. Each treatment was applied for 24 hours before determining sprouting using a computer-assisted microscope using Axiovision 4.5 (Zeiss) (scale bar = 100 μm ; n = 6). (F) The role of secreted VEGF was analyzed using a HUVEC spheroid-based angiogenic sprouting assay by stimulating spheroids with blank maintenance medium, 50 ng/mL VEGF, cell culture supernatants of neonatal rat cardiomyocytes that were treated with PE for 72 hours or cell culture supernatants of PE-treated neonatal rat cardiomyocytes that were supplemented with neutralizing anti-VEGF antibody (1:50, R&D Systems) before treating the HUVEC spheroids. Sprouting was determined by measuring the cumulative sprout length of ten randomly chosen spheroids using a computer-assisted microscope using Axiovision 4.5 (Zeiss) (scale bar = 100 μm ; n = 7). (G) To assess the role of VEGF also in the CTM system, CTMs were cultured for 10 days after HUVEC addition without PE, with 200 μM PE or with 200 μM PE + 1:50 neutralizing anti-VEGF antibodies (R&D Systems). Sprout length (GFP) was quantified using the Leica TCS SP8 confocal microscope and the LAS X software (scale bar = 100 μm ; n = 6). Data are shown as mean \pm SD. Statistical analysis was performed using the unpaired, two-sided T-test (B). For comparisons of >2 groups, multiple-group ANOVA with a post hoc Bonferroni test was used for Gaussian distributed data (E and F), for non-Gaussian distributed data, Kruskal-Wallis test with a Dunn's correction was used (C and G) indicated as follows: n.s. = not significant; * P <0.05; ** P <0.01; *** P <0.001 and **** P <0.0001.

β -receptor antagonist reduce PE-stimulated vascularization

As PE stimulation was observed to augment CTMs contraction (**Fig. 1F**), we asked if PE-induced mechanical activation of ECs could also contribute to the increase in CTM vascularization. To uncouple the contribution of contractile activation on angiogenesis, we incubated CTMs with the β -adrenergic receptor antagonists propranolol and metoprolol to inhibit CTM contraction [43, 44]. Propranolol and metoprolol reduced the frequency of CTM contraction (**Fig. 3A**), whereas propranolol additionally diminished PE-induced hypertrophic growth (**Fig. S5A**). Importantly, inhibition of CTM contraction significantly reduced PE-induced vascularization (**Fig. 3B, Fig. S5B**). As previous studies have reported a direct effect of β -adrenergic receptor antagonists on EC growth and vascular network expansion [40, 45, 46], we treated HUVEC monocultures in a network formation assay with propranolol and metoprolol. However, despite repeated attempts, we could not detect a direct impact of propranolol and metoprolol on EC network formation and growth (**Fig. 3C**). Finally, we cultured CM monocultures with PE and a combination of PE with propranolol or metoprolol. Collected supernatants were used as stimulus for HUVEC spheroids to exclude β -blocker induced secretomic changes. Interestingly, we found no significant alterations on endothelial sprouting, indicating the role of mechanical stress induced angiogenesis (**Fig. 3D**).

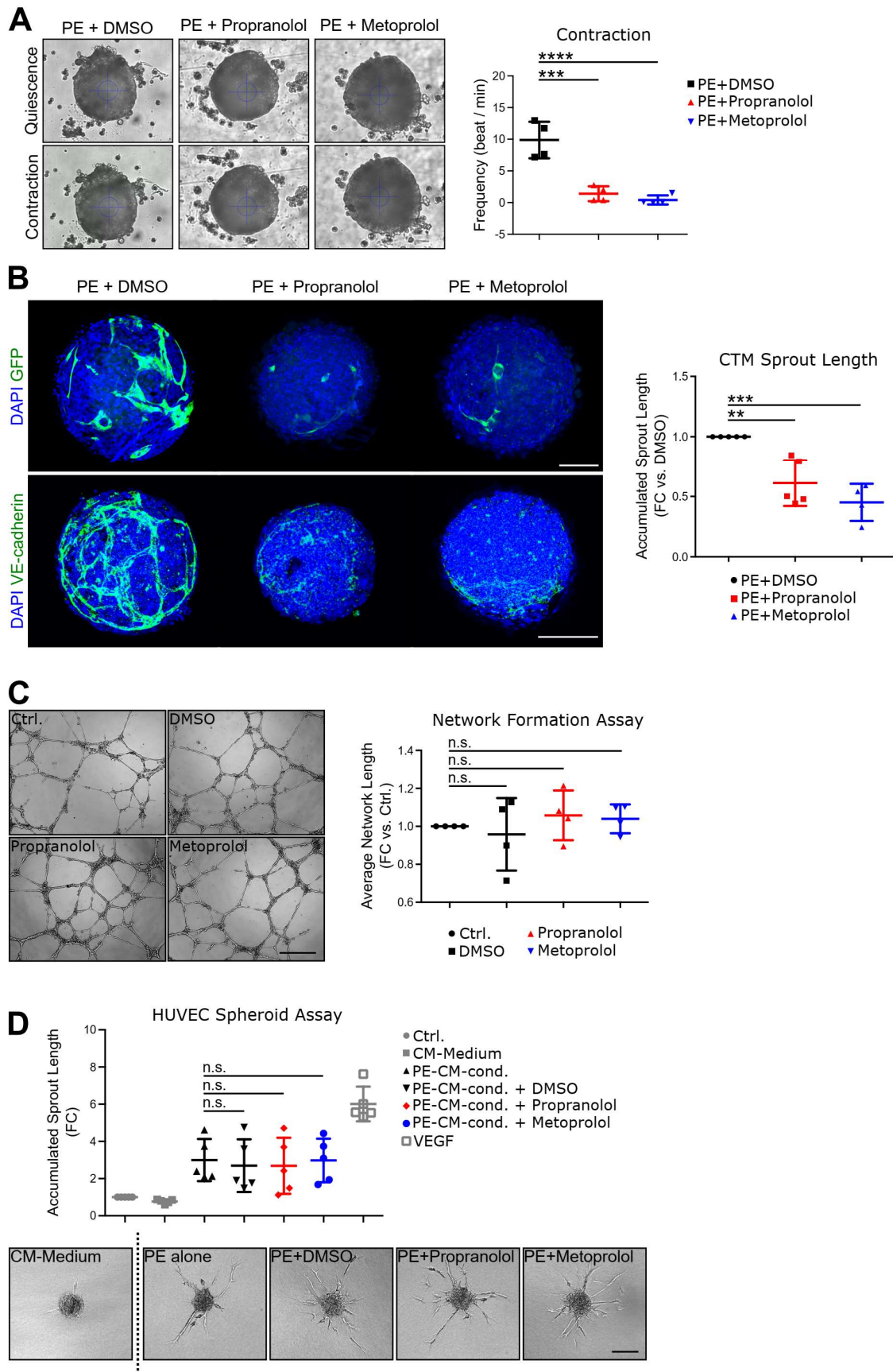


Figure 3: CTM contraction increases angiogenic sprouting. (A, B) To decrease beating, CTMs were cultured for 10 days in 200 μ M PE together with 1 μ M of the β -blocker propranolol, 50 μ M of the β -blocker metoprolol or 0.1% DMSO only (as solvent). propranolol and metoprolol both

significantly decreased CTM contraction as determined by counting beats per minute (A). 12 CTMs per condition were used for contractility measurements and representative images of quiescent and contracting CTMs are shown ($n = 5$). VE-cadherin staining (green; bottom) as well as the use of GFP-labeled HUVEC (green; top) in PE-treated CTMs under 0.1% DMSO (control), 1 μ M propranolol or 50 μ M metoprolol showed a significant decrease in angiogenic sprouting upon both β -blocker stimulations compared to DMSO (scale bar = 100 μ m; B) as quantified by using the Leica TCS SP8 confocal microscope and the LAS X software ($n = 5$ for PE+propranolol and PE+DMSO and $n = 4$ for PE+metoprolol). (C) A network formation assay was used to show that both β -blockers have no direct effect on HUVEC network formation. HUVEC were cultured for 24 hours on Matrigel in the presence of fully supplemented EBM (Ctrl.), 0.1% DMSO, 1 μ M propranolol or 50 μ M metoprolol. Quantification of the accumulated tube length showed no differences among the four conditions (scale bar = 200 μ m; $n = 4$). (D) To exclude secretomic changes in the β -blocker treated CTMs, neonatal rat cardiomyocytes were cultured for 72 hours with 200 μ M PE + 0.1% DMSO (served as solvent), 1 μ M propranolol, 50 μ M metoprolol or with no further supplement. A HUVEC spheroid-based angiogenesis assay was used with approx. 400 HUVEC per spheroid. The HUVEC spheroids incubated with 100 μ L of each cardiomyocyte supernatant, fully supplemented EBM, maintenance medium or 50 ng/mL VEGF for 24 hours. Sprouting was determined by measuring the cumulative sprout lengths of ten randomly chosen spheroids using a computer-assisted microscope using Axiovision 4.5 (Zeiss) (scale bar = 100 μ m; $n = 5$). Data are shown as mean \pm SD. Statistical analysis was performed using multiple-group ANOVA with a post hoc Bonferroni test for Gaussian distributed data (A, B and D), for non-Gaussian distributed data, a Kruskal-Wallis test with a Dunn's correction was used (D), indicated as follows: n.s. = not significant; ** $P < 0.01$ and *** $P < 0.001$.

Pathophysiological stressors interfere with cellular cross-talk in 3D CTMs

Next, we assessed whether 3D CTMs may be used as models to study stress related changes in cellular cross-talk. Therefore, we used transforming growth factor β 2 (TGF β 2), an established inducer of endothelial-mesenchymal transition (EndMT) and cardiac fibrosis, and hypoxia (0.1%) as a model of severe ischemia, both in combination with PE. The two stimuli were applied on mature CTMs (after 10 days of PE treatment) for 3 days.

TGF β 2 led to a slightly increased CTM vascularization (**Fig. 4A and B**). Vimentin fluorescence staining of mature CTMs in the presence or absence of TGF β 2 revealed evidence of cardiac fibroblast activation (**Fig. 4C**) as well as induced collagen deposition as visualized by second-harmonics generation (SHG) [47] and Sirius Red staining (**Fig. 4D-F**). Since TGF β 2 is a well-known EndMT inducer, we screened CTM cross-sections for ECs that were positive for vimentin, a commonly used FB marker [47]. Interestingly, we did find single ECs expressing vimentin but also SM22 α and collagen III suggesting that EndMT is occurring in pro-inflammatory CTMs (**Fig. 4G, Fig. S6A**). Furthermore, unlike TGF β 2, severe hypoxia at 1%O₂ and 0.1%O₂ significantly reduced CTM vascular network (**Fig. 4A and B, Fig. S7A and B**) and increased collagen deposition (**Fig. 4D-F**), indicating that this model accurately reflects changes observed in the native myocardium in response to severe myocardial hypoxia [48]. Finally, to ascertain that HUVECs were indeed differentiating into cells of the mesenchymal lineage, we utilized the SM22-GFP tracer reporter [31], wherein the mesenchyme lineage-specific SM22 promoter is utilized to drive expression of GFP upon promoter activation, as readout for activation of EndMT. HUVECs were transduced with the SM22-GFP reporter prior to integration into CTMs. CTMs were then stimulation with PE alone, or in combination with TGF β 2. As noted in **Fig. S6B**, SM22 promoter activation was detected specifically upon TGF β 2 stimulation, indicative of induction of EndMT in a subset of endothelial cells.

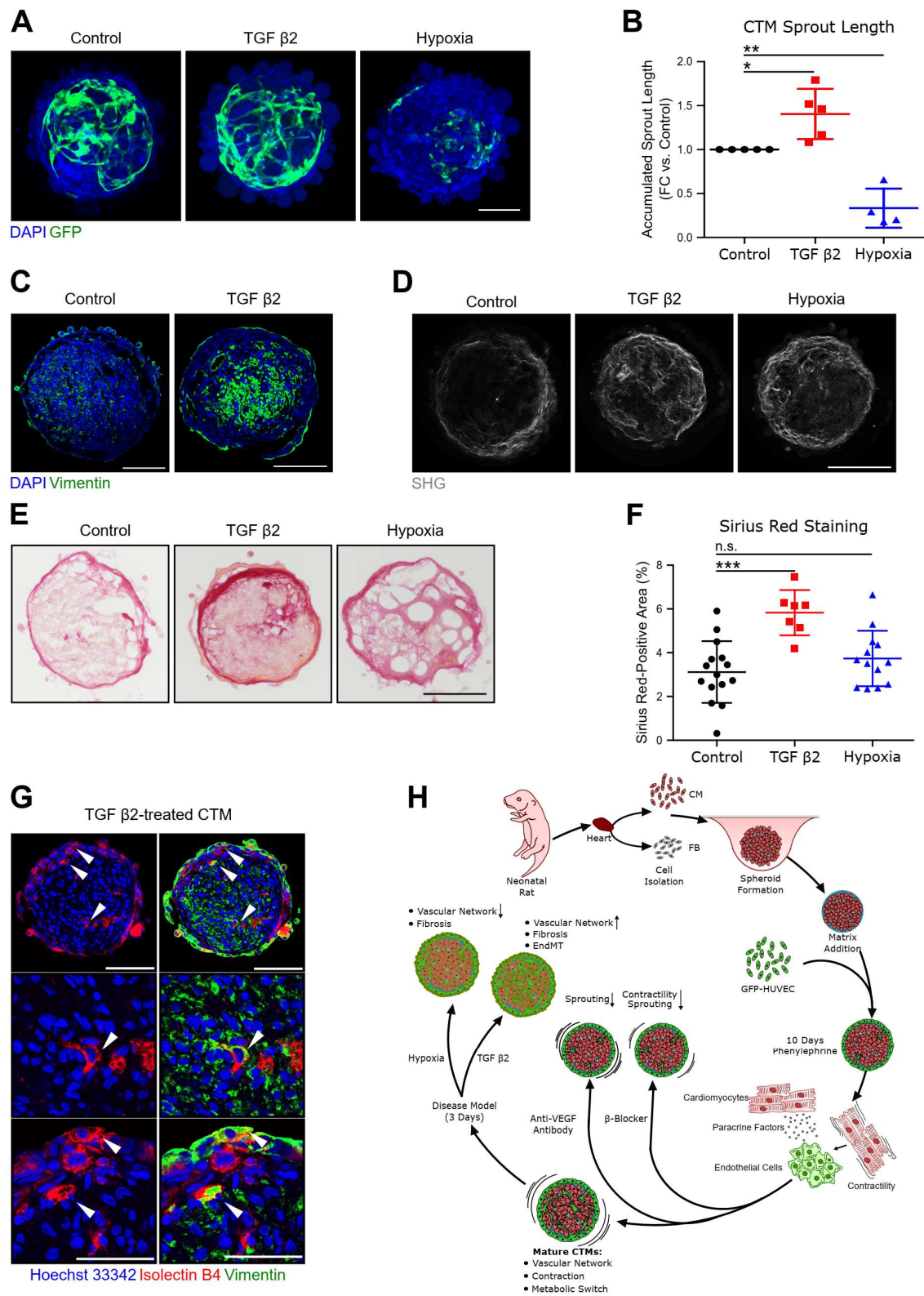


Figure 4: CTMs respond to stress stimuli. (A-G) After 10 days of culturing with 200 μ M PE, mature CTMs were cultured for further 3 days with 200 μ M PE (Control), 200 μ M PE + 10 ng / mL TGF β 2, or 0.1% O₂ (Hypoxia), to mimic an inflammatory / hypoxic stress condition in mature CTMs. (A-B) Angiogenic sprouting (GFP-labeled HUVEC) within the CTMs was observed using the Leica TCS SP8 confocal microscope (scale bar = 100 μ m) and quantified using the LAS X software (B, Control and TGF β 2: n = 5 and Hypoxia: n = 4). (C) Vimentin (green) was stained in CTMs that were treated with or without TGF β 2 (scale bar = 100 μ m). (D) Collagen deposition was

recorded using second-harmonics generation (SHG) microscopy on 10 μm thick CTM sections that were derived from mature CTMs cultured as described for panel A and B. SHG microscopy enables label-free visualization of biomolecules with a certain molecular structure, such as collagen fibrils. Shown are representative SHG images of mature CTMs under PE alone, PE+TGF β 2 or PE + hypoxia (scale bar = 100 μm). (**E and F**) Collagen deposition was further recorded using Sirius red staining on 10 μm thick CTM sections that were derived from mature CTMs cultured as described for panel A and B (scale bar = 100 μm ; n = 15 (control), n = 7 (TGF β 2), n = 13 (hypoxia)). (**G, top**) Representative overview image of a mature CTM that has been treated for 3 days with TGF β 2. Endothelial cells were stained with Isolectin B4 (red), whereas vimentin (green) was used as mesenchymal marker. Nuclei (blue) were counterstained with Hoechst 33342 (scale bar = 100). (**G, bottom**) High magnification images of endothelial cells (red; Isolectin B4) that are expressing vimentin (green) indicating endothelial-mesenchymal transition (white arrows). Nuclei (blue) were stained with Hoechst 33342 (scale bar = 50 μm). (**H**) Graphical abstract concluding the experimental data. Data are shown as mean \pm SD. Statistical analysis was performed using multiple-group ANOVA with a post hoc Bonferroni test was used (B and F), indicated as follows: n.s. = not significant, *P<0.05, **P<0.01 and ***P<0.001.

Discussion

This study reports a cardiac mimetic platform for the study of EC communication with CM under physiological and pathophysiological conditions. We demonstrate that physiological pro-hypertrophic stimuli augments vascularization of the CTMs at least in part by inducing VEGF-release by CM. The developed model additionally enabled dissection of cardiac response to ischemia and pro-fibrotic stress conditions.

Our tissue recapitulates cardiac responses to physiologic and pathologic stimuli at the level of tissue growth, vascularization, metabolism and function [28, 35] This is particularly striking in the response of the CTMs to high concentrations of PE, where we observed a significant increase in CTM growth, concomitant with the switch in metabolism from glycolysis to glucose oxidation (**Fig. 1G-I**). This switch reflects the dynamics and plasticity of our CTMs, which is further reflected at the gene expression level (**Fig. S2A, C**) [49, 50]. This mimicry of native tissue response was also observed with respect to cardiac function and contraction. In this regards, as reported *in vivo* [35], our CTM demonstrated an increase in the amplitude of contraction, thus reflecting a physiologic or adaptive hypertrophic response to PE stimulation. These changes in contractility were also reflected at the gene expression level (**Fig. S2A, D**).

Although 3D cardiac tissue engineering models have been previously used for therapeutic cardiac tissue engineering or drug testing [24, 51-55], these studies did not address the recapitulation of more complex, cellular communication-dependent *in vivo* phenotypes with their models. The use of heterogenic cell mixtures, pluripotent cells or the addition of ECs from different sources has allowed the formation of vascularized tissue constructs [21, 22, 55-57]. Despite the well-established importance of cellular interactions, few studies have used the 3D tissue engineering models for mechanistic studies. Here we provide a more in-depth elucidation of the role of cardiac microenvironment, particularly the impact of heterocellular cross-talk with respect to EC-CM interactions. Coating the pre-made spheroids with ECs allowed us to study the kinetics of angiogenic sprouting, which includes visualization of tip cells with filopodia. Our model further recapitulated the established pro-angiogenic response induced by cardiac hypertrophy and confirmed the importance of VEGF for mediating this effect [7, 8, 58-60]. Based on our previous work, we speculate that the induction of VEGF expression in cardiomyocytes in response to PE stimulation occurs through activation of Phosphoinositide 3-kinase (PI3K) signaling or direct induction of HIF1 α activation [49, 61, 62].

Of note, inhibition of VEGF did not fully prevent the induction of vascularization induced by PE suggesting that additional growth factors, cytokines, matrix proteins and/or mechanical factors contribute to the observed effect. Interestingly, the pro-angiogenic effect of PE was dependent on β_1/β_2 receptor and likely involved mechanical activation mediated by the contraction of CMs. Whether this effect occurs directly by mechanosensing of ECs or is due to an indirect effect mediated by a change in CM paracrine effects remains to be further elucidated. However, first supernatant experiments of CMs treated with PE and β -blockers showed no anti-angiogenic effect compared to CMs stimulated with PE alone, giving rise that mechanosensing of ECs induce sprouting. Of note, we exclude a direct pro- and anti-angiogenic effect of PE and β -blockers - at the concentrations used in the CTM experiments on EC sprouting. Interestingly, propranolol additionally reduced CTM hypertrophy whereas metoprolol did not, although we used very high concentrations of metoprolol that arose from previous experiences (data not shown). In line with our observations, previous studies have already reported in the 1990s that propranolol reverse ventricular hypertrophy [63, 64], while metoprolol is known to reduce hypertrophy to a lower extend only [65]. Another report even showed that metoprolol has no effect on left ventricular hypertrophy in systemic hypertension [66]. This nicely implicates that our 3D CTM platform mimics in vivo findings of β -blockers in terms of cardiac hypertrophy.

Adrenergic Receptors (AR) are key regulators in the cardiovascular system, through the activation of specific ARs on the endothelial surface by the release of catecholamines [67, 68]. The activation of these receptors maintain the release of NO via eNOS to control endothelial function [69]. Phenylephrine (PE) is a specific α AR agonist and the activation of the α_1 AR in endothelial cells is known to induce NO release in rodent arteries [70]. Interestingly, PE stimulation indeed induced vessel formation and maturation in our CTM model, whereas PE had no pro-angiogenic effect on HUVEC mono-spheroids. It might be that the release of NO in endothelial cells within CTMs has an autocrine effect, facilitating vessel maturation, while NO did not induce angiogenesis. During hypoxic conditions, endothelial cells release ROS rather than NO, a phenomenon that is referred to as “eNOS uncoupling” [71, 72]. While it is known that ROS contributes to many changes underlying endothelial injury, hypoxia may also alter the response to GPCR signaling and thereby control endothelial function as we reported for CTMs under severe hypoxia. A second main class of the endothelial ARs is the β_2 AR. Since PE is a selective α AR agonist, it doesn't activate β ARs. However, the endothelial β_2 AR signaling pathway also induces eNOS activation and although PE doesn't activate the endothelial β_2 AR, it could stimulate endothelial cells or other cells within the CTM via the α AR to release catecholamines that in turn activate the β_2 AR on endothelial cells and further promote eNOS activation [73]. In line with this assumption, Sorriento et al. found that endothelial cells are indeed able to produce catecholamines [74]. Of note, blocking β_2 AR in PE stimulated CTMs reduced endothelial sprouting. However, whether this effect is facilitated by a direct effect of the β_2 AR antagonist on endothelial cells or whether the reduction in CTM contraction was the main driver still needs to be studied in detail. A change in the CTM secretome cannot be excluded since we demonstrated no changes of soluble angiogenic factors in cardiomyocytes only. Fibroblasts and endothelial cells might also be affected and may display disturbances in catecholamine expression.

We applied this model to study pathophysiological conditions as they occur in cardiac ischemia and during cardiac remodeling after infarction. We showed that treatment of the CTMs with the prototypical inducer of a pro-fibrotic response, TGF β_2 , indeed augments collagen deposition in the CTMs. ECs increased sprouting and in addition, we found ECs

undergoing EndMT in CTMs under pro-inflammatory conditions, indicating that our model might also be used for studying EndMT in terms of cell-cell communication. Combinations of TGF β 2 with inflammatory cytokines may be an option to simulating pathophysiological conditions during cardiac remodeling and chronic heart failure. In addition, we showed that hypoxia exposure led to the induction of cell death, reduced contraction (data not shown) and increased collagen deposition, thus accurately reflecting changes in myocardial damage and dysfunction as result of severe ischemia [75, 76]. By further titrating graded levels of severe hypoxia from 0.1% O₂ to 1% O₂, we surprisingly observed a consistent decrease in endothelial vessel sprouting (**Fig. S7A and B**). These observations warrant further study, but as it stands, our data suggests that under conditions of severe hypoxia and consumption of oxygen by contracting myocytes vascular sprouting is impaired. Taken together, these data indicate that CTMs could serve as a robust 3D in vitro system to mimic severe myocardial ischemia and to potentially be utilized to identify efficacious pharmacological agent for therapy.

While our model represents in some way an advancement over current methodologies due to inclusion of the three main cells types of the heart and at ratios present in the native myocardium, further work will need to be performed to better understand the extent to which our model can accurately recapitulate native myocardium responses to more physiologically relevant stressors such as pressure or volume overload, and focal ischemia. It will also be important to determine if improvements to the culture protocol could further increase cardiomyocyte maturation and vascular organization to better reflect structural organization of these components in native tissue. It should also be noted that despite lengths taken to ensure purity of the respective cardiomyocyte, fibroblast and endothelial fractions prior to CTM formation, our CM and FB cultures compose of approximately 8% contaminating cells. Although we anticipate that this will not significant impact most macroscopic readouts, it is conceivable particularly when used as a model to study transdifferentiation events, that these contaminating cells could confound data interpretation and overestimate the efficiency of transdifferentiation. This issue can however be overcome by use of lineage tracers to enable precise determination of the frequency of such transdifferentiation events, as performed in this study.

In conclusion, such a model might be used for testing therapeutic modalities that go beyond targeting CM intrinsic functions such as calcium handling. Studying the vasculature may also provide a mean to determine putative detrimental side effects of therapeutic strategies on vascular growth under physiological stress responses. Finally, the knowledge acquired with such models might also be fundamental to develop novel therapeutics with specific biological targets for treatments of patients with heart disease.

Acknowledgements

The study was supported by the LOEWE Center for Cell and Gene Therapy, the Messer Foundation, and the German Research Foundation (Exc2026) to J.K. and S.D. and the German Research Foundation Council (CRC1366) and European Research Council (AngioInc) to S.D, and European Innovation Council (822455) to Genome Biologics.

Disclosures

All authors declare absence of any actual or potential conflict of interest including any financial, personal or other relationships with other people or organizations within three (3) years of beginning the work submitted that could inappropriately influence (bias) the work.

Author contributions

J.K. and S.D. designed and, M.D.P., J.U.G.W. and L.N. executed most experiments. M.H., T.Y. and K.B. performed stainings and metabolic assays. R.S. and D.J. performed all sequence analysis, M.M., M.H. and J.M. provided imaging and TEM data. S.D., J.K. and J.U.G.W., with help from M.D.P. wrote the paper.

Tables

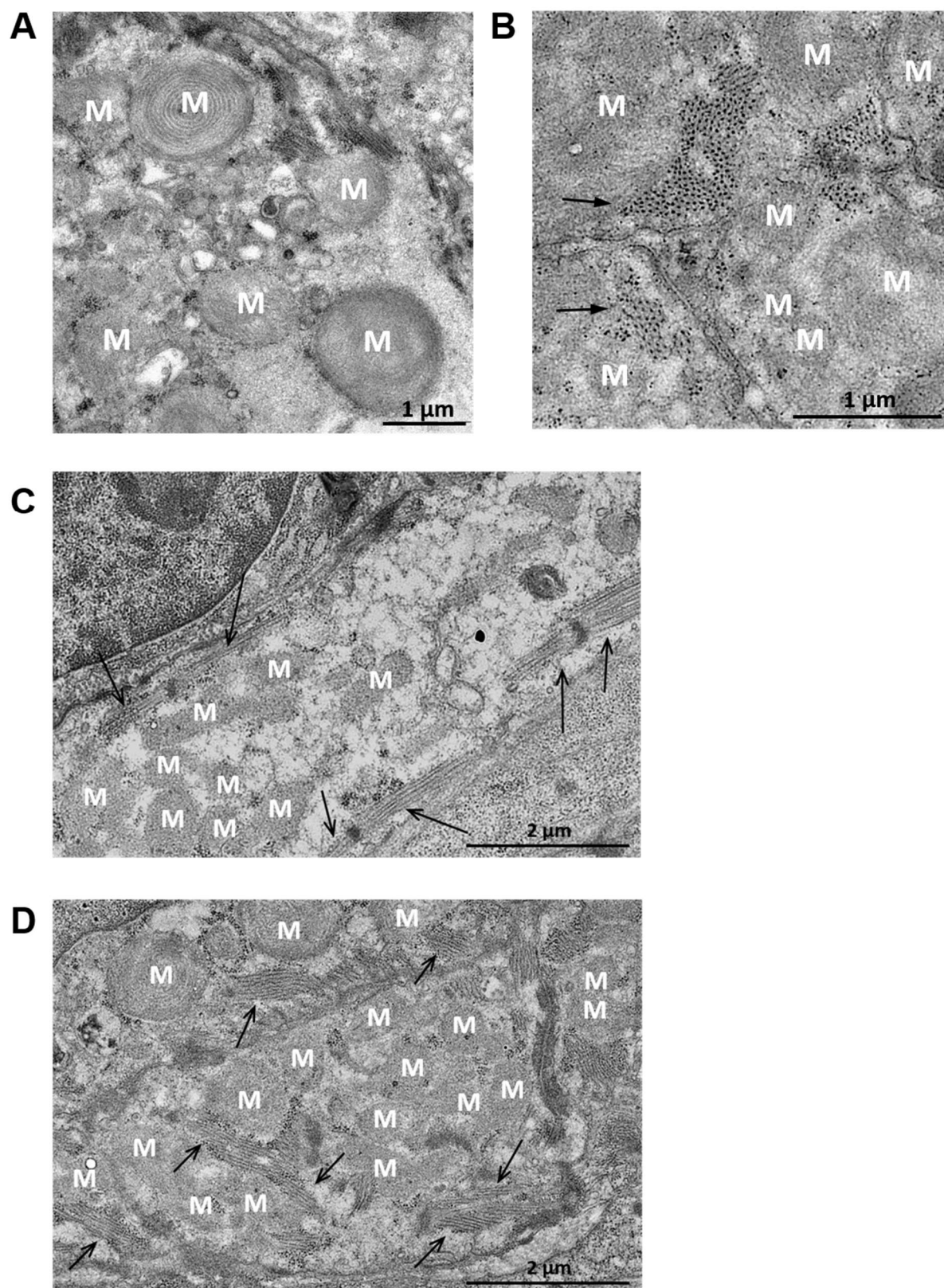
Table 2: List of antibodies.

Antibody	Company
Wheat Germ Agglutinin, Alexa Fluor™ 488 conjugate	Thermo Fischer (W11261)
anti-Phospho-Histone H2A.X (Ser139) (20E3) Rabbit mAb	Cell Signaling (9718S)
anti-VE-Cadherin antibody Rabbit	Cell Signaling (2500S)
anti- α -Actinin (Sarcomeric) antibody (clone: EA-53) Mouse mAb	Sigma-Aldrich (A7811)
anti-NG2 antibody Rabbit	Merck (AB5320)
Donkey anti-Mouse IgG (H+L) Cross-Adsorbed Antibody, Alexa Fluor 647	Invitrogen (A31571)
F(ab') ₂ -Goat anti-Mouse IgG (H+L) Cross-Adsorbed Antibody, Alexa Fluor 488	Invitrogen (A11017)
F(ab') ₂ -Goat anti-Rabbit IgG (H+L) Cross-Adsorbed Antibody, Alexa Fluor 488	Invitrogen (A11070)
F(ab') ₂ -Goat anti-Rabbit IgG (H+L) Cross-Adsorbed Antibody, Alexa Fluor 647	Invitrogen (A21246)
Goat anti-Mouse IgG (H+L) Cross-Adsorbed Antibody, Alexa Fluor 568	Invitrogen (A11004)
Goat anti-Rat IgG (H+L) Cross-Adsorbed Antibody, Alexa Fluor 488	Invitrogen (A11006)
Goat Anti-Vimentin antibody	Merck (AB1620)
Goat anti-Tagln antibody	Abcam (ab10135)
Anti-ATP5A antibody [15H4C4]	Abcam (ab14748)
Donkey anti-Goat IgG (H+L) HCross-Adsorbed Antibody, Alexa Fluor Plus 555	Invitrogen (A32816)
Rabbit anti-collagen III antibody	Abcam (ab7778)
Biotinylated Isolectin B4	Vector–Linaris (B1205)
Streptavidin Alexa Fluor 555	Invitrogen (A32355)

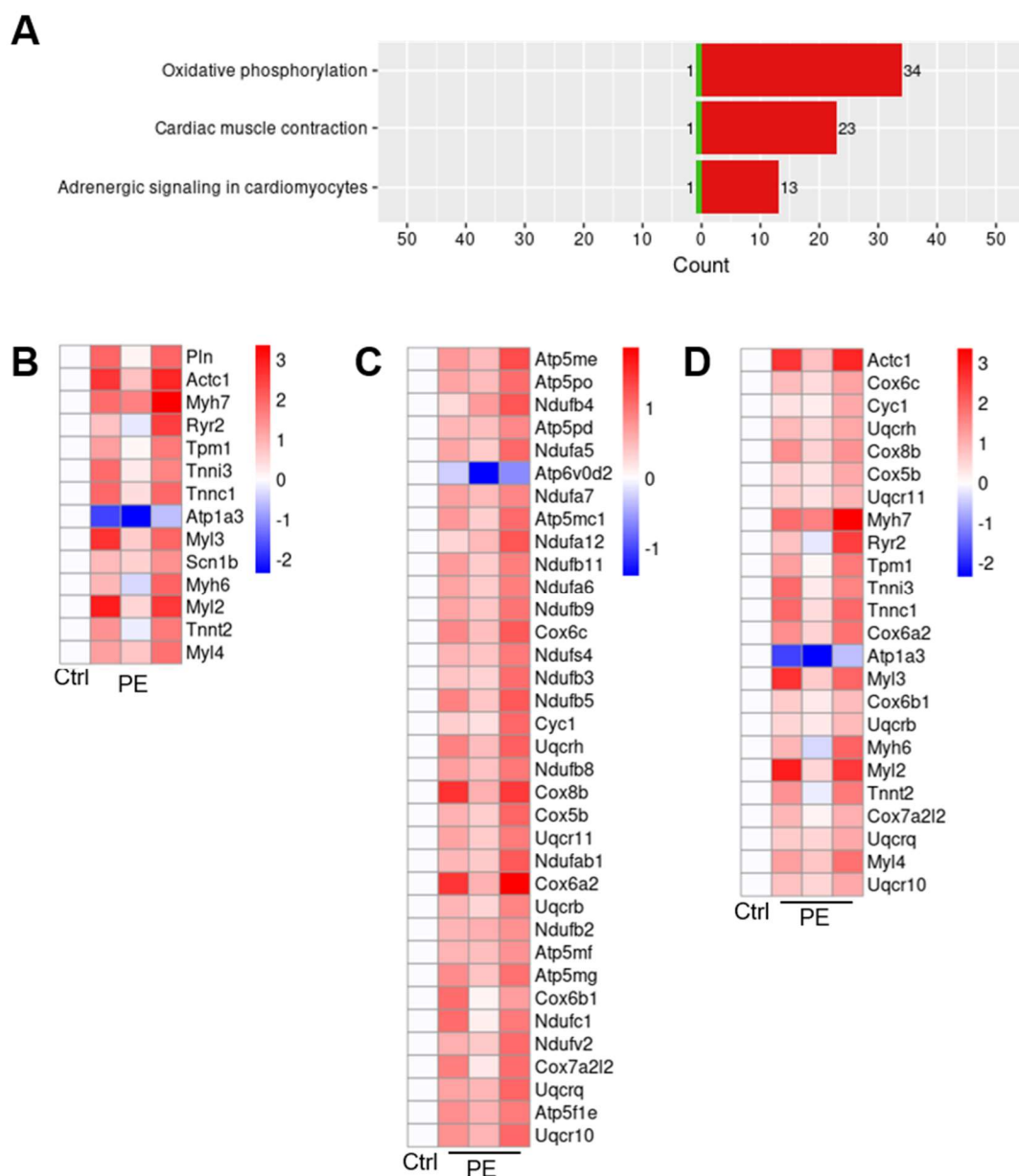
Table 2: List of primers used

Primer	Forward	Reverse
Total Titin	CCA AGC TCA CTG TGG GAG AAA	GCT ACT TCC AAG GGC TCA ATT C
N2B	CCA ACG AGT ATG GCA GTG TCA	TGG GTT CAG GCA GTA ATT TGC
N2BA-2	CCA ACG AGT ATG GCA GTG TCA	ACT ACA GGC GGA AAG CTA CTA AAA AC

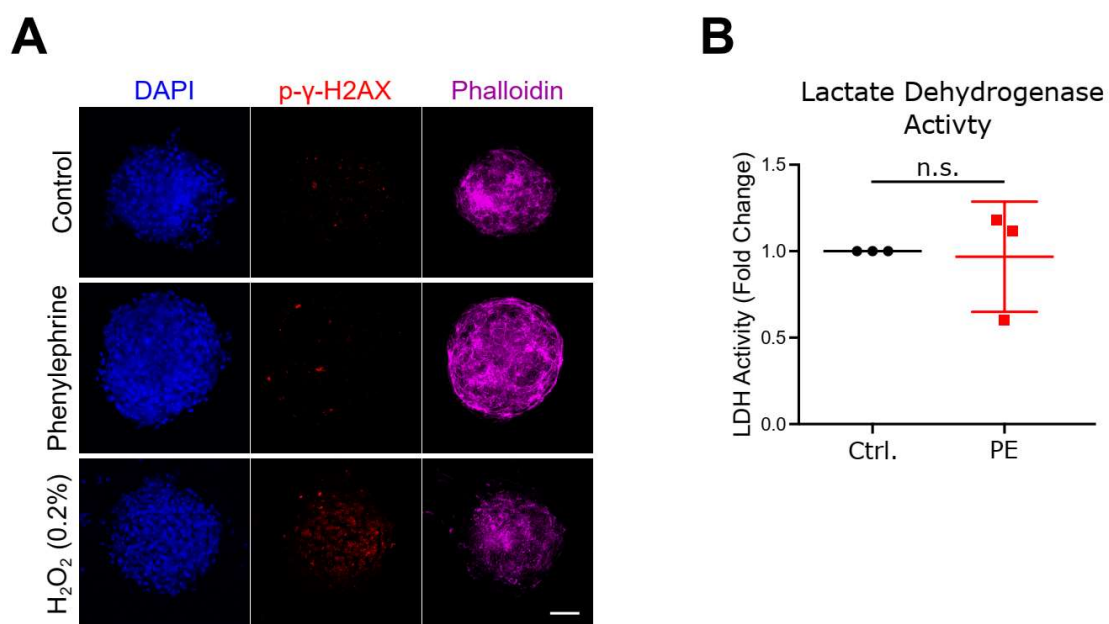
Supplemental Figures



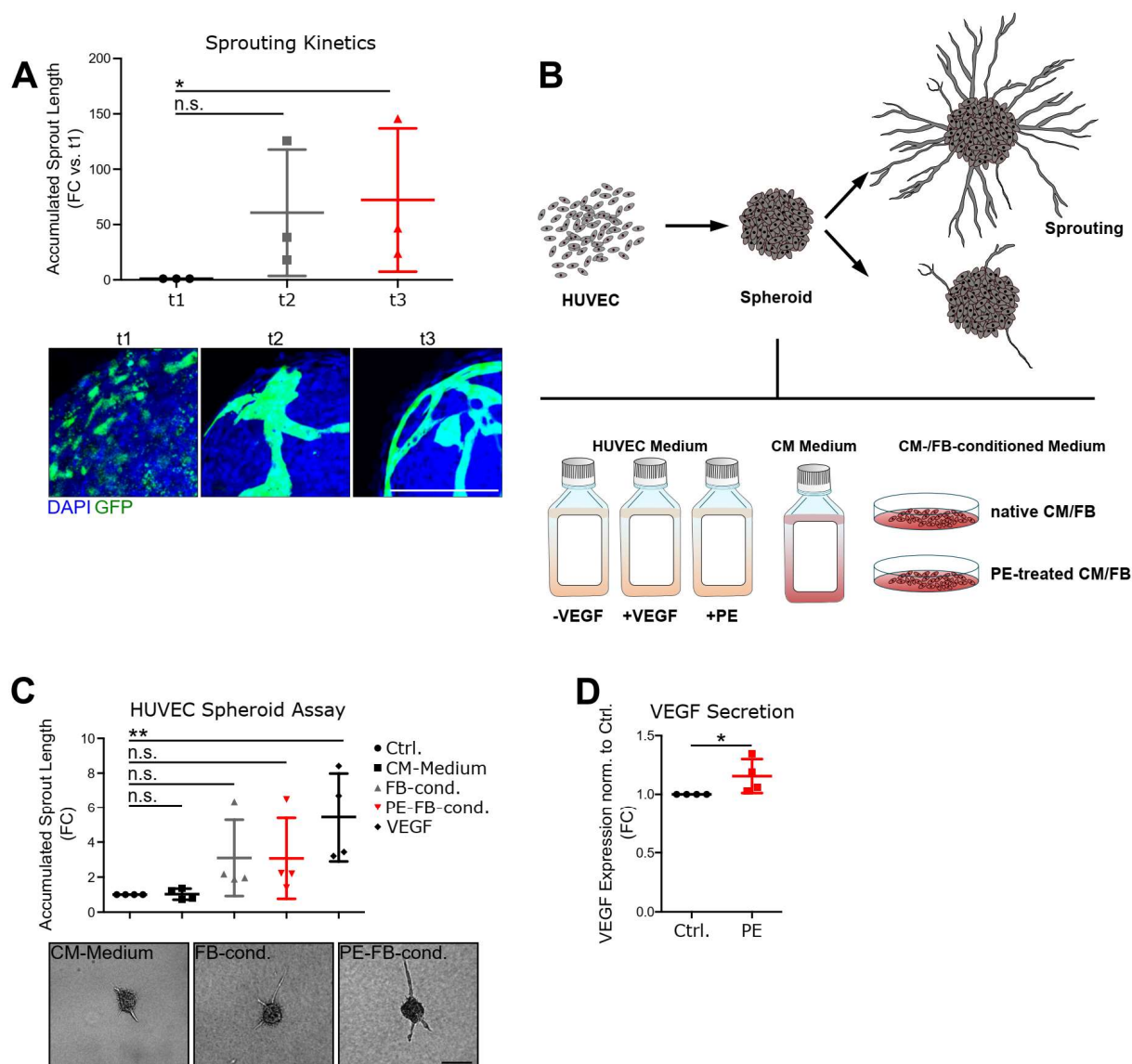
Supplemental Figure 1. Phenylephrine stimulation increases mitochondrial density. High magnifications of ultra-thin sections derived from untreated (A) and PE-treated (B) mature CTMs were analyzed by transmission electron microscopy. Low magnifications of untreated (C) and PE-treated CTMs (D) are shown in Panel C and D. Representative images are shown.



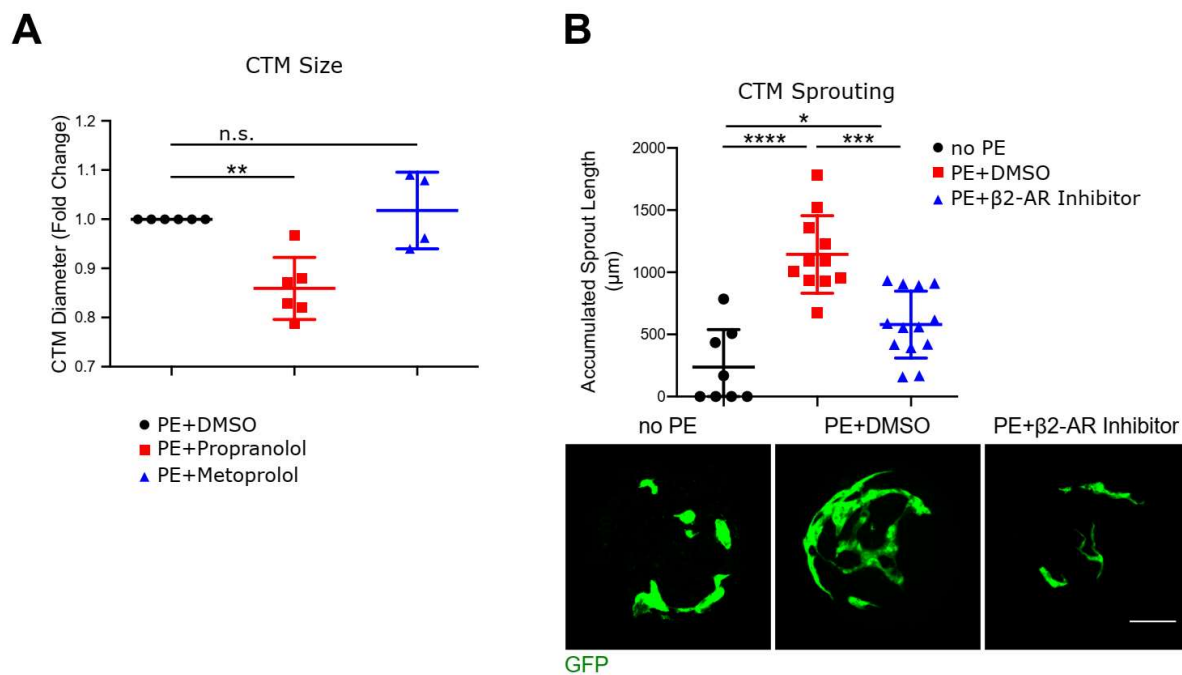
Supplemental Figure 2. Phenylephrine stimulation affects gene clusters implicated in angiogenesis, adrenergic signaling, angiogenesis, metabolism and contractility. (A) Relevant KEGG pathway enrichment in CTMs upon PE stimulation. (B-D) Heat map of differentially expressed adrenergic signalling pathway genes (B) metabolic genes (C) and genes involved in contraction (D) in phenylephrine-treated CTMs, normalized to log₂ FPKM of untreated control CTMs. Normalised Ctrl vales are shown (n=3) with the respective PE-treated replicates (n=3). *P<0.05 (A-D).



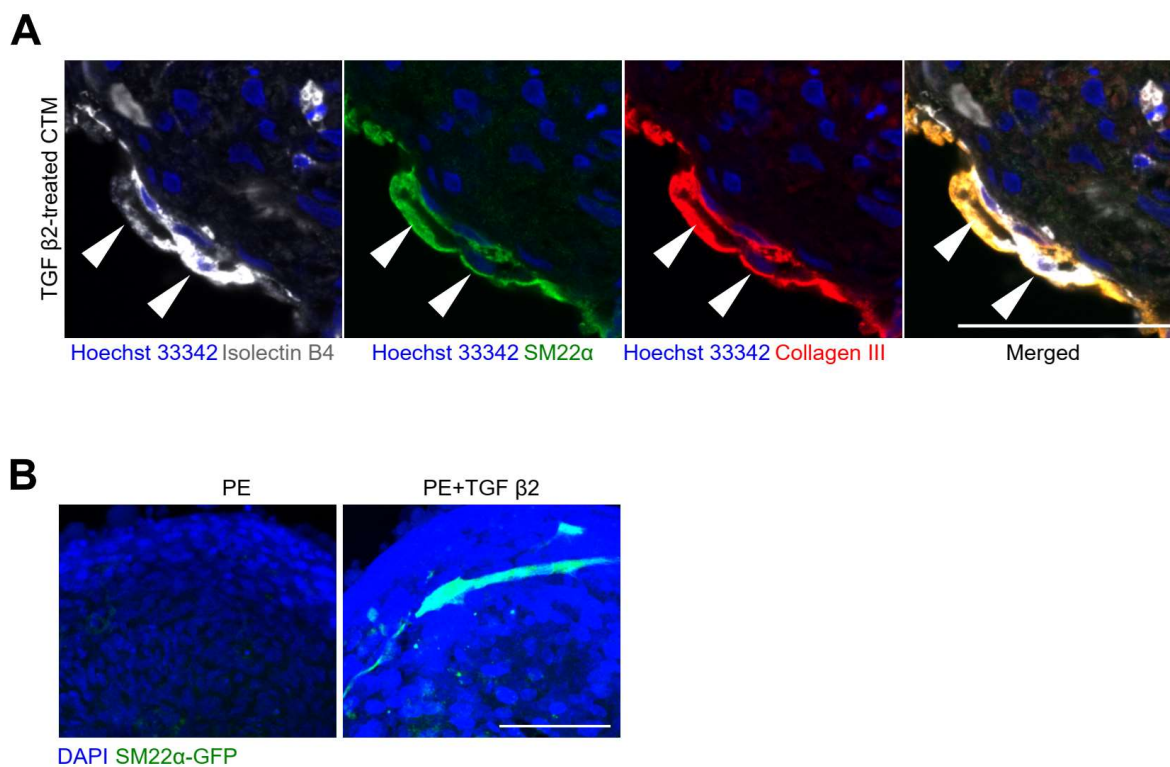
Supplemental Figure 3: Phenylephrine-treatment shows no cytotoxicity. (A) Mature CTMs were stained for p-γ-H2SX (red). One representative image per condition is shown where nuclei were stained with DAPI (blue) and cytoskeletal with phalloidin (magenta). As positive control served CTMs treated with 0.2% H₂O₂ for 30 minutes prior to immune staining (scale bar = 50 μm). (B) Lactate dehydrogenase activity was determined in mature CTMs treated with (PE) or without (Ctrl.) phenylephrine using the lactate dehydrogenase activity assay kit (Sigma-Aldrich) (n=3). Statistical power was determined using a Mann-Whitney test and data are shown as mean ± SD (n.s. = not significant).



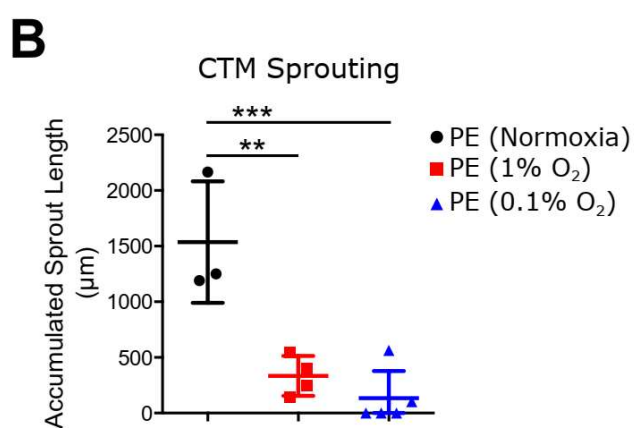
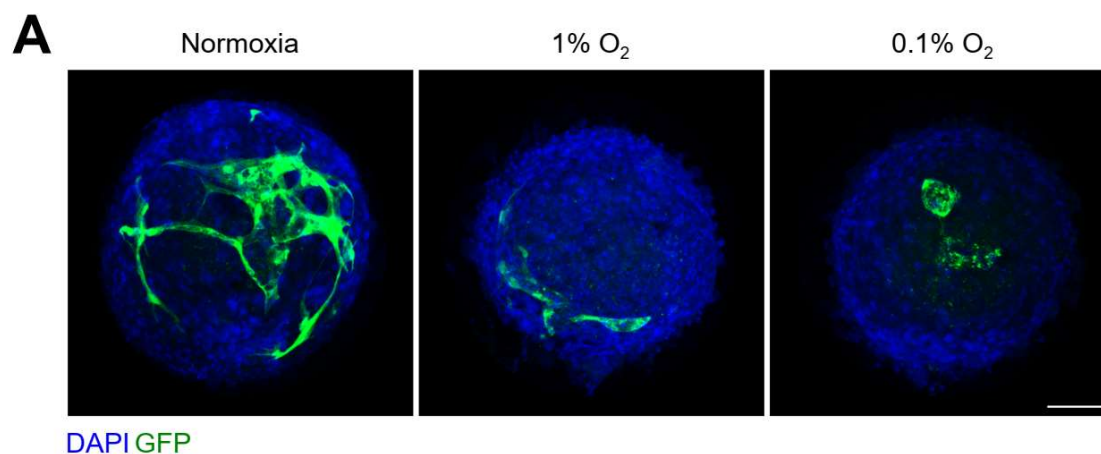
Supplemental Figure 4: Angiogenesis in CTMs upon phenylephrine-treatment. (A) Kinetic of angiogenic sprouting in CTMs upon phenylephrine-treatment. CTMs after 1 day (t1), 5 days (t2) and 10 days (t3) after GFP-HUVEC addition were fixed. Vascularization was determined using the Leica TCS SP8 confocal microscope and the LAS X software by measuring the accumulated HUVEC-sprout length (scale bar = 100 μ m; n=3). **(B)** Schematic set-up of spheroid based angiogenic sprouting assay. **(C)** To assess whether PE-treated cardiomyocytes secrete pro-angiogenic factors, a further HUVEC spheroid-based angiogenic sprouting assay was performed by stimulating the HUVEC spheroids with blank maintenance medium, 50 ng/mL VEGF or cell culture supernatants of neonatal rat fibroblasts that were treated either with no PE or PE for 72 hours. Each treatment was applied for 24 hours before determining sprouting using a computer-assisted microscope using Axiovision 4.5 (Zeiss) (scale bar = 100 μ m; n = 4). **(D)** VEGF levels in supernatants of CM-mono-cultures in the presence and absence of PE were determined using ELISA as fold change to no PE (n = 4). Data are shown as mean \pm SD. Statistical analysis was performed using a multiple-group Kruskal-Wallis test with a post hoc Dunn's correction test was used (A and C) and Mann-Whitney test (D). n.s. = not significant; *P<0.05 and **P<0.01.



Supplemental Figure 5: CTM size is altered upon β -blocker-treatment. (A) Size of mature CTMs treated for 10 days with PE+ 0.1% DMSO ($n = 6$) or treated with 200 μ M PE + 1 μ M propranolol ($n = 6$) / 50 μ M metoprolol ($n = 4$). CTM size is shown as fold change. **(B)** Sprout length of CTMs stimulated for 10 days with no PE ($n = 8$), PE + DMSO ($n = 11$) or PE+ the β 2-AR inhibitor ICI 118.551 ($n = 13$), scale bar = 100 μ m. Data are shown as mean \pm SD. Statistical analysis was performed using a multiple-group Kruskal-Wallis test with a post hoc Dunn's correction test was used (A), one-way ANOVA with a post-hoc Bonferroni test (B). n.s. = not significant, * $p < 0.05$; ** $p < 0.01$; *** $p < 0.001$ and **** $p < 0.0001$.



Supplemental Figure 6: Endothelial-mesenchymal transition occurs upon TGF β 2 treatment. After 10 days of culturing with 200 μ M PE, mature CTMs were cultured for further 3 days with 200 μ M PE (PE) or 200 μ M PE + 10 ng / mL TGF β 2. **(A)** Mature CTMs stimulated for 3 days with PE + TGF β 2. High magnification images of endothelial cells (white; Isolectin B4) that are expressing SM22 α (green) and collagen III (red) indicating endothelial-mesenchymal transition (white arrows). Nuclei (blue) were stained with Hoechst 33342 (scale bar = 50 μ m). **(B)** Mature CTMs were generated with endothelial cells that were transfected with a virus encoding GFP under the control of the SM22 α and were cultured for 3 days with PE or PE + TGF β 2. High magnification images of endothelial cells were taken that express GFP under the control of the SM22 α -promoter. Nuclei were stained with DAPI. (scale = 100 μ m).



Supplemental Figure 7: Effects of hypoxia on endothelial sprouting. (A) CTMs were cultured for 10 days with PE. After 10 days of PE stimulation, we kept CTMs 1% and 0.1% O₂ for three days (scale = 100 μm). (B) As read out accumulated sprout length was measured. Statistical power was determined using a One-way ANOVA with a pot-hoc Bonferroni test (**p<0.01; ***p<0.001).

References

- [1] R.G. Gourdie, S. Dimmeler, P. Kohl, Novel therapeutic strategies targeting fibroblasts and fibrosis in heart disease, *Nat Rev Drug Discov* 15(9) (2016) 620-38.
- [2] S.L. Lim, C.S. Lam, V.F. Segers, D.L. Brutsaert, G.W. De Keulenaer, Cardiac endothelium-myocyte interaction: clinical opportunities for new heart failure therapies regardless of ejection fraction, *European heart journal* 36(31) (2015) 2050-2060.
- [3] J.C. Del Alamo, D. Lemons, R. Serrano, A. Savchenko, F. Cerignoli, R. Bodmer, M. Mercola, High throughput physiological screening of iPSC-derived cardiomyocytes for drug development, *Biochimica et biophysica acta* 1863(7 Pt B) (2016) 1717-27.
- [4] J. Jabs, F.M. Zickgraf, J. Park, S. Wagner, X. Jiang, K. Jechow, K. Kleinheinz, U.H. Toprak, M.A. Schneider, M. Meister, S. Spaich, M. Sutterlin, M. Schlesner, A. Trumpp, M. Sprick, R. Eils, C. Conrad, Screening drug effects in patient-derived cancer cells links organoid responses to genome alterations, *Mol Syst Biol* 13(11) (2017) 955.
- [5] O. Bergmann, S. Zdunek, A. Felker, M. Salehpour, K. Alkass, S. Bernard, S.L. Sjostrom, M. Szewczykowska, T. Jackowska, C. Dos Remedios, T. Malm, M. Andra, R. Jashari, J.R. Nyengaard, G. Possnert, S. Jovinge, H. Druid, J. Frisen, Dynamics of Cell Generation and Turnover in the Human Heart, *Cell* 161(7) (2015) 1566-75.
- [6] Y. Tang, J.R. Nyengaard, J.B. Andersen, U. Baandrup, H.J. Gundersen, The application of stereological methods for estimating structural parameters in the human heart, *Anat Rec (Hoboken)* 292(10) (2009) 1630-47.
- [7] I. Shiojima, K. Sato, Y. Izumiya, S. Schiekofer, M. Ito, R. Liao, W.S. Colucci, K. Walsh, Disruption of coordinated cardiac hypertrophy and angiogenesis contributes to the transition to heart failure, *The Journal of clinical investigation* 115(8) (2005) 2108-18.
- [8] T. Oka, H. Akazawa, A.T. Naito, I. Komuro, Angiogenesis and cardiac hypertrophy: maintenance of cardiac function and causative roles in heart failure, *Circulation research* 114(3) (2014) 565-71.
- [9] F.J. Giordano, H.P. Gerber, S.P. Williams, N. VanBruggen, S. Bunting, P. Ruiz-Lozano, Y. Gu, A.K. Nath, Y. Huang, R. Hickey, N. Dalton, K.L. Peterson, J. Ross, Jr., K.R. Chien, N. Ferrara, A cardiac myocyte vascular endothelial growth factor paracrine pathway is required to maintain cardiac function, *Proceedings of the National Academy of Sciences of the United States of America* 98(10) (2001) 5780-5.
- [10] C. Daly, E. Pasnikowski, E. Burova, V. Wong, T.H. Aldrich, J. Griffiths, E. Ioffe, T.J. Daly, J.P. Fandl, N. Papadopoulos, D.M. McDonald, G. Thurston, G.D. Yancopoulos, J.S. Rudge, Angiotensin-2 functions as an autocrine protective factor in stressed endothelial cells, *Proceedings of the National Academy of Sciences of the United States of America* 103(42) (2006) 15491-6.
- [11] S.Y. Schubert, A. Benarroch, J. Monter-Solans, E.R. Edelman, Primary monocytes regulate endothelial cell survival through secretion of angiotensin-1 and activation of endothelial Tie2, *Arterioscler Thromb Vasc Biol* 31(4) (2011) 870-5.
- [12] J.A. Dougherty, N. Kumar, M. Noor, M.G. Angelos, M. Khan, C.A. Chen, M. Khan, Extracellular Vesicles Released by Human Induced-Pluripotent Stem Cell-Derived Cardiomyocytes Promote Angiogenesis, *Front Physiol* 9 (2018) 1794.

- [13] R.M. Palmer, D.S. Ashton, S. Moncada, Vascular endothelial cells synthesize nitric oxide from L-arginine, *Nature* 333(6174) (1988) 664-6.
- [14] S. Rafii, J.M. Butler, B.S. Ding, Angiocrine functions of organ-specific endothelial cells, *Nature* 529(7586) (2016) 316-25.
- [15] H.G. Augustin, G.Y. Koh, Organotypic vasculature: From descriptive heterogeneity to functional pathophysiology, *Science (New York, N.Y)* 357(6353) (2017).
- [16] Y. Manavski, T. Lucas, S.F. Glaser, L. Dorsheimer, S. Gunther, T. Braun, M.A. Rieger, A.M. Zeiher, R.A. Boon, S. Dimmeler, Clonal Expansion of Endothelial Cells Contributes to Ischemia-Induced Neovascularization, *Circulation research* 122(5) (2018) 670-677.
- [17] F. Perbellini, S.A. Watson, I. Bardi, C.M. Terracciano, Heterocellularity and Cellular Cross-Talk in the Cardiovascular System, *Front Cardiovasc Med* 5 (2018) 143.
- [18] J.J. Kim, L. Hou, N.F. Huang, Vascularization of three-dimensional engineered tissues for regenerative medicine applications, *Acta Biomater* 41 (2016) 17-26.
- [19] M.N. Hirt, A. Hansen, T. Eschenhagen, Cardiac tissue engineering: state of the art, *Circulation research* 114(2) (2014) 354-67.
- [20] D.B. Kolesky, K.A. Homan, M.A. Skylar-Scott, J.A. Lewis, Three-dimensional bioprinting of thick vascularized tissues, *Proceedings of the National Academy of Sciences of the United States of America* 113(12) (2016) 3179-84.
- [21] O. Caspi, A. Lesman, Y. Basevitch, A. Gepstein, G. Arbel, I.H. Habib, L. Gepstein, S. Levenberg, Tissue engineering of vascularized cardiac muscle from human embryonic stem cells, *Circulation research* 100(2) (2007) 263-72.
- [22] M.T. Valarmathi, J.W. Fuseler, J.M. Davis, R.L. Price, A Novel Human Tissue-Engineered 3-D Functional Vascularized Cardiac Muscle Construct, *Front Cell Dev Biol* 5 (2017) 2.
- [23] A. Moretti, K.L. Laugwitz, T. Dorn, D. Sinnecker, C. Mummery, Pluripotent stem cell models of human heart disease, *Cold Spring Harb Perspect Med* 3(11) (2013).
- [24] W.H. Zimmermann, C. Fink, D. Kralisch, U. Remmers, J. Weil, T. Eschenhagen, Three-dimensional engineered heart tissue from neonatal rat cardiac myocytes, *Biotechnol Bioeng* 68(1) (2000) 106-14.
- [25] A. Stoehr, M.N. Hirt, A. Hansen, M. Seiffert, L. Conradi, J. Uebeler, F.P. Limbourg, T. Eschenhagen, Spontaneous Formation of Extensive Vessel-Like Structures in Murine Engineered Heart Tissue, *Tissue Eng Part A* 22(3-4) (2016) 326-35.
- [26] H. Masumoto, T. Ikuno, M. Takeda, H. Fukushima, A. Marui, S. Katayama, T. Shimizu, T. Ikeda, T. Okano, R. Sakata, J.K. Yamashita, Human iPS cell-engineered cardiac tissue sheets with cardiomyocytes and vascular cells for cardiac regeneration, *Sci Rep* 4 (2014) 6716.
- [27] S. Sekiya, T. Shimizu, T. Okano, Vascularization in 3D tissue using cell sheet technology, *Regen Med* 8(3) (2013) 371-7.
- [28] T. Chen, G. Vunjak-Novakovic, In vitro Models of Ischemia-Reperfusion Injury, *Regen Eng Transl Med* 4(3) (2018) 142-153.
- [29] E. Ehler, T. Moore-Morris, S. Lange, Isolation and culture of neonatal mouse cardiomyocytes, *Journal of visualized experiments : JoVE* (79) (2013).
- [30] S. Arber, J.J. Hunter, J. Ross, Jr., M. Hongo, G. Sansig, J. Borg, J.C. Perriard, K.R. Chien, P. Caroni, MLP-deficient mice exhibit a disruption of cardiac

- cytoarchitectural organization, dilated cardiomyopathy, and heart failure, *Cell* 88(3) (1997) 393-403.
- [31] C.H. Yoon, M. Koyanagi, K. Iekushi, F. Seeger, C. Urbich, A.M. Zeiher, S. Dimmeler, Mechanism of improved cardiac function after bone marrow mononuclear cell therapy: role of cardiovascular lineage commitment, *Circulation* 121(18) (2010) 2001-11.
- [32] J.U.G. Wagner, E. Chavakis, E.M. Rogg, M. Muhly-Reinholz, S.F. Glaser, S. Gunther, D. John, F. Bonini, A.M. Zeiher, L. Schaefer, M.J. Hannocks, R.A. Boon, S. Dimmeler, Switch in Laminin beta2 to Laminin beta1 Isoforms During Aging Controls Endothelial Cell Functions-Brief Report, *Arterioscler Thromb Vasc Biol* 38(5) (2018) 1170-1177.
- [33] A. Dobin, C.A. Davis, F. Schlesinger, J. Drenkow, C. Zaleski, S. Jha, P. Batut, M. Chaisson, T.R. Gingeras, STAR: ultrafast universal RNA-seq aligner, *Bioinformatics (Oxford, England)* 29(1) (2013) 15-21.
- [34] Y. Liao, G.K. Smyth, W. Shi, featureCounts: an efficient general purpose program for assigning sequence reads to genomic features, *Bioinformatics (Oxford, England)* 30(7) (2014) 923-30.
- [35] B.C. Jensen, T.D. O'Connell, P.C. Simpson, Alpha-1-adrenergic receptors: targets for agonist drugs to treat heart failure, *J Mol Cell Cardiol* 51(4) (2011) 518-28.
- [36] C.A. Opitz, M.C. Leake, I. Makarenko, V. Benes, W.A. Linke, Developmentally regulated switching of titin size alters myofibrillar stiffness in the perinatal heart, *Circulation research* 94(7) (2004) 967-75.
- [37] C.A. Opitz, W.A. Linke, Plasticity of cardiac titin/connectin in heart development, *J Muscle Res Cell Motil* 26(6-8) (2005) 333-42.
- [38] S.P. Scott, T.K. Pandita, The cellular control of DNA double-strand breaks, *J Cell Biochem* 99(6) (2006) 1463-75.
- [39] J.E. Barker, E.C. McFarland, Hemopoietic precursor cell defects in nonanemic but stem cell-deficient W44/W44 mice, *J Cell Physiol* 135(3) (1988) 533-8.
- [40] H. Chen, D. Liu, Z. Yang, L. Sun, Q. Deng, S. Yang, L. Qian, L. Guo, M. Yu, M. Hu, M. Shi, N. Guo, Adrenergic signaling promotes angiogenesis through endothelial cell-tumor cell crosstalk, *Endocr Relat Cancer* 21(5) (2014) 783-95.
- [41] D. Chalothorn, H. Zhang, J.A. Clayton, S.A. Thomas, J.E. Faber, Catecholamines augment collateral vessel growth and angiogenesis in hindlimb ischemia, *Am J Physiol Heart Circ Physiol* 289(2) (2005) H947-59.
- [42] N. Nuamnaichati, V.H. Sato, P. Moongkarndi, W. Parichatikanond, S. Mangmool, Sustained beta-AR stimulation induces synthesis and secretion of growth factors in cardiac myocytes that affect on cardiac fibroblast activation, *Life Sci* 193 (2018) 257-269.
- [43] R.K. Amanfu, J.J. Saucerman, Modeling the effects of beta1-adrenergic receptor blockers and polymorphisms on cardiac myocyte Ca²⁺ handling, *Mol Pharmacol* 86(2) (2014) 222-30.
- [44] B.N. Prichard, Propranolol and beta-adrenergic receptor blocking drugs in the treatment of hypertension, *Br J Clin Pharmacol* 13(1) (1982) 51-60.
- [45] D. Sorriento, B. Trimarco, G. Iaccarino, Adrenergic mechanism in the control of endothelial function, *Transl Med UniSa* 1 (2011) 213-28.

- [46] Y. Ji, S. Chen, K. Li, X. Xiao, S. Zheng, T. Xu, The role of beta-adrenergic receptor signaling in the proliferation of hemangioma-derived endothelial cells, *Cell Div* 8(1) (2013) 1.
- [47] L. Mostaco-Guidolin, N.L. Rosin, T.L. Hackett, Imaging Collagen in Scar Tissue: Developments in Second Harmonic Generation Microscopy for Biomedical Applications, *Int J Mol Sci* 18(8) (2017).
- [48] N. Farbehi, R. Patrick, A. Dorison, M. Xaymardan, V. Janbandhu, K. Wystub-Lis, J.W. Ho, R.E. Nordon, R.P. Harvey, Single-cell expression profiling reveals dynamic flux of cardiac stromal, vascular and immune cells in health and injury, *Elife* 8 (2019).
- [49] J. Krishnan, M. Suter, R. Windak, T. Krebs, A. Felley, C. Montessuit, M. Tokarska-Schlattner, E. Aasum, A. Bogdanova, E. Perriard, J.C. Perriard, T. Larsen, T. Pedrazzini, W. Krek, Activation of a HIF1 α -PPAR γ axis underlies the integration of glycolytic and lipid anabolic pathways in pathologic cardiac hypertrophy, *Cell metabolism* 9(6) (2009) 512-24.
- [50] P. Mirtschink, J. Krishnan, F. Grimm, A. Sarre, M. Horl, M. Kayikci, N. Fankhauser, Y. Christinat, C. Cortijo, O. Feehan, A. Vukolic, S. Sossalla, S.N. Stehr, J. Ule, N. Zamboni, T. Pedrazzini, W. Krek, HIF-driven SF3B1 induces KHK-C to enforce fructolysis and heart disease, *Nature* 522(7557) (2015) 444-9.
- [51] T. Eschenhagen, C. Fink, U. Remmers, H. Scholz, J. Wattchow, J. Weil, W. Zimmermann, H.H. Dohmen, H. Schafer, N. Bishopric, T. Wakatsuki, E.L. Elson, Three-dimensional reconstitution of embryonic cardiomyocytes in a collagen matrix: a new heart muscle model system, *FASEB J* 11(8) (1997) 683-94.
- [52] A. Stohr, F.W. Friedrich, F. Flenner, B. Geertz, A. Eder, S. Schaaf, M.N. Hirt, J. Uebeler, S. Schlossarek, L. Carrier, A. Hansen, T. Eschenhagen, Contractile abnormalities and altered drug response in engineered heart tissue from Mybpc3-targeted knock-in mice, *J Mol Cell Cardiol* 63 (2013) 189-98.
- [53] T. Eschenhagen, W.H. Zimmermann, Engineering myocardial tissue, *Circulation research* 97(12) (2005) 1220-31.
- [54] W.H. Zimmermann, K. Schneiderbanger, P. Schubert, M. Didie, F. Munzel, J.F. Heubach, S. Kostin, W.L. Neuhuber, T. Eschenhagen, Tissue engineering of a differentiated cardiac muscle construct, *Circulation research* 90(2) (2002) 223-30.
- [55] A. Lesman, M. Habib, O. Caspi, A. Gepstein, G. Arbel, S. Levenberg, L. Gepstein, Transplantation of a tissue-engineered human vascularized cardiac muscle, *Tissue Eng Part A* 16(1) (2010) 115-25.
- [56] G.A. Figtree, K.J. Bubb, O. Tang, E. Kizana, C. Gentile, Vascularized Cardiac Spheroids as Novel 3D in vitro Models to Study Cardiac Fibrosis, *Cells Tissues Organs* 204(3-4) (2017) 191-198.
- [57] F. Maiullari, M. Costantini, M. Milan, V. Pace, M. Chirivi, S. Maiullari, A. Rainer, D. Baci, H.E. Marei, D. Seliktar, C. Gargioli, C. Bearzi, R. Rizzi, A multi-cellular 3D bioprinting approach for vascularized heart tissue engineering based on HUVECs and iPSC-derived cardiomyocytes, *Sci Rep* 8(1) (2018) 13532.
- [58] L.E. Benjamin, E. Keshet, Conditional switching of vascular endothelial growth factor (VEGF) expression in tumors: induction of endothelial cell shedding and regression of hemangioblastoma-like vessels by VEGF withdrawal, *Proceedings of the National Academy of Sciences of the United States of America* 94(16) (1997) 8761-6.

- [59] Y. Dor, V. Djonov, R. Abramovitch, A. Itin, G.I. Fishman, P. Carmeliet, G. Goelman, E. Keshet, Conditional switching of VEGF provides new insights into adult neovascularization and pro-angiogenic therapy, *The EMBO journal* 21(8) (2002) 1939-47.
- [60] Y. Dor, S.E. Klewer, J.A. McDonald, E. Keshet, T.D. Camenisch, VEGF modulates early heart valve formation, *Anat Rec* 271A(1) (2003) 202-8.
- [61] C.H. Kim, Y.S. Cho, Y.S. Chun, J.W. Park, M.S. Kim, Early expression of myocardial HIF-1 α in response to mechanical stresses: regulation by stretch-activated channels and the phosphatidylinositol 3-kinase signaling pathway, *Circulation research* 90(2) (2002) E25-33.
- [62] P.H. Sugden, Ras, Akt, and mechanotransduction in the cardiac myocyte, *Circulation research* 93(12) (2003) 1179-92.
- [63] C.I. Maina, M. Ogunde, Reversal of left ventricular hypertrophy by propranolol in hypertensive rats, *Afr Health Sci* 5(1) (2005) 29-32.
- [64] J. Szlachcic, W.D. Hall, J.F. Tubau, V. Porter, C. Vollmer, G. Wollam, A. Hirsch, B. Massie, Left ventricular hypertrophy reversal with labetalol and propranolol: a prospective randomized, double-blind study, *Cardiovasc Drugs Ther* 4(2) (1990) 427-33.
- [65] Y. Hui, Z. Dai, X. Chen, W. Wang, Effect of perindopril and metoprolol on left ventricular hypertrophy and performance in essential hypertension, *Chin Med J (Engl)* 108(9) (1995) 678-81.
- [66] G.P. Vyssoulis, E.A. Karpanou, C.E. Pitsavos, A.A. Paleologos, P.K. Toutouzas, Regression of left ventricular hypertrophy in systemic hypertension with beta blockers (propranolol, atenolol, metoprolol, pindolol and celiprolol), *Am J Cardiol* 70(13) (1992) 1209-11.
- [67] M. Ciccarelli, D. Sorriento, E. Cipolletta, G. Santulli, A. Fusco, R.H. Zhou, A.D. Eckhart, K. Peppel, W.J. Koch, B. Trimarco, G. Iaccarino, Impaired neoangiogenesis in beta(2)-adrenoceptor gene-deficient mice: restoration by intravascular human beta(2)-adrenoceptor gene transfer and role of NF κ B and CREB transcription factors, *Br J Pharmacol* 162(3) (2011) 712-21.
- [68] G. Iaccarino, E. Cipolletta, A. Fiorillo, M. Anecchiarico, M. Ciccarelli, V. Cimini, W.J. Koch, B. Trimarco, Beta(2)-adrenergic receptor gene delivery to the endothelium corrects impaired adrenergic vasorelaxation in hypertension, *Circulation* 106(3) (2002) 349-55.
- [69] S. Guimaraes, D. Moura, Vascular adrenoceptors: an update, *Pharmacol Rev* 53(2) (2001) 319-56.
- [70] Y. Mei, N. Yin, X. Jin, J. He, Z. Yin, The regulatory role of the adrenergic agonists phenylephrine and isoproterenol on fetal hemoglobin expression and erythroid differentiation, *Endocrinology* 154(12) (2013) 4640-9.
- [71] A. Bouloumie, J. Bauersachs, W. Linz, B.A. Scholkens, G. Wiemer, I. Fleming, R. Busse, Endothelial dysfunction coincides with an enhanced nitric oxide synthase expression and superoxide anion production, *Hypertension* 30(4) (1997) 934-41.
- [72] M. Ozaki, S. Kawashima, T. Yamashita, T. Hirase, M. Namiki, N. Inoue, K. Hirata, H. Yasui, H. Sakurai, Y. Yoshida, M. Masada, M. Yokoyama, Overexpression of

endothelial nitric oxide synthase accelerates atherosclerotic lesion formation in apoE-deficient mice, *The Journal of clinical investigation* 110(3) (2002) 331-40.

[73] G. Lembo, G. Iaccarino, C. Vecchione, E. Barbato, R. Izzo, D. Fontana, B. Trimarco, Insulin modulation of an endothelial nitric oxide component present in the alpha2- and beta-adrenergic responses in human forearm, *The Journal of clinical investigation* 100(8) (1997) 2007-14.

[74] D. Sorriento, G. Santulli, C. Del Giudice, A. Anastasio, B. Trimarco, G. Iaccarino, Endothelial cells are able to synthesize and release catecholamines both in vitro and in vivo, *Hypertension* 60(1) (2012) 129-36.

[75] G. Liu, C. Ma, H. Yang, P.Y. Zhang, Transforming growth factor beta and its role in heart disease, *Exp Ther Med* 13(5) (2017) 2123-2128.

[76] R.B. Jennings, C.E. Ganote, K.A. Reimer, Ischemic tissue injury, *Am J Pathol* 81(1) (1975) 179-98.

10 Curriculum Vitae

Personal Information

Name: Julian Uwe Gabriel Wagner, M.Sc.
 Address:
 Date / Place of Birth: April, 30th 1991, Limburg an der Lahn
 Nationality: German
 Marital status: unmarried
 E-mail:



Education & Training

2007 – 2010 “Allgemeine Hochschulreife”; Adolf-Reichwein Schule Limburg / Lahn (**Grade:** 1.9)

October 2011 – September 2014 Academic Bachelor studies of Biology at the Justus-Liebig University Giessen, Germany. (**Grade:** 1.7)

Summer semester 2014 **Bachelor thesis** at the department of Animal Physiology (Director: Prof. Dr. Wolfgang Clauss), Justus-Liebig University Giessen, Germany. **Supervisor:** Dr. Mike Althaus
Bachelor project: “H₂S as a molecular regulator of the CFTR in native tracheal epithelia”
Grade: very good (14 Notenpunkte)

October 2014 – August 2016 Academic Master studies of Biology (concentrated on Biochemistry and Animal Physiology) at the Justus-Liebig University Giessen, Germany. (**Grade:** 1.1)

October 2014 – October 2015 **Student assistant** at the Institute of Biochemistry, Department of Enzymology (Director: Prof. Dr. Katja Strässer), Justus-Liebig University Giessen, Germany.

Winter semester 2015/2016 **Master thesis** at the Institute of Biochemistry, Department of Enzymology (Director: Prof. Dr. Katja Strässer), Justus-Liebig University Giessen, Germany. **Supervisor:** Assoc. Prof. Dr. Peter Friedhoff
Master project: “CRISPR-Cas9 fusion proteins as a new tool for genome engineering”
Grade: very good (13 Notenpunkte)

August 2016 – present **PhD candidate** at the Institute of Cardiovascular Regeneration (Director: Prof. Dr. Stefanie Dimmeler), JW Goethe University of Frankfurt, Germany. **Supervisor:** Prof. Dr. Stefanie Dimmeler
PhD project: “Endothelial Cross-Talks in the Aging Heart”

Languages

German: native speaker

English: fluent in written and spoken

Latin: qualification in Latin ("*Latinum*")

Memberships and Fellowships

August 2016 – present	SFB 834 for "Endothelial Signaling and Vascular Repair". Student's Speaker since 2017.
April 2017 – present	Member of the DZHK (German Center for Cardiovascular Research).
August 2018 – present	CRC1366 for "Vascular Control of Organ Function".
January 2019 – July 2019	Student Member of the American Heart Association (AHA).
October 2019 – present	CPI Academy fellow of the Cardio Pulmonary Institute.

Contributions to conferences & Oral presentations (ONLY as first author)

March 2017	Poster presentation: "Aging modulates endothelial matrix protein expression thereby promoting endothelial cell senescence and endothelial mesenchymal transition". 12 years SFB/TR 23: 'From Vascular Differentiation and Remodeling to Organotypic Vasculature'. (Heidelberg, Germany).
April 2017	Oral presentation: "Aging modulates endothelial matrix protein expression thereby promoting endothelial cell senescence and endothelial mesenchymal transition". 83. Jahrestagung der Deutschen Gesellschaft für Kardiologie – Herz- und Kreislaufforschung e.V. (Mannheim, Germany).
May 2017	Invited oral presentation: "Ageing modulated endothelial matrix protein expression promotes autophagy in EC". Guest lecture at the Justus-Liebig University Giessen, Faculty of Biology (Giessen, Germany).
June 2017	Poster presentation: "A switch in Laminin $\beta 2$ to Laminin $\beta 1$ isoforms during aging enhances endothelial-mesenchymal transition". Symposium of the Excellence Cluster Cardio Pulmonary System (Bad Nauheim, Germany).

- July 2017 **Poster presentation:** “A switch in Laminin β 2 to Laminin β 1 isoforms during aging enhances endothelial-mesenchymal transition”. DZHK Retreat Rheine-Main 2017 (Frankfurt, Germany).
- March 2018 **Invited oral presentation:** “A switch in Lamb2 to Lamb1 isoforms during aging controls endothelial cell functions and enhances endothelial-to-mesenchymal transition”. 16th Dutch-German Joint Meeting of the Molecular Cardiology Working Groups (Amsterdam, The Netherlands).
- May 2018 **Webcast:** “A switch in Lamb2 to Lamb1 isoforms during aging controls endothelial cell functions and enhances endothelial-to-mesenchymal transition”. RISING STARS program – BioLamina.
- July 2018 **Poster presentation:** “Age-dependent regulations of the cardiac vascular niche”. Gordon Research Conference on “Endothelial Cell Phenotypes in Health and Disease” (Lucca, Italy).
- September 2018 **Poster presentation:** “Single-nucleus sequencing to identify cellular heterogeneity in the aging mouse heart”. 5th Young DZHK Retreat and 6th DZHK Retreat. (Königstein, Germany).
- November 2018 **Poster presentation:** “Developing a novel vascularized 3D cardiac spheroid culture to study interactions of cardiomyocytes, fibroblasts and endothelial cells”. Scientific Sessions of the American Heart Association (Chicago IL, USA).
- April 2019 **Oral Presentation:** “Single-nucleus sequencing identifies cellular heterogeneity in the aging mouse heart”. 85. Jahrestagung der Deutschen Gesellschaft für Kardiologie - Herz- und Kreislaufforschung e.V. (Mannheim, Germany).
- June 2019 **Poster presentation:** “Transcriptional dis-organization of fibroblasts is a hallmark of the aging heart”. Retreat of the Cardio Pulmonary Institute (CPI), Max-Planck Institute Bad Nauheim (Bad Nauheim, Germany).
- September 2019 **Poster presentation:** “Transcriptional heterogeneity of fibroblasts is a hallmark of the aging heart”. 6th Young DZHK Retreat and 7th DZHK Retreat. (Potsdam, Germany).
- October 2019 **Oral presentation and poster presentation:** “Dissection of heterocellular cross-talk in vascularized cardiac tissue mimetics”. Meeting of the German Society for Microcirculation and Vascular Biology (GfMVB). (Heidelberg, Germany).

